Vol.: 50(2)
June, 2026
ISSN: 0250-4758
Online ISSN: 0973-970X

IJVP-2026

INDIAN JOURNAL OF VETERINARY PATHOLOGY

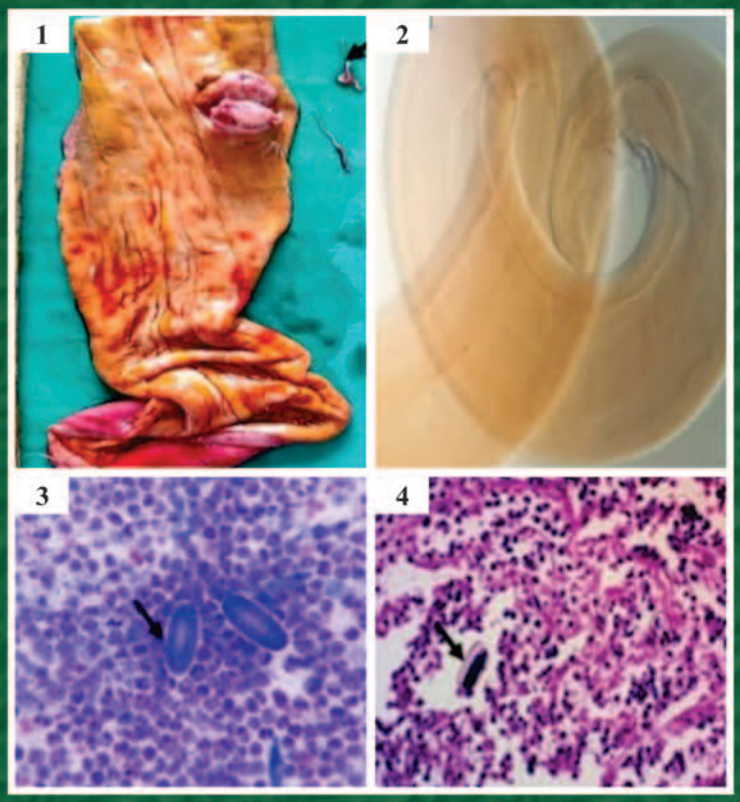

INDIAN ASSOCIATION OF VETERINARY PATHOLOGISTS
(Registered under article 21 of Societies Act 1860)

Visit us at: **www.iavp.org**
Journal available at: **www.indianjournals.com**

Vol. 50 (2)
June, 2026
ISSN: 0250-4758

INDIAN JOURNAL OF VETERINARY PATHOLOGY

Department of Veterinary Pathology, College of Veterinary Science,
Sri Venkateswara Veterinary University, Tirupati-517502, Andhra Pradesh
Mobile: +91-9441185383; E-mail: 7aakumar@gmail.com

INDIAN JOURNAL OF VETERINARY PATHOLOGY

Membership Fee and Subscription of Journal

- Individual life membership — Rs. 4,000/- (India) — US$ 600/- (Foreign)
- Individual life membership for the non-Indian citizens of the SAARC countries and other than North America, Europe and Australia — US$ 200/-
- Individual Annual Membership (for foreign only) — US $ 60/- (with free online access; no hard copy of journal)
- Library, Institutions, etc. (Annual) — Rs. 12,000/- (India) — US$ 400/- (Foreign)
- Individual Patron of IAVP — Rs. 1,00,000/- (Life member - paid patron for 5 years)
- Govt./Non-Govt./Corporate/ Institution Patrons — Rs. 5,00,000/ (for 5 years)

Advertisement Tariff

	Black and White	Full Colour
Regular full page	Rs. 4,000	Rs. 6,000
Regular half page	Rs. 2,000	Rs. 3,000
Inside front & back cover page	–	Rs. 10,000
Back cover page	–	Rs. 15,000

Note:

- Those submitting advertisement for two/four/six issues of the IJVP will be extended 15%/20%/25% discounts, respectively, on the above rates.
- The membership fee must be paid through Cash/Online/Crossed cheque or DD in favour of Treasurer "Indian Association of Veterinary Pathologists" payable at SBI, CARI Branch, Bareilly.

Contents

INDIAN JOURNAL OF VETERINARY PATHOLOGY

Cover Page Photo: Oesophageal Nodule with Spirocerca lupi: **1.** Photomicrographs showing focal nodule in the oesophagus of a dog with a Spirocerca lupi worm; **2.** Microscopic images of the Spirocerca lupi worm showing a vulval slit at the posterior end; **3.** Impression smear of the nodule showing Spirocerca lupi eggs; **4.** Parasitic eggs surrounded by infiltration of eosinophils, MNCs and PMNs.

Indian J. Vet. Pathol., 50(2) : 95-105, 2026: DOI: https://doi.org/10.56093/yas5sk24

REVIEW ARTICLE

West Nile Virus: Molecular epidemiology, pathogenesis, and global public health challenges

Divya Mudgal[1], Gaurav Joshi[1], Khushbu Dawra, Priya Mor, Gurmesh Bihnoi, Ritika Jangra, Nikita Bishnoi, Priyanka Luhauch, Nishant Vasdev, Manju Bernela, Taruna Anand, R.K.Vaid, B.C. Bera* and Nitin Virmani*

ICAR-National Research Centre on Equines, Sirsa Road, Hisar 125 001, Haryana, India

[1]The authors contributed equally and share first authorship

***Address of correspondence**

Nitin Virmani, Principal Scientist & Head, Equine Health Division, E-mail: nitin.virmani@icar.org.in and B.C. Bera, Principal Scientist, NCVTC, ICAR-NRCE, Hisar, E-mail: bcbpatent@gmail.com

Received: 3.2.26; Acepted: 13.4.26

ABSTRACT

The West Nile virus (WNV), belonging to *Flaviviridae*, is an RNA arbovirus and a member of the Japanese encephalitis virus serocomplex, and has materialized as a major growing health risk. Because of its swift geographic expansion and development of severe diseases, a small proportion of infected cases progress to neuroinvasive disease, tied to high fatality rates, mainly in geriatric and immunocompromised populations. The enzootic transmission of WNV occurs between avian hosts and Culicine mosquitoes, with humans and various mammals functioning as accidental terminal hosts. Molecular epidemiology has identified at least seven genetic lineages, with lineages 1, 2 and 5 responsible for human disease, and considerable phylogenetic diversity influenced by migratory bird dispersal. Acute flaccid paralysis, meningitis, encephalitis, fever, and long-term neurologic sequelae are among the clinical symptoms. Diagnosis relies on serological detection of WNV-specific IgM and confirmatory neutralization assays, though cross-reactivity with related flaviviruses complicates interpretation. Currently, no licensed human vaccines or specific antiviral therapies exist, and management remains supportive. Preventive strategies focus on vector control, blood donor screening, and personal protective measures. Advances in molecular virology, ecological surveillance, and vaccine development are improving understanding of viral transmission and pathogenesis. However, knowledge gaps remain regarding vector competence, host susceptibility, and predictive modelling of outbreaks. A multidisciplinary approach integrating genomic, ecological, and clinical data is essential to guide effective prevention, therapeutic innovation, and global preparedness against WNV.

Keywords: Encephalitis, Equines, *Flaviviridae*, JEV serocomplex, WNV

A. Introduction

A part of the Japanese encephalitis virus serocomplex, the West Nile virus (WNV) is an RNA virus that is carried by arthropods and belongs to the genus *Flavivirus* and family *Flaviviridae*[1]. Since its discovery in Uganda in 1937, WNV has proliferated throughout Africa, the Middle East, Australia, and the Americas, emerging as the most common virus carried by mosquitoes in temperate climate[2] (Table 1).

Transmission occurs primarily through Culicine mosquitoes, with birds serving as the main amplifying hosts[3]. Most infections are asymptomatic, but approximately 20% manifest as a self-limiting fever, and less than 1% develop neuroinvasive conditions such as acute flaccid paralysis, encephalitis or meningitis, which carry significant morbidity and mortality[4]. Molecular studies reveal several distinct viral lineages, of which lineages 1 and 5 are responsible for human and animal disease in India, and lineages 1 and 2 worldwide[5]. Various animals, including wildlife, domestic and companion animals, can be affected by the disease. When infected, most animals, including horses and humans, act as dead-end hosts owing to low levels of viraemia[6]. Most infections in horses and humans are asymptomatic with varying clinical manifestations, often involving nervous system functions. In other animals like bovines, ovines, camelids, canines and reptiles, WNV induces the formation of antibodies[7, 8].

The earliest serological evidence of West Nile virus infection in India was documented in Bombay in 1952, followed by confirmation in the South Arcot district of Tamil Nadu in 1982[9]. Over the subsequent three decades, recurrent outbreaks of WNV were reported predominantly from the southern states, including Tamil Nadu, Karnataka, and Andhra Pradesh[10]. Since 1974, serological investigations have demonstrated the presence of West Nile virus in animals across multiple regions of India[10]. Antibodies against WNV were

How to cite this article : Mudgal, D. Joshi, G., Dawra, K., Mor, P., Bihnoi, G., Jangra, R., Bishnoi, N., Luhauch, P., Vasdev, N., Bernela, M., Anand, T., Vaid, R.K., Bera, B.C. and Virmani, N. 2026. West Nile Virus: Molecular epidemiology, pathogenesis, and global public health challenges. Indian J. Vet. Pathol., 50(2) : 95-105.

Table 1. Historical perspective of West Nile Virus spread

Period/ Year	Key Event	Location	Significance
1937	First isolation of West Nile virus from a febrile woman	West Nile district, Uganda	Discovery of WNV; initially considered a mild dengue-like febrile illness[15, 16]
1950s	Ecological studies of virus transmission	Upper Nile region, Africa	Established Culex mosquitoes–bird transmission cycle; birds identified as amplification hosts and humans as dead-end hosts[17]
Late 1950s	First neurological disease observations	Egypt and Israel	Early evidence that WNV can cause neurological manifestations[18]
1960s–1980s	Sporadic outbreaks and equine cases	Africa, Europe, the Middle East	WNV is largely underestimated, as most infections were mild or asymptomatic[19, 20]
1970s–1980s	Identification of related virus variants	Australia	Discovery of Kunjin virus, a subtype/variant of WNV[21]
1996–1997	Large outbreak with neuroinvasive disease	Romania	Major turning point; high morbidity and mortality in elderly[22]
1999	First appearance in the Americas (NY99 strain)	New York City, USA	Major encephalitis outbreak in humans; high mortality in birds and horses[23]
2000–2003	Rapid geographic spread across North America	USA	Virus spread coast-to-coast by 2003 [24]
2000s	Expansion to other regions	Canada, Caribbean, Mexico, South America	Establishment of WNV across the Western Hemisphere[24, 25]
2000s	Development of surveillance systems	USA	ArboNET was established for monitoring human, avian, and mosquito infections[13]
2010s	Endemic establishment and emergence of lineage 2 in Europe	Hungary, Greece, Italy, Spain	Demonstrated spread of previously Africa-restricted lineage[20]
2012	Major outbreak in the USA	United States	One of the largest epidemics since its introduction in 1999[26]
2020s	Climate-change influenced transmission	North America and Europe	Extended mosquito season and expanded geographic range[27]
2025	Early seasonal cases detected	New York City, USA	Continued endemic circulation with positive mosquito pools across boroughs[10,28]

first detected in ardeid birds, including pond herons (*Ardeola grayii*) and cattle egrets (*Bubulcus ibis),* in Andhra Pradesh in 1981[10]. Subsequent studies confirmed viral circulation in both ardeid and terrestrial bird populations in Karnataka, as well as among wild resident and migratory avian species in eastern and northern parts of the country[11]. WNV-specific antibodies have also been identified in domestic pigs from Karnataka and Punjab, as well as in chickens from a poultry farm in Assam[12]. In Karnataka, pigs have been utilized as sentinel animals for monitoring WNV circulation. Longitudinal studies indicated that once pigs seroconverted to Japanese encephalitis (JE) and WNV, they retained immunity for up to three years[13]. Despite advances in surveillance and understanding of viral ecology, no licensed human vaccine or specific antiviral therapy exists, making prevention strategies reliant on vector control, personal protection, and public health monitoring[14].

Considering the increasing prevalence and emergence of WNV as an important neurotropic arbovirus, with potential for misdiagnosis in regions of co-existence of multiple flaviviruses, a comprehensive understanding of

public health significance of the disease and epidemiology is essential. This review, therefore, aims to underscore and summarize the current knowledge on epidemiology, transmission, pathogenesis, clinical manifestations, diagnostic challenges and control strategies from an Indian perspective, while at the same time highlighting the knowledge gaps that need further investigations.

B. Major Outbreaks of the Disease

Historically, several outbreaks of West Nile Virus (WNV) have been recorded, with major epidemics occurring in Israel (1951) and later in Romania, Tunisia, Russia, Canada, Greece, Algeria, the Czech Republic, and the Congo between 1994 and 1999[29, 30]. In animals, major outbreaks have primarily occurred among birds, particularly corvids and equines, although evidence of infection have been reported in over 35 animal species, most presenting asymptomatically. Notably, an outbreak of equine encephalitis attributed to WNV was recorded in Italy in 1998, affecting 14 horses and resulting in 4 deaths[31]. Another outbreak in France in 2003 resulted in several human cases and five equine meningoencephalitic cases, with a reported seroprevalence of 34% in equines[32]. North America has evidenced continuous outbreaks of WNV since 1999, affecting corvids, wild and exotic birds and equines, with thousands of avian mortalities and hundreds of equine cases documented so far[31]. In India, the prevalence of WNV has shown an upward trend, with serological evidence of infection in equines around Pune and 1,096 equines from five states. Additionally, serological evidence of WNV infection in pigs and frugivorous bats around Chandigarh suggests potential spillover into domestic and wild animals. In avian populations, neutralizing antibodies have been detected from pond herons, cattle egrets in southern parts of the country, as well as migratory and resident waterbirds from eastern and northern regions of the country[33].

C. Structure and Morphology of the Virus

The Virus's genome comprises single-stranded, positive-sense RNA with an approximate length of 11 kbp and codes for three structural and seven non-structural proteins, which are synthesised as a single polyprotein comprising around 3000 amino acids[3]. The virions are enveloped with icosahedral symmetry and approximately 50 nm in size. The structural proteins required for the formation of complete virions include capsid protein (C), pre-membrane protein (PrM) and envelope protein (E). The non-structural proteins include NS1, NS2A, NS2B, NS3, NS4A, NS4B and NS5, of which NS1 and NS2A are required for the processing of viral polyprotein along with NS2B, which acts as a cofactor for NS3 protease[34]. The NS1 protein also promotes neurodegeneration by promoting β-amyloid deposition in the CNS[35]. The NS5 protein, a methyltransferase, acts as RdRp (RNA-dependent RNA polymerase) and suppresses interferon signalling in anti-viral immune responses[36]. Whereas other non-structural proteins are small, hydrophobic and perform disparate functions[37]. All NSPs act together and facilitate viral replication, pathogenesis and immune evasion and are promising targets for drug design and development[38] (Figure 1).

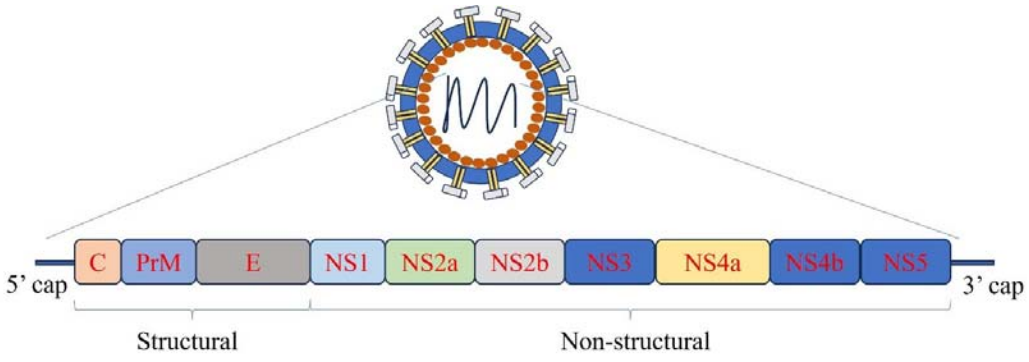

C	Capsid
PrM	Pre-membrane
E	Envelope

NS1	Replication/ evasion
NS2a	Replication
NS2b	Protease-cofactor
NS3	Protease/ helicase
NS4a	Membrane remodelling
NS4b	Immune evasion
NS5	Polymerase

Figure 1. Pictorial representation of the structure and genome of WNV

D. Molecular Epidemiology

Advances in genomic sequencing and global surveillance have substantially refined the phylogenetic classification of West Nile virus[18]. Current evidence indicates that WNV can be divided into at least seven distinct genetic lineages throughout the world, defined by nucleotide sequence divergence of approximately 25–30%[3]. Of these, only lineages 1 and 2 have been consistently associated with clinically significant mammalian and avian disease. In India, lineages 1 and 5 are predominant[18]. Importantly, phylogenetic clustering does not always align with the geographic distribution of the virus. This discordance is largely attributable to the long-distance dispersal of WNV through migratory avian hosts, which facilitates the intercontinental spread of genetically distinct strains[39]. Ongoing genomic surveillance continues to refine lineage boundaries and provides critical insights into viral evolution, epidemiology, and the emergence of strains with enhanced virulence or altered transmission dynamics.

Lineage 1

West Nile virus Lineage 1 exhibits a broad geographic distribution, encompassing North and Central America, Africa, Europe, Asia, Australia, and the Middle East[40]. Phylogenetic analyses subdivide lineage 1 into three major sublineages (1a, 1b, and 1c). Sublineage 1a is most often encountered and has been detected in Africa, Europe, the Middle East, Asia and the Americas, including the strain responsible for the 1999 New York outbreak (NY99). This sublineage has been implicated in virtually all major human encephalitis outbreaks concerning WNV worldwide, including the ongoing epidemics in North America. In 2011, sublineage 1a WNV was first reported in India, where it was detected from the serum of a febrile patient during an outbreak of neuroinvasive disease, further underscoring its pathogenic potential and global spread. Sublineage 1b, historically referred to as Kunjin virus (WNV-KUN), is endemic to Australia and likely extends into Papua New Guinea and parts of Southeast Asia[41]. Human disease caused by WNV-KUN is relatively uncommon; however, a notable 2011 equine outbreak in south-eastern Australia highlighted its ability to cause severe disease in horses under favourable ecological conditions. Sublineage 1c has thus far been reported exclusively from India[42]. However, recent phylogenetic studies suggest that isolates previously classified within sublineage 1c exhibit sufficient divergence to warrant reclassification as a distinct lineage, now proposed as lineage 5[43]. Newer Russian and Egyptian isolates, namely Ast01-182 and Eg101, have been isolated from Madurai, Tamil Nadu, which belong to lineage 1 of WNV[18].

Lineage 2

Historically, WNV lineage 2 was considered largely restricted to sub-Saharan Africa, where it was primarily associated with sporadic human infections manifesting as mild febrile illness and was not typically linked to large outbreaks or severe disease[43]. However, since the mid-2000s, the epidemiological profile of lineage 2 has shifted dramatically. Emerging evidence from Russia, Hungary, Italy, and Greece has demonstrated that lineage 2 strains are capable of causing severe neuroinvasive disease in humans, as well as fatal infections in birds and horses[44]. These findings established lineage 2 as an important cause of morbidity and mortality in both humans and animals, challenging the earlier perception of its limited pathogenicity and underscoring its expanding role in WNV epidemiology in Europe.

Lineage 5

The WNV lineage 5 mainly includes Indian isolates obtained from 13 different human cases showing genetic divergence from lineages 1, 2, and 3 (24-25% for lineage 1 and 2; 24-25% from lineage 3). Moreover, cross-neutralization studies employing lineage-1 strain Eg-101 specific polyclonal antibodies against Indian isolates suggest substantial antigenic variation[45].

E. Ecology

An enzootic transmitting cycle between a large number of mosquito vectors and a diverse range of avian hosts (more than 200 species) sustains the West Nile virus in nature[46]. Although representatives of the genus *Culex* are known to be the main vectors of WNV, over 60 different species of mosquito have been linked to the virus's spread[47]. Particularly significant in both North America and Europe is the *Culex pipiens* complex, which includes *Cx. pipiens pipiens*, *Cx. pipiens molestus*, and *Cx. Quinquefasciatus*[48]. The potential for local transmission is influenced by the physiology, behaviour, and ecological distribution of each species, as these factors determine vector competence, host preference, and population abundance.

Because the majority of Culicine mosquitoes are ornithophilic, or bird-feeding, they serve as effective enzootic vectors, maintaining the spread of viruses throughout bird populations. However, their frequent proximity to humans, especially in urban environments, also enables their role as epidemic vectors, bridging transmission from birds to humans. This is facilitated by the widespread presence of immature mosquito stages in aquatic habitats associated with artificial structures. Urban water management practices—such as the creation of wastewater treatment systems and conservation wetlands—may further alter vector and reservoir host communities, thereby modifying local WNV risk[49] (Figure 2).

F. Pathogenesis

The most frequent cause of West Nile virus infection is epidermal inoculation of viral material through

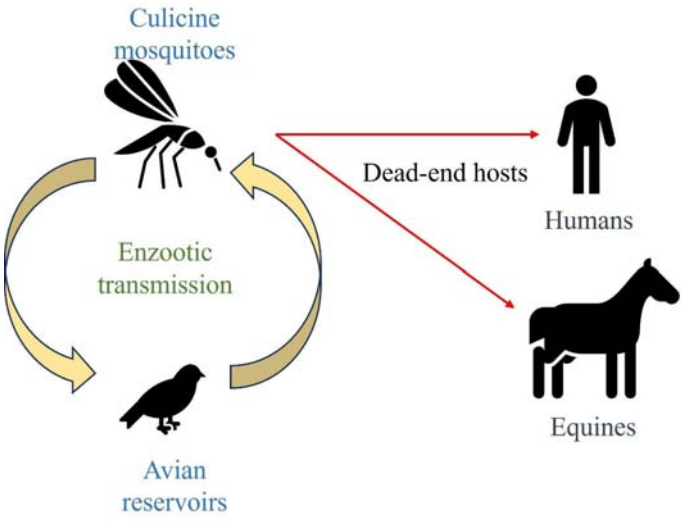

Figure 2. Representation of the transmission cycle of WNV

mosquito bites. Following entrance, the virus first replicates in dendritic cells (which are antigen-presenting cells) and epidermal keratinocytes at the injection site[38]. It then spreads to regional lymph nodes, where further replication occurs before disseminating into the bloodstream and subsequently infecting visceral organs[50,51]. In susceptible individuals, the virus may ultimately invade the central nervous system (CNS).

The early host response is mediated by the innate immune system. Infection induces production of proinflammatory cytokines, particularly type I interferons (IFNs), which play a critical role in restricting viral replication[52]. Additional mediators, including complement, chemokines, tumour necrosis factor (TNF), interleukin-1β, and innate cell-mediated responses, further contribute to viral control[53]. However, excessive or prolonged pro-inflammatory signalling can also cause immunopathologic damage. Viral clearance typically requires activation of the adaptive immune response, in which both humoral (B cell–mediated) and T cell–mediated immunity are necessary for limiting viral replication and preventing sustained inflammation-induced injury. Several mechanisms have been proposed for WNV neuroinvasion, including axonal transport along olfactory or peripheral neurons, cytokine-mediated disruption of the blood–brain barrier, migration of infected immune cells across endothelial tight junctions (the so-called "Trojan horse" mechanism), and direct infection of endothelial cells. Once within the CNS, WNV exhibits neurotropism with a predilection for extrapyramidal structures, including the brainstem, basal ganglia, thalami, and cerebellum; infection of neurons in these regions leads to cell death and contributes to the clinical manifestations of neuroinvasive disease[54]. The virus uses conserved receptors to enter the cells, which include neuronal $\alpha v\beta 3$ integrin and heparan sulphate[55]. The viral ligand E (envelope) glycoprotein binds the receptors, and internalization occurs by clathrin-mediated endocytosis and is recognised by TLR 3/7/9 along with other PRRs and leads to IFNAR signalling[56]. Furthermore, the immunopathological damage to neurons occurs by overactivation of NMDA receptors, leading to Ca2+ influx in neurons and causing neuronal death by excitotoxicity following virus-mediated astrocyte damage[57] (Figure 3).

G. Clinical Presentation

Most West Nile virus infections are asymptomatic (~80%), and approximately 20% of cases present as a self-limited febrile illness, while 0.4–0.7% progress to

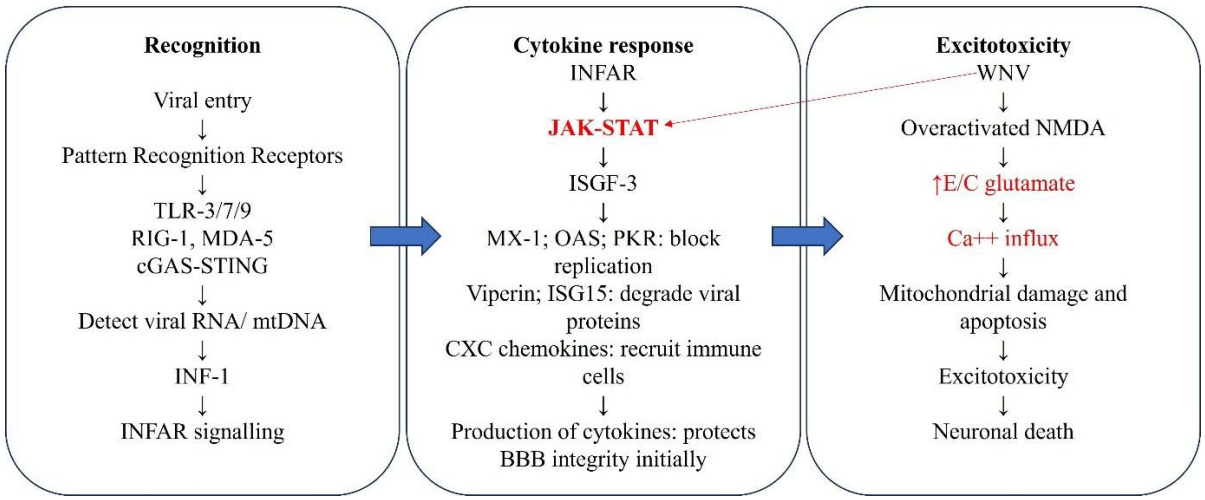

Figure 3. Molecular pathogenesis and immunopathological damage mechanism in the CNS by WNV

neuroinvasive disease[58]. The incubation period following mosquito exposure is typically 2–6 days (up to 14 days), though it may be prolonged in immunocompromised hosts, particularly transplant recipients and transfusion-related cases[59].

Neuroinvasive disease occurs in approximately 20% of horses infected with the virus and is characterised by fever and ataxia, including stumbling, incoordination, and staggering. Additional signs include limb paralysis, muscle fasciculations, weakness, prostration, defective proprioception and rarely acute death[60]. Among the horses developing neurological disease, 30% may die (CFR), and ~20 recover with neurological deficit. Clinical history, prevalence of mosquitoes, location and vaccination status of horses can support initial suspicion for the disease[60].

H. Diagnosis

West Nile virus infection should be considered in the differential diagnosis of patients presenting with febrile illness or neurologic symptoms during the summer and fall in endemic areas, particularly when there is a history of mosquito exposure, recent blood transfusion, or organ transplantation. Because clinical features overlap with other viral and bacterial infections, laboratory confirmation is essential[61]. The samples to be collected for diagnosis in case of suspicion for WNV include blood, serum and CSF from live animals and brain tissue from dead horses with a clinical history of severe neurological disease[60]. The signs of neurological disease often overlap with other neuroinvasive diseases like rabies, alphaviral equine encephalitis, Japanese encephalitis, etc. Hence, differential diagnosis with these diseases is also a necessity[60].

Serologic Testing

The principal and most sensitive method for diagnosing WNV infection in immunocompetent individuals involves detecting WNV-specific immunoglobulin M (IgM) antibodies in serum and/or cerebrospinal fluid (CSF). This is generally achieved through the use of IgM antibody-capture enzyme-linked immunosorbent assay (MAC-ELISA) or a duplex microsphere-based immunoassay technique[62]. WNV-specific IgM antibodies are detectable in >98% of patients by day 8 of illness; therefore, if initial IgM testing performed early in the course of infection is negative, repeat testing after day 8 is recommended[58]. Detection of WNV-specific IgM in non-bloody CSF is considered diagnostic of central nervous system (CNS) infection, as IgM does not ordinarily cross the intact blood–brain barrier[63].

However, interpretation of IgM results requires caution because antibodies may persist long after acute infection. Longitudinal studies have demonstrated persistence of serum IgM in 23–60% of patients for more than 16 months post-infection, and CSF IgM may remain detectable for up to 6 months[64]. Among viraemic blood donors, the average time to IgM negativity was approximately 5 months. For this reason, a positive IgM result does not necessarily distinguish acute infection from past exposure[65].

IgG testing alone is not diagnostic of acute disease, as it indicates prior infection with WNV or antigenically related flaviviruses. To confirm recent infection and exclude cross-reactivity with other flaviviruses (e.g., St. Louis encephalitis virus, Japanese encephalitis virus, Murray Valley encephalitis and Usutu virus), plaque reduction neutralization testing (PRNT) for WNV-specific neutralizing antibodies may be performed. PRNT remains the gold standard for serologic confirmation, though it is available only through reference laboratories such as the U.S. Centers for Disease Control and Prevention (CDC) and select state public health laboratories[62].

Molecular Testing

Detection of viral RNA by reverse transcription polymerase chain reaction (RT-PCR) is limited by the short duration of viremia, which typically resolves before the onset of neurologic disease in immunocompetent individuals. Sensitivity also varies by specimen type. In a cohort of 105 serologically confirmed patients with acute WNV disease, the sensitivity of RT-PCR was 26% for serum, 20% for plasma, and 17% for CSF[66]. Thus, RT-PCR is not considered a first-line diagnostic tool in the general population. Molecular testing, however, plays a critical role in immunocompromised patients who may not mount an antibody response. For example, individuals receiving B-cell–depleting monoclonal antibodies (e.g., rituximab, ocrelizumab) or transplant recipients are more reliably diagnosed with RT-PCR or metagenomic sequencing of serum, plasma, or CSF[58]. These molecular methods may be more sensitive than serology in such settings.

Tissue-Based Diagnosis

In certain cases, particularly postmortem evaluations, WNV infection can be confirmed by immunohistochemical staining (IHC) or RT-PCR detection of viral RNA in tissue samples. Histopathologic findings in neuroinvasive disease include microglial nodules, neuronal necrosis, and perivascular lymphocytic inflammation, predominantly affecting the brainstem, basal ganglia, thalami, and cerebellum. Patients with meningitis or meningoencephalitis may additionally exhibit leptomeningeal inflammation[67].

Rapid diagnostic platforms

Rapid diagnosis is essential in imparting the required treatment and also in surveillance and control of infections, especially in endemic areas. Several methods of diagnosis have been developed for rapid, pen-/

bed-side diagnosis of WNF, including Rapid Analyte Measurement Platform and chemiluminescent assays. These methods most commonly use serum or CSF as preferred diagnostic samples but can also be adapted to CNS tissue homogenates and cell-culture supernatant[68, 69].

I. Treatment and Prevention

Clinical management remains supportive, focusing on the stabilization of vital functions, mitigation of secondary brain injury, and long-term neurorehabilitation for patients with neuroinvasive disease. Investigational therapies—including interferon-α, ribavirin, immunoglobulins, and RNA-based strategies—have demonstrated antiviral activity in vitro or in animal models, but translation to human clinical efficacy has been inconsistent or absent[70]. High-titre immunoglobulins (e.g., Omr-IgG-am) and monoclonal antibodies show promise, yet their effectiveness in controlled human trials remains inconclusive. Similarly, RNA-targeted therapies (siRNA, antisense oligomers) and small-molecule inhibitors of viral protease or replication demonstrate preclinical efficacy but face challenges in timing of administration and CNS penetration[71].

Preventive strategies currently rely on mosquito vector control, personal protective measures, and blood safety screening. While effective equine vaccines exist, no human vaccine has been licensed. Several platforms—including inactivated, live-attenuated, chimeric, DNA, mRNA, and virus-like particle (VLP) vaccines—are in preclinical or early clinical phases, underscoring ongoing global efforts toward prophylaxis[72].

Critical gaps

The primary obstacles in WNV therapeutic development arise from both biological and logistical factors. First, the narrow therapeutic window presents challenges, as viremia often resolves by the time patients develop neuroinvasive disease, limiting antiviral efficacy[16]. Second, the blood–brain barrier restricts drug delivery to sites of neuroinflammation[73]. Third, the sporadic and geographically unpredictable nature of outbreaks hinders recruitment for large-scale clinical trials[74]. Additionally, most affected patients are elderly or immunocompromised, complicating trial design and therapeutic response evaluation.

Nevertheless, research suggests that early intervention with antibody-based therapies, RNA-targeted agents, or interferons could be effective if administered during the viraemic phase. Advances in nanoparticle delivery systems and host-targeted therapies may improve CNS penetration and broaden the therapeutic window[75]. Furthermore, preclinical data on monoclonal antibodies targeting the WNV envelope protein highlight their dual role as potential post-exposure prophylaxis and therapeutic agents[76].

The successful deployment of equine vaccines suggests technical feasibility; however, prioritization has been limited by the episodic nature of human outbreaks compared with other flaviviruses such as dengue, yellow fever, or Japanese encephalitis[77].

Translational gaps

Future research on West Nile virus must address the persistent translational gap between promising preclinical findings and demonstrable human efficacy. Despite substantial progress in animal models, the successful application of these discoveries in equine and human populations has been limited, largely due to the sporadic nature of outbreaks and the complexity of the virus's ecology. To bridge this divide, innovative approaches are required across trial design, therapeutic development, vaccine research, vector control, and integrated surveillance.

One key area of focus is clinical trial design. Traditional trial frameworks are poorly suited to an infection characterized by unpredictable and geographically variable outbreaks. Adaptive and platform trial models, deployed across endemic regions, could improve the efficiency and feasibility of evaluating both therapeutics and vaccines. Such designs would allow multiple interventions to be tested simultaneously, while also providing the flexibility to adapt as epidemiological conditions evolve.

Therapeutic strategies remain another critical frontier. Monoclonal antibody therapies, which have shown protection in preclinical studies, must now advance into controlled human trials. Similarly, novel approaches such as small interfering RNA (siRNA) and antisense oligomers require optimization to ensure effective delivery across the blood–brain barrier, one of the central challenges in treating WNV neuroinvasive disease[78]. Host-directed antivirals represent an additional avenue, with the potential to enhance innate immune defences while minimising the risk of immunopathology.

Vaccine development remains a high priority. Accelerated testing of DNA, mRNA, and chimeric vaccine platforms is urgently needed, particularly given the rapid advancements achieved during the COVID-19 pandemic[79]. Leveraging these established technologies may allow for scalable, cost-effective vaccines capable of providing durable protection in at-risk populations. Determining correlates of protection, such as neutralizing antibody titres and cellular immune responses, will be crucial for guiding both vaccine development and deployment strategies.

Finally, the adoption of the One Health approach is essential. Because WNV circulates at the intersection of human, animal, and environmental health, surveillance systems must integrate human clinical data with

veterinary and ecological monitoring. Strengthened cross-sectoral networks will be critical for identifying hotspots, predicting outbreak risk, and guiding targeted interventions such as vaccine deployment and intensified vector control.

Immunization and disease control measures

Currently, no vaccine is approved for human use; however, four vaccines are licensed for equine protection. WN InnovatorTM, Vetera WNV, and Prestige® WNV are three of these formulations that are whole-virus inactivated, while RecombitekTM Equine WNV is a live chimeric vaccination that expresses the prM/E genes in a canarypox vector[80]. All vaccines, except Vetera WNV, which is derived from the E159 equine isolate, are based on the NY99 strain. These vaccines have been shown to elicit protective immunity in horses, with efficacy lasting approximately one year[41].

Interestingly, an experimental study in mice reported that oral administration of vancomycin, neomycin, ampicillin, or metronidazole aggravated disease severity in multiple flavivirus infections[81]. These findings underscore the need for further well-designed, controlled investigations to establish effective therapeutic strategies for WNV. Prevention remains the primary strategy for controlling West Nile virus infections. The development of robust early warning systems and the implementation of targeted vector control programs are critical for reducing spillover transmission to humans. Effective entomological surveillance can provide advance indication of potential outbreaks, enabling timely intervention[82]. Immediate control measures should focus on reducing vector populations through the strategic use of organophosphate or synthetic pyrethroid insecticides. Recently, the adoption of the 'One Health' approach has gained prominence, promoting coordinated actions across human, animal, and environmental health sectors, as the virus circulates among humans, birds, horses, and mosquitoes, integrated surveillance systems are essential for early detection of viral activity in avian or equine populations which often precede human cases, and incorporating these signals into predictive models could provide vital early warnings. Research into climate change, avian migration patterns, and biodiversity shifts is also necessary to understand how ecological changes influence viral amplification and spillover into human populations. In Europe, this approach has enhanced the promptness of blood safety measures and facilitated the timely execution of vector control strategies[83].

Vector control remains a cornerstone of WNV prevention, but traditional methods such as larvicides, source reduction, and adulticides have not consistently prevented large-scale outbreaks. Research is needed to refine entomological surveillance, including the integration of molecular xeno-monitoring techniques that detect WNV RNA in mosquito pools as early outbreak indicators. Innovative biological control methods, such as the introduction of *Wolbachia*-infected mosquitoes, an entomopathogenic fungus, or larvivorous fishes like Gambusia, hold promise but require careful ecological risk assessments[80]. Genetic modification of mosquito populations through CRISPR-based gene drives, or sterile insect techniques (SIT), represents another frontier in vector control, though these approaches raise important ecological and ethical considerations[84]. Advances in mathematical modelling, which combine climate data, land-use patterns, and mosquito population dynamics, could further enhance the precision of outbreak prediction and improve targeted vector management.

Environmental management offers additional opportunities. Modifying urban water storage, improving sewage management systems, and managing wetlands can reduce breeding habitats, while public health campaigns can encourage behavioural changes that limit human–mosquito contact. Personal safety precautions, such as applying repellents, protective clothing, and avoidance of peak mosquito activity, remain effective, though research is needed to enhance compliance and long-term adoption.

Finally, the absence of nationwide equine vaccination and the licensed human vaccines highlight a critical prevention gap. Accelerated development and evaluation of DNA, mRNA, and chimeric vaccine platforms represent a promising research frontier. Integration of vaccination, once available, into a One Health–based prevention framework that coordinates human, veterinary, and ecological health responses will be essential for reducing the burden of WNV[85].

J. Future Perspectives

Future efforts to combat West Nile virus will focus on bridging the gap between existing preventive strategies and innovative interventions. In the short term, strengthening integrated surveillance systems that combine human, veterinary, and ecological data will be critical for early outbreak detection and targeted responses. Advances in vector control, including precision biological methods, genetic modification of mosquito populations, and climate-based predictive modelling, hold promise for reducing transmission but require rigorous ecological and ethical evaluation.

In the longer term, the development of a human vaccine remains the most important research priority. Novel platforms such as mRNA, DNA, and chimeric vaccines could accelerate progress, building on lessons from COVID-19 vaccine development. Parallel efforts in therapeutics, including monoclonal antibodies, RNA-based antivirals, and host-directed therapies, may offer new treatment options for neuroinvasive disease, which

currently lacks effective interventions. Finally, adopting a One Health framework that integrates environmental management, wildlife monitoring, and human health measures will be essential for sustainable control. As climate change, urbanization, and ecological shifts continue to expand the geographic range of WNV, multidisciplinary and globally coordinated research will be central to reducing its long-term public health impact[85].

K. Conclusion

West Nile virus remains an important emerging threat to global public and animal health. Classifying its epidemics into historical and contemporary phases provides valuable insight into its epidemiological patterns. As an emerging global pathogen, it also serves as a model for the international public health community to enhance communication, enhance collaborative networks, and improve preparedness strategies against presently neglected and future infectious disease threats. Strengthening diagnostic capacity in veterinary laboratories, promoting awareness among veterinarians and implementation of integrated vector control measures are crucial in mitigating the impact of virus. Furthermore, continued research on host-vector dynamics, reservoir patterns, and regional epidemiology will be essential in improving preparedness and prevention of future outbreaks affecting both human and animal populations.

Financial support & sponsorship: None

Conflicts of Interest: None

Use of Artificial Intelligence (AI)-Assisted Technology for manuscript preparation: The authors confirm that there was no use of AI-assisted technology for assisting in the writing of the manuscript and no images were manipulated using AI.

REFERENCES

1. Devine PA. 2003. West Nile virus infection. *Primary Care Update for OB/GYNS* **10(4):** 191–195.
2. Kakoti BB, Nongrang L, Borah C, Lahiri M, Ghosh M, Choudhary A. 2024. West Nile virus: evolutionary dynamics, advances in diagnostics, and therapeutic interventions. *Rising Contagious Diseases: Basics, Management, and Treatments*. 2024 John Wiley & Sons, Inc. 87-105.
3. Wehmeyer ML, Jaworsk, L, Jöst H, Șuleșco T, Rauhöft L, Afonso SMM, Lühken R. 2024. Host attraction and host feeding patterns indicate generalist feeding of Culex pipiens ss and Cx. torrentium. *Parasit Vectors* **17(1)**: 369.
4. Roberts J, Kim C, Hwang S, Hassan A, Covington E, Heydari K, Lyerly M, Sejvar J, Hasbun R, Prasad M, Thakur K. 2025. Clinical, Prognostic, and Longitudinal Functional and Neuropsychological Features of West Nile Virus Neuroinvasive Disease in the United States: A Systematic Review and Meta-Analysis. *Ann Neurol* **98.**
5. Koch R, Erazo D, Folly A, Johnson N, Dellicour S, Grubaugh N, Vogels C. 2023. Genomic epidemiology of West Nile virus in Europe. *One Health* **18**.
6. Zerbato V, Rossi B, Di Bella S, Bartalucci C, Cerchiaro M, Da Re D, Dentone C, Sepulcri C, Marini G, Delfino E, Sang Tran A, Di Biagio A, Giacobbe DR, Bassetti M. 2026. West Nile virus: epidemiology, prevention, clinical features, diagnosis, treatment, and open research questions. *Ann med*, **58(1)**: 2615482.
7. Gyure KA. 2009. West Nile virus infections. *J. neuropathol. exp neurol* **68(10):** 1053–1060. https://doi.org/10.1097/NEN.0b013e3181b88114
8. Vilibic-Cavlek T, Savic V, Klobucar A, Ferenc T, Ilic M, Bogdanic M, Tabain I, Stevanovic V, Santini M, Curman Posavec M, Petrinic S, Benvin I, Ferencak I, Rozac V and Barbic L. 2021. Emerging Trends in the West Nile Virus Epidemiology in Croatia in the 'One Health' Context, 2011-2020. *Trop. med. infect. dis.*, **6(3)**: 140.
9. Risbud AR, Sharma V, Rao CV, Rodrigues FM, Shaikh BH, Pinto BD and Verma SP. 1991. Post-epidemic serological survey for JE virus antibodies in south Arcot district (Tamil Nadu). *Indian J Med Res* **93**: 1-5.
10. Shanmugam L, Kumaresan M, Kundu R, Gunalan A, Dhodapkar R. 2022. Arboviruses in human disease: an Indian perspective. *Int J Adv Med Health Res* **9(2)**: 69–77.
11. Sedda L, Wrench E, Moore TC, Wolfe K, Tangena JAA, Brown HE. 2025. Challenges in the surveillance and control of mosquito-borne diseases in Europe and United States: the perspective from public health experts. *One Health* **21**: 101133.
12. Mackenzie JS, Lam SK. 2023. Human arboviruses in Eastern regions. *History of arbovirology: memories from the field. Vol II: virus family and regional perspectives*, *molecular biology and pathogenesis:* 313: Springer Nature Switzerland AG 2023.
13. Young JJ, Haussig JM, Aberle SW, Pervanidou D, Riccardo F, Sekulić N, Gossner CM. 2021. Epidemiology of human West Nile virus infections in the European Union and European Union enlargement countries, 2010–2018. *Euro surveill* **26(19)**: 2001095.
14. Mackenzie JS, Williams DT, van den Hurk AF, Smith DW, Currie BJ. 2022. Japanese encephalitis virus: the emergence of genotype IV in Australia and its potential endemicity. *Viruses* **14(11)**: 2480.
15. Simonin Y. 2024. Circulation of West Nile Virus and Usutu Virus in Europe: Overview and Challenges. *Viruses* **16(4)**: 599.
16. Singh P, Khatib MN, Ballal S, Kaur M, Nathiya D, Sharma S, Prasad GS, Sinha A, Gaidhane AM, Mohapatra P, Varma A. 2025. West Nile virus in a changing climate: epidemiology, pathology, advances in diagnosis and treatment, vaccine designing and control strategies, emerging public health challenges—a comprehensive review. *Emerg microbes infect*, **14(1):** 2437244.
17. Watts MJ, Sarto i Monteys V, Mortyn PG, Kotsila P. 2021. The rise of West Nile virus in southern and southeastern Europe: a spatial-temporal analysis investigating the combined effects of climate, land use and economic changes. *One Health*, **13**: 100315.
18. Rajaiah P, Mayilsamy M, Kumar A. 2023. West Nile virus in India: An update on its genetic lineages. *J. Vector Borne Dis* **60(3)**: 225-237.
19. Dachraoui K, Ben Osman R, Ben Slama S, Sayadi A, Maachach Y, Trifi M, Labidi I, Lachheb J, Badr C, Larbi I, Zhioua E. 2025. West Nile virus antibody prevalence in horses during the 2023 outbreak in Tunisia, North Africa. *Vector borne zoonotic dis*, **25(9)**: 558–564.
20. McDonald ES, Mathis S, Martin SW, Staples JE, Fischer M, Lindsey NP. 2021. Surveillance for West Nile virus disease—United States, 2009–2018. *MMWR morb mortal wkly rep* **70(1)**: 1–15.
21. Williams CR, Webb CE, Higgs S, van den Hurk AF. 2022. Japanese encephalitis virus emergence in Australia: public health importance and implications for future surveillance. *Vector borne*

zoonotic dis **22(11)**: 529–534.
22. Santini M, Haberle S, Židovec-Lepej S, Savić V, Kusulja M, Papić N, Vilibić-Čavlek T. 2022. Severe West Nile virus neuroinvasive disease: clinical characteristics, short- and long-term outcomes. *Pathogens* **11(1)**: 52.
23. Petersen LR, Roehrig JT. 2001. West Nile virus: a reemerging global pathogen. *Rev bioméd*, **12(3)**: 208–216.
24. Humphreys JM, Young KI, Cohnstaedt LW, Hanley KA, Peters DP. 2021. Vector surveillance, host species richness, and demographic factors as West Nile disease risk indicators. *Viruses* **13(5)**: 934.
25. Ferraguti M, Heesterbeek H, Martínez-de la Puente J, Jiménez-Clavero MA, Vázquez A, Ruiz S, Llorente F, Roiz D, Vernooij H, Soriguer R, Figuerola J. 2021. The role of different *Culex* mosquito species in the transmission of West Nile virus and avian malaria parasites in Mediterranean areas. *Transbound emerg dis* **68(2)**: 920–930.
26. Fair JM, Al-Hmoud N, Alrwashdeh MM, Bartlow AW, Balkhamishvili S, Daraselia I, Owen J. 2024. Transboundary determinants of avian zoonotic infectious diseases: challenges for strengthening research capacity and connecting surveillance networks. *Front microbiol* **15**: 1341842.
27. D'Amore C, Grimaldi P, Ascione T, Conti V, Sellitto C, Franci G, Kafil SH, Pagliano P. 2023. West Nile virus diffusion in temperate regions and climate change: a systematic review. *Le infez med* **31(1)**: 20.
28. Moreira-Soto A, Postigo-Hidalgo I, Tabares X, Roell Y, Fischer C, Gotuzzo E, Jaenisch T, Levi JE, Lustig Y, Drexler JF. 2025. Transfusion-transmitted infections: risks and mitigation strategies for Oropouche virus and other emerging arboviruses in Latin America and the Caribbean. *Lancet Reg Health Am* **46**.
29. Sejvar J J. 2003. West nile virus: an historical overview. Ochsner J 5(3): 6–10.
30. Klingelhöfer D, Braun M, Kramer IM, Reuss F, Müller R, Groneberg DA, Brüggmann D. 2023. A virus becomes a global concern: research activities on West Nile virus. *Emerging Microbes & Infections* 12(**2**): 2256424.
31. McLean RG, Ubico SR, Bourne D and Komar N. 2002. West Nile virus in livestock and wildlife. Curr Top Microbiol Immunol 267: 271–308.
32. Dauphin G, Zientara S, Zeller H and Murgue B. 2004. West Nile: worldwide current situation in animals and humans. Comp Immunol Microbiol Infect Dis 27(5): 343–355.
33. Gulati BR, Gupta AK and Kadian SK. 2014. West Nile virus infection among animals and humans in India. Adv. Anim. Vet 2(4S): 17–23.
34. Praveen M. 2024. Characterizing the West Nile Virus's polyprotein from nucleotide sequence to protein structure – Computational tools. J Taibah Univ Sci 19: 338 - 350.
35. Rossi SL, Ross TM and Evans JD. 2010. West Nile virus. *Clin Lab Med* **30(1)**: 47–65.
36. Beltrami S, Rizzo S, Schiuma G, Cianci G, Narducci M, Baroni M, Di Luca D, Rizzo R and Bortolotti D. 2025. West Nile virus non-structural protein 1 promotes amyloid Beta deposition and neurodegeneration. *Int J Biol Macromol* 141032
37. Brandolini M, De Pascali AM, Zaghi I, Dirani G, Zannoli S, Ingletto L, Lavazza A, Lelli D, Dottori M, Calzolari M, Guerra M. 2024. Advancing West Nile virus monitoring through whole genome sequencing: insights from a One Health genomic surveillance study in Romagna (Italy). *One Health* **19**: 100937.
38. Wessel A, Doyle M, Engdahl T, Rodriguez J, Crowe J and Diamond M. 2021. Human Monoclonal Antibodies against NS1 Protein Protect against Lethal West Nile Virus Infection. *mBio* **12**.
39. Mundhra S. 2024. West Nile virus: a comprehensive overview of epidemiology and pathology. *Emerg Hum Viral Dis* **2**: 193–219.
40. Chowdhury P, Khan SA. 2021. Global emergence of West Nile virus: threat and preparedness with special perspective to India. *Indian J Med Res* **154(1)**: 36–50.
41. Lopez KA. 2023. Evaluating adult mosquito control and insecticide resistance in a West Nile virus hotspot (dissertation): *University of Wisconsin–Madison*.
42. Mencattelli G, Ndione M, Rosà R, Marini G, Diagne C, Diagne M, Fall G, Faye O, Diallo M, Faye O, Savini G, Rizzoli A. 2022. Epidemiology of West Nile virus in Africa: an underestimated threat. *PLoS neg trop dis* **16**: e0010075.
43. Cavalleri JM, Korbacska-Kutasi O, Leblond A, Paillot R, Pusterla N, Steinmann E, Tomlinson J. 2022. European College of Equine Internal Medicine consensus statement on equine flaviviridae infections in Europe. *J Vet Intern Med* **36(6)**: 1858–1871.
44. Bondre VP, Jadi RS, Mishra AC, Yergolkar PN and Arankalle VA. 2007. West Nile virus isolates from India: evidence for a distinct genetic lineage. *J Gen Virol* **88(3)**: 875–884.
45. Bialosuknia SM, Dupuis II AP, Zink SD, Koetzner CA, Maffei JG, Owen JC, Landwerlen H, Kramer LD, Ciota AT. 2022. Adaptive evolution of West Nile virus facilitated increased transmissibility and prevalence in New York State. *Emerg Microbes Infect* **11(1)**: 988–999.
46. Soto A, Delang L. 2023. *Culex modestus*: the overlooked mosquito vector. *Parasites Vectors* **16(1)**: 373.
47. Haba Y, McBride L. 2022. Origin and status of *Culex pipiens* mosquito ecotypes. *Curr Biol* **32(5)**: R237–R246.
48. Chapman GE, Baylis M, Archer D, Daly JM. 2018. The challenges posed by equine arboviruses. *Equine Vet J* **50(4)**: 436–445.
49. Martí MM, Castanha PM, Barratt-Boyes SM. 2024. The dynamic relationship between dengue virus and the human cutaneous innate immune response. *Viruses* **16(5)**: 727.
50. Brisse ME, Hickman HD. 2025. Viral infection and dissemination through the lymphatic system. *Microorganisms* **13(2)**: 443.
51. Mertowska P, Smolak K, Mertowski S, Grywalska E. 2023. Immunomodulatory role of interferons in viral and bacterial infections. *Int J Mol Sci* **24(12)**: 10115.
52. Alghamdi A, Alissa M, Alshehri MA. 2025. Mechanisms of immune evasion of West Nile virus. *Rev Med Virol* **35(3)**: e70042.
53. Caldwell M, Boruah AP, Thakur KT. 2022. Acute neurologic emerging flaviviruses. *Ther Adv Infect Dis* **9**: 20499361221102664.
54. Chu J, Ng M. 2004. Interaction of West Nile virus with $\alpha v\beta 3$ integrin mediates virus entry into cells. *J Biol Chem* **279**: 54533–54541.
55. Evans J, Crown R, Sohn J, Seeger C. 2011. West Nile virus infection induces depletion of IFNAR1 protein levels. *Viral Immunol* **24(4)**: 253–263.
56. Getts D, Matsumoto I, Müller M, Getts M, Radford J, Shrestha B, Campbell I, King N. 2007. Role of IFN-γ in an experimental murine model of West Nile virus–induced seizures. *J Neurochem* **103**: 1–10.
57. Gould CV, Staples JE, Guagliardo SAJ, Martin SW, Lyons S, Hills SL, Nett RJ, Petersen LR. 2025. West Nile virus: a review. *JAMA*.
58. Szabó BG, Nagy A, Nagy O, Koroknai A, Csonka N, Korózs D, Jeszenszky K, Hardi A, Deézsi-Magyar N, Sztikler J, Bódi Z. 2025. First documented case of a fatal autochthonous Usutu virus infection in an immunocompromised patient in Hungary: a clinical-virological report and implications from the literature. *Virol J* **22(1)**: 261.
59. Paré J and Moore A. 2018. West Nile virus in horses - What do you need to know to diagnose the disease?. *Can Vet J* **59(10)**:

1119–1120.
60. Toribio RE. 2022. Arboviral equine encephalitides. *Vet Clin North Am Equine Pract* **38(2)**: 299–321.
61. Weatherhead JE, Ronca SE. 2022. Protocol of detection of West Nile virus in clinical samples. In: *West Nile virus: methods and protocols* **2585**: 119.
62. Pelz JO, Mühlberg C, Friedrich I, Weidhase L, Zimmermann S, Maier M, Pietsch C. 2024. A specific pattern of routine cerebrospinal fluid parameters might help to identify cases of West Nile virus neuroinvasive disease. Viruses **16(3)**: 341.
63. Schwarz ER, Long MT. 2023. Comparison of West Nile virus disease in humans and horses: exploiting similarities for enhancing syndromic surveillance. *Viruses* **15(6)**: 1230.
64. Ronca SE, Ruff JC, Murray KO. 2021. A 20-year historical review of West Nile virus since its initial emergence in North America: has West Nile virus become a neglected tropical disease? *PLoS Negl Trop Dis* **15(5)**: e0009190.
65. Zidovec-Lepej S, Vilibic-Cavlek T, Barbic L, Ilic M, Savic V, Tabain I, Savini G. 2021. Antiviral cytokine response in neuroinvasive and non-neuroinvasive West Nile virus infection. *Viruses* **13(2)**: 342.
66. Palmieri C, Franca M, Uzal F, Anderson M, Barr B, Woods L, Moore J, Woolcock P, Shivaprasad HL. 2011. Pathology and immunohistochemical findings of West Nile virus infection in psittaciformes. *Vet Pathol* **48(5)**: 975–984.
67. Gómez-Vicente E, Garcia R, Calatrava E, Duran O, Gutiérrez-Bautista J, Rodríguez-Granger J, Cobo F, Mari J, Sampedro-Martínez A. 2022. Comparative evaluation of chemiluminescent immunoassay and enzyme-linked immunosorbent assays for the diagnosis of West Nile virus infections. *APMIS* 130(**1**): 215–220.
68. Lustig Y, Sofer D, Bucris E, Mendelson E. 2018. Surveillance and diagnosis of West Nile virus in the face of flavivirus cross-reactivity. *Frontiers in Microbiology* **9**(**1**): 2421.
69. Mohanty P, Panda P, Acharya RK, Pande B, Bhaskar LVKS, Verma HK. 2023. Emerging perspectives on RNA virus-mediated infections: from pathogenesis to therapeutic interventions. *World Journal of Virology* **12**(**5**): 242.
70. Wang H, Liu T, Gao X, Wang H, Xiao J. 2024. Impact of climate change on the global circulation of West Nile virus and adaptation responses: a scoping review. *Infectious Diseases of Poverty* **13**(**1**): 1207.
71. Gupta R, Arora K, Roy SS, Joseph A, Rastogi R, Arora NM, Kundu PK. 2023. Platforms, advances, and technical challenges in virus-like particles-based vaccines. *Frontiers in Immunology* **14**(**1**): 1123805.
72. Pavesi A, Tiecco G, Rossi L, Sforza A, Ciccarone A, Compostella F, Lovatti S, Tomasoni LR, Castelli F, Quiros-Roldan E. 2024. Inflammatory response associated with West Nile neuroinvasive disease: a systematic review. *Viruses* **16**(**3**): 383.
73. Damus BJ, Amaeze NR, Yoo E, Kaur G. 2024. Ethoxy acetalated dextran-based biomaterials for therapeutic applications. *Polymers* **16**(**19**): 2756.
74. Mokhtary P, Pourhashem Z, Mehrizi AA, Sala C, Rappuoli R. 2022. Recent progress in the discovery and development of monoclonal antibodies against viral infections. *Biomedicines* **10**(**8**): 1861.
75. Saiz J. 2020. Animal and human vaccines against West Nile virus. *Pathogens* **9(12)**: 1073.
76. Wang MY, Zhao R, Wang YL, Wang DP, Cao JM. 2023. Challenges with the discovery of RNA-based therapeutics for flaviviruses. *Expert Opinion on Drug Discovery* **18**(**4**): 371–383.
77. Rando HM, Lordan R, Kolla L, Sell E, Lee AJ, Wellhausen N, COVID-19 Review Consortium. 2023. The coming of age of nucleic acid vaccines during COVID-19. *mSystems* **8(2)**: e00928-22.
78. Cendejas PM, Goodman AG. 2024. Vaccination and control methods of West Nile virus infection in equids and humans. *Vaccines* **12(5)**: 485.
79. Langendries L, Delang L, Neyts J. 2022. Classic and new strategies to fight arboviruses: effect of antiviral drugs and skin bacteria on virus infectivity. *Trends in Microbiology* **30(10)**: 1003–1016.
80. Taylor-Robinson AW. 2023. Harnessing artificial intelligence to enhance key surveillance and response measures for arbovirus disease outbreaks: the exemplar of Australia. *Frontiers in Microbiology* **14(1)**: 1284838.
81. Danasekaran R. 2024. One health: a holistic approach to tackling global health issues. *Indian Journal of Community Medicine* **49(2)**: 260–263.
82. Abbasi E. 2025. Innovative approaches to vector control: integrating genomic, biological, and chemical strategies. *Annals of Medicine and Surgery* **87(8)**: 5003–5011.
83. Edwards RTM. 2023. Development of a gene editing platform for sand fly vectors of *Leishmania* through CRISPR-Cas9 genetic modification targeting genes associated with olfaction (dissertation): London School of Hygiene & Tropical Medicine.
84. Lu B, Lim JM, Yu B, Song S, Neeli P, Sobhani N, K P, Bonam SR, Kurapati R, Zheng J, Chai D. 2024. The next-generation DNA vaccine platforms and delivery systems: advances, challenges and prospects. Frontiers in Immunology 15(1): 1332939.
85. Paternoster G, Tomassone L, Tamba M, Chiari M, Lavazza A, Piazzi M, Favretto A, Balduzzi G, Pautasso A, Vogler B. 2017. The degree of One Health implementation in the West Nile virus integrated surveillance in Northern Italy, 2016. *Frontiers in Public Health* **5(1)**: 236.

Indian J. Vet. Pathol., 50(2) : 106-111, 2026: DOI: https://doi.org/10.56093/sbph3n73

RESEARCH ARTICLE

Spontaneous lesions of the thyroid gland in goats (*Capra hircus*)

Poobitha Subbarayan[1], Madhavan Gopalakrishnan Nair[1], Kumar Raja[1]*, Varshney K.C.[1], Uma Maheswari D.[2], Uma S.[1] and Avinash Warundeo Lakkawar[1]

[1]Department of Veterinary Pathology, [2]Department of Animal Nutrition,
Rajiv Gandhi Institute of Veterinary Education and Research (RIVER), Kurumbapet,
Puducherry-605 009, India.

***Address for Correspondence**

Raja Kumar, Professor and Head, E-mail: kumarpath70@gmail.com

Received: 20.11.25; Accepted: 5.1.26

ABSTRACT

The thyroid glands play an important role in the development of various tissues, thermoregulation, metabolic function and reproduction. Abattoir and necropsy-based studies provide an excellent opportunity for detecting diseases of both economic and public health importance. In the present study, thyroid glands from 150 goats were collected and the lesions were characterized. Correlations of gross and histopathological findings, gross and histomorphometry were carried out. The macroscopic findings recorded in the thyroid gland of abattoir and necropsy cases were thyroid gland with normal appearance (87.33%); paler than normal (3.33%); darker than normal (8.33%); brownish black discolouration (0.66%); gland with solitary nodule in the parenchyma (0.33%) and cyst(s) in the hilar region (6.33%). Out of 150 thyroid glands studied, it was observed that the histology of both lobes was not uniform. The microscopic findings recorded were: thyroid gland with normal histoarchitecture (3.66%), ultimobranchial cyst (28.33%), vacuolar degeneration (25.66%), follicular degeneration (13%), cystic degeneration (6%), mineralization of cyst (0.33%), congestion (27.66%, inter-follicular haemorrhages (2.66%) and intra-follicular haemorrhages (4.66%), focal atrophy (7.66%), hypertrophy of follicular epithelium (14.66%), follicular epithelial hyperplasia (24.33%), C-cell hyperplasia (25.33%), colloid goitre (4%), melanin pigmentation (4%), macrofollicles (19.33%), microfollicles (5.33%), focal fibrosis (17.33%), signet ring variant of follicular cell adenoma (2%), C-cell adenoma (0.66%) and capillary hemangioma (0.33%). Morphological examination including histopathology of endocrine glands is a sensitive parameter for the detection of compounds that adversely affect gland function. This information would be useful in interpreting and grading the severity of changes related to any specified treatment effect.

Key words: Goat, pathology, thyroid gland

INTRODUCTION

Alterations in the structure and function of the endocrine glands may be brought about by genetic factors, infectious agents, malnutrition and environmental factors. Similarly, the disorders affecting the endocrine organs either individually or collectively have a remarkable effect on the animal body as a whole. Among the endocrine glands, the thyroid is one which mediates most of the reproductive performances of domestic animals. The thyroid is the largest endocrine organ and is usually bilobed[1]. Structurally, the thyroid gland consists of right and left lobes united by a narrow isthmus, which extends across the trachea anterior to second and third tracheal cartilages[2]. The morphology and location of the thyroid gland varies with species. It consists of follicles containing colloid; follicular cells called thyrocytes trap iodine and synthesize thyroglobulin and parafollicular cells (C-cells) produce the hormone thyrocalcitonin[3]. Thyroid gland contains 70-80 % of the total body iodine and produces two main iodine containing hormones, T4 and T3[4]. The final assembly of the hormones (thyroxine, T4 and triiodothyronine, T3) occurs extracellularly in the colloid within the follicular lumen. Thyroglobulin is a high molecular weight glycoprotein synthesized in successive subunits on the ribosomes of the endoplasmic reticulum in follicular cells[5]. The pathological conditions of thyroid gland adversely affect production and productivity of livestock[6,7]. Although hypothyroidism is reported to be the most common disorder affecting small ruminants, there are limited systematic studies carried out on the lesions affecting the thyroid gland in slaughtered animals, particularly in goats. The gross and histomorphometry of the thyroid gland of goats have been reported[8]. The present communication addresses the gross and histopathological features of spontaneous lesions recorded in the thyroid glands of goats that were either slaughtered at abattoirs or necropsied.

How to cite this article : Subbarayan, P., Nair, MG., Raja, K., Varshney. K.C., Maheswari, U.D., Uma, S. and Lakkawar, A.W. 2026. Spontaneous lesions of the thyroid gland in goats (*Capra hircus*). Indian J. Vet. Pathol., 50(2) : 106-111.

MATERIALS AND METHODS

The thyroid glands were collected from goats (n=145) at abattoirs and 5 from necropsy cases in Puducherry. The 145 crossbred goats were categorized according to their age and gender as: below 6 months (n=41, 28 M, 13 F), 6 months to 1 year (n=56, 32 M, 24 F) and above1 year to

3 years (n=48, 30 M, 18 F) and 5 necropsied goats were categorized as: below 6 months (n=1, M), 6 months to 1 year (n=1, M) and above 1 year to 3 years (n=3, F). After ascertaining the age, sex and breed, the right and left lobes of the thyroid glands were carefully dissected out. A detailed gross examination of all the thyroid glands with respect to size, shape, colour and consistency was carried out. After making longitudinal incisions, the glands (right and left lobes) were fixed in 10% neutered buffered formalin (NBF) in separate containers. Representative tissues from each of the glands were processed by routine paraffin embedding technique and microtomy and 4-5 μm thick sections were stained by routine Haematoxylin and Eosin (H&E) staining procedure and Periodic acid schiffs (PAS) wherever necessary[9]. The microscopic changes of the thyroid gland were classified as described earlier[5]. All images were captured by using a trinocular microscope (Optika, Italy) fitted with Optika B5 camera.

RESULTS

The macroscopic features recorded in the thyroid gland of abattoir and necropsy cases were: (a) thyroid gland with normal features, 262/300 lobes, 87.33%); (b) paler than normal (10/300,3.33%); (c) darker than normal (25/300, 8.33%); (d) brownish black discolouration (2/300, 0.66%), a lobe with solitary nodule (1/300, 0.33%); (e) cyst (s) in the hilar region (20/300, 6.33%).

The thyroid glands with normal histoarchitecture had characteristically, a thin capsule made of irregular connective tissue. The parenchyma comprised of thyroid follicles, parafollicular (C) cells, sparse interstitial loose connective tissue, and dense network of capillaries. Follicles were round to oval in shape and lined by a single layer of follicular epithelial cells that were either flattened or low columnar, depending on the degree of activity of the gland. Occasionally, follicular cells with abundant granular acidophilic cytoplasm (Hürthle cells) were noticed. In some of the cases, the thyroid gland appeared to be active. These cases were characterized by the presence of a row of small vacuoles located at the interface between follicular epithelium and the colloid and the phenomenon is referred to as scalloping (Fig.1). Ultimobranchial cysts were recorded in 85/290 lobes, 29.31% (27 in left lobe, 30 in right lobe and 14 bilaterally) in the abattoir cases.

Histopathological changes recorded in the thyroid glands were categorized as congenital anomalies, degenerative changes, vascular disturbances, growth disturbances, pigmentation, neoplasms and miscellaneous conditions. Degenerative changes in the thyroid lobes were recorded in both abattoir and necropsy cases. The various degenerative changes were categorized as vacuolar degeneration, follicular degeneration, cystic degeneration (follicular cysts) and cystic mineralization. However, it is emphasized that, few degenerative changes were also seen concomitantly with various other thyroid lesions recorded.

Vacuolar degeneration was recorded in 72/290 lobes (24.82%) of the abattoir cases and 5/10 lobes (50%) of the necropsy cases. Amongst these 77 lobes, vacuolar degeneration occurred in 25 of the left lobes, 18 of the right lobes and bilaterally in 17 cases. Vacuolar degeneration was characterized by clear vacuoles, that were located either in a supra nuclear or infra nuclear position within the cytoplasm of the follicular epithelium (Fig.2). The degree of vacuolar degeneration varied from mild to severe. Follicular degeneration with desquamation was recorded in 37/290 lobes (12.75%) of the abattoir cases and in 2/10 (20%) of necropsy cases. Amongst these 39 cases, the feature was observed in 10 of the left lobes, 19 of the right lobes and bilaterally in 5 lobes characterized by partial to complete exfoliation of the follicular epithelial cells into follicular lumen. The severity of follicular degeneration varied from mild to severe. In severe cases, there was extensive desquamation with lack of colloid. Cystic degeneration of the follicles was recorded in 18/290lobes (6.20%) of the abattoir cases, of which, 8 occurred in the left, 8 in the right and bilaterally in 1 case characterized by cystic dilatation of the degenerating follicles. These cysts were lined by flattened epithelial cells and contained degenerated follicular epithelial cells that gave a granular appearance (Fig.3). Mineralization was characterized by the formation of densely basophilic spherules or granules in the lumen of cysts. These appeared to represent the precipitation of minerals on the degenerated cellular debris (Fig.4). Mineralization was recorded in only one lobe of an abattoir case.

Vascular disturbances were recorded in 98/290 lobes (33.79%) of the abattoir cases and 7/10 lobes (70%) of the necropsy cases. The vascular disturbances recorded were congestion and haemorrhages. Grossly, congested thyroid glands appeared deep red in colour, normal in shape and consistency (Fig.5). Microscopically, congestion was multi-focal and varied from mild to severe degree. Haemorrhages were not grossly discernible. Microscopically, haemorrhages occurred in focal areas within the parenchyma and varied from mild to moderate degree. Based on the location, haemorrhages were categorized as either inter-follicular or intra-follicular (Fig.6).

The growth disturbances were categorized as focal atrophy, hypertrophy and hyperplasia. Focal areas of follicular atrophy were observed in 22/290 lobes (7.58%) of the abattoir cases and in 1/10 lobes (10%) of the necropsy cases. Amongst these 23 cases, focal follicular atrophy was noticed in 13 of the left lobes and 10 of the right lobes, with no bilateral involvement. Microscopically,

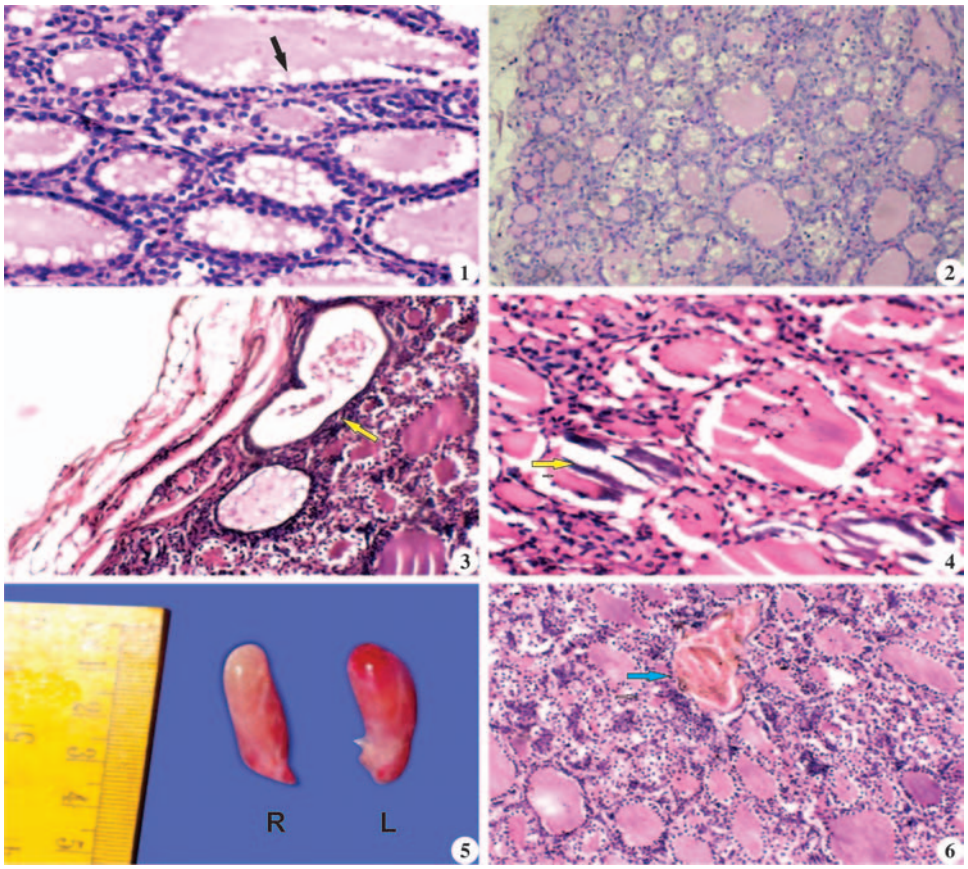

Fig. 1. Thyroid gland showing resorption vacuoles (arrow) at the interface between follicular epithelial cells and colloid [Scalloping]. H&E x200; **Fig.2.** Thyroid gland showing vacuolar degeneration of follicular epithelial cells. H&E x200; **Fig.3.** Thyroid gland showing cystic egeneration of the follicles, presence of granular material in the lumen (arrow).H&Ex100; **Fig.4.** Thyroid gland showing mineralization of follicular cyst(arrow). H&E x200; **Fig. 5.** Thyroid glands showing mild degree of congestion (L-leftlobe, R-rightlobe); **Fig.6.** Thyroid gland showing intra-follicular haemorrhage (arrow). H&E x200.

hyperplasia was recorded in 33/290 lobes (11.37%) of abattoir cases and 5/10 lobes (50%) of necropsy cases. Diffuse hyperplasia of intra-follicular epithelium was recorded in 4/290 lobes (1.37%) of the abattoir cases. Occasionally, an irregular papillary projection of hyperplastic epithelium was noticed extending into the lumen of cystic follicles. Both hyperplasia and hypertrophy of follicular epithelium were observed in 14/290 lobes (4.83%) of the abattoir cases. C-cell hyperplasia recorded in the present study was characterized by the presence of ovoid to round cells and had a distinct pale or light cytoplasm in the interstitium. The hyperplastic response of C-cells was either focal or diffuse and the proliferation response varied from mild to moderate degree. C-cell hyperplasia was recorded in 75/290 lobes (25.86%) of the abattoir cases and 1/10 lobes (10%) of the necropsy cases. The distribution of lesion was even in both the lobes. Colloid goitre was recorded in 11/290 lobes (3.79%) of the abattoir cases and 1/10 lobes (10%) of the necropsy cases. Colloid goitre occurred in 7 of the left lobes and 3 of the right lobes. Microscopically, the parenchyma comprised of large sized follicles, distended with pale pink-stained colloid, lined by low cuboidal to completely flattened single layer of epithelial cells (Fig. 10). Bilateral involvement was observed in only one case.

Neoplastic conditions of the thyroid gland were recorded in 9/290 lobes (3.10%) and all were from the abattoir cases. These were categorized as signet ring variant of follicular cell adenoma (6 cases), C-cell adenoma (2 cases) and capillary hemangioma (1 case). Miscellaneous conditions recorded were: (i) melanin pigmentation of the thyroid glands in 12/290 lobes (4.13%) of the abattoir cases. Melanin pigmentation was recorded in 5 left lobes, 3 right lobes and bilateral in two cases. Grossly, the affected thyroid lobes were dark brown in colour, had a firmer consistency (Fig.11). Microscopically, melanin deposition was noticed predominantly in the interstitium (Fig.12) and occasionally in the follicular epithelium. The distribution of the pigment varied from focal to diffuse. (ii) Macrofollicles, characterized by large the follicles appeared smaller and collapsed and invariably devoid of colloid. There was an increase in the inter-follicular connective tissue separated and compressed the follicles (Fig.7). Hypertrophy of follicular epithelium (Fig.8), characterized by the transformation of cuboidal epithelial cells into tall columnar cells with concomitant reduction in colloid, was recorded in 43/290 lobes (14.82%) of the abattoir cases and in 1/10 lobes (10%) of the necropsied cases. The hypertrophied follicular epithelial cells were significantly larger compared to normal cases. Follicular epithelial hyperplasia (Fig.9) was recorded in 68/290 lobes (23.44%) of abattoir cases and 5/10 lobes (50%) of necropsied cases. Hyperplasia of follicular epithelium occurred either as focal, diffuse or sometimes cystic. Focal intra-follicular epithelial hyperplasia was recorded in 31/290 lobes (10.68%) of the abattoir cases. Minimal follicular epithelial

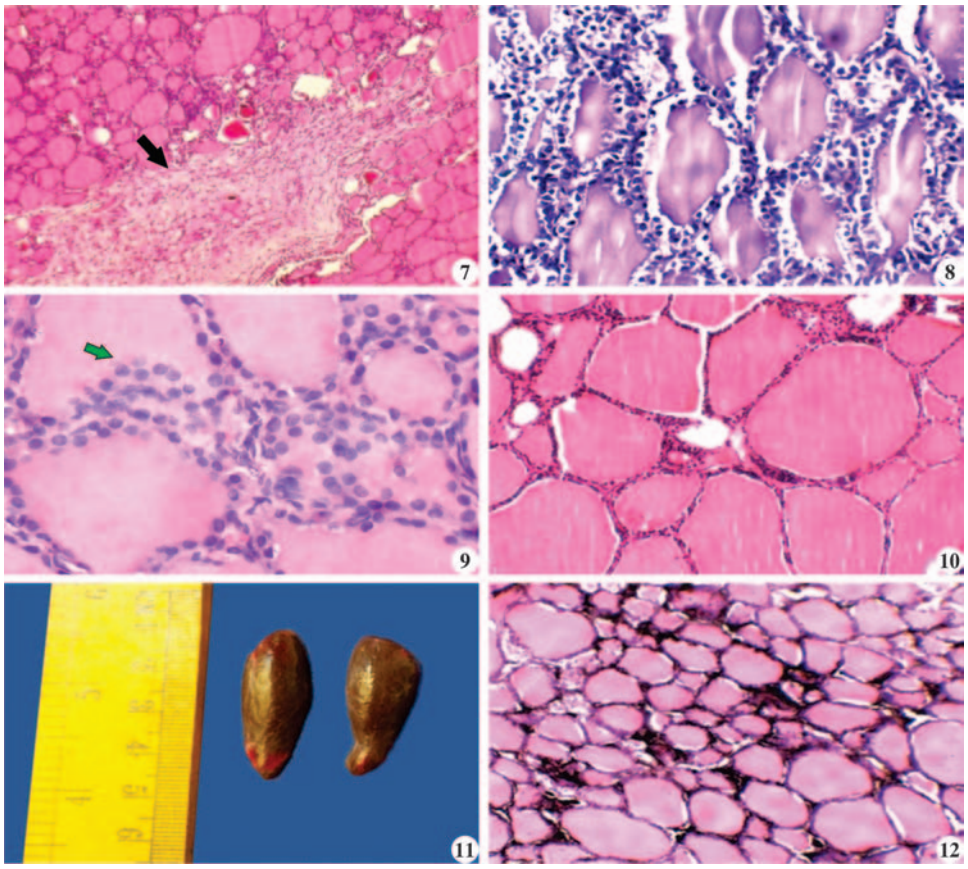

Fig.7. Thyroid gland showing focal follicular atrophy, follicular degeneration and fibrous tissue proliferation (arrow) in the interstitium. H&E x100; **Fig.8.** Thyroid gland showing moderate degree of hypertrophy of follicular epithelium. H&E x200; **Fig.9.** Thyroid gland showing focal hyperplasia of follicular epithelium (arrow). H&E x400; **Fig.10.** Thyroid gland showing moderately distended follicles lined by single layer of flattened epithelium. H&E x200; **Fig. 11.** Melanin pigmentation of the thyroid gland; **Fig.12.** Thyroid gland showing extensive deposition of melanin pigment in the interstitium. H&E x200.

follicles that were severely distended with completely flattened single layer of epithelial cells with abundant colloid were recorded in 53/290 lobes (18.27%) of the abattoir cases and 3/10 lobes (30%) of the necropsy cases. They were recorded in left lobes (29), right lobes (11) and bilaterally (8). Macrofollicles either occurred singly or in combination in focal areas within the thyroid parenchyma. (iii) Microfollicles, characterized by very small follicles lined by cuboidal epithelium with prominent nuclei and contained little or no colloid were recorded in 16/290 lobes (5.51%) of the abattoir cases, 6 in the left lobe, 4 in the right lobe and 3 bilaterally. (iv) Fibro-collagen tissue deposition was recorded in focal areas within the thyroid parenchyma in 49/290 lobes (16.89%) of the abattoir cases and in 3/10 lobes (30%) of the necropsy cases. Focal areas of fibrosis were recorded in 24 left lobes, 20 right lobes and 4 bilaterally.

DISCUSSION

Thyroid glands with normal histoarchitecture could be recorded only in 3.79% of the cases. Interestingly, only one case had normal histoarchitecture of both the lobes and in the rest of the cases normal histological features were observed either in the right lobe or in the left lobe. In an abattoir-based study on the thyroid gland of sheep at Puducherry[10], normal histoarchitecture was recorded in 19/170 (11.17%) of the cases. In some of the cases recorded in the present study, the thyroid gland appeared to be active. These were characterized by either vacuolations at the periphery of the colloid in follicles (scalloping) or hypertrophy of the follicular epithelial cells. It has been reported that a row of small vacuoles that occur at the interface between follicular epithelium and the colloid is a feature of actively functioning glands and nomenclatured as resorption vacuoles. Functional polarity is apparent at the level of the follicle and the follicular cell. A single follicle may have flattened cells on one side and cuboidal or low columnar cells on the other, the best expression of the functional activity of the thyroid gland[11]. Histopathological changes recorded in the thyroid glands in the present study were categorized as congenital anomaly, degenerative changes, vascular disturbances, growth disturbances, pigmentation, neoplasms and miscellaneous conditions.

Ultimobranchial cysts, the only congenital anomaly recorded, were located predominantly at the hilar region either as single or multiple cysts in the parenchyma. A detailed report on ultimobranchial cysts of the thyroid gland of goats has been published[12]. Degenerative changes in the thyroid lobes varied in severity from mild to severe which was in accordance an earlier study[13]. Vacuolar degeneration of the follicular epithelium of thyroid in sheep has been reported following experimental locoweed poisoning in sheep and Methylthiouracil (MTU) poisoning in cattle respectively[14,15]. Spontaneous occurrence of vacuolar degeneration in the thyroid gland of slaughtered animals has been reported as: 18.6% in sheep and 0.4% in buffaloes, respectively[4,10]. Vacuolar

degeneration of the thyroid follicular epithelium has been reported in *Ipomea carnea* toxicity in goats[16].It has been postulated that Swainsonine, an indolizidine alkaloid in *Ipomea carnea*, promoted the cellular accumulation of non-metabolized oligosaccharides that lead to the inhibition of acid or lysosomal alpha mannosidase enzyme and resultant cellular vacuolation. Follicular degeneration has been attributed as a manifestation of aging process in cynomolgus monkeys[17] and sheep[10]. Although degenerative changes were reported in apparently normal abattoir cases, experimental studies indicated that factors such as malnourishment, hypothyroidism and exposure to chemicals such as O-chlorobenzylidene malononitrile could induce degenerative changes in the thyroid gland[18,19]. Spontaneous occurrence of cystic changes in the follicles has also been reported in sheep, buffaloes and rats[4, 10, 19].

Vascular changes (congestion and haemorrhages) observed in the present study have been reported on abattoir studies in sheep[10,20]and experimentally induced hypothyroidism cases in goats[21].Vascular disturbances recorded in abattoir cases could be attributed as agonal changes and those in necropsy cases, associated with generalized systemic involvement.

Growth disturbances recorded in the present study were focal atrophy, hypertrophy and hyperplasia. Atrophic changes of the thyroid gland have been reported in ruminants[4, 10, 20, 22] varied from 2.5% in cattle to 43.26% in sheep. Hypertrophic changes of the thyroid follicular epithelium following thiourea induced hypothyroidism in sheep have been reported[23].

Hyperplasia of follicular lining epithelial cells have been reported in experimentally induced hypothyroidism in goats (13, 21), sheep[24] and cattle[15].Follicular epithelial hyperplasia was recorded after the experimental dosing with sulfonamides in rats, mouse and dog[25]. C-cell hyperplasia in the present study (25.86%) in abattoir cases and 10% in necropsied cases was comparatively higher than that reported in cattle[26] and sheep[10]. Hyperplasia and hypertrophy of the follicular cells with concomitant reduction in thyroid hormones in blood due to the interference of iodination of tyrosine by thiourea was reported in experimental hypothyroidism in sheep[23]. Inadequate iodine in the thyroid gland results in the synthesis of uniodinated inactive pre hormone instead of thyroxine, which stimulates the pituitary gland to secrete thyroid stimulating hormone (TSH). This commonly results in hyperplasia of the thyroid tissue and considerable enlargement of the gland leads to goitre[27]. Colloid goitre cases recorded in the present study were in accordance with earlier reports in goats (2.4% to 10%) [28,29]and in sheep (5.88%) (10). Colloid goitre is the most frequent type of goitre reported in goat and sheep and has been proven to be either due to deficiency of iodine or the consumption of goitrogens[7,30].

Melanin pigmentation of the thyroid lobes was recorded in 4.13% of the abattoir cases. Accumulation of melanin-like pigments in the cytoplasm of follicular cells as a phenomenon of aging has been reported in man. This phenomenon becomes massive after the administration of drugs such as minocycline and when intense, it is appreciable grossly and referred to as melanosis thyroid or less pompously as black thyroid[31]. Details of the neoplasms of the thyroid gland recorded in the present study have already been published[32].

The recording of macrofollicles and microfollicles were indicative of relatively inactive and as active follicles respectively in accordance with aging studies reported in man and animals[33].

Fibrosis of the thyroid gland of varying proportions (0.66% to 10%) has been reported in abattoir-based studies of cattle, goat, buffaloes, and sheep, respectively[4,29,34, 35]. In the present study, a relatively higher percentage (16.89%) of focal fibrosis of the thyroid gland was recorded. A recent report on the combined utility of ultrasonography with morphometric features ofthe thyroid and parathyroid gland of goats[2]would aid in detecting and monitoring focal lesions of the thyroid gland for clinical interventions.

CONCLUSION

Abattoir and necropsy-based study highlighted the importance of gross and microscopic examination of thyroid glands. Occult lesions that had no macroscopic alterations could be detected and characterized by microscopic studies. A large-scale study including the functional aspect of the thyroid glands would definitely help in elucidating the pathogenesis of thyroid abnormalities in goats.

ACKNOWLEDGEMENT

The authors are thankful to The Dean, Rajiv Gandhi Institute of Veterinary and Education and Research (RIVER), Puducherry for providing facilities to carry out this study.

Financial support & sponsorship: None.

Conflicts of interest: None.

Use of artificial intelligence (AI)-Assisted Technology for manuscript preparation: The authors confirm that there was no use of AI-assisted technology for assisting in the writing of the manuscript and no images were manipulated using AI.

REFERENCES

1. Ali SA, El-Sayed SA, Goda NIA and Beheiry RR.2020. Morphological characteristics of the goat thyroid glands among summer and winter seasons. *Adv Anim Vet Sci***8(3):** 252-259.
2. Pankowski F, Paśko S, Bonecka J, Szaluś-Jordanow O, Mickiewicz M, Moroz A and Bartyzel BJ. 2020. Ultrasonographic and anatomical examination of normal thyroid and internal parathyroid glands in goats. *PLoS ONE***15(5):** e0233685. https://doi.org/10.1371/journal.pone.0233685.
3. Sarma K, Sarma M and Devi J. 2017. Age Related Post Natal Histological Studies on the Thyroid Gland in Male Assam Goat (*Capra hircus*). *Indian Vet J***94:** 14-17.
4. Salunke SB, Kulkarani GB andGangane GR. 2008. Pathology of thyroid gland in buffaloes. *Asian J Anim Sci***3:** 215-218.
5. Jubb KVF, Kennedy PC and Palmer N. 2005. Pathology of Domestic Animals**,** 4thed., Academic Press, California, USA.
6. Davoodi F, Zakian A, Rocky A and Raisi A. 2022. Incidence of iodine deficiency and congenital goitre in goats and kids of Darreh Garm region, Khorramabad, *Iran Vet Med Sci* **8:** 336–342.
7. Radostits OM, Gay CC, Blood DC and Hinchcliff KF. 2000. Veterinary Medicine, 9th*ed*., W.B. Saunders Co, Philadelphia, pp. 1503-1505.
8. Poobitha S, Nair MG, Kumar R, Varshney KC, Uma Maheswari, D, Uma S and Lakkawar AW.2020. Gross and Histomorphology of the Thyroid gland in Goats. *J EntomolZool Stud* **8:**2283-2287.
9. Luna LG. 1968. Manual of Histological Staining Methods of the Armed Forces Institute of Pathology, McGraw-Hill, New York, USA.
10. Sridhar BG. 2011. Patho-morphological studies on thyroid gland in sheep. M. V. Sc. Dissertation submitted to Pondicherry University, Puducherry.
11. Carcangiu ML. 2002. Thyroid gland, In: Histology for Pathologists, Lippincott Williams, Philadelphia, pp. 1130-1149.
12. Poobitha S, Nair MG, Kumar R, Sivakumar M, Varshney KC, Uma Maheswari D and Lakkawar, A.W.2020. Ultimobranchial Cysts in the Thyroid of Goats. *J EntomolZool Stud* **8:** 1794-1797.
13. Kadum NB and Luaibi OK. 2017. Clinical study hypothyroidism in goats and treatment by iodine compounds. *J EntomolZool Stud* **5:** 1956-1961.
14. Van Kampen KR and James LF. 1969. Pathology of locoweed poisoning in sheep. *VetPathol* **6:** 413-423.
15. Serakides R, Nunes VA, Santos RL, Cassali GD and Costa PP. 1999. Histomorphometry and quantification of nucleolar organizer regions in bovine thyroid containing methylthiouracil residues. *Vet Pathol* **36:** 574-582.
16. Schumaher-Henrique B, Gorniak SL, Dagli, MLZ and Spinosa HS.2003. The clinical, biochemical, haematological and pathological effects of long-term administration of *Ipomea carnea* to growing goats. *Vet Res Commun* **27:** 311-319.
17. Ishida K, Narita K, Ito K, Izumisawa N, Nii A, Okamiya H and Hanada T. 2000. Morphologic variations in the thyroid glands of Cynomolgus monkeys. *JToxicolPathol* **13:** 189-191.
18. Chowdhury AR, Deshmukh MB, Raghuveeran CD, NashikkarAB and Chatterjee AK. 1978. Histological changes in thyroid of rat under the acute exposure of O-chloro- benzylidine malononitrile. *Experientia* **34:**1327.
19. Takaoka M, Teranishi M, Furukawa T, Manabe S and Goto N. 1995. Age-related changes in thyroid lesions and function in F344/DuCrj rats. *Experimental Animals* **44:**57-62.
20. Nouri M, Mohammadian B and Pourjamshid R. 2010. An abattoir study of thyroid histopathology in ewes and their fetus in Ahvaz city of Iran. *Vet Res Forum* **1:** 50-53.
21. Sreekumaran T and Rajan A. 1978. Clinicopathological studies in experimental hypothyroidism in goats. *VetPathol* **15:** 549-555.
22. Saber APR, Jalali MT, Mohjeri D, Akhoole AA, Teymourluei HZN, Nouri M and Garachorlo S. 2009. The effect of ambient temperature on thyroid hormones concentration and histopathological changes of thyroid gland in cattle in Tabriz, Iran. *Asian J Anim Vet Adv* **4:**28-33.
23. Mostaghni K, Badiei K, Tafti AK and Maafi AB. 2008. Pathological and biochemical studies of experimental hypothyroidism in sheep. *Vet Arh* **78:**209-216.
24. Sokkar SM, Soror AH, Ahmed YF, Ezzo OH and Hamouda MA. 2000. Pathology and biochemical studies on experimental hypothyroidism in growing lambs. *J Vet Med* **47:** 639-652.
25. Haschek WM and Rousseaux CG. 1998. Fundamentals of Toxicologic pathology, Academic Press, California, USA.
26. Puttanaiah GB and Seshadri SJ. 1981. Pathology of the thyroid gland in cows. *Indian J VetPathol* **5:** 1-5.
27. Bhardwaj RK. 2018. Iodine deficiency in Goats. *Goat Science* http://dx.doi.org/10.5772/intechopen.72728.
28. Dutt B and Kehar ND. 1959. Incidence of goitre in goats and sheep in India. *British Vet J* **115:**176-178.
29. Ramakrishna C and Prasad MC. 1992. Pathomorphological study of experimental hypothyroidism in goats. *Indian Vet J* ***69****:111*-114.
30. Nourani H and Sadr S. 2023. Case report of congenital goitre in a goat kid: Clinical and pathological findings. *Vet Med Sci* **9:** 2796–2799.
31. Rosai J. 2004. The Thyroid gland. In Rosai & Ackerman's Surgical pathology, 9thed., Elsevier, New York.
32. Poobitha S, Nair MG, Kumar R, Sivakumar M, Varshney KC, Uma Maheswari D and Lakkawar AW. 2021. Neoplasms of the thyroid gland in goats (*Capra hircus*) - A abattoir based study. *Indian J VetPathol* **45:** 209-211.
33. Faggiano A, Coulot J, Belbon N, Talbot M and Caillou B. 2004. Age-dependent variation of follicular size and expression of iodine transporters in human thyroid tissue. *J NuclMed* **45:**232-237.
34. LambhateYS. 2000. Studies on thyroid gland of slaughtered sheep and goats with special reference to T3 and T4 values. M.V.Sc dissertation, Post Graduate Institute of Veterinary and Animal Sciences, Akola, MAFSU.
35. Shelke VM, Pathak VP, Bedre DK, Patil DM and Mote CS. 2009. Study of histopathological changes in thyroid gland in buffaloes. *Vet World* 387-389.

Indian J. Vet. Pathol., 50(2) : 112-116, 2026: DOI: https://doi.org/10.56093/4xxvgd67

RESEARCH ARTICLE

Clinicopathological evaluation of Autoimmune skin diseases in dogs

Kothapalli Mounika[1], T. Devi[*], K. Nagarajan[2], B. Gowri[3] and S. Kavitha[4]

[1]PG Scholar, Department of Veterinary Clinical Medicine, Madras Veterinary College, TANUVAS, Chennai- 600007

[2]Professor, Department of Veterinary Pathology, Madras Veterinary College, TANUVAS, Chennai- 600007

[3]Professor and Head, Department of Veterinary Medicine, VC&RI, Udumalpet, TANUVAS

[4]Professor and Head, Department of Veterinary Clinical Medicine, Madras Veterinary College, TANUVAS, Chennai- 600007

***Address for Correspondence**

Dr. T. Devi, Assistant Professor, Dept. of Veterinary Public Health and Epidemiology, Madras veterinary College, Chennai -7; E-mail: drdevi.t@gmail.com

Received: 24.11.25; Accepted: 24.12.25

ABSTRACT

Autoimmune skin diseases in dogs are uncommon but clinically important disorders arising from immune-mediated injury to epidermal, vascular or melanocytic structures. The present study was undertaken to document the clinicopathological features of autoimmune skin diseases in dogs and to establish diagnostic patterns essential for accurate identification. A total of 2,811 dogs presented to the Madras Veterinary College Teaching Hospital, Chennai, were screened for a period of one year (2024-2025). Detailed diagnostic evaluation including clinical examination, dermatoscopy, cytology, haematology, serum biochemistry and histopathology was carried out in suspected cases. Twelve dogs (0.43%) were diagnosed with autoimmune skin diseases, comprising pemphigus foliaceus, pemphigus vulgaris, ear-tip vasculitis and vitiligo. Pemphigus foliaceus presented with crusts, scales and superficial erosions and subcorneal pustules in histopathology, whereas pemphigus vulgaris exhibited severe mucosal ulceration and acantholytic cells on cytology. Ear-tip vasculitis showed ischemic necrosis with fibrinoid vascular changes, while vitiligo was characterized by distinct depigmentation with loss of melanocytes. Dermatoscopic, cytological and histopathological findings supported clinical diagnosis. Haematological and biochemical alterations were mild and not clinically significant. The study highlights that comprehensive clinicopathological evaluation is essential for the early and reliable diagnosis of autoimmune dermatological disorders in dogs.

Keywords: Autoimmune diseases, clinicopathology, dog, pemphigus, vasculitis, vitiligo

INTRODUCTION

Autoimmune skin diseases in dogs occur when immunological tolerance is lost, resulting in immune-mediated destruction of epidermal adhesion complexes, dermal vasculature or melanocytes. Although their overall prevalence in canine dermatology is low, these disorders often present with chronic, progressive skin lesions that mimic allergic, infectious or endocrine conditions. This diagnostic overlap contributes to delays in appropriate therapy. Pemphigus foliaceus (PF) and pemphigus vulgaris (PV) represent the major autoimmune blistering diseases in dogs, while immune-mediated vasculitis and vitiligo constitute important vascular and pigmentary autoimmune conditions. Early diagnosis requires a combination of clinical evaluation, dermatoscopy, cytology and histopathology. Detailed documentation of clinicopathological characteristics is particularly important in Indian veterinary settings, where published reports remain limited. The present study was conducted to establish the clinical and pathological features of autoimmune skin diseases observed in dogs presented to a tertiary referral center.

How to cite this article : Mounika, K., Devi, T., Nagarajan, K., Gowri, B and Kavitha, S. 2026. Clinicopathological evaluation of Autoimmune skin diseases in dogs. Indian J. Vet. Pathol., 50(2) : 112-116.

MATERIALS AND METHODS

The study involved dogs presented to the Small Animal Dermatology Outpatient Unit of the Madras Veterinary College Teaching Hospital (Chennai, India) for a period of one year (2024-2025). All the enrolled dogs underwent a routine and thorough dermatological examination, including detailed anamnesis, assessment of lesion distribution, and characterization of primary and secondary skin lesions. Dogs exhibiting chronic, recurrent, or therapy-resistant lesions clinically suggestive of an underlying autoimmune etiology were selected for further diagnostic evaluation. Prior to definitive diagnosis, common infectious and parasitic causes of skin disease were rigorously excluded using standard diagnostic methods[2,3].

Skin scrapings (deep and superficial) were collected and examined microscopically in potassium hydroxide (KOH) solution (10%) or mineral oil to exclude ectoparasites such as Demodex spp. and Sarcoptes spp[5] . Culture (aerobic bacterial

culture and fungal culture, e.g., Dermatophyte Test Medium - DTM) was performed on samples from affected areas to rule out bacterial pyoderma and dermatophytosis[8]. The presence of Malassezia pachydermatis was assessed using tape cytology[5,6].

Dermatoscopic examination was performed on all selected lesions using a handheld digital dermatoscope (DermLite DL4) to document surface changes, including vascular patterns, scale, crusts, and follicular openings. This served visually to guide biopsy selection and document gross morphology[1]. Cytological samples were collected from lesions (e.g., vesicles, bullae, erosions, or pustules) for rapid assessment of the cellular profile. Direct Impression Smears were used for ulcerated or moist lesions. Tape Preparations (Acetate Tape Strips) applied directly to skin surfaces to lift debris and cells, primarily for evaluation of superficial inflammation and the presence of Malassezia or acantholytic cells[2,3,6,].

All cytological smears were stained using a Romanowsky-type stain (Diff-Quik) and examined under light microscopy to identify cellular patterns, inflammatory cell types (neutrophils, eosinophils, macrophages), and the presence of infectious agents or acantholytic cells (diagnostic for Pemphigus complex)[13,11]. Routine haematological and biochemical analyses were performed on venous blood samples collected from all dogs. Analyses were carried out using standard automated methods (e.g., automated cell counter for Complete Blood Count - CBC; automated chemistry analyzer for serum biochemistry profile)[14]. To assess systemic health, detect concurrent diseases, and identify hematological changes often associated with chronic inflammation or specific autoimmune diseases (e.g., non-regenerative anemia, leukocytosis, or alterations in globulin levels).

Skin biopsies were collected as the definitive diagnostic procedure. Representative biopsies (minimum of 3 samples per dog) were collected from active, untreated lesions (e.g., an intact blister, crust, or margin of an ulcer) under aseptic conditions using a 4-6 mm punch biopsy tool following local anesthesia (e.g., 2% Lidocaine)[6,7]. Specimens were immediately placed into 10% neutral buffered formalin (NBF) at a ratio of approximately 10:1 (formalin:tissue volume) for a minimum of 24 hours. The fixed tissues were then routinely processed (dehydrated in graded alcohol, cleared in xylene, and embedded in paraffin wax). Sections of 4-5µ thickness were cut using a rotary microtome, mounted on glass slides, and stained with Hematoxylin and Eosin (H & E) stain[7].

The final diagnosis of autoimmune skin disease (e.g., Pemphigus Foliaceus, Systemic Lupus Erythematosus etc.) was established by correlating three essential elements *viz*., Specific distribution and morphology of lesions (e.g., bilateral symmetry, mucocutaneous involvement). Demonstration of relevant cells, such as acantholytic cells for Pemphigus, and identification of characteristic histopathological changes such as acantholysis (for Pemphigus) or interface dermatitis, ensuring that all infectious and parasitic etiologies had been excluded[1,2,3].

RESULTS

A total of 2,811 dogs were screened during the study period of one year which twelve dogs (0.43%) were confirmed to have autoimmune skin diseases. Pemphigus vulgaris accounted for 41.66% (5/12) of cases, followed by pemphigus foliaceus accounting 33.33% (4/12), ear-tip vasculitis accounting 16.66% (2/12) and vitiligo accounting 8.33% (1/12). Dogs aged four to six years were most commonly affected, and males and females were equally represented. Clinically, pemphigus foliaceus presented with crusting, scaling and superficial erosions involving the face, ears and distal extremities (Fig 1). Dogs affected with pemphigus vulgaris exhibited deep mucocutaneous involvement with painful oral ulcers and gingival bleeding, with a positive Nikolsky sign indicating loss of intercellular adhesion within the epidermis. Ear-tip vasculitis was characterized by sharply demarcated ischemic necrosis and ulcerated margins of the ear tip (Table 1 and 2) (Fig 1). Across the 12 cases, autoimmune skin diseases in dogs predominantly exhibited mild to moderate severity with isolated instances of severe and extensive involvement. PF and PV were the most frequently encountered diseases.

Table 1. Clinical signs in Autoimmune skin diseases

Autoimmune Skin Diseases	Clinical Signs (with Percentage)
Pemphigus Foliaceus	Pustules (25%), Erosions (50%), Crusts and Scales (75%)
Pemphigus Vulgaris	Oral Ulcers (80.0%), Erythematous scabs (20%), Gums Bleeding (60%)
Ear tip Vasculitis	Necrosed Ear Tip (50%), Debrided Wound (50%)
Vitiligo	Depigmentation (100.0%)

Table 2. Severity score index

Disease	No. of Cases	Score Range (Min–Max)	Severity Grade
Pemphigus foliaceus (PDAI)	4	5 – 26	Mild to Moderate–Severe
Pemphigus vulgaris (ODSS-PDAI)	5	15 – >48.5	Mild to Moderate–Severe
Ear tip vasculitis (Vasculitis severity score)	2	5/20-14/20	Mild to Severe
Vitiligo (VASI)	1	6.75	Moderate

Fig.1. Clinical signs of Autoimmune skin diseases in dogs. (a) Skin and paw pad area - Erythema, ulceration, and deep ecchymoses into the subcutaneous tissue and paw margins; **(b)** Erosive and Ulcerative Nasal/Periocular Dermatitis - Markedly erythematous, swollen, eroded and ulcerated nasal planum; **(c)** Face - Erythema, crusting, erosion and ulceration on the Nasal planum, periocular and muzzle regions, and distal limb paw in Pemphigus foliaceus; **(d)** Severe necrotic, erosive and hemorrhagic crust on pinna – necrotic ear tip and debraded wound in ear tip - vasculitis; **(e)** Oral Cavity-Erythematous scab (arrow) and depigmentation over the lip lining and buccal mucosa - Pemphigus vulgaris; **(f)** Periorbital dermatitis - marked depigmentation, erythema and ulcerative cheilitis; **(g)** Crusting and Erosions around periocular area in a pemphigus foliaceus dog; **(h)** Paw - black and hyperkeratotic, with noticeable fine white scales/crusts, Pododermatitis - Pustules (arrow) on paw; **(i)** Severe gingivitis/mucositis - intensely erythematous and swollen mucosal surface with highly inflamed and small, bleeding spots or erosions.

Dermatoscopy revealed disease-specific patterns including erythematous backgrounds, ruptured pustules, white and yellow crusts, hemorrhagic dots, pigment loss and necrotic cores. Cytology demonstrated numerous acantholytic keratinocytes and non-degenerated neutrophils in pemphigus complex (Fig.3), degenerated neutrophils with erythrocyte extravasation in vasculitis, and melanin-laden keratinocytes without inflammation in vitiligo. Histopathology confirmed classical lesions: sub corneal pustules and acantholysis in PF, fibrinoid necrosis with perivascular inflammation in vasculitis, and melanocyte loss with pigmentary incontinence in vitiligo. Moderate neutrophilia and lymphocytosis. These alterations were within physiological limits and are consistent with inflammatory changes commonly reported in autoimmune skin diseases (Fig.2). Serum biochemistry remained largely stable, with occasional mild increases in total protein and ALT, suggesting limited systemic involvement.

The diagnosis of pemphigus foliaceus was established through the combined evaluation of cytology and confirmatory histopathology. Pemphigus vulgaris was primarily diagnosed based on the characteristic lesion distribution, further supported

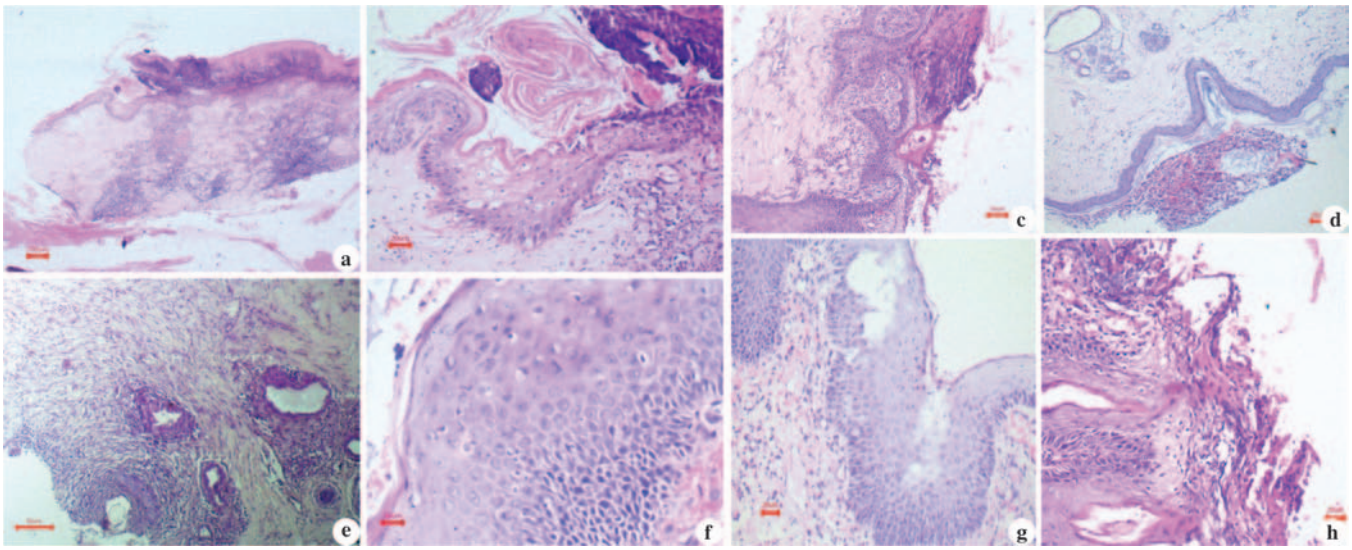

Figure 2. Histopathology of Autoimmune skin diseases. (a) Skin- Histopathology (HP)-Pemphigus foliaceus -Hyperkeratosis (Arrow) of stratum corneum and Granuloma formation in dermis H&E, 40x; **(b)** Skin – HP - Pemphigus foliaceus Pemphigus foliaceus –Lhasaapso-Hemorrhages(Arrow); Edema and ballooning degeneration of the dermis H&E, 200x; **(c)** Skin- HP- Pemphigus foliaceus- –Rajapalayam - Erosion and MNC infiltration H&E, 100x; **(d)** Skin- HP- Eartip Vasculitis - Ear tip vasculitis- ND-Granuloma formation with multinucleated gaint cells H&E,200x; **(e)** Skin- HP-Vitiligo-Lab- Vitiligo-Lab-Fibroblast proliferation and fibrosis H&E,100x; **(f)** Skin- HP-Pemphigus foliaceus – Beagle-Vacuolar degeneration(Arrow) of stratum spinosum and cell edema H&E,400x; (**g**) Skin- HP-Pemphigus foliaceus - Beagle- Cell edema, plasma cells, Mononuclear infiltration (MNC) infiltration, acantholysis,sub corneal pustule H&E, 100x; (**h**) Skin – HP- Pemphigus foliaceus - Beagle – Desquamation- Erosion with MNC Infiltration, H&E, 100X

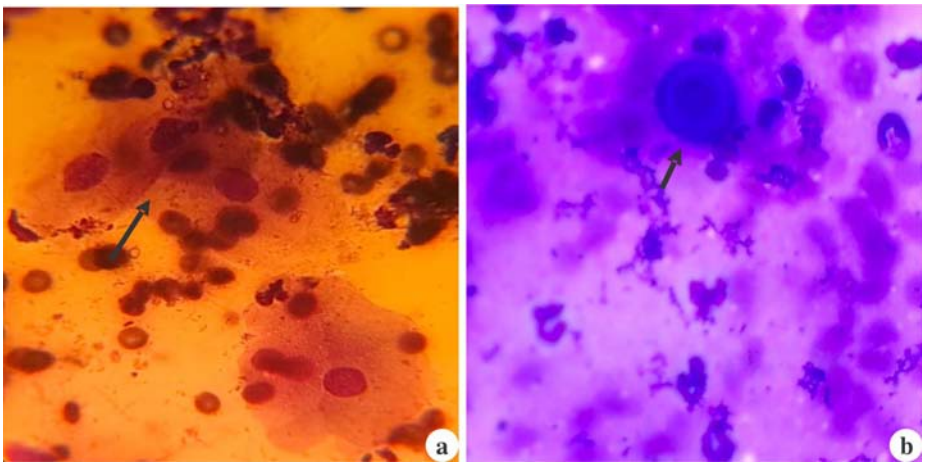

Fig. 3. Cytology showing Acantholytic cells. (a) Skin – Direct impression cytology - Acantholytic cells (Arrows) with non degenerative neutrophils Diff quik stain, 200x; **(b)** Skin – Direct impression cytology - Acantholytic cell (Arrow) along with neutrophils Diff quik stain, 1000x

blistering disorders, depigmentation or vasculitis[4,8,10,13]. In this study, the clinicopathological patterns closely resembled classical descriptions of canine autoimmune dermatoses, with chronic, relapsing lesions and poor response to empirical antibiotics supporting an immune-mediated aetiology[2,5,8,11]. Pemphigus foliaceus exhibited characteristic crusts, scales and erosions, with dermatoscopic yellow-white crusts and inflamed surfaces reflecting subcorneal pustules and acantholysis[10]. Pemphigus vulgaris presented with deep mucocutaneous ulceration, gingival bleeding and Nikolsky positivity, by cytological identification of non-degenerate neutrophils and acantholytic keratinocytes (Fig.3). Vitiligo and ear-tip vasculitis were diagnosed on the basis of their distinct clinical presentation and lesion localization, with histopathological findings providing definitive confirmation.

DISCUSSION

Autoimmune skin diseases in dogs arise from immune dysregulation in which autoantibodies target desmosomes, melanocytes or dermal vessels, leading to consistent with suprabasal clefting and severe epithelial disruption[10,13]. Ear-tip vasculitis showed ischemic necrosis and purpuric lesions, and dermatoscopy demonstrated hemorrhagic dots and vascular injury patterns typical of immune-complex vasculopathies[1,4]. Vitiligo cases revealed sharply marginated depigmented patches with dermatoscopic loss of pigment network and perifollicular changes indicative of melanocyte destruction[1]. Cytology further supported these diagnoses by demonstrating acantholytic keratinocytes in pemphigus and degenerated neutrophils with erythrocyte extravasation

in vasculitis[4,11]. Histopathology confirmed hallmark features including subcorneal pustules and acantholysis in PF, fibrinoid necrosis in vasculitis and melanocyte loss with pigmentary incontinence in vitiligo[12]. Overall, the integration of clinical lesions, dermatoscopy, cytology and histopathology provided a strong diagnostic framework consistent with established immunopathological mechanisms reported in veterinary dermatology[8,10,13]. Haematology showed mild inflammatory changes, notably neutrophilia and lymphocytosis, while serum biochemistry remained largely within normal limits except for increased total protein due to chronic inflammation[8,14]. Collectively, the clinical, dermatoscopic, cytological and histopathological features observed strongly align with classical immune-mediated mechanisms described in veterinary dermatology and confirm their diagnostic value in autoimmune skin diseases of dogs.

CONCLUSION

The present study confirms that autoimmune skin diseases in dogs although uncommon exhibit distinct clinicopathological characteristics that permit reliable diagnosis. Pemphigus foliaceus and pemphigus vulgaris were the predominant autoimmune dermatoses encountered, followed by immune-mediated vasculitis and vitiligo. Dermatoscopy, cytology and histopathology played key roles in differentiating among disease categories, while haematology and biochemistry provided supportive information. The findings highlights the importance of comprehensive clinicopathological evaluation for early diagnosis and successful clinical management of autoimmune dermatological disorders in dogs.

Financial support & sponsorship: None.

Conflicts of interest: None.

Use of artificial intelligence (AI)-Assisted Technology for manuscript preparation: The authors confirm that there was no use of AI-assisted technology for assisting in the writing of the manuscript and no images were manipulated using AI.

REFERENCES

1. Errichetti E and Stinco G. 2016. Dermoscopy in inflammatory skin disorders. *Dermatol Ther* **29:** 1–12.
2. Gross TL, Ihrke PJ, Walder EJ and Affolter VK. 2008. *Skin Diseases of the Dog and Cat: Clinical and Histopathologic Diagnosis.* John Wiley & Sons, Oxford.
3. Hnilica KA and Patterson AP. 2017. *Small Animal Dermatology: A Color Atlas and Therapeutic Guide.* 4th Edn. Elsevier, St. Louis.
4. Innera M. 2012. Cutaneous vasculitis in dogs: A Review. *Vet Dermatol* **23:** 5–14.
5. Jackson HA and Marsella R. 2021. *BSAVA Manual of Canine and Feline Dermatology.* 4th Edn. BSAVA, Gloucester.
6. Latimer KS. 2011. *Duncan and Prasse's Veterinary Laboratory Medicine: Clinical Pathology.* John Wiley & Sons, Ames.
7. Luna, LG. 1968. *Manual of Histologic Staining Methods of the Armed Forces Institute of Pathology.* 3rd Edn. McGraw-Hill, New York, pp-285.
8. Miller WH, Griffin, CE and Campbell KL. 2013. *Muller and Kirk's Small Animal Dermatology.* 7th Edn. Elsevier, St. Louis.
9. Moriello KA. 2004. Diagnostic techniques for dermatophytosis. *Clin Tech Small Anim Pract* **19:** 211–215.
10. Olivry T and Linder KE. 2009. Pemphigus and pemphigoid in dogs and cats. *Vet Clin North Am Small Anim Pract* **39:** 745–760.
11. Paterson S. 2009. *Manual of Skin Diseases of the Dog and Cat.* John Wiley & Sons, Chichester.
12. Tham HL, Linder KE and Olivry T, 2019. Autoimmune diseases affecting skin melanocytes in dogs, cats and horses: vitiligo and the uveodermatological syndrome: a comprehensive review. *BMC Vet Res* **15(1):** 251.
13. Tham HL, Linder KE and Olivry T. 2020. Deep pemphigus (pemphigus vulgaris, pemphigus vegetans and paraneoplastic pemphigus) in dogs, cats and horses: a comprehensive review. *BMC Vet Res* **16(1):** 457.
14. Thrall MA. 2012. *Veterinary Hematology and Clinical Chemistry.* 2nd Edn. Wiley-Blackwell, Ames.

Indian J. Vet. Pathol., 50(2) : 117-123, 2026: DOI: https://doi.org/10.56093/8btmjy77

RESEARCH ARTICLE

Hematopathological studies on Feline Panleukopenia with emphasis on bone marrow assessment

J. Thilahayswari[1], K. Nagarajan[*], S. Hemalatha and M. Chandrasekar[2]
Department of Veterinary Pathology, Madras Veterinary College, Tamil Nadu Veterinary and Animal Sciences University, Chennai, India
[1]PG Scholar; [2]Resident Veterinary Services Section, Madras Veterinary College, Tamil Nadu Veterinary and Animal Sciences University, Chennai, India

***Address for Correspondence**
K. Nagarajan, Professor, E-mail: nagavet@gmail.com

Received:21.11.25; Accepted: 12.1.26

ABSTRACT

Feline Panleukopenia Virus (FPV) is a highly contagious viral disease causing severe hematological abnormalities in cats. This study was aimed to evaluate the hematological, biochemical, and bone marrow changes in naturally infected cats and to characterize FPV at the molecular level. A total of 22 cats exhibiting clinical signs of anorexia, pallor of mucus membrane, recumbency, and emaciation were examined. Out of this 7 were subjected to detailed post-mortem evaluation. Hematological analysis revealed significant anemia, leukopenia, and thrombocytopenia in FPV-infected cats, accompanied by hypoglycemia and hypoproteinemia, while liver and kidney parameters remained largely unaffected. Blood smear and bone marrow cytology showed predominant erythroid hypoplasia, myeloid hypoplasia and megakaryocytic hyperplasia, indicating compensatory hematopoietic responses. Necropsy findings included generalized pallor of visceral organs, thickened intestines with mucosal petechiae, mild hepatomegaly, and pulmonary edema. Molecular detection of DNA of FPV from 19 bone marrow samples via PCR targeting the VP2 gene confirmed infection in 15 cats (78.95%). Phylogenetic analysis revealed that the Indian bone marrow isolate clustered closely with other Indian FPV strains, forming a distinct clade separated from strains reported in Europe, Africa, and East Asia, suggesting geographic evolution patterns. These findings highlight the critical role of bone marrow in FPV pathogenesis, the systemic impact of infection, and the regional genetic distinctness of circulating FPV strains in India, which has implications for disease surveillance and vaccine strategies.

Keywords: Bone marrow, cytology, Feline Panleukopenia Virus, hematology, PCR, phylogenetic analysis

INTRODUCTION

Panleukopenia is a hematologic abnormality characterized by a marked reduction in all circulating white blood cell types, most often detected through complete blood count (CBC) evaluation in veterinary practice [1]. Beyond being considered as a hematological abnormality, it is actually a clinical syndrome reflecting systemic viral infection affecting immune and haemopoietic organs [2].Though there are many causes of panleukopenia in cats, the most common and prime cause is Feline parvovirus and the infection is termed as Feline panleukopenia or feline distemper. It is a linear, single-stranded DNA molecule with unique hairpin structures at both ends that is around 5 kb long. It belongs to the Parvoviridae family and the genus Protoparvovirus[3].

Following the virus' initial replication in oropharyngeal lymphoid tissue, it spreads throughout the body through the blood to all tissues, causing viraemia which could be identified clinically after 2–10 days of incubation and diagnosed after 2–7 days post-infection [4]. Significant changes in occur especially to the bone marrow and lymphoid tissue causing severe destruction of whole leukocytes ,thereby substantiating the disease name [5]. Given the central role of bone marrow in hematopoiesis, its evaluation is critical in understanding the severity of FPV infection. This study aims to investigate the presence of parvovirus within the bone marrow and to perform molecular characterization, thereby addressing the existing gaps in knowledge regarding the circulating whole-genome sequences of FPV in India.

How to cite this article : Thilahayswari, J., Nagarajan, K., Hemalatha, S. and Chandrasekar, M. 2026. Hematopathological studies on Feline Panleukopenia with emphasis on bone marrow assessment. Indian J. Vet. Pathol., 50(2) : 117-123.

MATERIALS AND METHODS

A total of 22 cats clinically diagnosed with Feline panleukopenia (FPV) were included in this study. These animals were selected based on the presence of clinical signs indicative of panleukopenia, including anorexia, pale mucous membranes, recumbency, hypothermia, and emaciation. Cats of varying ages and both sexes were included to assess age- and sex-related susceptibility. Each cat underwent a detailed

clinical examination to record general health status and specific signs. Seven cats succumbed to death due to late clinical presentation and they were subjected to detailed necropsy examination.

Peripheral blood was collected aseptically from all the cats to perform complete blood counts and serum biochemical parameters using an automated hematology analyzer (BC-2800Vet, Mind ray Medical Instrumentation, China) and automated serum biochemistry analyzer (A15 Random Access Analyzer, Biosystems, Barcelona, Spain). A total of 22 Bone marrow aspirates and biopsy including 15 from live animals and 7 from dead cats were collected from the trocanteric fossa of proximal femur under sedation using standard aseptic techniques for cytological examination and viral detection. Control samples were collected from 6 apparently healthy domestic short haired cats of age ranging from 6 months to 2 years to serve as reference for hematological analyses.

Aspirate cytology smears were stained with Leishman-Giemsa stain as per the standard protocol. Tissue samples were routinely processed, with bone tissue decalcified before embedding. Sections 3–5 µm thick were stained with hematoxylin and eosin (H&E) for routine histopathology[6]. Additionally, special stain—Masson's trichrome were performed to check for myelofibrosis for differentiating collagen and semi-quantifying collagen deposition in the bone marrow.

Out of the 22 bone marrow samples, only 19 were subjected to PCR due to insufficient sample quantity in the remaining cases. DNA was extracted from bone marrow samples (approximately 25 mg of tissue) using the commercially standardized DNeasy Blood and Tissue Kit (QIAGEN, Germany). Samples were subjected to PCR targeting the VP2 gene of Feline parvovirus using the following primers: Forward primer (FPL-FP): 5'–GCT TTA GAT GAT ACT CAT GT–3'; Reverse primer (FPL-RP): 5'–GTA GCT TCA GTA ATA TAG TC–3'.Those samples yielding a positive 698 base pair (bp) band by PCR amplification were further subjected to genetic sequencing. The sequence data were compared with VP2 reference sequences from the NCBI database, and phylogenetic tree was generated using MEGA12 software to analyze the genetic relationships of the isolates of different geographical location.

RESULTS

Sex, age and breed wise incidence

Sex, age and breed wise incidence of feline panleukopenia were tabulated (Table 1) and interpreted diagrammatically (Fig. 1). Out of the 22 cats diagnosed with Feline panleukopenia, male cats were more commonly affected compared to females. Age-wise, the highest proportion of cases was observed in cats younger than 6 months among all age groups, indicating a higher susceptibility among younger animals. Regarding breed distribution, the majority of affected cats were Domestic Shorthaired was affected, suggesting that FPV infection predominantly occurs in the common domestic population rather than

Fig. 1. Bar chart depicting Sex, age and breed wise incidence of feline panleukopenia

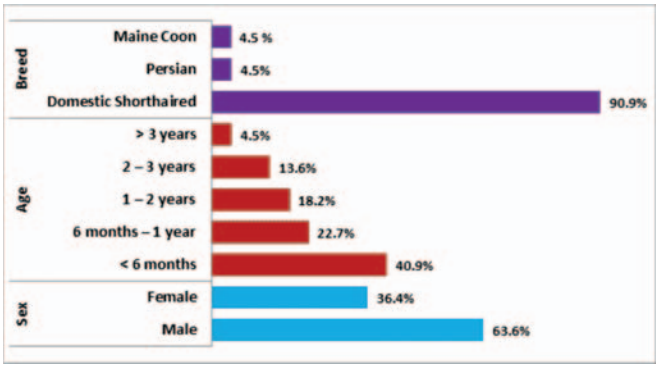

Table 1. Sex, age and breed wise incidence of feline panleukopenia

Parameter	Category	Number of Cats	Percentage (%)
Sex	Male	14	63.6
	Female	8	36.4
Age	< 6 Months	9	40.9
	6 Months – 1 Year	5	22.7
	1 – 2 Years	4	18.2
	2 – 3 Years	3	13.6
	> 3 Years	1	4.5
Breed	Domestic Shorthaired	20	90.9
	Persian	1	4.5
	Maine Coon	1	4.5

** Highly Significant ($p<0.01$); *Significant ($p<0.05$); NS – Not Significant

Table 2. Hematological Comparison between Healthy and FPV-Infected Cats

Parameter	Unit	Group 1 Apparently healthy (n=6)	Group 2 Feline panleukopenia (n=22)	t statistic
Hemoglobin	(g/dl)	11.3±0.41	8.7±0.44	2.97**
PCV	(%)	36.33±2.060	27.58±2.35	1.87^{NS}
RBC	(mil/µl)	7.18±0.34	5.06±0.41	2.29*
WBC	(/cmm)	13633.33±1373.48	6543.18±344.16	10.58**
Platelets	(/cmm)	401916.67±45134.69	242863.64±24939.35	2.98**
Neutrophils	(%)	56±4.03	61.77±2.51	-1.09^{NS}
Neutrophil count	(/cmm)	7715.33±1023.33	2245.63±246.98	7.84**
Lymphocytes	(%)	38±3.68	30.29±2.07	1.74^{NS}
Lymphocyte count	(/cmm)	5771±727.59	1031.38±117.02	9.72**
Monocytes	(%)	3.07±0.55	4.56±0.49	-1.52^{NS}
Monocyte count	(/cmm)	386.07±35.75	160.30±23.04	4.69**
Eosinophils	(%)	2.93±0.65	3.38±0.53	-0.415^{NS}
Eosinophils count	(/cmm)	360.93±54.76	104.88±16.10	6.19**

** Highly significant (p<0.01); *Significant (p<0.05); NS – Not Significant

Table 3. Serum Biochemistry findings comparison between Healthy and FPV-Infected Cats

Parameter	Unit	Group 1 Apparently healthy (n=6)	Group 2 Feline panleukopenia (n=22)	t statistic
Glucose	(mg/dl)	95±3.25	76.27±3.88	2.43*
Total protein	(g/dl)	6.75±0.29	5.15±0.28	2.84**
Albumin	(g/dl)	2.9±0.19	2.81±0.19	0.22^{NS}
BUN	(mg/dl)	23.27±2.05	20.23±1.11	1.27^{NS}
Creatinine	(mg/dl)	0.81±0.09	1.08±0.10	1.33^{NS}
ALT	(mg/dl)	53.33±2.51	46.14±2.95	1.22^{NS}
ALP	(mg/dl)	22.33±3.66	34±4.48	1.31^{NS}

** Highly significant (p<0.01); *Significant (p<0.05); NS – Not Significant

Table 4. Histological and Cytomorphological evaluation of bone marrow

Parameter	Observation	Number of Cats (n = 22)	Percentage (%)
	Normocellular	2	9.1
Marrow Cellularity	Hypocellular	20	90.9
	Hypercellular	-	-
	Normal	-	-
Erythroid Lineage	Hypoplasia	20	90.9
	Hyperplasia	2	9.1
	Normal	-	-
Myeloid Lineage	Hypoplasia	17	77.3
	Hyperplasia	5	22.7
	Normal	8	36.3
Megakaryocytic Lineage	Hyperplasia	10	45.5
	Hypoplasia	4	18.2

purebred cats. The most prominent clinical signs were anorexia, pale mucous membranes, recumbency, hypothermia, and emaciation. Additional findings included vomiting, dyspnea, and absence of pupillary light reflex (PLR). Less frequently, cats exhibited loss of nociception, nystagmus, seizures, and hyperthermia, reflecting the variable severity and systemic impact of Feline panleukopenia.

Haematology and serum biochemistry findings

Comparison between apparently healthy cats and Feline Panleukopenia-infected cats revealed significant alterations in several hematological and serum bichemistry parameters as listed in the table 2 and table 3 respectively. Hemoglobin levels were significantly reduced in FPV-infected cats (8.7±0.44 g/dl) compared to healthy controls (11.3±0.41 g/dl), indicating anemia. Similarly, RBC counts (5.06±0.41 mil/µl) and platelet counts (242863.64±24939.35 /cmm) were significantly lower in infected cats. White blood cell analysis showed a marked decrease in total WBC count (6543.18±344.16/cmm), neutrophil (2245.63±246.98/cmm) and lymphocyte counts (1031.38±117.02/cmm) while the percentages of neutrophils (61.77±2.51%) and lymphocytes (30.29±2.07%) did not differ significantly. Monocyte counts (160.30±23.04 /cmm) were significantly decreased in FPV-infected cats, whereas monocyte percentage (4.56±0.49%) remained unchanged. Eosinophil counts (104.88±16.10/cmm) were also significantly reduced, although eosinophil percentage (3.38±0.58%) did not differ. Overall, these findings demonstrate that Feline Panleukopenia induces severe leukopenia, anemia, and thrombocytopenia, reflecting profound bone marrow suppression and systemic hematological impact in infected cats.

Glucose levels were significantly lower in infected cats compared to healthy controls, indicating potential hypoglycemia. Similarly, total protein levels were significantly reduced in infected cats, suggesting protein loss or impaired synthesis. Other parameters, including albumin, BUN, creatinine, ALT and ALP did not show significant differences between the two groups, indicating that renal and hepatic functions were largely unaffected in this cohort.

Necropsy findings

Necropsy revealed generalized pallor of visceral organs, Mild hepatomegaly and pulmonary edema with predominant lesions in the gastrointestinal tract showing thickened intestines, mucosal petechiae (Fig. 2a) and mesenteric lymphadenopathy (Fig. 2b).

Blood smear and bone marrow examination:

Cats infected with Feline Panleukopenia Virus exhibited anaemia, hypochromasia and acanthocytosis of RBC, leukopenia and thrombocytopenia on peripheral blood smear, reflecting significant hematological compromise. Bone marrow histopathological examination revealed marked hypocellularity (Fig. 2c) with predominance of clear ring shaped adipocytes and reduced hematopoietic cells and no myelofibrosis. Both histopathological and cytological evaluation (Table 4) (Fig.3) showed erythroid hypoplasia (Fig. 2d) predominantly characterized by less number of erythroid cells with dense nucleus and basophilic cytoplasm, suggesting impaired red blood cell production. Myeloid hypoplasia characterized by comparatively less number of myeloid cells with less dense, unlobed/lobed nucleus and pale pink to grey cytoplasm was seen in most of the cases with dysplastic erythroid precursors (Fig. 4a), highlighting compromised granulopoiesis and a mechanism for the observed leukopenia in peripheral blood. A few cases

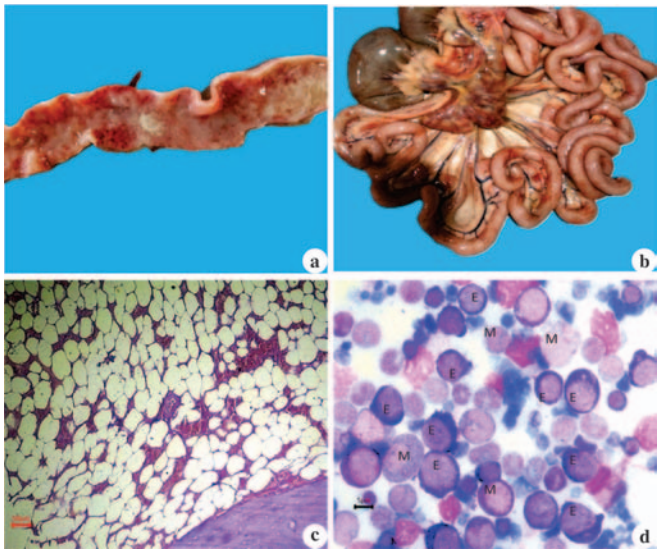

Fig. 2. (a) Intestine- Catarrhal enteritis characterized by excessive mucus coating the mucosa along with multifocal mucosal petechiae; **(b)** Mesentery- Haemorrhagic mesenteric lymphadenopathy characterized by enlarged, dark-red lymph nodes with serosal congestion; **(c)** Bone marrow histopathology- Hypocellular marrow with predominance of clear ring shaped adipocytes and reduced hematopoietic cells; H&E x100; **(d)** Bone marrow cytology- Erythroid cell(E) with basophilic cytoplasm; Myeloid cell(M) with pale pink to grey cytoplasm; Erythroid hypoplasia and myeloid hyperplasia (Leishman-Giemsa x1000).

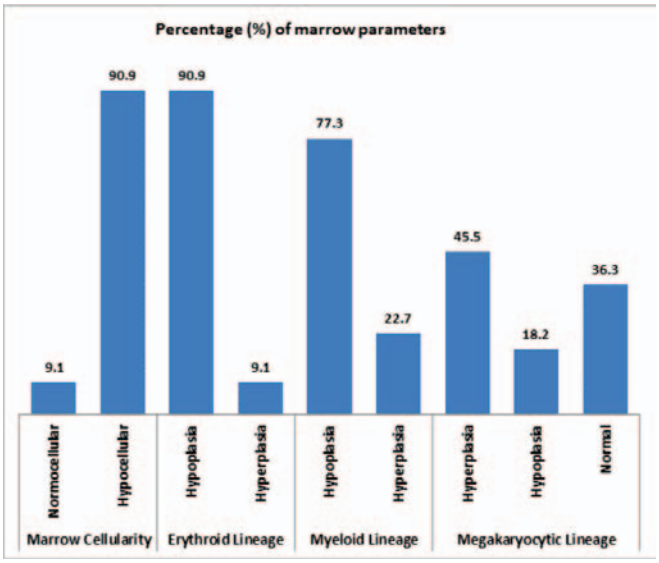

Fig. 3. Histological and Cytomorphological evaluation of bone marrow

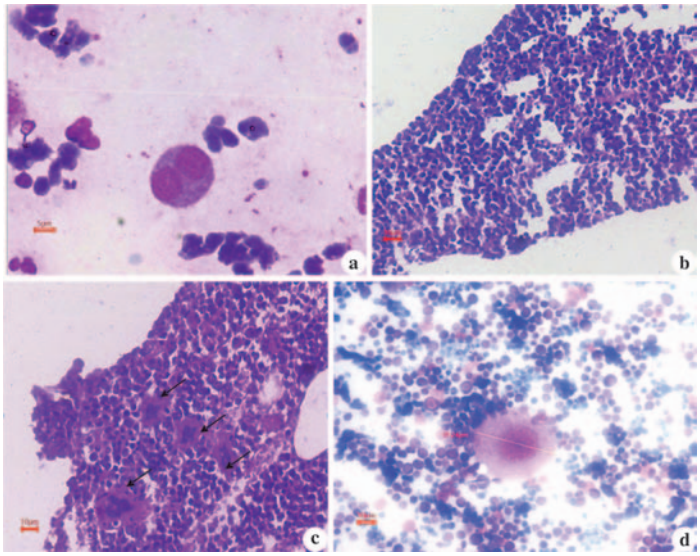

Fig. 4. **(a)** Bone marrow cytology- Binucleate (dysplastic) erythroid cell with basophilic cytoplasm indicative of dysplastic erythropoiesis; LG x1000; **(b)** Bone marrow histopathology- Erythroid hyperplasia and Myeloid hypoplasia- Numerous erythroid cells with dark, dense nucleus and basophilic cytoplasm; H&E x400; **(c)** Bone marrow histopathology- Megakaryocytic hyperplasia (Black arrows) showing >3 megakaryocytes/ low power field; H&E x100; **(d)** Bone marrow cytology- Mature megakaryocyte (59.24 μm) with abundant cytoplasm and multilobulated nucleus (Leishman-Giemsa x400).

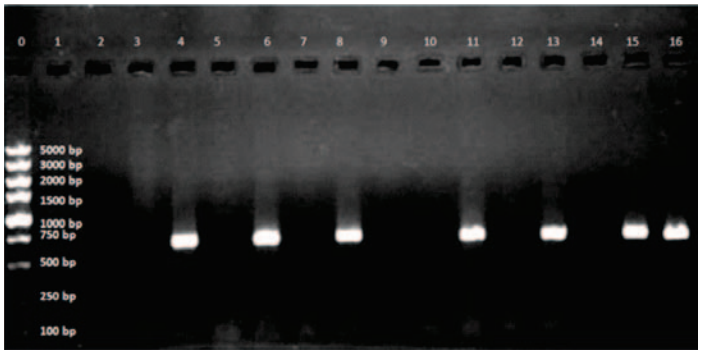

Fig. 5. Feline parvovirus targeting VP2 gene- Lane:0- DNA ladder; Lane:4,6,8,11,13,15- Positive bands at 698 base pairs; Lane:16- Positive control; Lane:2- Negative control

of erythroid hyperplasia (Fig.4b) and myeloid hyperplasia were observed, evident of compensatory erythropoiesis and granulopoiesis representing early infection or recovery stage. A very few cases showed megakaryocytic hyperplasia (Fig.4c), indicating a compensatory response to peripheral thrombocytopenia comparing normal picture (Fig.4d)

Molecular characterisation:

PCR amplification of DNA from bone marrow targeting the VP2 gene produced a specific 698 bp band (Fig.5), confirming FPV in 15 out of 19 samples (78.95%). Phylogenetic analysis (Fig. 6) revealed that the bone marrow isolate clustered closely with Indian FPV strains (OQ266795.1, MK052678.1, MH559110.1), forming a distinct clade

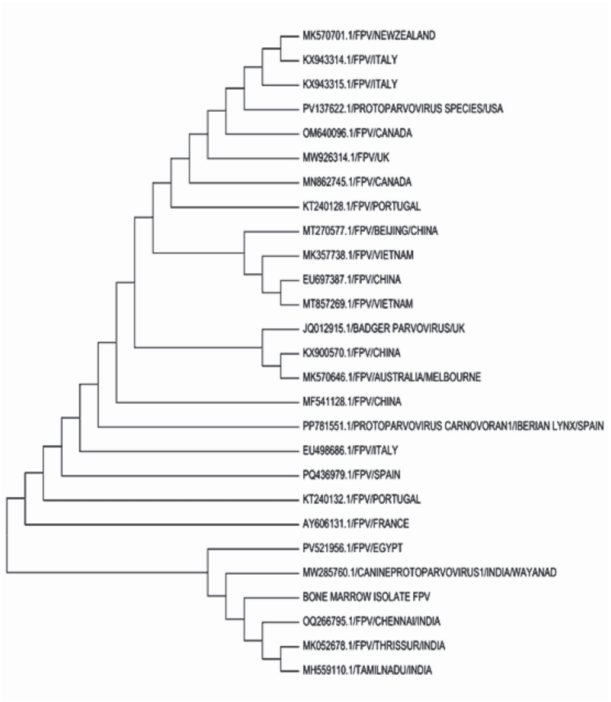

Fig.6. Phylogenetic analysis of feline parvovirus from bone marrow isolate by maximum likelihood method

separated from isolates from Portugal, France, Egypt, China, Vietnam, Australia, and New Zealand. North American and European isolates formed a separate cluster, while other protoparvoviruses appeared as distinct branches, indicating both geographical divergence and the genetic distinctness of the Indian FPV lineage.

DISCUSSION

In the study, cats with Feline Panleukopenia Virus (FPV) infection with significantly reduced hemoglobin, RBC, WBC, and platelet counts, consistent with severe bone marrow suppression align with established literature[5]. The classic pathophysiology involves viral damage to rapidly dividing hematopoietic progenitors in the bone marrow, as demonstrated in vitro studies, exhibiting strong inhibition of colony formation of both myeloid (CFU-GM) and erythroid progenitors[7]. In one study[5] of 187 cats with panleukopenia, leukopenia was detected in 65%, thrombocytopenia in 54% and anemia in 48%. The peripheral cytopenias especially leukopenia and thrombocytopenia are congruent with classical myelogram findings [8], especially immature erythroid and myeloid precursors, in both natural and experimental panleukopenia cases. These data strongly support that bone marrow suppression is a major contributor to the cytopenias seen in peripheral blood of FPV-infected cats.

Hypoglycemia and significant hypoproteinemia has also been reported in FPV-infected cats[5,9,10], including changes in total protein and other metabolic markers reflecting poor nutritional intake, gastrointestinal loss, sepsis, or impaired gluconeogenesis during systemic viral illness.

Some studies[11,12,13] have reported pronounced reductions in albumin in FPV-infected cats which result from compromised intestinal protein absorption and substantial protein leakage into the gut lumen secondary to mucosal epithelial injury [13]. However, in our study, albumin did not differ significantly. This discrepancy may be attributed to variations in the stage of disease at the time of sampling, with many animals possibly being evaluated during the early or recovery phase before substantial protein loss occurred. In addition, differences in disease severity, extent of intestinal villous damage, and hydration status at presentation may have masked hypoalbuminemia. Supportive fluid therapy prior to sampling could also have contributed to the maintenance of near-normal albumin concentrations despite ongoing intestinal pathology.

The absence of significant changes in BUN, creatinine, ALT, and ALP suggests that renal and hepatic functions remained relatively stable in many of the cats in the study. This is consistent with findings in a study, where overt azotemia or marked liver enzyme elevation is not a universal feature[5]. But a report has documented mild to moderate increases in liver enzymes in FPV-infected cats, possibly due to hypoxia, dehydration, or secondary sepsis[12]. Overall, these findings suggest that glucose and protein metabolism were only affected, while liver and kidney function remain relatively stable in the acute phase of infection.

Necropsy findings are in accordance with a study[14] conducted by Kadam *et al.,* including mucosal hemorrhages in the stomach and intestines, enlarged mesenteric lymph nodes, slightly pale bone marrow, and liver congestion in naturally infected cats. These parallels support the notion that systemic hypoxia, bone marrow depletion, and vascular damage are central in feline panleukopenia pathology.

The pronounced erythroid and myeloid hypoplasia aligns closely with the *in vitro* observations where FPV propagates and significantly inhibits colony formation from both myeloid progenitors (CFU-GM) and erythroid progenitors (BFU-E and CFU-E) in feline bone marrow cultures[7]. Another report[8] also documented hypoplastic changes in both erythroid and myeloid series in bone marrow aspirates in an experimental *in vivo* infection study.

Although erythroid and myeloid hypoplasia were dominant in our study, few cases of myeloid hyperplasia were also noticed in some cats suggesting a compensatory or reactive component in marrow response. This is echoed in a large retrospective cytological study[15] in which 46.7% of 152 feline bone marrow samples showed hyperplasia, with granulocytic (50.7%) and erythroid (45.1%) hyperplasia being the most frequent patterns. This substantiates that the feline bone marrow retains a notable capacity for regeneration or reactive proliferation, even during severe systemic stress or infection.

A prominent finding in our study was the frequent megakaryocytic hyperplasia, which may represent a compensatory response to peripheral platelet loss or destruction. While classical FPV literature has mostly focused on erythroid and myeloid suppression, the data on megakaryocytic dynamics remain less well-characterized. Our observations expand on this by suggesting that platelet lineage may mount a regenerative response, perhaps driven by peripheral thrombocytopenia. The variability in the megakaryocytic response may also reflect host-specific factors, such as the timing of sampling, the severity of infection, or the individual capacity for lineage recovery.

The high detection rate of FPV DNA (78.95%) in bone marrow samples strongly suggests that the virus actively invades and persists in hematopoietic tissue, underscoring the bone marrow as an important site for viral replication or reservoir. This observation is in agreement with a study[16] where the presence of FPV genomic material was demonstrated in bone marrow using molecular techniques including conventional PCR, qPCR, and in situ hybridization, thereby supporting the diagnostic value of bone marrow PCR, particularly in cases where faecal or antigen-based assays yield inconclusive results.

Phylogenetic analysis showed that our isolate clusters tightly with other Indian FPV strains (e.g., OQ266795.1, MK052678.1, MH559110.1), forming a well-supported clade- a finding that is consistent with previous molecular epidemiological work in India[17,18].

The clear genetic divergence of this Indian clade from FPV strains reported in Europe, Africa, and East Asia (e.g., Portugal, France, Egypt, China, Vietnam, Australia, New Zealand) suggests distinct geographical evolutionary patterns, possibly driven by regional viral ecology, host population structure, and transmission dynamics. This aligns with broader observations of FPV genetic diversity in southern India, where phylodynamic studies identified novel mutations and potential recombination events in VP2 among cat populations[18]. But this is in contrast to a report of phylogenetic analysis[19] based on the full VP2 gene of FPV which demonstrated close genetic affinity of FPV strains circulating in Mizoram state of India with the non-Indian isolates from Thailand

(MW589472), Italy (MZ508524) and China (OR727315). A recent study[20] also reported novel amino acid mutations in VP2 at positions 303, 441, 554 plus a recombination event, indicating high genetic heterogeneity in feline parvoviruses, warranting the need for genetic sequencing and phylogenetic analysis.

Altogether, our findings support the hypothesis of a regionally circulating FPV lineage in India, which may have co-evolved locally. This has important implications for disease surveillance and vaccine design, since antigenic drift in VP2 could affect viral pathogenicity and the effectiveness of vaccines derived from non-local strains.

ACKNOWLEDGEMENT

The authors are grateful for the support received from the Tamil Nadu Veterinary and Animal Sciences University (TANUVAS), Chennai, for providing the necessary facilities and infrastructure to complete this study.

Financial support & sponsorship: None.

Conflicts of interest: None.

Use of artificial intelligence (AI)-Assisted Technology for manuscript preparation: The authors confirm that there was no use of AI-assisted technology for assisting in the writing of the manuscript and no images were manipulated using AI.

REFERENCES

1. Stockham SL and Scott MA. 2008. Fundamentals of Veterinary Clinical Pathology. 2nd edn. Ames: Wiley-Blackwell.
2. Stuetzer B and Hartmann K. 2014. Feline parvovirus infection and associated diseases. *Vet J* **201**: 150–155.
3. Parthiban M, Aarthi KS, Balagangatharathilagar M and Kumanan K. 2014. Evidence of feline panleukopenia infection in cats in India. *Virus Dis* **25**: 497–499.
4. Barrs VR. 2019. Feline Panleukopenia: A Re-emergent Disease. *Vet Clin North Am Small Anim Pract* **49**: 651–70.
5. Sykes JE. 2013. Feline Panleukopenia Virus Infection and Other Viral Enteritides. *Canine Feline Infect Dis* 187-194.
6. Bancroft JD and Gamble M. 2008. Theory and Practice of Histological Techniques. 6th ed. UK: Churchill Livingstone Elsevier.
7. Kurtzman GJ, Platanias L, Lustig L, Frickhofen N and Young NS. 1989. Feline parvovirus propagates in cat bone marrow cultures and inhibits hematopoietic colony formation in vitro. *Blood* **74**: 71-81.
8. Hosokawa S, Ichijo S and Goto H. 1987. Clinical, hematological, and pathological findings in specific pathogen-free cats experimentally infected with feline panleukopenia virus. *Jpn J Vet Sci* **49**: 43-50.
9. Irgashev A, Ishenbaeva S, Asanova E, Kasieva G, Zholoibekov A, Vityala Y, Tagaev T and Vityala S. 2023. Changes in hematological and biochemical parameters in feline panleukopenia. *Explor Anim Med Res* **13**: 216–219.
10. Kolomak I. 2023. Clinical and hematological changes in viral panleukopenia in cats. *Sci Messin LNU Vet Med Biotech* **25**: 17–22.
11. Manikantaswamy BM, Anil Kumar MC, Anjan Kumar KR, Lathamani VS, Chetan Kumar GK, Veena MP and Sumathi BR. 2022. Haemato-biochemical alteration in cats infected with feline panleukopenia. *Pharma Innov J* **11**: 228–30.
12. Lh M, Rao N, Raval S, Chaudhry J and Mathakiya R. 2024. Hematobiochemical alterations in feline panleukopenia affected cats. *Int J Vet Sci Anim Husb* **9**: 949–53.
13. Mayur TC, Kamran AC and Ramesh PT. 2016. Diagnosis of feline panleukopenia and feline leukemia virus using rapid test kits. *Int J Agric Sci Vet Med* **4**:1-75.
14. Kadam MB, Sawale GK, Gandge RS, Ingle SA, Rohi RR and Meshram PV. 2024. Prevalence and Pathology of Feline Panleukopenia in Domestic Cats. *Acta Sci Vet Sci* **6**: 40-47.
15. Turinelli V and Gavazza A. 2018. Retrospective study of 152 feline cytological bone marrow examinations: preliminary classification and ranges. *J Feline Med Surg* **20**: 1158.
16. Haynes SM and Holloway SA. 2012. Identification of parvovirus in the bone marrow of eight cats. *Aust Vet J* 90: 136–139.
17. Karanam B, Srinivas MV, Vasu J, Xavier AP, Karuppiah R, Shanmugam VP and Mukhopadhyay HK. 2022. Phylodynamic and genetic diversity of parvoviruses of cats in southern India. *Virus Dis* **33**: 108–13.
18. Raja P, Mallika KS, Viva VY, Parthiban M, Sathish G, Vinitha V, Parthiban S and Dhinakar RG. 2024. Complete genome sequence and phylogenetic analysis of feline panleukopenia virus from India. *Virus Dis* **35**: 34–40.
19. Zochampuii T, Rajkhowa TK and Jayappa K. 2025. Molecular detection and phylogenetic analysis of feline panleukopenia virus in domestic cat population of Mizoram state, India. *Vet Res Forum* **16**: 585-590.
20. Karanam B, Srinivas MV, Vasu J, Xavier AP, Karuppiah R, Shanmugam VP and Mukhopadhyay HK. 2022. Phylodynamic and genetic diversity of parvoviruses of cats in southern India. *Virus Dis.* **33**(1): 108–113.

Indian J. Vet. Pathol., 50(2) : 124-130, 2026: DOI: https://doi.org/10.56093/gp521x46

RESEARCH ARTICLE

Phytotherapeutic attenuation of patho-biochemical and oxidative alterations using *Artemisia annua* L. plant extract in experimentally induced *E. coli* (O101) infection in poultry birds

Sahil Choudhary, Rakesh Kumar*, R.K. Asrani, Mridul Soni and R.D. Patil
Department of Veterinary Pathology, Dr. G.C. Negi College of Veterinary and Animal Sciences, CSK Himachal Pradesh Agricultural University, Palampur, Himachal Pradesh, 176062, India

***Address for Correspondence**
Rakesh Kumar, E-mail: rkvetpath@gmail.com

Received: 22.11.25; Accepted: 1.1.26

ABSTRACT

The present experimental study was planned to investigate the effect of *Artemisia annua* (*A. annua*) against experimental *E. coli* (O101) organisms intraperitoneally in Delham Red (DR) chicks. In the experiment study, 300 day-old Delham Red (DR) birds were randomly divided into 6 groups. Group I acted as a control group, group II was given *E. coli* infection only, and groups III, IV, and V were administered with both *E. coli* and 70% aqua-ethanolic extract of *A. annua* at the dose rates of 500 mg, 1000 mg and 2000 mg/L water, respectively. The group VI was provided with 70% aqua-ethanolic extract of *A. annua* only at the dose rate of 2000 mg/L of water. *E. coli* (O101) infection was given to the birds intraperitoneally on the 7th day of age. The 70% aqua-ethanolic extract of *A. annua* was given in drinking water to birds from 0 days to day 14. The birds from each group were sacrificed at 1, 3, 5, 7, 10 and 14 days post-infection (DPI). The values of biochemical parameters such as ALT, AST and creatinine were increased, whereas concentrations of total protein and albumin were decreased in group II (*E. coli* infection only) as compared to group I (control group). However, the clinical signs and serum biochemical values in the groups III, IV and V were significantly lower in a dose-dependent manner as compared to group II (*E. coli* infection only). The gross pathology comprised fibrinous perihepatitis, fibrinous pericarditis, air sacculitis, splenomegaly and peritonitis with higher severity in group II, and there was a significant reduction in the gross lesions in groups III, IV and V in a dose-dependent manner. Microscopically, the liver and heart of group II showed severe perihepatitis, pericarditis, vacuolar changes, leukocytic infiltration, degenerative changes and enhanced cytoplasmic granularity. Similarly, in group II, the microscopic lesions in the spleen were characterized by reticuloendothelial cell hyperplasia and an increase in eosinophilic coagulum material. The microscopic lesions in the liver, heart, spleen and air sacs were of less severity in groups III, IV and V, which were attributed to the antibacterial effect of the plant extract used in the present study.

Keywords: *Artemisia annua, E. coli* (O101), hepatoprotective, liver damage, oxidative stress, serum biochemistry

INTRODUCTION

Avian colibacillosis is an infectious disease of poultry and is caused by *E. coli*, regarded as one of the main reasons for heavy morbidity and mortality in birds. Colibacillosis occurs in almost all species of domestic and wild birds as a highly acute fatal septicaemic disease[1]. Colibacillosis is characterised by colisepticemia, coligranuloma (Hjarre's disease), omphalitis/yolk sac infection, coliform cellulitis, peritonitis, salpingitis, haemorrhagic septicaemia, orchitis, osteomyelitis/synovitis, panophthalmitis, enteritis, and swollen head syndrome. In its acute form, it causes septicaemia that results in death and its subacute form, it causes pericarditis, perihepatitis, air saculitis, and other abnormalities. Various organ surfaces of birds get covered with a fibrin layer as an inflammatory response including the heart, liver, intestines, ovary, oviduct and lungs[2] .

Antibiotic administration is the most common and fastest approach for treating *E.coli* infection in broiler chickens, however, the main problem is the emergence of drug-resistant strains to the medications employed [3]. Antimicrobial drugs added to feed at low doses (sub-therapeutic dose) over a prolonged period may cause resistance development[4,5]. Antimicrobial resistance (AMR) for *E. coli* strains is a severe threat to public health because they could be transferred to humans through the food chain[6,7]. The WHO has suggested creating and utilising environment-friendly alternative techniques to prevent infections in poultry and other food-producing animals[10]. Therefore, it is important to develop or identify more potent, more natural and environment-friendly products to prevent or treat avian colibacillosis. The plant-based dietary supplement may turn out to be an effective and useful tool for treating and preventing *E. coli* infections as well as growth promoter.

How to cite this article : Choudhary, S., Kumar, R., Asrani, R.K., Soni, M. and Patil, R.D. 2026. Phytotherapeutic attenuation of patho-biochemical and oxidative alterations using *Artemisia annua* L. plant extract in experimentally induced *E. coli* (0101) infection in poultry birds. Indian J. Vet. Pathol., 50(2): 124-130.

Artemisia annua L. (Annual mugwort, Sweet Wormwood, Sweet Annie, Sweet Sage wort,

Annual Wormwood) is an annual herb used for a very long time in Chinese and Hindu traditional medicine in Asia[11]. The naturally occurring bioactive components in *Artemisia annua* include monoterpenes, diterpenes, sterols and triterpenes, sesquiterpenes, phenylpropanoids, flavonoids, aliphatic (hydrocarbons, aldehydes and acids), aromatic (alcohols, ketones and acids). *A. annua* possesses various biological activities such as antibacterial, antifungal, anti-inflammatory, anticancer, antiviral, antiparasitic, anti-ulcerogenic, anti-adipogenic, anti-asthmatic, anti-osteoporotic, anti-nocicepetive and immunoregulatory etc[13].

Therefore, the current study was conducted to assess the antimicrobial properties of *Artemisia annua* L. plant extract against experimental *E. coli* infection in broiler chicks.

MATERIALS AND METHODS

Collection and Identification of plant material

In this study, *Artemisia annua* plant free from any dirt and dust was collected from Lahaul & Spiti (32.6192N, 77.3784E) district of Himachal Pradesh, India. Identification of the plant was done at CSIR-IHBT (Institute of Himalayan Bioresource Technology), Palampur, Himachal Pradesh, India.

Assessment of inhibition of bacterial growth

The 70% aqua-ethanolic extract of *Artemisia annua* plant was prepared as per the standard procedure[2]. *E.coli* organism was procured from the Department of Public Health, Lala Lajpat Rai University of Veterinary and Animal Sciences (LUVAS), Hisar, Haryana, India. The serotyping of the isolate was done at the Central Research Institute (CRI), Kasauli and maintained in the Microbiology laboratory of the Department of Veterinary Pathology, DGCN COVAS, Palampur, Himachal Pradesh, India. The disc diffusion method was used to assess the antibacterial action of the plant extract.

DMSO, which was taken as a solvent for impregnating the discs, was used as a negative control. The isolated organism was tested against various antibiotics like Gentamicin (GEN50), Amikacin (AK30), Oxytetracycline (O30), Ciprofloxacin (CIP30), Levofloxacin (LE5), Enrofloxacin (EX10), Ceftriaxone (CTR10 and CTR30), Amoxicillin & Salbactum (AMS30/15), Amoxicillin & Clavulanic acid (AMC20/10). Among all the antibiotics used in the *in vitro* trial, Ceftriaxone (CTR10) determined to be the most effective and thus the disc impregnated with Ceftriaxone (CTR10) served as the positive control. The empty sterile disc was mounted on inoculated plates to check for any inhibition.

Viable bacterial count

The viable count of the bacteria was determined by counting the colonies on EMB plates by performing serial dilutions of the *Escherichia coli* O101 culture, which was incubated in the nutrient broth for 18 hours. The serial dilutions were made in normal saline solution (NSS) diluted from 10^{-1} to 10^{-7} and from each dilution 0.1ml was uniformly distributed across EMB plates. These plates were incubated for 24 to 36 hours at 37^0C and after incubation; these plates were counted for colony-forming units (cfu) per ml.

Determination of LD_{50} of *E. coli* O101

The study was conducted on day-old chicks (N=48) procured from the University Poultry farm, COVAS, CSKHPKV, Palampur, India. The birds were randomly divided into six groups, each group have 8 birds. On the 7th day, the *E.coli* organism was given to the birds through the intraperitoneal route. In the first five groups, the birds were infected with 1ml of normal saline solution with different concentrations of organisms (3.3×10^8, 3.3×10^7, 3.3×10^6, 3.3×10^5, and 3.3×10^4 cfu/ml, respectively). The sixth group acts as a control, having no infection. The birds were closely observed for up to 10 days for any mortality.

Animal experimentation

The final experiment was conducted on 300; day-old Delham Red (DR) birds procured from Animal Genetics and Breeding Department of DGCN COVAS, Palampur and were reared under strict hygienic conditions. Birds were purchased and maintained as per the recommendations of CCSEA. On the 7th day, infection was induced to the birds intraperitoneally and this day was

Table 1. Experimental design

Group	Treatment	Dosing level of infection + 70% aqua-ethanolic extract	No. of birds
I	Feed only (control)	0+0	50
II	*E. coli* infection only	3.6×10^7cfu/ ml +0	50
III	*E. coli* infection + 70% aqua-ethanolic extract of *Artemisia annua*	3.6×10^7cfu/ml+500 mg extract per litre of water	50
IV	*E. coli* infection + 70% aquaethanolic extract of *Artemisia annua*	3.6×10^7cfu/ml+1000 mg extract per litre of water	50
V	*E. coli* infection + 70% aqua-ethanolic extract of *Artemisia annua*	3.6×10^7cfu/ml+2000 mg per litre of water	50
VI	70% aqua-ethanolic extract of *Artemisia annua*	0 + 2000 mg per litre of water	50

considered as the 0 DPI. Table 1 provides an overview of the various treatments administered to each group. The birds were repeatedly monitored throughout the experimental trial up to 14 DPI (21 days of age).

Clinical symptoms, mortality and body weight

The clinical symptoms to be observed at least three times a day included loss of appetite, restlessness, dullness, weight loss and diarrhoea. The mortality pattern was recorded throughout the experimental trial. To determine the effect of 70% aqua-ethanolic extract of *Artemisia annua* on the body weight, three birds from each treatment group were weighed on 0, 1, 2, 3, 5, 7, and 14 DPI and weight was recorded.

Serum Biochemistry

The blood samples were collected at 1, 3, 5, 7, 10 and 14 DPI from 3 birds in each group by cardiac puncture before sacrifice for the estimation of serum biochemicals like aspartate aminotransferase (AST), alanine aminotransferase (ALT), creatinine (CRT), albumin (ALB) and total protein (TP) by using a semi-automatic biochemistry analyzer (Model AGAPPE MISPA neo).

Gross pathological examination

A detailed necropsy examination was done on the birds that were sacrificed and died throughout the experiment. Gross lesions were properly recorded, photographed and scored per a modified protocol given by Thakur et al.,[2]. After detailed necropsy examination, approximately 0.5 cm representative tissue sections from the liver, heart, spleen, and air sacs were collected for histopathological examinations in 10% neutral buffered formalin (NBF) from three chicks of each group at 1, 3, 5, 7, 10 and 14 DPI.

Histopathological examination

The microscopic lesions were scored as per the modified protocol given by Thakur et al.[2] The fixed tissues were washed overnight in running tap water, processed in various grades of alcohol, cleared in benzene, and embedded in paraffin wax. The sections were cut into a thickness of 3 to 5 micron and stained with routine Haematoxylin and Eosin stain (H&E) as per the standard protocol[14].

Reisolation of *E. coli*

Reisolation attempts for *E. coli* organisms were made at different intervals from the birds, which were sacrificed at different intervals. The obtained heart and liver swabs were aseptically collected and streaked directly on EMB plates. The plates were further incubated at 37^0C for 24 to 48 hours and subsequently checked for any bacterial growth.

Statistical analysis of data

The statistical evaluation of the results were subjected to ANOVA using the GraphPad Prism (10.2.1) statistical software and the means were compared using Tukey's test ($P \leq 0.05$).

RESULTS

***In vitro* antimicrobial activity of *Artemisia annua extract* against *E. coli* (O101)**

Ceftriaxone (CTR 10) was found to be the most effective among all antibiotics used in the *in vitro* study followed by Ceftriaxone (CTR 30) and Gentamycin (GEN 50). *Artemisia annua* extract showed a zone of inhibition measuring 18 mm at 200 mg/ml concentration and 70% aqua-ethanolic extract of *Artemisia annua* was further used in poultry birds (DR) infected with *E. coli* (O101).

Clinical Signs and mortality

The birds in-group I i.e. control group and group VI i.e. highest dose of 70% aqua-ethanolic extract of *Artemisia annua* were completely healthy and active throughout the experiment. The clinical symptoms in *Artemisia annua* treated groups appeared after 18h post-infection and included reduced feed and water intake, ruffled feather, abdominal breathing and whitish diarrhoea. The intensity of clinical symptoms was however much less in the groups III, IV and V in a dose-dependent manner in comparison to the group given infection alone i.e. group II.

No mortality was observed in group I and group VI throughout the experiment. The mortality in groups III, IV and V was relatively lower as compared with group II. The decline in the mortality rate in the groups III, IV and V reflects the antimicrobial potential of *Artemisia annua* against *E. coli* in infected birds.

Effect on body weight

In all six groups i.e. I, II, III, IV, V and VI, there was sequential growth in the body weight as the experiment progressed. The group IV and V exhibited a significant increase ($P \leq 0.05$) in the values of body weight at 5 DPI while the birds in group III showed a significant increase ($P \leq 0.05$) in body weight at 14 DPI in comparison to group II kept on plain infection only. The decrease in body weight in group II was linked to a decrease in feed consumption.

Biochemical changes

The serum ALT and AST values were significantly ($P \leq 0.05$) found to decline in the groups treated with the 70% aqua-ethanolic extract of *Artemisia annua* in a dose-dependent manner as compared with the group given *E. coli* infection only (group II) on days 3, 5 and 14 DPI. The group IV and V exhibited a significant reduction ($P \leq 0.05$) in the values of serum ALT at 7 DPI as compared with group II. An increase in the values of serum albumin was observed in the groups treated with *Artemisia annua* extract at different time intervals in a dose-dependent

manner. However, a significant increase (P≤0.05) in serum albumin was observed in group V treated with the highest dose of *Artemisia annua* extract (2000 mg) at 3DPI as compared with the group II administered with plain *E. coli* infection only.

Gross pathological examination

The lesions were in general, comprised of fibrinous perihepatitis, fibrinous pericarditis, airsacculitis, splenomegaly and peritonitis. The total gross lesion score and mean lesion score of fibrinous perihepatitis were higher in-group II throughout the experiment as compared to other treatment groups at different DPI. Severe fibrinous pericarditis was indicated by a thickened pericardial layer and caused adhesions to the epicardial surface of the heart in the birds of group II. Group II had the highest total gross lesion and mean lesion scores for the air sacs as compared to the other treatment groups at different time intervals post-infection (Fig. 1).

Histopathological changes

The histopathological examination of the liver in group II (*E. coli* infection only) included fibrin deposition, vaculoar changes, sinusoidal congestion, heterophilic and mononuclear cell infiltration, degenerative changes and increased cytoplasmic granularity. The intensity of microscopic lesions in the liver was highest in group II at 3, 5 and 7 DPI. Similar trend was noticed in other treatment groups III, IV and V but the intensity of lesions in liver was reduced in dose-dependent manner. Group V showed the lowest intensity of lesions among different treatment groups (Fig. 2). The lesions in the heart comprised of fibrinous pericarditis, infiltration of heterophils and mononuclear cells, congestion, muscle fibre degeneration and increased cytoplasmic granularity. Maximum lesion score intensity was observed in group II at 3, 5 and 7 DPI. Similar changes were observed in treatment groups III, IV and V but the changes were of lesser severity as compared to group II (*E. coli* infection only). Minimum microscopic lesion score was seen in group V among various treatment groups (Fig. 3). The lesions present in the

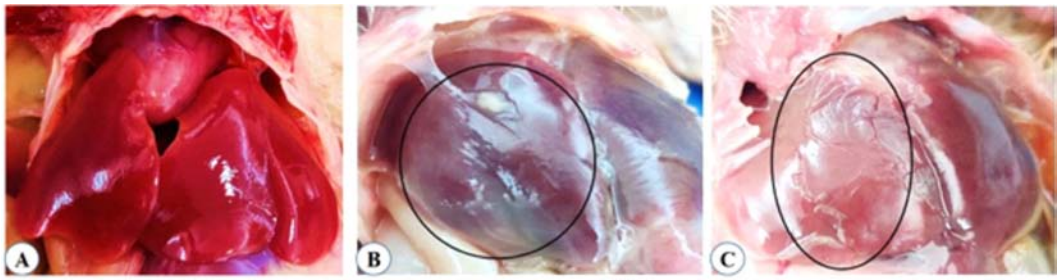

Fig.1. Gross pathology depicting the effect of different treatments on the liver of poultry birds. **A.** Control group showing normal liver. **B.** Group II treated with *E. coli* infection only depicting severe fibrinous perihepatitis. **C.** Group V treated with *E. coli* infection along with aqua-ethanolic extract of *Artemisia annua* exhibiting minimal fibrinous perihepatitis

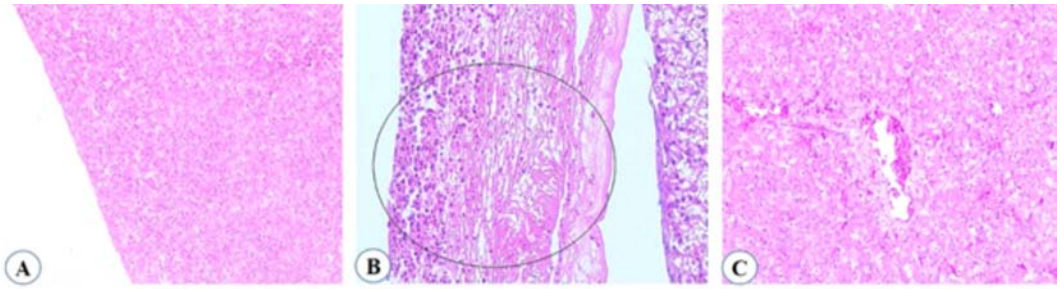

Fig.2. Histopathology depicting the effect of different treatments on the liver of poultry birds. **A.** Control group with normal architecture. **B.** Group II treated with *E. coli* infection only exhibiting severe fibrin deposition. **C.** Group V treated with *E. coli* infection along with aqua-ethanolic extract of *Artemisia annua* exhibiting mild fibrin deposition along with congestion

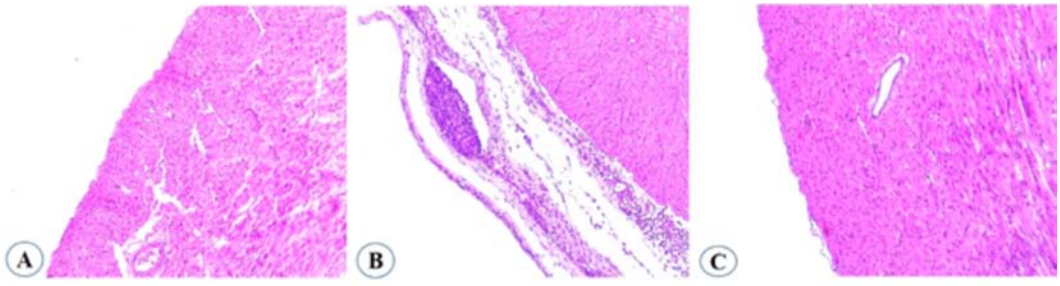

Fig.3. Histopathology depicting the effect of different treatments on the heart of poultry birds. **A.** Control group with normal architecture. **B.** Group II treated with *E. coli* infection only exhibiting severe fibrin deposition. **C.** Group V treated with *E. coli* infection along with aqua-ethanolic extract of *Artemisia annua* exhibiting mild fibrin deposition

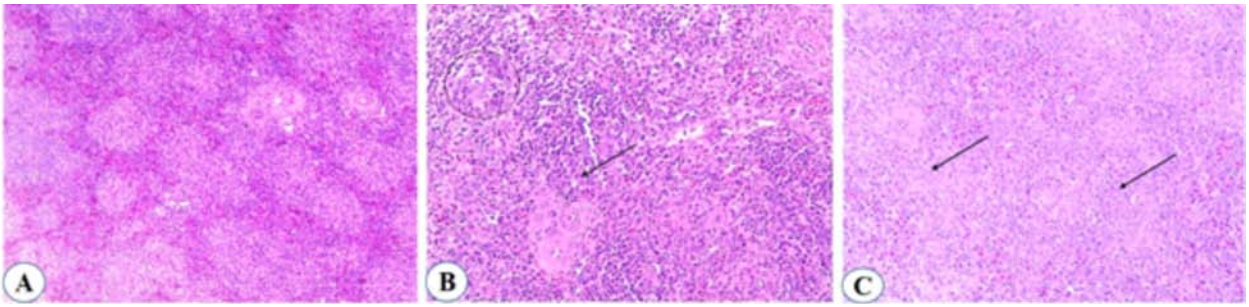

Fig.4. Histopathology depicting the effect of different treatments on the spleen of poultry birds. **A.** Control group with normal architecture. **B.** Group II treated with *E. coli* infection only exhibiting severe reticuloendothelial cell hyperplasia, and an increase in eosinophilic coagulum. **C.** Group V treated with *E. coli* infection along with aqua-ethanolic extract of *Artemisia annua* exhibiting mild reticuloendothelial cell hyperplasia

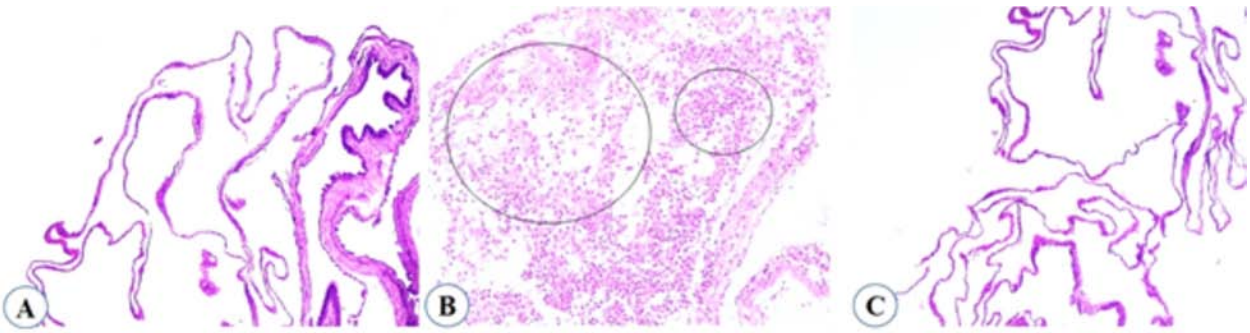

Fig.5. Histopathology depicting the effect of different treatments on the air sacs of poultry birds. **A.** Control group with normal architecture. **B.** Group II treated with *E. coli* infection only exhibiting severe fibrinous air sacculitis along with the infiltration of heterophils. **C.** Group V treated with *E. coli* infection along with aqua-ethanolic extract of *Artemisia annua* showing almost normal air sacs

spleen were reticuloendothelial cell hyperplasia, an increase in eosinophilic coagulum and congestion.

The maximum severity of lesions in the spleen were present in group II at 3, 5 and 7 DPI. The lesions intensity was reduced in dose-dependent manner in treatment groups III, IV and V. Group V showed lesions of reduced intensity in the spleen (Fig. 4). In the air sacs, fibrinous airsacculitis, infiltration of heterophils and mononuclear cells and congestion was observed largely at 3, 5 and 7 DPI in group II. In treatment groups III, IV and V similar trend was noticed but the severity of lesions was much lower than group II and the effect of plant extract was also dose-dependent (Fig. 5).

DISCUSSION

In the present study, *Artemisia annua* ought to show antibacterial activity by disc diffusion method with a zone of inhibition measuring 18 mm at 200 mg/ml concentration. The antimicrobial activity of aqua-ethanolic extract of *Artemisia annua* against *E. coli* were in accordance with Ikram et al.[15]Therefore, 70% aqua-ethanolic extract of *Artemisia annua* was further planned to be used in poultry birds infected with *E. coli* (O101).

In the *in vivo* study the clinical symptoms and mortality pattern were monitored regularly. The clinical symptoms, in general, in all the infected groups include a reduced feed and water intake, dullness, depression, huddling, ruffling of feathers, reluctance to move, and whitish watery diarrhoea. The mortality was reduced in the groups treated with *Artemisia annua* extract as compared with the group II provided with *E. coli* (O101).

The mean serum activity of ALT, AST and creatinine appeared increased whereas concentrations of total protein and albumin were lower in the infected groups as compared to the control group. But these values were highest the group treated with *E. coli* (O101) as compared with the groups provided with *Artemisia annua* extract in a dose dependent manner.

An elevation in the values of serum ALT in the *E. coli* infected group is associated with hepatocellular damage resulting into the alteration in cell membrane permeability and allowing the cytoplasmic ALT to leak into the circulation in accordance with previous study concluded by earlier workers[2]. The increase in the values of serum AST signify a damage to the hepatic system causing leakage of the enzyme into circulation. The increased level of serum creatinine in the infected group II as compared with the control and treatment groups may be associated with the renal damage and the finding of

our research has a correlation with previous observations documented by earlier[2]. The mean serum total protein values were lowest in group II as compared to the other treated group III, IV, V and VI. These findings were in accordance with the observations of Thakur *et al*.[2].

Fibrin deposition on the liver surface may be related to the endothelial damage of the blood vessels causing leakage of fibrin. The total gross lesion score and mean lesion score of fibrinous perihepatitis was higher in the group II throughout the experiment as compared to other treatment groups at different DPI. The similar type of fibrinous changes on hepatic parenchyma in *E coli* infection was observed in several studies conducted earlier[19]. In group III, IV, and V the total gross lesion score and mean lesion score were comparatively lower as compared to the group II given *E. coli* infection only at different time intervals post infection. The decline in the intensity of fibrin deposition on the liver may be related to antimicrobial potential and hepatoprotective effect of the *Artemisia annua* plant as reported in previous study[2]. Severe fibrinous pericarditis indicated by thickened pericardial layer and caused adhesions with epicardial surface of the heart were profoundly reported in the group II provided with *E coli* infection as compared with the other treatment groups. The severity of airsacculitis in the treatment groups III, IV and V treated with *Artemisia annua* extract showed a dose-dependent decline as compared to the group II given *E. coli* infection only.

The hepatocytes in the group II treated with *E. coli* infection only were markedly swollen with degenerative changes and increased cytoplasmic granularity. The fibrin layer was seen with moderate to severe intensity along with mononuclear cells and occasional heterophils. The total microscopic lesions and the mean microscopic lesion score of fibrinous perihepatitis, vacuolar changes and leukocytic infiltration in the liver were comparatively lower in all the treatment groups as compared to the group II given with *E. coli* infection only.

Severe fibrinous pericarditis in association with leukocytic infiltration predominantly MNCs were observed in the group provided with *E. coli* infection only. The inflammatory response majorly involved mononuclear cell infiltration admixed with few heterophils and fibroblast cells. Fibrinous pericarditis was however comparatively milder in the groups provided with *Artemisia annua* as compared to the group II administered with *E. coli* infection only. In group II, the total microscopic lesions and mean lesion score of reticuloendothelial cell hyperplasia and eosinophilic coagulum in the spleen were found to be higher as compared to the other groups at different intervals post-infection. In group V, severity of total microscopic lesion score and mean lesion score of reticuloendothelial cell hyperplasia and the presence of eosinophilic coagulum in the spleen was lower as compared to all the other treatment groups.

CONCLUSIONS

The 70% aqua-ethanolic extract of aerial parts of *Artemisia annua* exhibited antibacterial activity against *E. coli* (O101) as indicated by the results of *in vitro* as well *in vivo* studies. In the *in vivo* experiment, the extract significantly reduced serum liver enzyme levels, indicating notable hepatoprotective effects. Treated groups also exhibited markedly reduced gross and microscopic lesions on the liver, heart, air sacs and spleen, confirming the effective antibacterial and tissue-protective properties. In addition, the overall clinical response of the treated birds improved, as evidenced by reduced mortality, minimal clinical manifestations, and better feed intake. These findings collectively support the therapeutic potential of the 70% aqua-ethanolic extract of *Artemisia annua* as a natural antimicrobial, hepatoprotective, cardioprotective, and immunoprotective agent against *E. coli* (O101) infections in poultry birds.

ACKNOWLEDGEMENT

The authors are thankful to Dean, COVAS, CSK HPKV, Palampur for providing necessary facilities to carry out the research.

Financial support & sponsorship: None.

Conflicts of interest: None.

Use of artificial intelligence (AI)-Assisted Technology for manuscript preparation: The authors confirm that there was no use of AI-assisted technology for assisting in the writing of the manuscript and no images were manipulated using AI.

REFERENCES

1. Sara GR, Sur SK, Mitra M, Nag NC and Das AK. 1995. "Colibacillosis in capitive birds at Alipore Zoo". *J Anim Health* **34(1):** 43-45.
2. Thakur, S., Kumar, R., Asrani, R. K., Thakur, M., Patel, S. K., Patil, R. D., Obaidullah, A. J., & Emran, T. B. 2024. "Hepatoprotective and cardioprotective effect of *Artemisia nilagirica* leaf extract on *E. coli* challenged broiler chicken". *Heliyon*, **10(4)**, e25709. https://doi.org/10.1016/j.heliyon.2024.e25709
3. Saidi, B., Mafirakureva, P and Mbanga J. 2013. "Antimicrobial resistance of Escherichia coli isolated from chickens with colibacillosis in and around Harare, Zimbabwe". *Avian dis* **57(1):** 152-4.
4. Apata, DF. 2009. "Antibiotic resistance in poultry". *Inter J Poult Sci* **8(4):** 404-8.
5. Diarra, M.S and Malouin F. 2014. "Antibiotics in Canadian poultry productions and anticipated alternatives". *Front Microbiol* **17: 5**:282.
6. Akond, M.A., Alam, S., Hassan, S.M and Shirin M. 2009. "Antibiotic resistance of *Escherichia coli* isolated from poultry and poultry environment of Bangladesh". *Inter J Food safety*

11: 19-23.
7. Murray, M., Salvatierra, G., Dávila-Barclay, A., Ayzanoa, B., Castillo-Vilcahuaman, C., Huang, M., Pajuelo, M.J., Lescano, A.G., Cabrera, L., Calderón, M and Berg D.E. 2021. "Market chickens as a source of antibiotic-resistant Escherichia coli in a Peri-urban community in Lima, Peru". *Front Microbiol* **2(12):** 635871.
8. Nhung, N.T., Chansiripornchai, N and Carrique-Mas J.J. 2017. "Antimicrobial resistance in bacterial poultry pathogens: a review". *Front Vet Sci* **10(4):**126.
9. Aworh, M.K., Kwaga, J.K., Hendriksen, R.S., Okolocha, E.C and Thakur, S. 2021. "Genetic relatedness of multidrug resistant Escherichia coli isolated from humans, chickens and poultry environments". *Antimicrob Resist & Infec Control* **10(1):** 1-13.
10. WHO. 2001. "Antimicrobials in animal feed- a threat to human use". *WHO Drug Information* **15:** 160-162.
11. Ekiert. H., Świątkowska, J., Klin, P., Rzepiela, A and Szopa, A. 2021. "*Artemisia annua*– Importance in Traditional Medicine and Current State of Knowledge on the Chemistry, Biological Activity and Possible Applications". *Planta Medica* **87(08):** 584-99.
12. Gupta, P.C., Dutta, B., Pant, D., Joshi, Pand and Lohar, D.R. 2009. "*In vitro* antibacterial activity of *Artemisia annua Linn*. growing in India". *Inter J Green Pharm (IJGP)***3(3).**
13. Feng, X., Cao, S., Qiu, F and Zhang, B. 2020. "Traditional application and modern pharmacological research of Artemisia annua L". *Pharmacol & Therap* **216:** 107650.
14. Luna, L.G. 1968. "Manual of Histological Staining Methods. *Armed Forces Insti of Pathol*. New York, NY: McGraw Hill Book Company.
15. Ikram, M., Jan, G., Khan, S.D., Jan, F.G., Ullah, A., Shaheen, S., Ijaz, F., Rehman,S., Bahadar, S., Ziaulhaq, A.A and Iqbal, Z. 2015. "Antimicrobial activity and phytochemical screening of *Artemisia annua L*. and *Millotus philippensis (Lam.) Mull. Arg.* Leaves". *Am Eurasian J Agricul & Environ Sci* **15(12):** 2437-2441.

Indian J. Vet. Pathol., 50(2) : 131-142, 2026: DOI: https://doi.org/10.56093/b1yk9637

RESEARCH ARTICLE

Protective effects of *Citrus limon* supplementation against arsenic-induced clinicopathological, ultrastructural, and genotoxic alterations in Swiss Albino mice

Kuldeep Kumar, Mamta Kumari*, Anita Rathore, Kamal Purohit, Balram Yadav, Mamta, Naresh Meena and Pooja Gill

Department of Veterinary Pathology, College of Veterinary and Animal Science, Navania, Vallabhnagar, Udaipur-313601 Rajasthan University of Veterinary and Animal Sciences, Bikaner, Rajasthan, India

***Address for Correspondence**

Mamta Kumari, Department of Veterinary Pathology, College of Veterinary and Animal Science, Navania, Vallabhnagar, Udaipur-313601, E-mail: mamtabijarnia@gmail.com; ORCID is 0000-0002-8595-2312

Received: 29.12.25; Accepted: 28.2.26

ABSTRACT

Arsenic exposure poses significant toxic effects on various biological systems, and this study investigates the ameliorative potential of *Citrus limon* (lemon) on arsenic-induced toxicity in mice. For the experimental study, 24 Swiss albino mice were randomly divided into four groups of six mice each. Group A served as control group (C). Group B (SA) was exposed to arsenic for 28 days. Group C (CL) was supplemented *C. limon* and Group D (SA+CL) received arsenic treatment for 28 days along with *Citrus limon* supplementation. Hemato-biochemical analysis revealed that arsenic exposure resulted in macrocytic hypochromic anemia, significantly elevated liver enzymes (alanine aminotransferase, aspartate aminotransfera, alkaline phosphatase)), creatinine, cholesterol, and total bilirubin levels, and significantly reduced total protein and albumin levels. Oxidative stress markers indicated increased lipid peroxidation (LPO) and decreased levels of superoxide dismutase (SOD), glutathione reductase (GR), and catalase. Group D (SA+CL)) revealed fewer ultrastructural changes like irregular nuclear membranes, fragmented chromatin, lipid droplet accumulation, and swelling of mitochondria and rough ER and microscopic changes like hydropic degeneration, fatty changes and inflammatory changes in liver as compared to group B (SA). The sperm head abnormalities were significantly reduced and the sperm count was normal in lemon supplemented arsenic toxicity group. The formation of micronuclei in normochromatic and polychromatic RBCs was reduced in arsenic treated lemon supplemented group. In conclusion, *C. limon* administration in mice exhibited a significant protective effect against arsenic-induced alterations in hematological and biochemical parameters, along with a marked reduction in oxidative stress, pathological lesions, and genotoxic damage.

Keywords: Anemia, biochemical enzymes, gross lesions, hematology, histopathology, lemon, micronuclei, oxidative stress, sperm abnormalities

INTRODUCTION

Arsenic is a hazardous metalloid that contaminates air, water, soil, and food sources[1]. It exists in multiple chemical forms, including elemental arsenic (As^0), arsenite (As^{3+}), arsenate (As^{5+}), and arsine gas. Arsenite (As^{3+}) is considerably more toxic than organic forms[2]. Natural processes such as mineral dissolution, groundwater movement, geothermal activity; human activities like mining, industrial operations, and use of arsenic-based pesticides contribute to its environmental dissemination. Groundwater contamination with arsenic has emerged as a critical public health issue, especially in regions of India, and other parts of Southeast Asia. Human and animal exposure occurs primarily through ingestion, inhalation, and dermal absorption, with contaminated drinking water and food particularly rice and seafood being the main sources. Pesticides and insecticides, dipping fluid used to treat ectoparasites, are also significant sources of arsenic exposure for livestock.The WHO safe limit for arsenic in drinking water is 10 µg/L; however, groundwater arsenic levels in India frequently exceed this limit. Severe contamination is reported from the Gangetic plains and states such as West Bengal (50 to 3700 µg/l), Punjab, Haryana, Bihar, Assam, Uttar Pradesh, Jharkhand, Chhattisgarh, Karnataka, Madhya Pradesh, Rajasthan and northeastern states including Manipur and Tripura, with concentrations reaching up to 9,886 µg/L[50]. In West Bengal, arsenic is also elevated in rivers and ponds. Elevated blood arsenic levels, particularly noted in Bihar, have been associated with increased disease susceptibility and a higher prevalence in carcinoma patients, suggesting a link between arsenic exposure and cancer.[51] Acute exposure can cause gastrointestinal distress, neurological symptoms, and, in

How to cite this article : Kumar, K., Kumari, M., Rathore, A., Purohit, K., Yadav, B., Mamta, Meena, N. and Gill, P. 2026. Protective effects of Citrus lemon supplementation against arsenic-induced clinicopathological, ultrastructural, and genotoxic alterations in Swiss Albino mice. Indian J. Vet. Pathol., 50(2) : 131-142.

extreme cases, death. Chronic exposure is associated with a range of health complications, including cardiovascular diseases, various forms of cancer, and neurotoxicity[2]. At the cellular level, arsenic induces toxicity through the generation of reactive oxygen species (ROS) and reactive nitrogen species (RNS), disruption of enzymatic functions, impairment of mitochondrial activity, and interference with key cellular signalling pathways involved in cell development, proliferation and death. These effects can lead to apoptosis and a variety of pathological conditions[3]. It also alters DNA methylation and histone modifications, which can be passed down to subsequent generations via sperm from exposed males[52].

Given the widespread exposure and severe health consequences of arsenic toxicity, the search for effective protective agents is of paramount importance. Natural compounds with antioxidant and detoxifying properties may show promise in this regard. As arsenic affects the intracellular anti-oxidant machinery; therefore, exogenous anti-oxidant supplementation can counteract the anti-oxidant stress caused by it. *Citrus limon* (lemon) is known for its high vitamin C content, flavonoids, limonoids, terpenes, fiber, pectin and other phytochemicals that offer antioxidant, vascular-protective, anti-inflammatory, anti-microbial, anti-allergic and potential anticancer effects[5]. Its phenols and flavones are known to suppress tumoro-genesis and neoplasia. It has demonstrated the ability to combat oxidative stress and enhance detoxification pathways, making it a promising candidate for the alleviation of arsenic-induced health effects. So, the present study was performed to evaluate the ameliorating effec of *Citrus limon* fruit supplementation in experimentally induced sub-acute arsenic toxicity in Swiss albino mice.

MATERIALS AND METHODS

Collection and Identification of Plant Materials

Citrus limon were collected from Local agriculture farm and were authenticated by Department of Pharmacognosy, Faculty of Pharmacy, Bhupal Nobles' University, Udaipur.

Phytochemical Analysis

Qualitative Phytochemical Analysis

The phytochemical analysis was done as per standard tests. The detection of alkaloid was done by Mayer's test; phenol by lead acetate test; flavonoid by sulphuric acid test; cardiac glycosides by Keller-Kiliani test; and terpenoids by Salkowski test[6,7].

Quantitative Phytochemical Analysis

Determination of Total Phenol by Folin-Ciocalteu Reagent Method

Total phenol content was determined by Folin-Ciocalteu reagent method with some modification and employing gallic acid as standard. The absorbance was measured for solution by using UV-spectrophotometer (UV 5704 SS, ECIL, India) at constant wavelength 750 nm. The yield of total phenolic compound was expressed in mg gallic acid per ml of plants.

Determination of Total Flavonoids by Colourimetric Method

The total flavonoids content was measured by using a modified colourimetric method with employing quercetin as standard (mg/L). The total flavonoids contents of crude extracts were estimated by aluminium chloride colourimetric method. The absorbance of samples was measured at 510 nm wavelength using spectrophotometer. Quercetin standard was used for the calibration curve.

Determination of in vitro antioxidant activity of plants by 2, 2-di-phenyl-1-picrylhydrazyl (DPPH) method

The potential of extracts to scavenge DPPH radicals was determined according to the method of Blois (1958)[8]. The absorbance of the samples and control solutions were determined at 517 nm against water. The % DPPH radical scavenging activity was calculated as follows:

% DPPH radical scavenging activity =

$[1– (A_{517}\text{nm sample} / A_{517}\text{nm control})] \times 100$

Experimental animals

A total of twenty-four healthy Swiss albino mice, weighing between 25–30 grams, were procured from the Disease-Free Small Animal House, College of Veterinary Sciences, Lala Lajpat Rai University of Veterinary and Animal Sciences, Hisar. The animals were housed in the Animal House Facility of the institute under strict hygienic conditions and a controlled environment, in accordance with the guidelines of the Committee for Control and Supervision of Experiments on Animals (CCSEA). All mice had free access to pelletized feed and clean drinking water throughout the study. Prior to the commencement of the experiment, the animals were acclimatized for one week. Necessary approval was obtained from the Institutional Animal Ethics Committee (IAEC/RES/04/01) before the initiation of the experiment.

Experimental Design

Twenty-four mice were randomly divided into four groups, each consisting of six mice. Group A served as the control group. Group B, the toxicity group, received 3 mg/kg body weight (BW) of sodium arsenite (SA) orally, once daily for 28 days. Groups C was treated with 10 ml/kg BW of *Citrus limon* juice orally, once daily for 28 days. Group D received sodium arsenite and *Citrus limon* juice orally, once daily for 28 days.

Hematological analysis

Blood was collected from the retro-orbital sinus of each mouse in all experimental groups at the time of euthanasia on 28th day. Samples were drawn into dry, sterilized vials containing ethylene diamine tetra acetic acid (EDTA) and hematological parameters [Hemoglobin content (Hb),

Total Erythrocyte count (TEC), Packed Cell Volume (PCV), Total Leucocyte count (TLC), Different Leucocyte count (DLC), Total platelets count (PLT), Mean platelet volume (MPV), were analyzed using a Mindray hematology analyzer (Model No. RM-303-03, Serial No. 3903).

Biochemical analysis

To evaluate changes in serum enzyme levels induced by arsenic toxicity in Swiss albino mice, blood samples were collected in clean, sterile tubes without anticoagulant. The samples were centrifuged at 3000 rpm for 15 minutes at 4°C to separate the serum, which was then stored at -20°C until further analysis. Serum enzyme levels were estimated by using liquid stable reagent kits (Aekray Healthcare Pvt. Ltd., Surat, India). The serum analysis was carried out with the help of a biochemistry auto analyzer (CAT No. BGS–246, Biogen). The various parameters such as total protein, albumin, alanine aminotransferase (ALT), aspartate aminotransferase (AST), alkaline phosphatase (ALP), creatinine, blood urea nitrogen (BUN), cholesterol (CHOL), triglyceride (TRIG) and total bilirubin (TB) were analyzed.

Oxidative stress

The liver tissue homogenate was prepared and assessed for oxidative stress as well as antioxidant enzyme activities by microprocessor UV-VIS double beam spectrophotometer (Chino Scientific Instruments MFG, Ajmer, India).

Preparation of liver tissue homogenates

A 500 mg of individually weighed liver tissue samples were dissected and washed with phosphate buffer saline (PBS). After washing, samples were taken in 5ml ice-cold PBS (pH 7.4). By the help of a teflon homogenizer MSW 346 (IKA), under ice cold condition, 10% tissue homogenate was prepared in PBS, then it was centrifuged (3000 rpm under 4°C) for 10 min to purge cellular debris and supernatant was collected. The resulting supernatant was used for determination of oxidative stress marker.

Lipid peroxidation (LPO)

Lipid peroxidation was evaluated in terms of malondialdehyde (MDA) production by using thiobarbituric acid-reactive substances (TBARS) test[9]. The absorbance was read at 535 nm. Calculation was done using the molar extinction coefficient (EC) of MDA-TBA complex (TBARS) at 535 nm, i.e. $1.56x10^8$/M/cm. The amount of LPO was expressed as nanomole of MDA formed per gm of tissue.

$$\text{LPO (nmole MDA. G}^{-1}) = \frac{\text{OD of test}}{\text{EC}} \times \frac{\text{Total volume of reaction mixture}}{\text{Volume of sample taken}} \times 10^9 \times \text{DF}$$

DF = Dilution factor i.e. 10

Superoxide dismutase

Superoxide dismutase (SOD) was estimated as per the method described earlier[10]. The absorbance was read at 570 nm against distilled water (blank). The result was expressed as SOD units (one unit of SOD was the amount of protein required to inhibit the MTT reduction by 50%).

Glutathione reductase activity

Glutathione reductase (GR) activity from tissue was estimated as per method described earlier[11] with some modification. A high GSH/GSSG ratio is essential for protection against oxidative stress and the oxidation of NADPH to NADP+ is accompanied by a decrease in absorbance at 340 nm. The enzyme activity was expressed as µmole of NADPH oxidized to NADP/mg of protein/min using the molar extinction coefficient of 6200/M/cm at 340 nm

Catalase

Catalase activity was determined by measuring the decomposition of hydrogen peroxide (H_2O_2) at 240 nm according to the method decribed earlier[12]. The decomposition of H_2O_2 was followed directly by the decrease in extinction per unit time at 240 nm. The difference in extinction per unit time is a measure of catalase. Activity of catalase was calculated using the molar extinction coefficient of 43.6 cm^{-1} and expressed a mmoles of H_2O_2 decomposed/min/mg protein.

Pathological studies

Thorough necropsy examination of all mice was carried out and gross lesions were recorded. For histopathological examination, organs (lungs, heart, liver, spleen, kidney, brain, stomach, intestines and testes) were collected in 10% neutral buffered formalin. The formalin fixed tissue were washed and processed for paraffin embedding technique[53] and then stained with routine hematoxylin and eosin staining method[54].

Ultrastructural studies

Liver samples of two mice from arsenic treated groups were processed for transmission electron microscopy following the standard method described earlier[55,56,57] with slight modifications at AIIMS, New Delhi.

Semen Evaluation

Semen was collected after the termination of study from the entire cauda epididymis. Sperm count[13] and sperm head abnormality assays (SHA) were done in mice of all groups.

Micronucleus test

The occurrence of micronuclei in control, arsenic treated and all other treatment groups were assessed by the test as described earlier[14,15].

Statistical analysis

The data for various parameters were subjected to

statistical analysis using analysis of variance (ANOVA) and t-test. Differences between group means were evaluated for statistical significance using Duncan's multiple range test at $P< 0.05$[16].

RESULTS

Phytochemical Analysis

Qualitative Estimation

Phytochemicals help to protect against various diseases due to the presence of alkaloids, flavonoids, terpenoids, cardiac glycosides and phenolic compounds. The phytoconstituents present in *Citrus limon* juice were phenols, terpenoids and flavonoids.

Quantitative Estimation

The total phenol and total flavonoid contents in *Citrus limon* juice were 4.65 mg/ml and 1.67 mg/ml, respectively.

In vitro Antioxidant activity assay

DPPH radical scavenging activity was evaluated using serial two-fold dilutions (corresponding to 0.125–8 ml juice equivalents) of *Citrus limon* juice. The results indicated a dose-dependent antioxidant activity for *Citrus limon* (lemon) juice, with higher concentrations exhibiting greater radical-scavenging activity, increasing from 27.21% to 51.41% .

Hemato-biochemical analysis

The present study revealed decreased total RBC count, hemoglobin levels, elevated Mean corpuscular volume (MCV) and reduced Mean corpuscular hemoglobin (MCH) and Mean corpuscular hemoglobin concentration (MCHC) values in arsenic-exposed mice (Table 1). Mean values of hemoglobin (g/dl) value was significantly (P<0.05) lower in arsenic intoxicated group B (SA) as compared to *C. limon* group C, and arsenic intoxicated group supplemented with Citrus limon groupD (SA+CL). The arsenic intoxicated group B had a significantly (P<0.05) higher total leukocyte count as compared to groups C (CL), and D (SA+CL) (Table 2). The group B had significantly (P<0.05) lower platelet count compared to group D (Table 2).

The results of various biochemical parameters are presented in Table 3. The AST level of arsenic intoxicated group B (SA) mice was significantly (P<0.05) higher as compared to control group A and *Citrus limon* group C (CL). The ALT levels of group B (SA) were significantly (P<0.05) higher as compared to all other groups. Similarly, ALP levels of group B (SA) were significantly (P<0.05) higher as compared to groups A, C and D (arsenic intoxicated group supplemented with *Citrus limon*). Additionally, creatinine levels in group B (arsenic intoxicated) were significantly (P<0.05) higher than other groups. The total protein level in group B (arsenic intoxicated) was significantly (P<0.05) lower compared to groups A (control), C (CL), D (arsenic intoxicated group supplemented with *Citrus limon*). Similarly, albumin level was significantly (P<0.05) lower in arsenic intoxicated group B as compared to control group A. Regarding serum cholesterol values, group B (SA) showed significantly (P<0.05) higher levels than all other groups and group C (CL) showed significantly lower level as compared to control group. Triglycerides

Table 1. Mean (Mean ± SEM) values of erythrocyte parameters of different experimental groups.

Groups	Mean ± SEM Value of Parameters					
	RBC ($10^6/\mu l$)	Hb (g/dl)	HCT (%)	MCV (fL)	MCH (pg)	MCHC (g/dl)
A (Control)	$8.63^{ab} \pm 0.24$	$15.35^{b} \pm 0.55$	$56.38^{a} \pm 1.58$	$65.55^{a} \pm 2.44$	$17.78^{a} \pm 0.34$	$27.30^{b} \pm 1.16$
B (SA)	$7.80^{a} \pm 0.20$	$13.67^{a} \pm 0.35$	$58.38^{a} \pm 1.46$	$74.96^{b} \pm 1.38$	$17.58^{a} \pm 0.57$	$23.47^{a} \pm 0.72$
C (CL)	$8.20^{ab} \pm 0.17$	$15.18^{b} \pm 0.37$	$56.87^{a} \pm 0.74$	$69.48^{ab} \pm 1.80$	$18.54^{a} \pm 0.56$	$26.68^{b} \pm 0.36$
D (SA+CL)	$8.30^{ab} \pm 0.19$	$16.03^{b} \pm 0.29$	$56.95^{a} \pm 1.51$	$68.60^{ab} \pm 0.60$	$19.37^{a} \pm 0.55$	$28.24^{b} \pm 0.83$

All values are represented as Mean ± SEM; n=6 in each group; values bearing different superscript in the same column differ significantly at P<0.05.

Table 2. Mean values of leucocyte and platelet parameters of different experimental groups.

Group	Lymphocyte ($10^3/\mu l$)	Other granulocytes ($10^3/\mu l$)	Neutrophils ($10^3/\mu l$)	Platelets ($10^3/\mu l$)	Mean Platelet Volume (fL)
A(Control)	$6.73^{a} \pm 0.42$	$0.45^{a} \pm 0.12$	$9.27^{ab} \pm 0.63$	$421.17^{b} \pm 8.57$	$8.52^{a} \pm 0.14$
B (SA)	$5.85^{a} \pm 0.74$	$0.78^{a} \pm 0.16$	$10.88^{b} \pm 0.81$	$383.17^{a} \pm 10.79$	$8.22^{a} \pm 0.18$
C (CL)	$6.37^{a} \pm 0.60$	$0.65^{a} \pm 0.29$	$8.20^{a} \pm 0.65$	$403.00^{ab} \pm 10.63$	$8.35^{a} \pm 0.20$
D (SA+CL)	$6.17^{a} \pm 0.54$	$0.72^{a} \pm 0.09$	$8.25^{a} \pm 0.51$	$420.50^{b} \pm 6.51$	$8.28^{a} \pm 0.18$

All values are represented as Mean ± SEM; n=6 in each group; values bearing different superscript in the same column differ significantly at P<0.05.

Table 3. Mean values of biochemical parameters in mice of different experimental groups.

Groups	Mean ± SEM Value of Parameters									
	Aspartate aminotrasferase (U/L)	Alanine aminotransferase (U/L)	Alkaline phosphatase (U/L)	Blood urea nitrogen (mg/dl)	Creatinine (mg/dl)	Total Protein (mg/dl)	Albumin (mg/dl)	Cholesterol (mg/dl)	Triglycerides (mg/dl)	Total bilirubin (mg/dl)
A (Control)	$55.16^{a} \pm 4.58$	$38.40^{a} \pm 4.11$	$56.80^{a} \pm 4.46$	$44.50^{a} \pm 1.86$	$0.41^{a} \pm 0.03$	$5.87^{b} \pm 0.44$	$4.60^{c} \pm 0.41$	$76.06^{a} \pm 3.49$	$259.56^{a} \pm 10.86$	$0.86^{ab} \pm 0.10$
B (SA)	$74.37^{b} \pm 6.57$	$53.25^{b} \pm 5.23$	$85.69^{b} \pm 3.30$	$48.34^{a} \pm 3.49$	$0.58^{b} \pm 0.08$	$4.77^{a} \pm 0.19$	$3.22^{a} \pm 0.13$	$128.41^{c} \pm 9.54$	$342.29^{b} \pm 13.56$	$1.26^{b} \pm 0.18$
C (CL)	$56.27^{a} \pm 3.63$	$34.43^{a} \pm 2.41$	$57.48^{a} \pm 4.88$	$42.44^{a} \pm 2.33$	$0.33^{a} \pm 0.03$	$5.83^{b} \pm 0.19$	$3.95^{abc} \pm 0.11$	$74.17^{b} \pm 5.13$	$275.82^{a} \pm 9.69$	$0.86^{ab} \pm 0.11$
D (SA+CL)	$62.32^{ab} \pm 5.01$	$44.58^{ab} \pm 2.60$	$60.81^{a} \pm 4.85$	$43.36^{a} \pm 4.19$	$0.33^{a} \pm 0.03$	$5.80^{b} \pm 0.35$	$3.57^{ab} \pm 0.25$	$61.99^{a} \pm 3.37$	$280.45^{a} \pm 13.54$	$0.85^{ab} \pm 0.13$

All values are represented as Mean ± SEM; n=6 in each group; values bearing different superscript in the same column differ significantly at P<0.05.

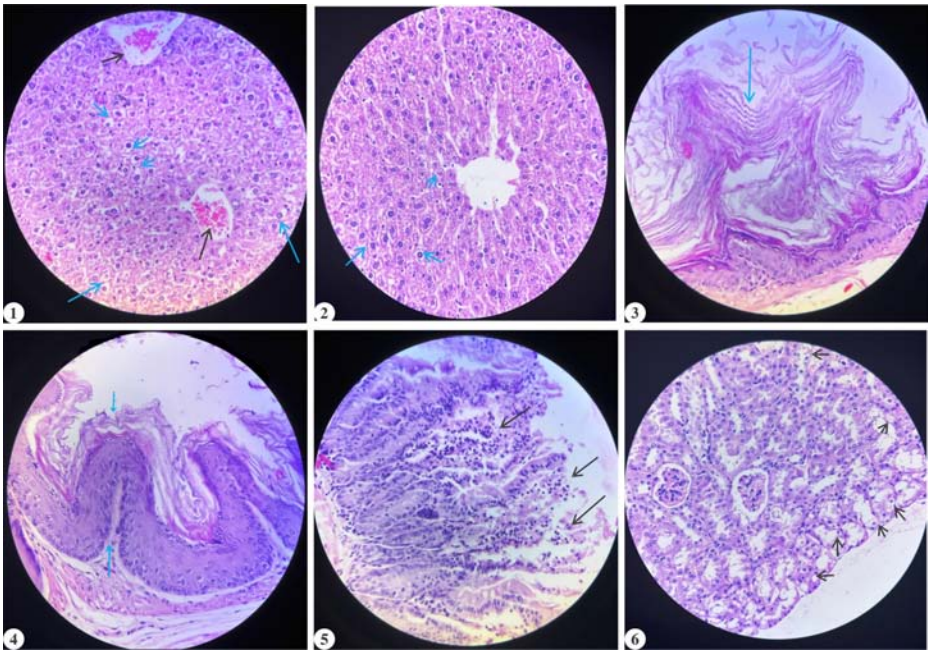

Fig. (1) and (2). Liver of arsenic intoxicated group B (1) showing hydropic degeneration and congested veins, while arsenic intoxicated and *Citrus limon* supplemented group D (2) showing mild degenerative changes (H&E 400X); **Fig. (3) and (4)**. Stomach of arsenic intoxicated group B (3) revealing hyperkeratosis in mucosa, and arsenic intoxicated and *Citrus limon* supplemented group D (4) revealing mild hyperplasia (H&E 400X); **Fig. 5.** Intestine of arsenic intoxicated group B showing villus destruction, and lymphocytic infiltration (H&E 400X); **Fig. 6.** Kidney of arsenic intoxicated group B showing hydropic degeneration in tubules (H&E 400X).

Table 4. Mean oxidative satress related parameters of mice of different experimental groups.

Groups	Mean ± SEM Value of Parameters			
	Superoxide dismutase (U/mg protein)	Lipid peroxidation (nmol/μL)	Glutathione reductase (μg/mg tissue)	Catalase (U/mg protein)
A (Control)	$17.51^{c} \pm 0.59$	$73.09^{a} \pm 0.93$	$3.86^{bc} \pm 0.23$	$40.12^{c} \pm 0.58$
B (SA)	$13.66^{a} \pm 0.41$	$93.3^{b} \pm 0.44$	$1.58^{a} \pm 0.11$	$23.67^{a} \pm 0.68$
C (CL)	$19.33^{d} \pm 0.61$	$71.84^{a} \pm 1.05$	$3.87^{bc} \pm 0.10$	$41.13^{c} \pm 0.73$
D(SA+CL)	$15.94^{b} \pm 0.26$	$73.88^{a} \pm 0.89$	$3.63^{b} \pm 0.09$	$37.28^{b} \pm 0.74$

All values are represented as Mean ± SEM; n=6 in each group; values bearing different superscript in the same column differ significantly at P<0.05.

values in group B (arsenic intoxicated) were significantly (P<0.05) higher than all other groups.

Oxidative stress

The mean values of different antioxidant enzymes are presented in Table 4. LPO (nmol/μL) levels observed was significantly (P<0.05) higher in arsenic intoxicated group B as compared to control group A, *C. limon* group C, and arsenic intoxicated group D supplemented with *Citrus limon*. SOD (U/mg protein) levels were significantly (P<0.05) lower in group B compared to all other groups (A, C, and D);. Additionally, SOD activity in group B was significantly (P<0.05) lower than in groups A, D, but remained higher than in group B. While group D showed significantly higher SOD levels than group A indicating antioxidant effect

Table 5: Mean (Mean ± SEM) values of total sperm count, and number of normal sperms, and abnormal sperms (out of total 200 sperms examined) in mice of different experimental groups.

Groups	Sperm Count ((x10^6 sperm/ml))	Normal	Sperm Head Abnormality Assay				
			Head less tail	Detached head	Pairing phenomena	Amorphous head	Hook less Head
A	36.67^{bc} ± 2.47	183.83^{b} ± 0.60	6.17^{ab} ± 0.31	5.17^{a} ± 0.54	4.82^{a} ± 0.48	0.00^{a} ± 0.00	0.00^{a} ± 0.00
B	26.67^{a} ± 1.67	177.50^{a} ± 0.76	8.50^{b} ± 0.43	6.83^{b} ± 0.60	5.65^{bc} ± 0.56	0.83^{b} ± 0.17	0.67^{b} ± 0.42
C	41.67^{c} ± 4.22	184.50^{b} ± 0.97	5.50^{a} ± 0.43	5.33^{ab} ± 0.40	4.66^{a} ± 0.42	0.00^{a} ± 0.00	0.00^{a} ± 0.00
D	30.83^{ab} ± 3.75	183.33^{b} ± 0.84	4.82^{a} ± 0.48	5.67^{ab} ± 0.56	5.50^{b} ± 0.43	0.50^{a} ± 0.22	0.17^{a} ± 0.17

All values are represented as Mean ± SEM; n=6 in each group; values bearing different superscript in the same column differ significantly at P<0.05.

Fig. 7. Kidney of arsenic intoxicated group B showing marked interstitial inflammatory cell infiltration, mainly in the peritubular and perivascular areas (mainly lymphocytes and some macrophages) (H&E 400X); **Fig. 8.** Arsenic intoxicated *Citrus limon* supplemented group D Kidney section shows marked perivascular mononuclear cell infiltration with congestion and mild tubular epithelial degeneration (H&E 400X); **Fig. 9.** Testes of arsenic intoxicated group B show degeneration of seminiferous tubule characterized by disorganization of germinal epithelium and reduction in mature spermatozoa within the lumen (H&E 400X); **Fig. 10.** Testes of arsenic intoxicated *Citrus limon* supplemented group D show normal testicular structure (H&E 400X); **Fig. 11.** Arsenic intoxicated group B indicates perivascular cuffing, slight increase in small, dark glial nuclei scattered in neuropil (H&E 400X); **Fig. 12.** Arsenic intoxicated *Citrus limon* supplemented group D showing mild clear spaces surrounding neurons and small vessels representing edema (H&E 400X).

of plant extract that led to increased SOD activity and better neutralization of free radicals formed as a result of arsenic toxicity.

Glutathione reductase (μg/mg tissue) activity was significantly lower (P<0.05) in group B compared to groups A, C, and D. Catalase (μg/mg tissue) activity was significantly lower (P<0.05) in group B compared to all other groups. Additionally, catalase activity in groups A, and C, was significantly (P<0.05) higher than in groups B, and D. Similarly, arsenic intoxicated group D supplemented with *C. limon* showed significantly (P<0.05) higher catalase activity compared to arsenic intoxicated group B.

Pathological studies

Control group A and *Citrus limon* group C did not show pathological lesions in any organ. Arsenic exposure (group B) induced mild to moderate gross pathological alterations in liver, lung, heart, kidney, spleen, brain, stomach, intestines and testes. Microscopically, the liver of arsenic intoxicated group B exhibited edema, hepatocellular vacuolation, hydropic degeneration and congested veins, while arsenic intoxicated group D supplemented with *Citrus limon* showed mild changes (Fig. 1and 2). Gastric lesions in group B included mucosal congestion, and hyperkeratoses, these changes were milder in group D (Fig.3 and 4). The intestine of group B revealed mucosal congestion, hemorrhages, focal villus destruction, and lymphocytic infiltration (Fig. 5). These effects were absent in treated groups, which showed normal architecture. Similarly, kidneys of group B showed congestion, tubular degeneration, vacuolization and lymphocytic infiltration (Fig. 6 and 7). Marked perivascular mononuclear cell infiltration with vascular congestion and mild

Table 6. Mean values of polychromatic erythrocytes (PCE), normochromatic erythrocytes (NCE) and micronucleated polychromatic (MNPCE) and micronucleated normochromatic erythrocytes (MNNCE) in mice of different experimental groups

Groups	PCE (%)	NCE (%)	PCE/NCE	MNPCE (%)	MNNCE (%)
A (Control)	$28.57^{b} \pm 1.07$	$71.43^{b} \pm 1.07$	$0.40^{b} \pm 0.02$	$0.16^{a} \pm 0.03$	$0.16^{a} \pm 0.03$
B (SA)	$35.00^{c} \pm 0.34$	$65.00^{a} \pm 0.34$	$0.54^{c} \pm 0.01$	$0.26^{b} \pm 0.03$	$0.29^{b} \pm 0.03$
C (CL)	$26.63^{ab} \pm 1.35$	$73.37^{bc} \pm 1.35$	$0.37^{ab} \pm 0.03$	$0.12^{a} \pm 0.02$	$0.13^{a} \pm 0.02$
D(SA+CL)	$27.73^{ab} \pm 0.90$	$72.27^{bc} \pm 0.90$	$0.38^{ab} \pm 0.02$	$0.15^{a} \pm 0.01$	$0.17^{a} \pm 0.02$

All values are represented as Mean ± SEM; n=6 in each group; values bearing different superscript in the same column differ significantly at P<0.05.

tubular epithelial degeneration and were noted in group D (Fig. 8). Lastly, the testes of group B showed degeneration of seminiferous tubules, characterized by disorganization of germinal epithelium, reduced stratification of spermatogenic cells, marked reduction in mature spermatozoa within the lumen, detached germ cells visible within tubular lumen and slight widening of interstitial spaces (Fig. 9) while group D maintained normal testicular structure (Fig. 10), indicating protective efficacy against arsenic-induced testicular damage. Lung examination revealed congestion, and edema in group B, while groups D had mild changes. Brain of arsenic intoxicated group B, revealed mild cerebral edema and perivascular cuffing, slight increase in small, dark glial nuclei scattered in neuropil (Fig. 11), while group D revealed no marked perivascular cuffing, though clear spaces surrounding neurons and small vessels (Fig. 12) were noticed.

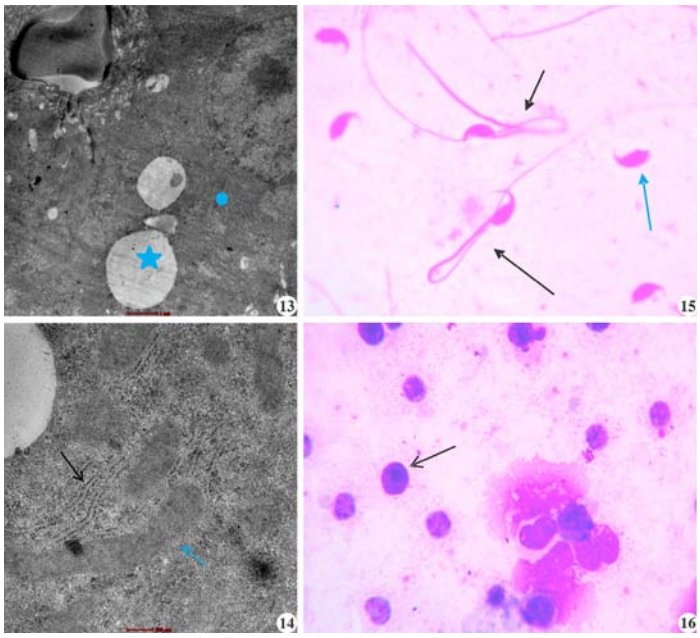

Fig. 13. Arsenic intoxicated group B liver tissue revealed vacuolation in the cytoplasm (*) and unclear mitochondrial cristae and RER (•); **Fig. 14.** Arsenic intoxicated *Citrus limon* supplemented group D the endoplasmic reticulum (ER) showed normal ribosomal attachment, mild mitochondrial swelling and mild vacuolation was observed; **Fig. 15.** Photomicrograph of sperms of group B showing Pairing Phenomena (black arrow) and detached head (blue arrow) (1000X); **Fig. 16.** Bone marrow slide of group B showing polychromatic erythrocytes (PCEs) with moderate basophilia and prominent small, dark purple body consistent with micronuclei (1000X).

Ultrastructural studies

The ultra-structural analysis of arsenic intoxicated group B liver tissue revealed significant cellular alterations, including vacuolation in the cytoplasm indicating hydropic degeneration**,** an irregular nuclear membrane, mitochondrial cristae and intact RER were not clearly defined (Fig. 13). In group D (arsenic intoxicated group supplemented with *Citrus limon*), the endoplasmic reticulum (ER) showed normal ribosomal attachment, mild mitochondrial swelling and mild vacuolation was observed (Fig. 14).

Semen evaluation

Sperm count- The mean values of sperm count of all mice of different experimental groups are presented in Table 5. The sperm count was significantly lower (P<0.05) in arsenic intoxicated group B compared to all other groups A, C and D (arsenic intoxicated group supplemented with *Citrus limon*).

Sperm head abnormality assay (SHA)

The mean value of frequency of sperm head abnormalities in all groups of mice are shown in Table 5. Head-less tail, detached head, amorphous head, and hook-less head was significantly (P<0.05) increased in arsenic intoxicated group B compared to groups A, and C. Pairing phenomena (Fig. 15) were also significantly (P<0.05) higher in group B compared to control D group .

Micronucleus test (MNT)

The mean value of frequency of PCE, NCE and PCE/NCE ratio and mean value of frequency of MNPCE (Fig. 16), and MNNCE of all groups of mice are shown in Table 6. The PCE (%) was significantly (P< 0.05) higher in group B (arsenic intoxicated) compared to all other groups. The NCE (%) was

significantly (P< 0.05) lower in group B as compared to other groups (A, C and D). The PCE/NCE ratio was significantly (P<0.05) higher in group B as compared to the other groups. The percentages of MNPCE, and MNNCE were significantly (P<0.05) increased in group B compared to groups A, C and D.

DISCUSSION

The phytochemical analysis of *C. limon* fruit revealed the presence of flavonoids, terpenoids, and phenolic compounds, similar to other researchers work[17,18]. The phenolic compounds are recognized for their ability to mitigate oxidative damage. These compounds can directly neutralize free radicals or engage with antioxidant enzymes to scavenge them. Additionally, phenolic substances have been shown to contribute to the stabilization of lipid peroxidation. The flavonoids present in *C. limon* also contribute to good free radical scavenging activity of these plants and play a crucial role in mitigating the toxicity of heavy metals in plants. These bioactive compounds act as potent antioxidants, chelating metal ions and reduce oxidative stress induced by metal toxicity and therefore protect cellular structures from damage[19].

Hematological parameters are critical indicators of an animal's health status, providing insights into the physiological impact of intoxication. In the present study, arsenic exposure in Swiss albino mice led to significant hematological alterations, notably a decrease in RBC count and hemoglobin levels, alongside elevated mean corpuscular volume (MCV) and reduced mean corpuscular hemoglobin (MCH) and mean corpuscular hemoglobin concentration (MCHC). These changes suggest arsenic-induced macrocytic hypochromic anemia, likely due to liver dysfunction, disrupted erythropoiesis and oxidative damage to erythrocytes. Ola-Davies and Akinrinde (2016)[20] reported that arsenic inhibits porphyrin and haem synthesis, resulting in decreased hemoglobin and RBC levels.

In contrast, supplemented group showed hematological values comparable to the control group, indicating the protective role of *C. limon* (lemon). Their ameliorative effects are attributed to bioactive compounds such as polyphenols, flavonoids, ascorbic acid, steroidal saponins, and alkaloids.. Lemon juice has been shown to improve RBC count and hemoglobin levels, attributed to its rich antioxidant content[23]. Flavonoids in lemon juice protect hemoglobin from oxidative degradation, and antioxidants mitigate erythrocyte destruction[23].

Arsenic exposure significantly increased total WBC count (P<0.05) in group B compared to other groups, with elevated neutrophil levels, while lymphocytes and other [mid-sized cells (MID) *viz*. Monocyte, eosinophils and basophils)cell counts remained unchanged. These findings suggest an immune response to arsenic toxicity, consistent with previous reports linking arsenic exposure to leukocytosis and immune system activation[24]. The supplemented groups exhibited no significant changes in total and differential leukocyte counts, suggesting immune-protective effects of *C. limon*. Vitamin C, a key constituent of *C. limon*, supports immune function by accumulating in neutrophils and enhancing chemotaxis, phagocytosis, and microbial killing[25].

Biochemical markers of liver and kidney function such as ALT, AST, ALP, creatinine, and urea were significantly elevated in arsenic-exposed mice, indicating hepatocellular damage and renal impairment. These findings were consistent with earlier findings attributing these changes to arsenic-induced oxidative stress, lipid peroxidation, and membrane disruption[26]. Elevated creatinine further confirms nephrotoxicity. Serum total protein and albumin levels were significantly reduced in arsenic-exposed mice, reflecting impaired liver function and possibly increased renal protein loss. These findings corroborated previous studies reporting arsenic-induced hypoproteinemia, likely due to oxidative damage and altered protein metabolism[20]. Additionally, arsenic exposure disrupted lipid metabolism, causing hepatic fat degeneration and elevated serum cholesterol and triglycerides[27]. Arsenic-induced hyperbilirubinemia may result from hemolysis, impaired hepatic uptake, and oxidative modification of bilirubin. In this study, arsenic exposure significantly increased total cholesterol, triglycerides, and total bilirubin levels. Co-treatment with *C. limon* restored serum ALT, AST, ALP, BUN, and creatinine levels to near normal[28].

Arsenic exposure disturbs redox homeostasis by inducing excessive ROS production, resulting in oxidative damage to cells. The arsenic-induced oxidative stress leads to an overproduction of superoxide anion radicals, resulting in a significant reduction in superoxide dismutase (SOD) activity. This reduction causes the down-regulation of SOD2 gene expression, which has been linked to oxidative stress in various tissues. Additionally, reduced SOD and catalase levels indicate a compromised antioxidant defense system, unable to neutralize the excessive ROS generated during arsenic metabolism[29]. Similarly, in the current study the significant decrease (P<0.05) in Superoxide dismutase activity in As-exposed mice group compared to the control group was observed. Arsenic-induced oxidative damage reduces GR activity, impairing GSH regeneration and causing cellular dysfunction[30]. Similarly, in the current study the significant (P<0.05) decrease in glutathione reductase activity in As-exposed mice group compared to the control group was observed. In the present study, a significant decrease (P<0.05) in CAT

activity was observed in arsenic-exposed mice compared to the control group. Arsenic exposure reduces CAT activity by depleting NADPH, which is essential for reactivating CAT from its inactive form during arsenic metabolism. Similar to the present results, Khuntia *et al*. (2023)[31] reported a significant reduction (P<0.05) in CAT activity in arsenic trioxide-treated groups compared to controls[31].

In the present study, *C. limon* reduced the free radical stress by increasing the activity of antioxidant enzymes. Lemon juice exhibits strong antioxidant and hepatoprotective properties due to its rich content of citrate, flavonoids, vitamin C, vitamin E, and limonoids[32]. It restores SOD and CAT activities in pesticide-treated animals, reducing ROS accumulation. Additionally, lemon juice lowers MDA levels and improves glutathione redox status, supporting liver health[33,34].

Arsenic-induced hepatotoxicity primarily results from oxidative stress, leading to cellular injury. Histopathological findings in arsenic-intoxicated animals revealed hepatocyte vacuolation, hydropic degenration, mild haemorrhages, neutrophil infiltration, and vascular congestion. Similar degenerative changes, including vacuolar degeneration, swollen hepatocytes, and bile duct hyperplasia, have also been reported by other researchers[35]. *Citrus limon* significantly mitigated hepatic damage in arsenic intoxicated group D. It preserved hepatocyte integrity, reduced necrosis, and protected against oxidative lipid damage. Renal histology in arsenic-treated mice showed tubular vacuolization, glomerular hyaline degeneration, increased Bowman's space, hemorrhage, and inflammatory infiltration, consistent with previous reports[36]. These changes correlate with biochemical alterations and are attributed to increased glomerular filtration and protein leakage. *C. limon* supplementation reduced renal damage, with near-normal histology observed in group D. The nephroprotective effects are linked to their phenolic content and antioxidant activity. Arsenic intoxicated mice exhibited hyperkeratinization in the stomach mucosa and intestinal villus necrosis with leukocyte infiltration, similar to prior observations. These effects were ameliorated in groups receiving *C. limon*. Vitamin C, abundant in *C. limon*, enhances antioxidant defense and immune function reducing gastrointestinal tissue damage.

Arsenic exposure caused pulmonary congestion, hemorrhage, and inflammation, aligning with previous studies[35]. In arsenic intoxicated and *C. limon* supplemented group D, *C. limon* significantly reduced lung injury. Arsenic neurotoxicity results from ROS-induced oxidative stress, leading to neural degeneration, edema, and inflammation. The brain's vulnerability is intensified by its high oxygen demand and low antioxidant defenses. Histological changes included vacuolar changes and gliosis. Supplementation with *C. limon* reduced these alterations, likely due to their antioxidant properties. Vitamin C has demonstrated neuroprotective effects by preserving brain architecture and reducing oxidative damage[37]. The present study found that *C. limon* supplementation preserved spleen architecture. Histological changes in seminiferous tubules were due to arsenic-induced oxidative stress. These were markedly reduced in antioxidant-supplemented groups, indicating the protective efficacy of *C. limon.*

The ultra-structural analysis of group B liver tissue revealed irregular nuclear membrane and fragmented chromatin, swelling of both mitochondria and rough ER. Additionally, lipid droplet accumulation in the cytoplasm was noted In contrast, group D showed normal ultrastructural features, showing only minor lipid droplet presence, indicating mild cellular injury and apoptotic changes. This mild injury suggests the potential ameliorating effects *Citrus limon* in mitigating arsenic-induced hepatotoxicity.

Arsenic exposure triggers oxidative stress, leading to the generation of reactive oxygen species (ROS) that damage sperm cells. These cells are particularly vulnerable due to their limited cytoplasm and high concentration of unsaturated fatty acids. The combined effects of hormonal imbalance and oxidative stress contribute to sperm abnormalities and DNA damage, ultimately leading to infertility. The histological studies in the present study have revealed that arsenic exposure caused damage to seminiferous tubules. Moreover, arsenic exposure has been reported to induce oxidative stress and damage to spermatogenic cells within the seminiferous tubules and significantly reduce sperm count as reported by other researchers[38,39]. Due to the toxic effects of arsenic, dietary interventions like *Citrus limon* (lemon) has been investigated for its potential protective benefits. The use of this plant showed reduced injury to testes in the present study. Moreover, lemons contain vitamin C, which acts as an antioxidant and supports male reproductive health by maintaining sperm function, testicular integrity, and stimulating testosterone production. Vitamin C enhances sperm concentration, morphology, and motility while protecting sperm from oxidative damage caused by free radicals[40]. It neutralizes ROS, preventing DNA damage and oxidative stress. Additionally, lemon juice contains essential minerals like potassium, calcium, and phosphorus, which play vital roles in sperm motility and testosterone production[41].

Reproductive toxicity is also assessed by evaluating sperm head abnormalities, which is considered one of the most predictive methods for analysing *in-vivo* germ cell genotoxicity. An increase in sperm head abnormalities may result from chromosomal aberrations during the

packaging of genetic material in the sperm head or due to point mutations in testicular DNA. ROS increases genetic material damage in sperm[42]. Ijaz *et al*. (2023)[39] reported increased sperm defects in arsenic-exposed rats, affecting the head, mid-piece, and tail. Similarly, Morakinyo *et al*. (2010)[43] observed a significant rise (P<0.01) in sperm abnormalities in arsenite-treated rats. Furthermore, Kesari *et al*. (2012)[44] observed a significant increase in sperm head abnormalities in male mice due to the genotoxic effects of arsenic exposure.

Presence of micronuclei serves as a key biomarker for chromosomal damage caused by clastogenic or aneugenic mechanisms[45]. Arsenic disrupts normal cellular and mitotic processes, potentially by inhibiting DNA repair mechanisms and interfering with the mitotic spindle apparatus[46]. Its genotoxic effects are largely attributed to the generation of ROS, which trigger oxidative stress and DNA damage[47]. ROS can lead to double-stranded DNA breaks, chromosomal fragmentation, and mitotic spindle disruption, ultimately resulting in the formation of micronuclei (MN)[1]. Sub-chronic arsenic exposure significantly increases micronucleus formation due to its clastogenic potential[48]. A dose-dependent increase in micronucleus formation in polychromatic erythrocytes, further reinforces the link between arsenic exposure and cytogenetic damage[49]. Similarly, in the present study the significant increase (P<0.05) in percentages of micronucleated polychromatic erythrocytes (MNPCE), micronucleated normochromatic erythrocytes (MNNCE) and micronucleated erythrocytes (MNE) was observed in sodium arsenite exposed mice.

CONCLUSION

The present study demonstrates that *Citrus limon* supplementation offers a significant protection against arsenic-induced toxicity in mice. Arsenic exposure caused marked haematological alterations, liver and kidney dysfunction, oxidative stress, tissue damage, and genotoxic effects. Co-administration of *C. limon* effectively ameliorated these adverse changes by improving blood parameters, restoring liver and kidney function markers, enhancing antioxidant enzyme activity, and reducing lipid peroxidation. Additionally, *C. limon* supplementation minimized histopathological and ultrastructural tissue alterations, normalized sperm count, reduced sperm head abnormalities, and decreased micronuclei formation. Overall, *C. limon* exhibits substantial antioxidative and cytoprotective potential, indicating its promise as a protective agent against arsenic-induced systemic toxicity. Long-term exposure models and dose-dependent studies could provide deeper insights into its efficacy and safety profile. Additionally, exploring its protective potential in other animal species and in human populations exposed to arsenic may broaden its applicability. Molecular studies focusing on gene expression, signalling pathways, and epigenetic alterations would further clarify its role in mitigating arsenic-induced oxidative stress, organ damage, and genotoxicity.

ACKNOWLEDGMENT

The authors acknowledge the help of Bhupal Nobels' University for identification of the plant.

Financial support & sponsorship: None.

Conflicts of interest: None.

Use of artificial intelligence (AI)-Assisted Technology for manuscript preparation: The authors confirm that there was no use of AI-assisted technology for assisting in the writing of the manuscript and no images were manipulated using AI.

REFERENCES

1. Jomova K, Jenisova Z, Feszterova M, Baros S, Liska J, Hudecova D, Valko M. 2011. Arsenic: toxicity, oxidative stress and human disease. *J Appl Toxicol* **31(2):** 95-107.
2. Rehman MU, Khan R, Khan A, Qamar W, Arafah A, Ahmad A and Ahmad P. 2021. Fate of arsenic in living systems: Implications for sustainable and safe food chains. *J Hazard Mater* **417:** 126050.
3. Birben E, Sahiner UM, Sackesen C, Erzurum S and Kalayci O. 2012. Oxidative stress and antioxidant defense. *World Allergy Organ J* **5(1):** 9–19.
4. Ponnusha BS, Subramaniyam S and Pasupathi P. 2011. Antioxidant and antimicrobial properties of Glycine max – a review. *Int J Curr Biol Med Sci* **1(2):** 49–62.
5. Maqbool Z, Khalid W, Atiq HT, Koraqi H, Javaid Z, Alhag SK and Al-Farga A. 2023. Citrus waste as source of bioactive compounds: Extraction and utilization in health and food industry. *Molecules* **28(4):** 1636.
6. Roghini R and Vijayalakshmi K. 2018. Phytochemical screening and quantitative analysis of flavonoids and minerals in ethanolic extract of Citrus paradisi. *Int J Pharm Sci Res* **9(11):** 4859–4864.
7. Balamurugan V, Fatima S and Velurajan S. 2019. A guide to phytochemical analysis. *Int J Adv Res Innov Ideas Educ* **5(1):** 236–245.
8. Blois MS. 1958. Antioxidant determinations by the use of a stable free radical. *Nature* **181:** 1199–1250.
9. Fernanda BAP, Cibele MCPG, Patricia PA and Ione S. 2005. Protective action of hexane crude extract of Pterodon emarginatus fruits against oxidative and nitrosative stress induced by acute exercise in rats. *BMC Complement Altern Med* **5:** 17–21.
10. Madesh M and Balasubramanian KA. 1998. Microtiter plate assay for superoxide dismutase using MTT reduction by superoxide. *Indian J Biochem Biophys* **35:** 184–188.
11. Goldberg DM and Spooner RJ. 1983. Assay of glutathione reductase. *Methods Enzym Anal* **3:** 258–265.
12. Aebi HE. 1983. Catalase. *Methods Enzym Anal* **3:** 273–286.
13. Bairy L, Paul V and Rao Y. 2010. Reproductive toxicity of sodium valproate in male rats. *Indian J Pharmacol* **42(2):** 90–94.
14. Boller K and Schmid W. 1970. The Chinese hamster bone marrow as an *in vivo* test system: Hematological findings after

treatment with trenimon. *Humangenetik* **11(1):** 35–54.
15. Heddle JA. 1973. A rapid in vivo test for chromosomal damage. *Mutat Res* **18:** 187–190.
16. Snedecor GW and Cochran WG. 1989. Statistical Methods. Iowa State University Press 1191(2).
17. Ijege KO, Umar I and Suleiman R. 2023. Assessment of mineral contents, phytochemicals and proximate analysis of seeds and peels of *Citrus limon* (lemon). *Niger J Chem Res* **28(1):** 40–50.
18. Anuradha N, Saravana Kumar S, Himabindu N, Gnanavel A and Karthick S. 2024. Quantitative analysis of phytocompounds and GC–MS profiling of methanolic extract of Citrus limon peel. *J Clin Diagn Res* **18(8):** 7–10.
19. Zahra M, Abrahamse H and George BP. 2024. Flavonoids: Antioxidant powerhouses and their role in nanomedicine. *Antioxidants* **13(8):** 922.
20. Ola-Davies OE and Akinrinde AS. 2016. Acute sodium arsenite-induced hematological and biochemical changes in Wistar rats: protective effects of ethanol extract of Ageratum conyzoides. *Pharmacogn Res* **8(1):** S26–S21.
21. Alada ARA, Akande OO and Ajayi FF. 2004. Effect of soya bean diet preparations on hematological and biochemical indices in rats. *Afr J Biomed Res* **7(2):** 71–74.
22. Hu M, Zhou J, Qiu L, Song R, Qin X, Tan Z and Wang X. 2024. Effects of soy protein on alleviating iron deficiency anemia in suckling rats with different iron supplements. *Food Biosci* **61:** 104555.
23. Manthou E, Georgakouli K, Deli CK, Sotiropoulos A, Fatouros IG, Kouretas D and Jamurtas AZ. 2017. Effect of pomegranate juice consumption on biochemical parameters and complete blood count. *Exp Ther Med* **14(2):** 1756–1762.
24. Akter R, Neelotpol S and Kabir MT. 2022. Effect of Allium sativum methanol extract in amelioration of arsenic-induced toxicity in Swiss albino mice. *Phytomed Plus* **2(1):** 100192.
25. Carr AC and Maggini S. 2017. Vitamin C and immune function. *Nutrients* **9(11):** 1211.
26. Norouzzadeh M, Kalantar H, Khorsandi L, Mohtadi S and Khodayar MJ. 2024. Betaine ameliorates arsenic-induced kidney injury in mice by mitigating oxidative stress-mediated inflammation. *Arch Biochem Biophys* **758:** 110076.
27. Chi L, Lai Y, Tu P, Liu CW, Xue J, Ru H and Lu K. 2019. Lipid and cholesterol homeostasis after arsenic exposure and antibiotic treatment in mice: potential role of the microbiota. *Environ Health Perspect* **127(9):** 097002.
28. Kingsley UI, Steven OO, Agu CE, Orji OC, Chekwube BE and Nwosu TF. 2017. Anti-hyperlipidemic effect of crude methanolic extracts of Glycine max in high cholesterol diet-fed albino rats. *J Med Allied Sci* **7(1):** 34–40.
29. Rana T, Bera AK, Bhattacharya D, Das S, Pan D and Das SK. 2012. Chronic arsenicosis in goats: exposure, excretion and deposition in an arsenic-contaminated zone. Environ *Toxicol Pharmacol* **33(2):** 372–376.
30. Nithyananthan S and Thirunavukkarasu C. 2019. Arsenic trioxide delays hepatic regeneration by oxidative stress and hepatocyte apoptosis in partially hepatectomized rats. *Toxicol Appl Pharmacol* **382:** 114760.
31. Khuntia G, Dash JR, Jena B, Mishra UK and Parija SC. 2023. Hesperidin attenuates arsenic trioxide-induced cardiac toxicity in rats. *Asian Pac J Trop Biomed* **13(4):** 156–164.
32. Yu J, Wang L, Walzem RL, Miller EG, Pike LM and Patil BS. 2005. Antioxidant activity of citrus limonoids, flavonoids and coumarins. *J Agric Food Chem* **53(6):** 2009–2014.
33. Haidari F, Mohammad Shahi M, Zarei M and Fathi M. 2019. Protective effect of Citrus limon on inflammation and adipokine levels in acrylamide-induced oxidative stress in rats. *Braz J Pharm Sci* **55:** 18285.
34. Ndefo JC, Okagu IU, Chiazor CC and Aham EC. 2021. A polyherbal formulation reverses hydrogen peroxide-induced hematological and biochemical aberrations in rats. *Indian J Trad Know* **20(4):** 927–933.
35. Himat K, Kumari M, Purohit K, Singh G, Rathore A, Daranga D, Poonam P, Khatik PC, Rolania S and Katara S. 2023. Pathological changes in experimentally induced arsenic toxicity in mice and its amelioration with Aegle marmelos. *Indian J Vet Pathol* **47(4):** 319–324.
36. Thangapandiyan S, Ramesh M, Miltonprabu S, Hema T, Jothi GB and Nandhini V. 2019. Sulforaphane attenuates arsenic-induced nephrotoxicity via the PI3K/Akt/Nrf2 pathway in Wistar rats. *Environ Sci Pollut Res* **26(12):** 12247–12263.
37. Chahrazed M, Hassina KO, Soumya B, Yasmine O, Houda Z and Nacira DZ. 2021. Protective effects of vitamin C on ivermectin-induced toxicity in kidney and brain tissues of rabbits. *Egypt Acad J Biol Sci D Histol Histochem* **13(1):** 63–77.
38. Niraj PK, Singh RV, Shankar P, Ghosh AK and Kumar A. 2024. Protective and antidote effect of Foeniculum vulgare against sodium arsenite-induced hepatotoxicity and testicular toxicity in Charles Foster rats. *J Adv Zool* **45(3):** 360–372.
39. Ijaz MU, Haider S, Tahir A, Afsar T, Almajwal A, Amor H and Razak S. 2023. Protective effects of fisetin against arsenic-induced reproductive toxicity in male rats. *Sci Rep* **13(1):** 3080.
40. Noorul H, Mujahid M, Khalid M, Vartika S, Nesar A, Zafar K and Zohrameena S. 2017. Physico-phytochemical analysis and estimation of phenolic, flavonoid and proanthocyanidin content of Persea americana seed extracts. *World J Pharm Sci* **5(4):** 70–77.
41. Hamad AWR, Al-Daghistani HI, Shquirat WD, Abdel-Dayem M and Al-Swaifi M. 2014. Sodium, potassium, calcium and copper levels in seminal plasma and their association with sperm quality. *Biochem Pharmacol* **3(4):** 1–7.
42. Das S, Langthasa P, Barhoi D, Upadhaya P and Giri S. 2018. Effect of nutritional status on arsenic- and smokeless tobacco-induced genotoxicity, sperm abnormality and oxidative stress in mice. *Environ Mol Mutagen* **59(5):** 386–400.
43. Morakinyo AO, Achema PU and Adegoke OA. 2010. Effect of Zingiber officinale on sodium arsenite-induced reproductive toxicity in male rats. *Afr J Biomed Res* **13(1):** 39–45.
44. Kesari VP, Kumar A and Khan PK. 2012. Genotoxic potential of arsenic at its reference dose. *Ecotoxicol Environ Saf* **80:** 126–131.
45. Ambasta SK, Trivedi I, Kumari S, Kumar A, Verma P, Prasad B and Sinha UK. 2017. Anticlastogenic effects of *Tinospora cordifolia* against arsenic-induced genotoxicity using micronucleus assay in Swiss albino mice. *IOSR J Environ Sci Toxicol Food Technol* **11(1):** 97–100.
46. Aposhian HV and Aposhian MM. 2006. Arsenic toxicology: five questions. *Chem Res Toxicol* **19(1):** 1–15.
47. Dopp E, von Recklinghausen U, Diaz-Bone R, Hirner AV and Rettenmeier AW. 2010. Cellular uptake, subcellular distribution and toxicity of arsenic compounds in methylating and non-methylating cells. *Environ Res* **110(5):** 435–442.
48. Kaushal S, Ahsan AU, Sharma VL and Chopra M. 2019. Epigallocatechin gallate attenuates arsenic-induced genotoxicity via regulation of oxidative stress in BALB/C mice. *Mol Biol Rep* **46(5):** 5355–5369.
49. Patlolla AK and Tchounwou PB. 2005. Cytogenetic evaluation of arsenic trioxide toxicity in Sprague–Dawley rats. *Mutat Res Genet Toxicol Environ Mutagen* **587(1–2):** 126–133.

50. Central Ground Water Board, Ministry of Jal Shakti, Department of Water Resources, River Development and Ganga Rejuvenation, Government of India. Retrieved June 10, 2024 from https://cgwb.gov.in/sites/default/files/inline-files/districts-contamination.pdf
51. Chakraborti D, Singh SK, Rahman MM, Dutta RN, Mukherjee SC, Pati S and Kar PB. 2018. Groundwater arsenic contamination in the Ganga River Basin: a future health danger. *Int J Environ Res Public Health 15(2):* 180.
52. Nohara K, Suzuki T and Okamura K. 2020. Gestational arsenic exposure and paternal intergenerational epigenetic inheritance. *Toxicol Appl Pharmacol* **409:** 115319.
53. Lillie RD. 1965. Histopathological technique and practical histochemistry, Mc Graw Hill Book Co., New York and London, pp. 616-617.
54. Luna G. 1968. Manual of histologic staining methods of the Armed Forces Institute of Pathology, 3rd Edition. McGraw Hill Book Company, New York, pp. xii-258.
55. Karnovsky MJ. 1965. A formaldehyde–glutaraldehyde fixative of high osmolality for use in electron microscopy. *J Cell Biol* **27:** 137A–138A.
56. Hayat MA. 1981. Principles and Techniques of Electron Microscopy: Biological Applications. Vol. 1. CRC Press.
57. Watson ML. 1958. Staining of tissue sections for electron microscopy with heavy metals. *J Biophys Biochem Cytol* **4:** 475–478.

Indian J. Vet. Pathol., 50(2) : 143-149, 2026: DOI: https://doi.org/10.56093/7mp01m36

RESEARCH ARTICLE

Toxicopathological assessment revealed expanded tissue tropism of fipronil in experimental Wistar albino rats

Nakul P., K. Sujatha[1*], A. Anand Kumar and S. Vijayalakshmi[2]

Department of Veterinary Pathology, College of Veterinary Science, Sri Venkateswara Veterinary University, Tirupati- 517502, Andhra Pradesh

[1]Centre for Continuing Veterinary Education and Communication, SVVU, Tirupati

[2] Professor& Head, Department of Veterinary Microbiology, CVSc, Proddatur

***Address for correspondence**

K. Sujatha, Coordinator, Centre for Continuing Veterinary Education and Communication, SVVU, Tirupati, E-mail: karamalasujatha@gmail.com

Received: 3.1.26; Accepted: 27.1.26

ABSTRACT

Fipronil is a widely used phenylpyrazole insecticide known primarily for its neurotoxic action, however, increasing evidence suggests that its toxic effects extend beyond the nervous system in non-target mammals. The present study was undertaken to evaluate the expanded tissue tropism of fipronil in Wistar albino rats with particular emphasis on organs that have received limited attention in earlier studies. Twenty-four healthy male Wistar albino rats were randomly divided into four groups (n = 6). Group I served as control, Group II received fipronil (10 mg/kg) orally for 45 days, Group III received *Punica granatum* peel extract (200 mg/kg) alone, and Group IV received *Punica granatum* concurrently with fipronil. Histopathological evaluation of fipronil treated rats revealed distinct toxic alterations in multiple organs, including the heart, spleen, pancreas, adrenal glands, thymus, lymph nodes and gastrointestinal tract. Cardiac lesions were characterized by myocardial degeneration, inflammatory infiltration and fibroblastic proliferation and lymphoid organs exhibited lymphoid depletion and vascular congestion indicating immunosuppressive effects. Pancreatic tissue showed ductular hyperplasia, acinar degeneration and islet atrophy. Intestinal and gastric sections revealed mucosal degeneration, inflammatory infiltration and villous disruption, while adrenal glands demonstrated cortical vacuolar degeneration and medullary haemorrhages. In contrast, rats receiving *Punica granatum* supplementation along with fipronil showed marked attenuation of these lesions, with near-normal histoarchitecture in most tissues. The findings of the present study demonstrate that fipronil exhibits expanded tissue tropism involving cardiovascular, immune, endocrine and gastrointestinal systems in rats. These results highlight the need for comprehensive multisystem toxicological evaluation of fipronil in non-target organisms.

Keywords: Adrenal, fipronil, heart, pancreas, *Punica granatum,* wistar rats

How to cite this article : Nakul P., Sujatha, K.; Kumar, A.A. and Vijayalakshmi, S. 2026. Toxicopathological assessment revealed expanded tissue tropism of fipronil in experimental Wistar albino rats. Indian J. Vet. Pathol., 50(2) : 143-149.

INTRODUCTION

Over the past several decades, numerous arthropod species have progressively developed resistance to conventional insecticides[1]. This growing resistance necessitated the development and global introduction of newer insecticidal compounds, including fipronil (FIP). Fipronil is a synthetic, second-generation phenylpyrazole insecticide that primarily targets the central nervous system of invertebrates[2]. Nevertheless, evidence suggests that FIP may also exert effects on other physiological systems, such as the reproductive system, as documented in ticks[3]. As a phenylpyrazole class insecticide, fipronil (FIP) exerts its toxic effects by inhibiting γ-aminobutyric acid (GABA) gated receptors and by promoting oxidative stress through the excessive generation of reactive oxygen species[4,5,6]. Fipronil may exert adverse effects beyond its primary neurotoxic action by targeting non-neuronal organs such as the liver, kidney, thyroid, and by disrupting reproductive functions in non-target species[6]. Chronic exposure to fipronil in rats has been shown to predominantly affect the liver, kidney, and thyroid, where marked toxic alterations were observed[7]. Additionally, short-term fipronil exposure has been reported to induce oxidative stress in the kidney, brain, and liver of mice[11].

Although it primarily exerts its insecticidal action by blocking γ-aminobutyric acid (GABA) gated chloride channels in invertebrates, increasing evidence suggests that FIP is not selectively neurotoxic and can adversely affect multiple organ systems in non-target mammals[8,9]. Experimental studies have demonstrated that FIP exposure induces oxidative stress, mitochondrial dysfunction and apoptotic signalling, mechanisms that may contribute to its systemic toxicity[10]. Among mammalian organs, the liver has been identified as a major target of FIP toxicity, with several rodent studies reporting hepatotoxic effects following acute, sub-chronic and chronic exposure[11,12]. Similarly,

nephrotoxicity has been consistently documented, indicating that the kidney is highly susceptible to FIP induced oxidative and metabolic disturbances[13,14]. Neurotoxicity remains one of the most well-established outcomes of FIP exposure, affecting both central and peripheral nervous systems[15,16], while pulmonary involvement has also been described in experimental models[17]. Collectively, these findings indicate that FIP exhibits a broad toxicological profile rather than being restricted to neural tissues. In contrast, information regarding the effects of FIP on other vital tissues involved in cardiovascular function, immune regulation, endocrine balance and metabolism is sparse. Organs such as the heart, spleen, adrenal glands, thymus, pancreas and gastrointestinal tract play critical roles in maintaining physiological homeostasis, and toxic insults to these tissues may have far-reaching systemic consequences[18,19]. However, systematic toxicopathological evaluations of these organs following FIP exposure are lacking.

In this context, the present study was undertaken to investigate the expanded tissue tropism of FIP in Wistar rats by examining its potential toxic effects on the heart, spleen, adrenal glands, thymus, pancreas and gastrointestinal tract. By focusing on these relatively under-explored tissues, the study aims to provide a more comprehensive understanding of fipronil induced multisystem toxicity and to bridge existing gaps in the toxicological assessment of this widely used insecticide.

MATERIALS AND METHODS

Source and Management of Experimental Animals and Test Compounds

Healthy male Wistar albino rats weighing between 100 and 120 g were utilized for the present investigation. The animals were obtained from Sri Venkateshwara Enterprises, Bengaluru. Following procurement, the rats were allowed a two-week acclimation period before initiation of the experimental protocol. Animals were maintained in polypropylene cages under controlled environmental conditions, with three rats housed per cage. The animal room temperature was regulated at 25 ± 1 °C, and a consistent 12-hour light and 12-hour dark photoperiod was maintained throughout the six-week study duration. Standard laboratory animal feed and potable water were provided ad libitum, and appropriate hygienic and management practices were followed in accordance with laboratory animal care guidelines. The test toxicant, fipronil (technical grade, 99% purity; Batch No. FIP92B5266), was sourced from Gharda Chemicals Ltd. The *Punica granatum* (pomegranate) peel extract used in the study (Product code: Dadim LC23030077) was procured from Chemiloids Life Science Pvt. Ltd., Andhra Pradesh

Ethical approval: Prior approval for the experimental design was obtained from the Institutional Animal Ethics Committee (IAEC approval No. 281/GO/ReBi/S/2000/CPCSEA/CVSc/TPTY/010/Veterinary Pathology/2023, dated 08-05-2023), and all procedures were conducted in compliance with CPCSEA regulations.

Experimental design: Twenty-four clinically healthy young male Wistar albino rats were enrolled in the study and randomly allocated into control and treatment groups. The animals were divided into four experimental groups, each comprising six rats. Fipronil was administered orally by gavage, using distilled water as the vehicle, once daily throughout the 45-day experimental period. The experimental grouping and dosage regimen followed in the present investigation are depicted below. All rats were maintained for 6 weeks and animals were sacrificed by overdose of inhalational

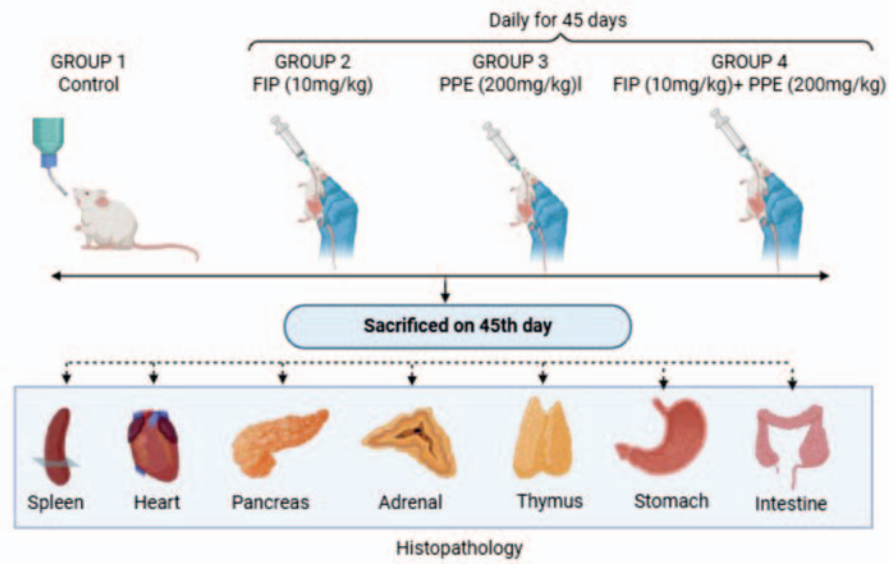

Elements of this figure were created using Biorender.com

anaesthetic agent in a closed chamber at the end of the research study (45th day).

Histopathology

A comprehensive postmortem examination was carried out on all animals sacrificed from each experimental group. Representative tissue samples from the heart, spleen, pancreas, intestine, thymus, lymph nodes and gastro-intestinal systems were collected and fixed in 10% neutral buffered formalin for histopathological evaluation. The fixed tissues were routinely processed using the paraffin embedding technique. Tissue sections of 5–6 μm thickness were prepared and stained with Haematoxylin and Eosin (H&E) following standard procedures[20]. Special histochemical stains were applied wherever required to aid in diagnosis.

RESULTS

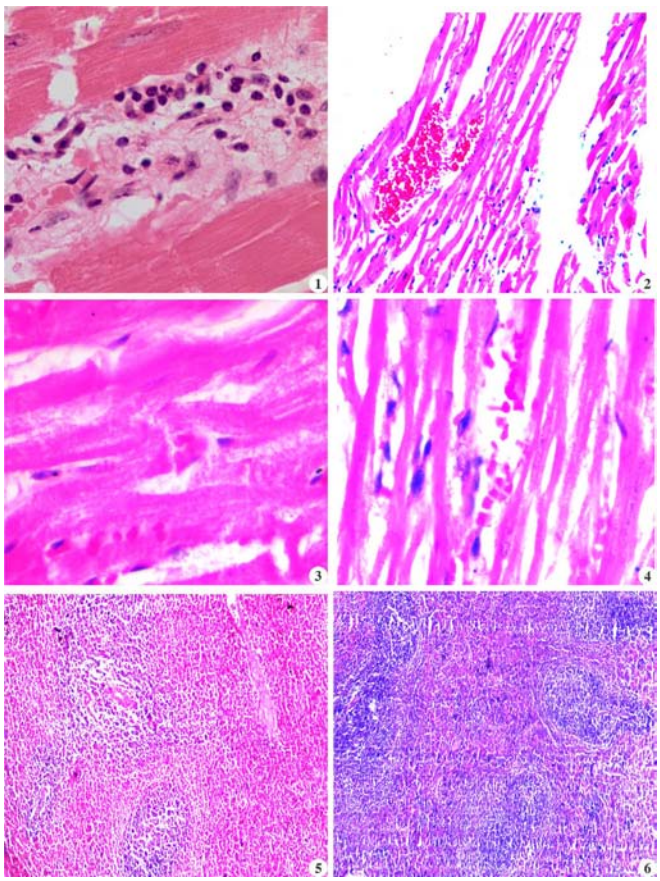

Fig. 1. Heart: Group II: showing mixed inflammatory cell infiltration and fibrin in the cardiac interstitium. H&E X400; **Fig. 2.** Heart: Group II: Section showing pockets of hemorrhages in between cardiac muscle fibres. H&E X100; **Fig. 3.** Heart: Group II: Section showing swollen and granular cytoplasm of cardiac muscle fibres. H&E X400; **Fig. 4.** Heart: Group II: Note reduced thickening of cardiac muscle fibres. H&E X400; **Fig. 5.** Spleen: Group II: Section showing mild to moderate depletion of lymphocytes in the white pulp. H&E X40; **Fig. 6.** Spleen: Group IV: Section showing normal appearance of white pulp and presence of more lymphoid follicles. H&E X40

At the completion of the experimental duration (sixth week), rats belonging to the control group (Group I) and the *Punica granatum* control group (Group III) did not exhibit any gross or histological alterations of pathological relevance. In contrast, histological examination of the heart in Group II (fipronil-treated) rats revealed moderated mononuclear inflammatory cell infiltration, proliferation of fibroblasts (Fig. 1), and focal interstitial haemorrhages between cardiac muscle bundles (Fig. 2). Additionally, several regions showed swollen myocardial fibres with granular cytoplasm and features consistent with coagulative necrosis (Fig. 3). In

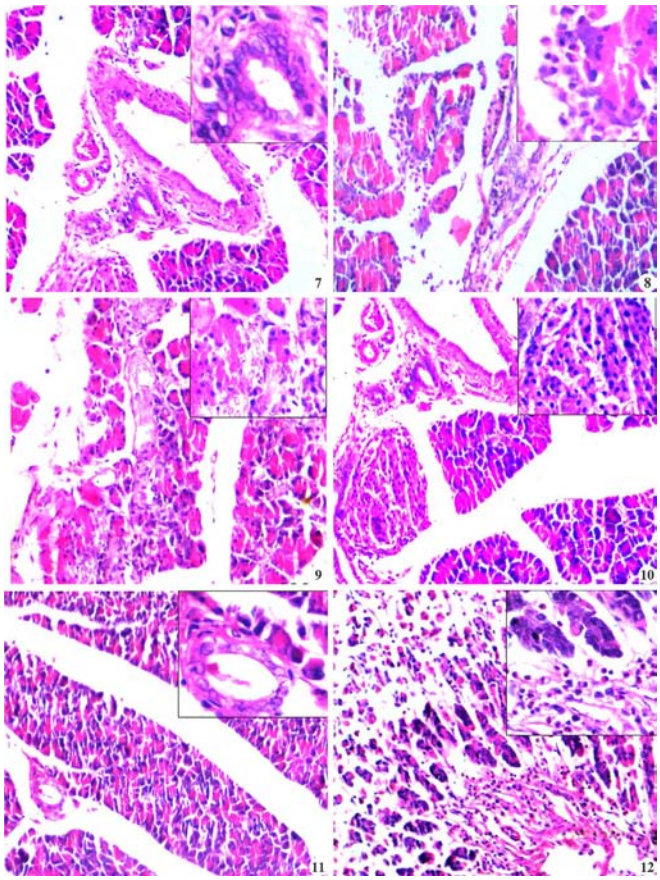

Fig. 7. Pancreas: Group II: Note thickened interlobular ducts with fibrous tissue deposition and hyperplasia of ductular epithelium. H&E X100, (Insight microphotograph X400); **Fig. 8.** Pancreas: Group II: Section showing infiltration of eosinophils and MNC's in inter-acinar spaces. H&E X100, (Insight microphotograph X400); **Fig. 9.** Pancreas: Group II: Section showing degenerated and complete architectural loss of pancreatic acini with replacement of acinar cells by fibrous tissue and MNC's. H&E X100 (Insight microphotograph X400); **Fig. 10.** Pancreas: Group II: Section showing congestion and degeneration with focal loss of islets of Langerhans. H&E X100 (Insight microphotograph x 400); **Fig. 11**. Pancreas: Group IV: Section showing normal appearance of lining epithelium of pancreatic ducts. H&E X100 (Insight microphotograph X400); **Fig. 12.** Stomach: Group II: Section showing moderate degenerative changes with desquamation of mucosal lining and severe infiltration of inflammatory cells mainly eosinophils in mucosa. H&E X100 (Insight microphotograph X400)

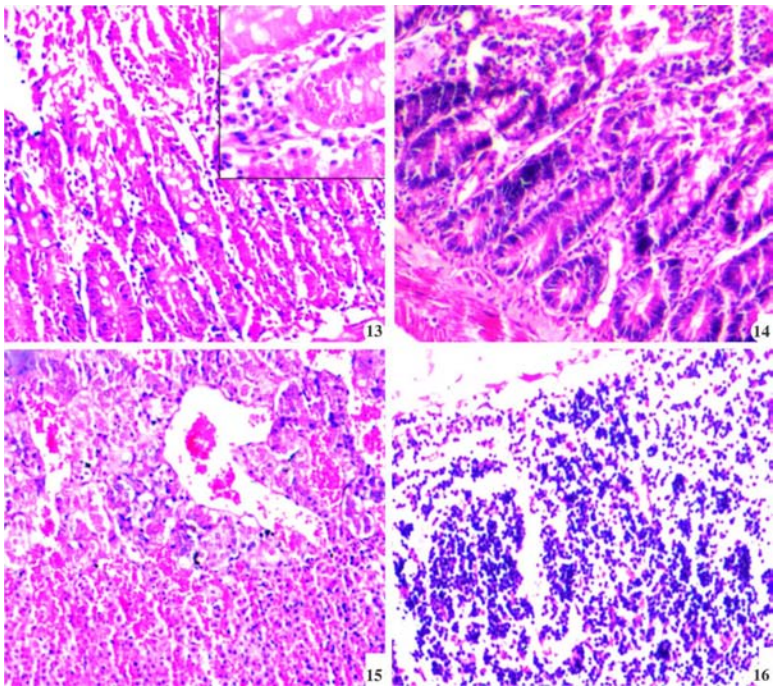

Fig. 13. Intestine: Group II: Section showing increased number of goblet cells in the mucosa and severe infiltration of eosinophils and MNC's in submucosa. H&E X100 (Insight microphotograph X400); **Fig. 14.** Intestine: Group IV: Section showing mild degenerative changes and less MNC's infiltration in the villous structure. H&E X100; **Fig. 15.** Adrenal: Group II: Section showing congestion and haemorrhages in adrenal medulla. H&E X100; **Fig. 16.** Lymph node: Group II: Section showing mild to moderate depletion of lymphocytes in the cortex. H&E X100.

a few animals, myocardial atrophy characterized by thinning of muscle fibres and expansion of intermuscular spaces was evident (Fig. 4). Mild to moderate sarcolytic degeneration accompanied by fibroblastic proliferation was also observed, along with congestion and thickening of myocardial blood vessels, which became more pronounced by the end of the sixth week. Conversely, the cardiac tissue of Group IV (ameliorated) rats exhibited only mild degenerative alterations, minimal haemorrhage, and slight inflammatory infiltration, with an overall preservation of myocardial architecture. The heart of *Punica granatum* treated rats displayed normal histomorphology comparable to that of control animals.

Microscopic evaluation of the spleen in fipronil-exposed rats demonstrated mild to moderate lymphoid depletion within the white pulp (Fig. 5), prominence of splenic trabeculae, and congested, thickened blood vessels at the end of the experimental period. In the ameliorated group, similar splenic changes were present but with reduced severity, including mild lymphocytolysis, minimal congestion, reactive hyperplasia of the white pulp, and an increased number of lymphoid follicles. The splenic architecture in *Punica granatum* treated rats remained comparable to that observed in the control group (Fig. 6).

Histopathological examination of the pancreas in Group II animals revealed thickening of interlobular ducts with deposition of fibrous connective tissue, ductular epithelial hyperplasia (Fig. 7), vascular congestion, and infiltration of eosinophils and mononuclear cells within the inter-acinar regions (Fig. 8). The islets of Langerhans showed prominent congestion, degenerative alterations, and atrophy in most animals (Fig. 9). Multifocal areas exhibited moderate to severe degeneration of pancreatic acini with disruption of normal lobular architecture, wherein acinar cells were replaced by fibrous tissue and inflammatory cells (Fig. 10). Intralobular ductular hyperplasia was consistently noted in all fipronil-treated rats. The pancreas of Group IV rats showed similar lesions but of lesser magnitude, characterized by mild acinar degeneration with preservation of normal ductal structures and islets. Pancreatic sections from *Punica granatum* treated rats appeared histologically normal and comparable to controls (Fig. 11).

Examination of the stomach in fipronil-treated rats showed moderate degenerative changes, sloughing of the gastric mucosal epithelium, and intense inflammatory cell infiltration predominantly eosinophils within the mucosal glands. These alterations were also observed in the ameliorated group but with diminished severity (Fig. 12). Microscopic assessment of the intestine in Group II rats revealed marked goblet cell hyperplasia within the mucosa, dense infiltration of eosinophils and mononuclear cells between the mucosal glands, and focal necrosis of the mucosal layer (Fig. 13). Structural disruption and desquamation of intestinal villi were also evident by the end of the sixth week. The ameliorated group exhibited similar intestinal lesions but with noticeably reduced intensity. Intestinal histology of *Punica granatum* treated rats was comparable to that of the control group (Fig. 14).

Histological examination of the adrenal glands in fipronil-exposed rats demonstrated vacuolar degeneration within the adrenal cortex, along with congestion and focal haemorrhages in the medulla (Fig. 15). The ameliorated group showed similar adrenal changes, albeit milder in nature. Lymph nodes from Group II rats exhibited mild to moderate cortical lymphoid depletion and vascular congestion, while the ameliorated group displayed the same lesions with reduced intensity (Fig. 16). Thymic sections from fipronil-treated animals showed mild

to moderate haemorrhages and congestion of blood vessels, whereas the ameliorated group demonstrated comparable but less pronounced changes.

DISCUSSION

In the current study, histological evaluation of the cardiac tissue in most fipronil exposed rats showed moderate mononuclear inflammatory infiltration, fibroblastic proliferation, focal hemorrhages and swollen myocardial fibers exhibiting granular cytoplasm. Sarcolytic degeneration and necrotic alterations, along with focal fibroblast proliferation were consistently observed. In addition, myocardial atrophy characterized by thinning of muscle fibers and widening of intermyocardial spaces was evident in all treated animals. Comparable myocardial alterations following fipronil exposure have been reported in earlier studies[18,22]. These pathological changes may be attributed to mitochondrial dysfunction in cardiomyocytes, resulting from excessive mitochondrial reactive oxygen species (ROS) generation, loss of mitochondrial membrane potential, and subsequent release of cytochrome-c, ultimately leading to cardiomyocyte injury [18]. Rats belonging to the *Punica granatum* ameliorated group (Group IV) exhibited only minimal histological alterations in the heart when compared with the fipronil-treated group (Group II). This protective effect may be associated with the potent antioxidant and free radical scavenging properties of *Punica granatum* [23,24,25,26], which likely neutralize excess ROS generated within cardiac mitochondria and thereby mitigate oxidative damage to myocardial tissue.

Microscopic examination of the spleen from fipronil treated rats revealed mild to moderate lymphoid depletion in the white pulp, prominence of trabecular structures, and marked vascular congestion with thickened vessel walls. These findings corroborate earlier findings in the literature[19,27,28]. The observed lymphocytolytic changes may be linked to the immunosuppressive action of fipronil on lymphoid tissues. Fipronil induced ROS can directly damage cellular lipids, proteins, and DNA in immune cells, while also activating stress responsive intracellular signalling pathways that compromise immune function[29].

In the *Punica granatum* supplemented group, similar splenic alterations were evident but with markedly reduced severity when compared to the fipronil only group. This improvement may be attributed to the immunomodulatory potential [30] and antioxidant capacity of *Punica granatum*[23-26.]

Histopathological assessment of the pancreas in fipronil treated rats showed thickening of interlobular ducts due to fibrous tissue deposition, hyperplasia of ductular epithelium, vascular congestion, and infiltration of eosinophils within inter-acinar spaces. The islets of Langerhans exhibited degenerative and atrophic changes. Marked disruption of pancreatic acinar architecture was evident, with extensive degeneration and replacement of acinar structures by fibrous tissue and desquamated epithelial cells. Hyperplasia of intralobular ductular epithelium was consistently observed across all treated animals. As comparable reports were unavailable in the literature, these pancreatic alterations are likely attributable to the direct cytotoxic effects of fipronil. In contrast, pancreatic tissue from the ameliorated group appeared largely preserved and near normal when compared with fipronil fed rats.

Microscopic examination of the intestine in fipronil exposed rats revealed severe necrosis of intestinal villi, loss and desquamation of villous architecture, goblet cell hyperplasia, and dense infiltration of eosinophils and mononuclear cells between mucosal glands. Similarly, gastric sections showed moderate degenerative alterations, sloughing of the mucosal epithelium, and intense inflammatory cell infiltration predominantly eosinophils at the base of mucosal glands. Due to the absence of comparable studies in the literature, these findings could not be directly correlated. However, only minimal histological changes were observed in the intestine and stomach of *Punica granatum* ameliorated rats, which may be attributed to its established anti-inflammatory properties[31].

In the present study, adrenal sections from Group II rats demonstrated vacuolar degeneration of the adrenal cortex along with hemorrhages within the medulla. As no comparable reports were available, these findings appear novel. The adrenal glands of ameliorated rats showed near to normal histological features by the end of the experimental period. Microscopic evaluation of lymph nodes from fipronil treated animals revealed mild to moderate cortical lymphocyte depletion accompanied by vascular congestion, consistent with previous findings[19]. These alterations may result from fipronil induced immunosuppression and oxidative injury to immune cells[29]. Although similar lesions were observed in the ameliorated group, their severity was considerably reduced, possibly due to the immunomodulatory effects of *Punica granatum*[30]. Histological examination of the thymus in Group II animals showed mild to moderate hemorrhages and congestion of blood vessels. In the absence of comparable literature, these findings could not be directly contrasted. However, the ameliorated group exhibited similar thymic changes with reduced severity, which may again be attributed to the immunomodulatory action of *Punica granatum*[30.]

CONCLUSION

The present toxicopathological study clearly demonstrates that fipronil is not restricted to neurotoxicity but exhibits expanded tissue tropism affecting the cardiovascular, immune, endocrine, pancreatic, and gastrointestinal systems in Wistar albino rats following sub-chronic exposure. The consistent histological alterations observed in the heart, spleen, pancreas, adrenal glands, thymus, lymph nodes, and gastrointestinal tract indicate a broad multisystem toxic potential of fipronil, likely mediated through oxidative stress–induced cellular and mitochondrial damage. Importantly, concurrent administration of *Punica granatum* peel extract significantly attenuated the severity of these lesions, suggesting its protective antioxidant and immunomodulatory role. These findings underscore the necessity for comprehensive multisystem toxicological evaluation of fipronil in non-target mammals and highlight the potential of *Punica granatum* as a natural ameliorative agent against fipronil-induced toxicity.

ACKNOWLEDGEMENTS

The authors are thankful to the Sri Venkateswara Veterinary University, Tirupati for providing various facilities to carry out the present research work.

Financial support & sponsorship: None

Conflicts of Interest: None

Use of Artificial Intelligence (AI)-Assisted Technology for manuscript preparation: The authors confirm that there was no use of AI-assisted technology for assisting in the writing of the manuscript and no images were manipulated using AI.

REFERENCES

1. Awad MA, Ahmed ZSO, AbuBakr HO, Elbargeesy GAEFH and Moussa MH. 2021. Fipronil induced oxidative stress in neural tissue of albino rat with subsequent apoptosis and tissue reactivity. *Acta Histochemica* **123**: 151764.
2. De Oliveira PR, Bechara GH, Denardi SE, Oliveira RJ and Mathias MIC. 2012. Genotoxic and mutagenic effects of fipronil on mice. *Exp Toxicol Pathol* **64**: 569-573.
3. Oliveira PR, Bechara GH, Morales MAM and Mathias MIC. 2009. Action of the chemical agent fipronil on the reproductive process of semi-engorged females of the tick Rhipicephalus sanguineus. *Food Chem Toxicol* **47**: 1255-1264.
4. Vidau C, Gonzalez RA, Nisosantano M, Gomezsanchez R and Fuentes. 2011. Fipronil is a powerful uncoupler of oxidative phosphorylation that triggers apoptosis in human neuronal cell line SH-SY5Y. *Neurotoxicol* **32**: 935-943.
5. Hussain R, Khan A, Mahmood F, Rehan S and Ali F. 2014. Clinico-hematological and tissue changes induced by butachlor in male Japanese quail (Coturnix japonica). *Pestic Biochem Physiol* **109**: 58-63.
6. Khan S, Jan MH, Kumar D and Telang AG. 2015. Firpronil induced spermotoxicity is associated with oxidative stress, DNA damage and apoptosis in male rats. *Pestic Biochem Physiol* **124**: 8-14.
7. Badgujar PC, Pawar NN, Chandratre GA, Telang AG and Sharma AK. 2015. Fipronil induced oxidative stress in kidney and brain of mice: protective effect of vitamin E and vitamin C. *Pestic Biochem Physiol* **118**: 10-18.
8. Bharatiya R, Chagraoui A, De Deurwaerdere S, Argiolas A, Melis MR, Sanna F and De Deurwaerdere P. 2007. Chronic administration of fipronil heterogeneously alters the neurochemistry of monoaminergic systems in the rat brain. *Int J Mol Sci* **21**: 5711.
9. Gunasekara AS, Truong T, Goh KS, Spurlock F and Tjeerdema RS. 2007. Environmental fate and toxicology of fipronil. *J Pest Sci* **32**: 189-199.
10. Ortiz-Ortiz MA, Morán JM, González-Polo RA, Niso-Santano M, Soler G, Bravo-San Pedro JM and Fuentes JM. 2009. Nitric oxide-mediated toxicity in paraquat exposed SH-SY5Y cells: a protective role of 7-nitroindazole. *Neurotox Res* **16:** 160-173.
11. Badgujar PC, Chandratre G, Pawar NN, Telang AG and Kurade NP. 2016. Fipronil induced oxidative stress involves alterations in SOD1 and catalase gene expression in male mice liver: protection by vitamins E and C. *Environ Toxicol* **31**: 1147-1158.
12. Da Cunha ELR, da Silva Matos R, Pereira NRC, de Oliveira PR, Daemon E and Camargo-Mathias MI. 2017. Histopathological changes in the liver and thyroid of mice caused by the acaricides fipronil and thymol. *J Histol Histopathol* **4**: 9.
13. Khalaf AA, Ibrahim MA, Galal MK, Abdallah AA, Mansour R and Afify MM. 2020. Protective effects of Terminalia laxiflora extract on hepato-nephrotoxicity induced by fipronil in male rats. *Environ Sci Pollut Res* **27**: 39507-39515.
14. Abou-Zeid SM, Tahoun EA and AbuBakr HO. 2021. Ameliorative effects of jojoba oil on fipronil-induced hepatorenal and neurotoxicity: antioxidant status and apoptotic marker expression in rats. *Environ Sci Pollut Res* **28**: 25959-25971.
15. Nakul P, Sujatha K, Kumar AA, Lekshmi S and Vijayalakshmi S. 2025. Ameliorative potential of *Punica granatum* peel extract against fipronil induced neuronal toxicity in male Wistar albino rats. *Indian J Vet Pathol* **49**: 224-231.
16. Elshony N, Nassar AM, El-Sayed YS, Samak D, Noreldin A, Wasef L and Shaheen HM. 2021. Ameliorative role of cerium oxide nanoparticles against fipronil impact on brain function, oxidative stress and apoptotic cascades in albino rats. *Front Neurosci* **15**: 651471.
17. Nakul P, Sujatha K, Anand Kumar A and Vijayalakshmi S. 2025. Protective effects of pomegranate peel extract against fipronil-induced lung toxicity in Wistar albino rats. *J Vet Anim Sci* **56**: 476-481.
18. Seydi E, Mehrpouya L, Sadeghi H, Rahimi S and Pourahmad J. 2021. Luteolin attenuates fipronil-induced neurotoxicity through reduction of ROS-mediated oxidative stress in rat brain mitochondria. *Pestic Biochem Physiol* **173**: 104785.
19. Aldayel TS, Abdel-Rahman HG, El-Hak HNG, Abdelrazek HM, Mohamed RM and El-Sayed RM. 2021. Modulatory activity of *Uncaria tomentosa* extract against fipronil immunotoxicity in male rats. *Ecotoxicol Environ Saf* **224**: 112674.
20. Culling CFA. 1974. Handbook of Histopathological and Histochemical Techniques. 3rd edn. London: Butterworths, p. **361**.
21. Snedecor WG and Cochran GW. 1967. Statistical Methods. 6th edn. New Delhi: Oxford and IBH Publishing Company, pp. **258-268**.
22. Abdelgadir EH, Al-Qudsi J, Al-Saleh LN and Emara HA. 2020. Sub-acute exposure of fipronil induces biochemical and histopathological changes in liver, kidney and heart of male albino rats. *J Forensic Toxicol Pharmacol* **9**: 4.
23. Moneim AEA. 2012. Evaluating the potential role of pome-

granate peel in aluminum-induced oxidative stress and histopathological alterations in brain of female rats. *Biol Trace Elem Res* **150**: 328-336.
24. Shiban MS, Al-Otaibi MM and Al-Zoreky NS. 2012. Antioxidant activity of pomegranate (*Punica granatum* L.) fruit peels. *Food Nutr Sci* **3**: 991-996.
25. Dkhil MA. 2013. Anti-coccidial, anthelmintic and antioxidant activities of pomegranate peel extract. *Parasitol Res* **112**: 2639-2646.
26. Hasan S, Elrahman A, Abou-Rawash A, Bekheet M and Hassan S. 2016. Protective role of aqueous extract of *Punica granatum* peel on lead-induced anemia in rats. *Alexan J of Vety Sci* **50**:1.
27. Senthilkumar T. 2010. Studies on the pathological effects of fipronil and their amelioration by curcumin in rats. PhD Thesis, College of Veterinary and Animal Sciences, Mannuthy.
28. Bano F and Mohanty B. 2020. Thyroxine modulation of immune toxicity induced by mixture pesticides mancozeb and fipronil in mice. *Life Sci* **240**: 117078.
29. Campoio TR, Oliveira FA and Otton R. 2011. Oxidative stress in human lymphocytes treated with fatty acid mixture: role of carotenoid astaxanthin. *Toxicol In Vitro* **25**: 1448-1456.
30. Labsi M, Khelifi L, Mezioug D, Soufli I and Touil-Boukoffa C. 2016. Antihydatic and immunomodulatory effects of *Punica granatum* peel aqueous extract in a murine model of echinococcosis. *Asian Pac J Trop Med* **9**: 211-220.
31. Pfohl M, DaSilva NA, Marques E, Agudelo J, Liu C, Goedken M, Slitt AL, Seeram NP and Ma H. 2021. Hepatoprotective and anti-inflammatory effects of standardized pomegranate fruit extract in high fat diet-induced obese mice. *Int J Food Sci Nutr* **72**: 499-510.

Indian J. Vet. Pathol., 50(2) : 150-154, 2026: DOI: https://doi.org/10.56093/07j1wr59

SHORT COMMUNICATION

Epidemiological study on enterotoxaemia in small ruminants from Namakkal and Karur districts of Tamil Nadu

S. Sivaraj, M. Sasikala*, K. Ramya[1] and P. Srinivasan
Department of Veterinary Pathology, Veterinary College and Research Institute, Namakkal, TANUVAS
[1]Associate Professor, Department of Veterinary Microbiology, V C R I, Udumalpet

***Address for correspondence**
M. Sasikala, Assistant Professor, VCRI, Udumalpet, E.mail: vetsasi.pathologist@gmail.com / sivarajvetpatho@gmail.com

Received: 20.11.25; Accepted: 28.12.25

ABSTRACT

Enterotoxaemia remains one of the most economically important *Clostridial* diseases of small ruminants, which often occurs in peracute form with sudden mortality without any premonitory signs. Thus, the present study was undertaken to determine the occurrence of enterotoxaemia in sheep and goat flocks with the history of sudden death in Namakkal and Karur regions of Tamil Nadu. Totally, 62 flocks with the history of sudden death were investigated and samples like intestinal contents in necropsied animals and faecal swabs from live animals were collected. Among these, 22 flocks were found positive for different toxinotypes of *Clostridium perfringens* by multiplex PCR, which include 14 sheep flocks and 8 goat flocks. The study revealed that the major etiological agent for sudden death in small ruminants was *C. perfringens* type D and highest occurrence was recorded in sheep. Similarly, male lambs and kids were more susceptible than females. With respect to age, lambs and kids in the age group of 4 to 6 months were mostly affected. The findings also revealed, enterotoxaemia is more prevalent in the extensive system of management. Among the different toxinotypes, Type D is most commonly observed in both dead and live animals, followed by Type A. Thus, the present study highlights the continued endemicity of enterotoxaemia in this region and stresses the need for periodical vaccination, proper dietary management, disease surveillance and regular monitoring for effective disease control.

Keywords: Enterotoxaemia, small ruminants, occurrence, mPCR

INTRODUCTION

Sheep and goat husbandry in India remains largely traditional, with animals reared under extensive grazing systems that predispose them to soil-borne infections and parasitic infestations. Among these, enterotoxaemia is one of the most devastating diseases of young feedlot sheep and goats, leading to high mortality and significant economic losses[1]. Seasonal outbreaks, particularly during the onset of the monsoon, are common even in vaccinated flocks[2].

Enterotoxaemia in small ruminants is caused by *Clostridium perfringens*, a Gram positive, spore forming anaerobe, usually a commensal organism of the intestinal tract that proliferates rapidly under favourable intestinal conditions, resulting in the production of potent toxins. Of its five toxinotypes (A–E), type D, producing alpha and epsilon toxin, is mainly responsible for enterotoxaemia in small ruminants[3].

While case history, clinical signs and gross pathological findings are useful for arriving at presumptive diagnosis of enterotoxaemia by *C. perfringens* in sheep and goats, definitive diagnosis of these diseases cannot be established without molecular confirmation of relevant toxin genes[4]. Recent studies have investigated the role of different toxin genes of *C. perfringens* in the intestinal contents in the definitive diagnosis of the diseases[5]. Based on these studies, the definitive diagnosis of enterotoxaemia relies on identification of specific toxin genes in the intestinal contents in conjunction with characteristic clinical signs and gross lesions of the affected animals.

The disease occurs sporadically or in outbreaks, often influenced by sudden dietary changes, climatic stress and management practices that favour the rapid intestinal proliferation of *C. perfringens.* The occurrence varies widely between regions and seasons, reflecting differences in husbandry systems, feeding patterns and vaccination coverage. Young and fast-growing animals are particularly vulnerable and the disease often remains underreported due to its per-acute nature.

Therefore, evaluating the occurrence of enterotoxaemia across different age groups, management systems and different seasons remains crucial for understanding disease dynamics and formulating evidence-based control measures and effective vaccination programmes. With this background, the present communication reports the occurrence of enterotoxaemia in

How to cite this article : Sivaraj, S., Sasikala, M., Ramya, K. and Srinivasan, P. 2026. Epidemiological study on enterotoxaemia in small ruminants from Namakkal and Karur districts of Tamil Nadu. Indian J. Vet. Pathol., 50(2) : 150-154.

sheep and goats of Namakkal and Karur districts of Tamil Nadu, a well-known hub for small-ruminant farming.

MATERIAL AND METHODS

Study area

Occurrence of enterotoxaemia was assessed in sheep and goat flocks located in and around the Namakkal and Karur districts of Tamil Nadu during the period from December 2024 to September 2025.

Study population

During the study period, a total of 75 dead animals from 62 flocks were investigated and 31 flocks were suspected to have enterotoxaemia outbreaks. With respect to live animals, a total of 181 faecal samples were collected from the flocks confirmed with enterotoxaemia outbreak. Data like species, sexes, age, month of occurrence and different toxinotypes were recorded.

Sampling

Case history

Dead animals with a history of sudden death, neurological signs, abdominal bloating along with good body condition were considered for sample selection and subsequent screening for enterotoxaemia by multiplex PCR. Meanwhile, samples from live animals were collected based on the presence of clinical signs such as diarrhoea and abdominal distension in flocks with a confirmed enterotoxaemia outbreak.

Sample collection

During the study period, a total of 75 animals from 62 flocks were reported to have sudden death and postmortem samples were collected from these cases. The collected samples were subjected to isolation by culture method and confirmed by molecular detection of *C. perfringens* toxin genes associated with enterotoxaemia by multiplex PCR. Faecal swabs and blood samples were collected from 181 live animals that manifested clinical signs such as depression and diarrhoea and subjected to bacteriological and molecular detection of *C. perfringens*.

Laboratory diagnostics

The collected samples, such as intestinal contents and faecal swabs, were inoculated into Robertson's cooked meat medium and milk medium, followed by incubation at 37 °C for 24 hours. Subsequently, the positive samples were then subcultured onto blood agar and egg yolk agar and then incubated for 24 hours[6]. Colonies exhibiting characteristic growth were then subjected to molecular detection of different toxinotypes of *C. perfringens* by multiplex PCR[7]. The intestinal contents were also tested for the presence of epsilon toxin for confirmation of type D enterotoxaemia by using commercial ELISA kit (Bio-X, Belgium; BIO K 268).

RESULTS AND DISCUSSION

Laboratory Diagnosis of Enterotoxaemia Using PCR and ELISA

DNA was extracted from the positive cultures of *C. perfringens* by the hot and cold lysis method. Multiplex PCR was carried out for the detection of different toxin genes of *C. perfringens* using the extracted DNA and specific primers. Polymerase chain reaction yielded positive results in 29 out of 75 intestinal samples collected during necropsy and 69 out of 181 clinical samples collected from enterotoxaemia suspected animals.

ELISA performed on intestinal contents of PCR positive samples for the detection of epsilon toxin revealed varying levels of epsilon toxin, ranging from 27.2% to 87.6%, which were significantly than the levels detected in other clinically suspected animals.

Species-wise occurrence

In the present study, the distribution of enterotoxaemia differed between sheep and goats, indicating a species-related variation in susceptibility to *C. perfringens* infection. The occurrence of enterotoxaemia was more in sheep with 19 cases (45.23%) from 14 flocks than in goats with 10 cases (30.30%) from 8 flocks (Table 1). Similarly, in live animals, out of 181 samples screened, 69 samples were positive for enterotoxaemia, with 52 (40.94%) samples from sheep and 17 (31.48%) samples from goats (Table 2). Such differences have been documented in earlier reports as well. 25% of sheep from 20 flocks in Egypt exhibited clinical signs of enterotoxaemia, with a mortality rate of 16.25%, highlighting the significant disease burden in ovine populations observed by[8]. Similarly, [7]reported a higher prevalence of *C. perfringens* in sheep (72.36%) than in goats (60%), suggesting that sheep may be comparatively more prone to infection and clinical disease expression.

Table 1. Species-wise occurrence of Enterotoxaemia in affected flocks (Dead animals)

S.No.	Species	No of animals died with history sudden death	No of ET positive animals	Per cent positivity
1.	Sheep	42	19 (14 flocks)	45.23
2.	Goats	33	10 (8 flocks)	30.30
	Total	**75**	**29 (22 flocks)**	**38.66**

Table 2. Species-wise occurrence of Enterotoxaemia in affected flocks (Live animals)

S.No.	Species	No of sample collected	No of ET positive samples	Per cent positivity
1.	Sheep	127	52	40.94
2.	Goats	54	17	31.48
	Total	**181**	**69**	**38.12**

Table 3. Sex-wise occurrence of Enterotoxaemia in affected flocks

S.No.	Sex	Total no. of samples		No. of Positives		Per cent positivity	
		Dead	Live	Dead	Live	Dead	Live
1.	Male	41	110	17	48	41.46	43.63
2.	Female	34	71	12	21	35.29	29.58
	Total	**75**	**181**	**29**	**69**	**38.66**	**38.12**

Sex-wise occurrence

In the present study, males showed a higher occurrence of enterotoxaemia than females, *viz*., 41.46% of dead animals and 43.63% of live animals were males (Table 3). Similar findings were reported earlier[9,10] who also observed a higher prevalence of enterotoxaemia in males. This pattern might be due to managemental practices where males are often maintained for fattening and are commonly preferred in intensive farming systems. Such management conditions may expose them to higher nutritional stress and sudden dietary changes, making them more susceptible to *C. perfringens* infection.

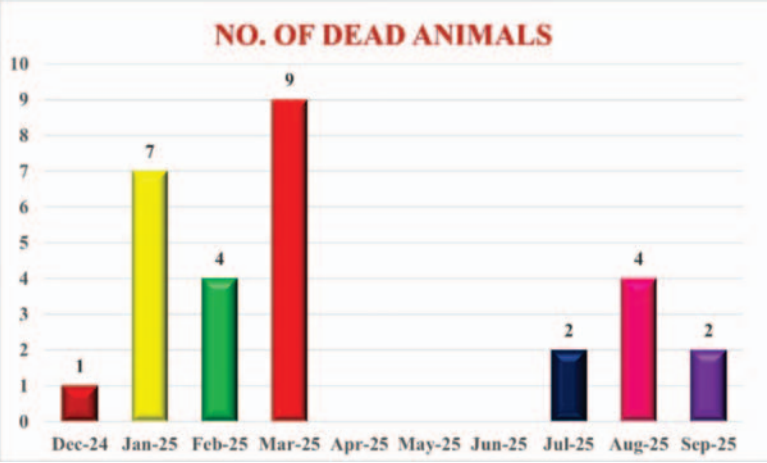

Fig 1. Month-wise occurrence of Enterotoxaemia among dead animals

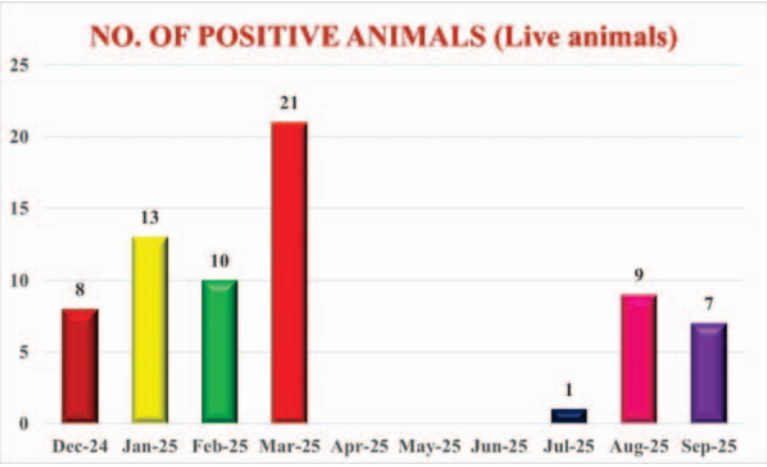

Fig 2. Month-wise occurrence of Enterotoxaemia among live animals

Age-wise occurrence

In the present study, enterotoxaemia occurred in all age groups, but the highest occurrence was seen in animals aged 4–6 months, both in dead (57.14%) and live (46.47%) animals. The 7–12 month group followed this, while the lowest occurrence was recorded in animals above one year of age (Table 4). These findings indicate that young growing animals are more susceptible to the

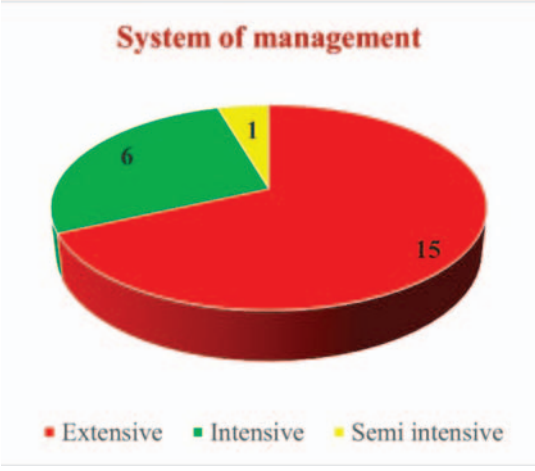

Fig 3. Occurrence of Enterotoxaemia based on the System of Management

Table 4. Age-wise occurrence of Enterotoxaemia in affected flocks

S. No.	Age group	Total no. of samples		No. of positive		Per cent positivity	
		Dead	Live	Dead	Live	Dead	Live
1.	0 – 3 Months	21	52	5	16	23.80	30.77
2.	4 – 6 Months	28	71	16	33	57.14	46.47
3.	7 – 12 Months	12	48	6	19	50.00	39.58
4.	Above 12 Months	14	10	2	01	14.28	10.00
	Total	**75**	**181**	**29**	**69**	**38.66**	**38.12**

Table 5. Occurrence of different toxinotypes of *C. perfringens*

S. No.	*Clostridium* toxinotypes	Dead			Live			Total no of animals
		Sheep	Goats	Total	Sheep	Goats	Total	
1.	*C. perfringens* type A	7	3	10	21	6	27	37
2.	*C. perfringens* type B	0	0	0	0	0	0	0
3.	*C. perfringens* type C	0	0	0	0	0	0	0
4.	*C. perfringens* type D	12	7	19	31	11	42	61
	Total	**19**	**10**	**29**	**52**	**17**	**69**	**98**

disease. Seroprevalence of epsilon toxin was highest in sheep aged 6–12 months, followed by animals below 6 months and lowest in adults[10].

Month-wise occurrence

In the present study, the highest number of enterotoxaemia-related mortality occurred during March, with 9 animals out of 14 animals examined (64.28%), followed by January with 7 mortality (50.00%) and February and August with 4 mortalities each (Figure 1). A similar temporal trend was noted in live animals, with 21 positive animals (35.00%) in March, followed by January with 13 positive animals (38.23%) and February with 10 positive animals (50.00%) (Figure 2). The clustering of cases during the late winter and early summer months indicates that seasonal factors may influence disease expression.

The present findings agree previous worker[11] who reported that *C. perfringens* infection in small ruminants was more frequent during winter and autumn, suggesting that cooler seasons favour disease occurrence. Likewise, [12]emphasized that humid conditions and rainy periods predispose sheep to enterotoxaemia, indicating that fluctuations in environmental moisture may enhance bacterial proliferation or toxin expression. Peak occurrence during the monsoon season in unvaccinated lambs from Andhra Pradesh, highlighting the role of climatic stressors and management conditions documented by [2].

System of management

In contrast to the earlier worker [14] who observed a higher prevalence of *Clostridium perfringens* in closed (intensive) farms, the present study showed a different distribution pattern. Among the 22 positive flocks detected, 15 (68.18%) were from extensive systems, 6 (85.71%) from intensive farms and 1 (50.00%) from a semi-intensive system (Figure 3). The higher occurrence of enterotoxaemia in extensive (open) farms may be due to frequent grazing, wider environmental exposure, irregular dietary changes during grazing shifts, the ingestion of lush pasture or high-carbohydrate feeds and improper vaccinations.

Toxinotypes

In the present study, *C. perfringens* type D was the predominant toxinotype in both dead (65.51%) and live (60.86%) animals, followed by type A, while types B and C were not detected (Table 5). The higher occurrence of type D in clinically affected animals coincides with earlier observations, who reported that type D constituted 45.76% of isolates from diseased sheep[13]. Similarly, consistent involvement of type D in field outbreaks of enterotoxaemia has been reported[2,14]. The detection of type A in both live and dead animals also agrees with the reports[2,8] who observed substantial proportions of type A in suspected and healthy animals, suggesting that type A remains a common intestinal inhabitant that may become pathogenic under conducive conditions. With agreement to this, in our study, a total of 10 dead animals were positive for *C. perfringens* type A and 27 live animals were positive for *C. perfringens* type A. The absence of toxinotypes B and C in the present work is also in agreement with recent studies, which also documented their limited or negligible occurrence[2,8].

CONCLUSION

In conclusion, the present study provides

a comprehensive overview of the occurrence of enterotoxaemia in small ruminants across different species, age groups, sexes, seasons and management systems. The distribution of toxinotypes further highlights the epidemiological complexity of the disease. These findings emphasize the continued vulnerability of young animals and the critical role of management and environmental factors in disease occurrence. Overall, the insights gained from this study can support the development of more targeted vaccination programmes, strengthen preventive health strategies, and guide improvements in farm management practices to mitigate the burden of enterotoxaemia in endemic areas.

Financial support & sponsorship: None.

Conflicts of interest: None.

Use of artificial intelligence (AI)-Assisted Technology for manuscript preparation: The authors confirm that there was no use of AI-assisted technology for assisting in the writing of the manuscript and no images were manipulated using AI.

REFERENCES

1. Niilo L. 1980. *Clostridium perfringens* in animal disease: a review of current knowledge. *Can Vet J.* **21:** 141–8
2. Kumar NV, Sreenivasulu D and Reddy YN. 2014. Prevalence of *Clostridium perfringens* toxin genotypes in enterotoxemia suspected sheep flocks of Andhra Pradesh. *Vet. World.* **7(12):** 1132–1136.
3. Uzal FA and Kelly WR. 1996. Enterotoxaemia in goats: a review. *Vet Res Commun.* **20:** 481–92.
4. Uzal FA. 2004. Diagnosis of *Clostridium perfringens* intestinal infections in sheep and goats. *Anaerobe*., **10(2):** 135-143.
5. Gkiourtzidis K, Frey J, Bourtzi-Hatzopoulou E, Iliadis N, Sarris K. 2001. PCR detection and prevalence of alpha, beta, beta 2, epsilon, iota and enterotoxin genes in Clostridium perfringens isolated from lambs with *clostridial* dysentery. *Vet Microbiol*., **82:** 39–43.
6. Quinn, PJ, Markey BK, Leonard FC, FitzPatrick ES, Fanning S and Hartigan PJ. 2011. Veterinary microbiology and microbial disease, 2nd Edn. Wiley-Blackwell.
7. Nazki S, Wani SA, Parveen R, Ahangar SA, Kashoo ZA, Hamid S, Dar ZA, Dar TA and Dar PA. 2017. Isolation, molecular characterization and prevalence of *Clostridium perfringens* in sheep and goats of Kashmir Himalayas, India. *Vet. World*, **10(12):** 1501.
8. Elsify A, Tarabess R, Nayel MA, Salama A, Allaam M, Abd El-Gaber M, Hassan H, Zaghawa A and Elballal S. 2016. Bacteriological and molecular studies on *Clostridium perfringens* isolated from sheep in three Egyptian provinces. *Afr. J. Microbiol. Res.*, **10(20):** 725-732.
9. Singh DD, Pawaiya RVS, Gururaj K, Gangwar NK, Mishra AK, Andani D, Singh MK, Bhushan S and Kumar A. 2018. Molecular detection of *Clostridium perfringens* toxinotypes, enteropathogenic *Escherichia coli*, rotavirus and coronavirus in diarrheic fecal samples of neonatal goat kids. *Indian J. Anim. Sci.,* **88(6):** 655–661
10. Suresha M, Karela P, Gururaj K and Chahar A. 2024. Prevalence of enterotoxaemia in sheep in Bikaner district of Rajasthan. *Int. J. Adv. Biochem. Res.*, **8(1):** 899–902.
11. Omar AA, Baker NM, Bkheet AA, Khder AM, and Nasr MY. 2018. Epidemiological studies and molecular characterization of Clostridium perfringens in small ruminants at El-Behera governorate, Egypt. *Assiut Vet. Med. J.,* **64(156):** 81–88.
12. Javed MT, Irfan M, Mukhtar N and Hussain R. 2009. An outbreak of enterotoxaemia at livestock farm during subtropical summer. *Acta Trop.*, **112(2):** 225-227.
13. Nayel M, El-Sify A, Akram S, Allaam M, Abdeen E and Hassan H. 2013. Molecular typing of *Clostridium perfringens* isolates from soil, healthy, and diseased sheep in Egypt by multiplex PCR. *J. Vet. Med. Res.*, **22(1):** 53-57
14. Fayez MM, Al Musallam A, Al Marzoog A and Suleiman MB. 2013. Prevalence and toxinotyping of the toxigenic *Clostridium perfringens* in sheep with suspected enterotoxemia. *Nat. Sci*., **11(8):** 15-21.

Indian J. Vet. Pathol., 50(2) : 155-159, 2026: DOI: https://doi.org/10.56093/38yafg36

SHORT COMMUNICATION

Evaluation of proliferative status of bitch mammary gland osteosarcoma using modified methods of AgNOR staining

Sanjiv Kumar*, Rajesh Kumar[1] and Puja Kumari Bhagat
Department of Veterinary Pathology, Bihar Veterinary College, BASU, Patna, Bihar, India
[1]Department of Veterinary Surgery & Radiology

***Address for correspondence**
Sanjiv Kumar, Department of Veterinary Pathology, Bihar Veterinary College, BASU, Patna, Bihar,
E-mail: mrsanvet@rediffmail.com

Received: 15.1.26; Accepted: 17.2.26

ABSTRACT

Canine mammary osteosarcoma is a rare but highly aggressive extra medullary tumour, predominantly affecting older female dogs and marked by rapid progression and a high metastatic potential. While histopathology is the standard diagnostic and prognostic tool, it does not always accurately represent the true proliferative activity of tumour cells, necessitating more sensitive adjunct techniques. Nucleolar organizer regions (NORs), which contain argyrophilic proteins involved in ribosomal RNA synthesis, can be visualized using silver staining (AgNOR). AgNOR quantification has emerged as a valuable adjunct to routine histopathology, as increased AgNOR counts correlate with higher metabolic activity, faster cell cycles, and greater tumour proliferation. Recent advances involving zinc and silver co-localization have further improved the sensitivity and consistency of AgNOR-based assessments. The present study investigated naturally occurring mammary gland osteosarcoma in bitches. Tumour tissues were collected, formalin-fixed, and subjected to routine histopathology, followed by AgNOR staining and zinc–silver co-localization analysis. Proliferative activity was evaluated through quantitative assessment of cell-cycle phases and mitotic figures. Results revealed a significant positive association between mitotic counts and proliferative phases of the cell cycle, along with a negative correlation with the G1 phase across all staining methods. These findings highlight the reliability of AgNOR techniques and zinc-silver co-localization as sensitive markers for assessing tumour proliferation and biological aggressiveness in canine mammary osteosarcoma.

Key words: AgNOR, Bitch, Co-localization, grading, mammary osteosarcoma, mitotic index, proliferative status

INTRODUCTION

Cancer remains a leading cause of death in animals due to limited therapeutic options and poor prognosis. Mammary tumours are the second most common tumour in dogs, accounting for 52% alone of all tumour cases[1]. Although histopathological grading remains the gold standard, it often fails to reflect true proliferative activity, necessitating newer techniques. Histochemistry is a potent supplement to conventional histopathological procedures because it improves diagnostic accuracy, offers functional insights and directs targeted therapy[2]. Histochemical techniques localize and demonstrate specific chemical constituents such as biomolecules and nucleic acids within cells and tissues. Nucleolar organizing regions having a group of argyrophilic proteins that are preferentially stained with silver techniques. Nucleolar organizing regions (NOR) contains a set of argyrophilic proteins, which can be selectively stained by silver methods. AgNOR ((Argyrophilic nucleolar organizer region) staining technique can be used as an adjunct to histopathology in differentiating benign and malignant tumours, particularly borderline cases. AgNOR staining is one of them that is becoming more and more popular since it is simple to use, correlates with the proportion of cell cycling, and is more intense when the cell cycle speed increases. rRNA is responsible for the production of many such proteins in the cell. Protein synthesis is an important step in cell development. Therefore, a relationship between NOR and cell proliferation has been suggested[3]. After silver staining, AgNOR appears as discrete brown to black dots in formalin-fixed tissues. The AgNOR index is a count of the number of such black dots, in a cell nucleus. The AgNOR index is a marker used to assess tumour proliferation rates and differentiate between benign and malignant tumours. They have the advantage that their numbers are increased only in actively and dividing cells. Their increased number indicates high metabolic activity which probably correlates with increased speed[4]. These silver-stained sites correspond to zinc-binding nucleolar proteins involved in replication and transcription[5]. Co-localization studies of zinc and silver binding sites may improve understanding of AgNOR formation and provide a more reliable, sensitive marker for tumour proliferation assessment[6].

How to cite this article : Kumar, S., Kumar, R. and Bhagat, P.K. 2026. Evaluation of proliferative status of bitch mammary gland osteosarcoma using modified methods of AgNOR staining. Indian J. Vet. Pathol., 50(2): 155-159.

MATERIALS AND METHODS

Samples from 11 different adult bitches of different breeds, showing lesions of swelling and growth in the mammary gland, were collected from cases presented in the Teaching Veterinary Clinical Complex, Bihar Veterinary College, Patna or the nearby pet clinics for treatment. The bitches mostly aged between 8–10 years, were affected six to eight months back for which they were treated but showed no response. The growths of variable sizes were seen in different mammary glands in different cases, however, the growth were unanimously hard and firm with few ulcerated points (Fig. 1). These cases were therefore, suspected for mammary tumour. Clinically these animals were found anaemic and dull.

The representative tissue samples were collected and preserved in 10% formalin for further laboratory examination for diagnosis of neoplasia and its proliferative behaviour. These samples were subjected for evaluation of their biological aggressiveness in light of co-localization of zinc and argyrophilic sites in nuclei and counting of number of cells in different phases of cell cycle developed[7].

Samples collected from different regions of the tumour mass were subjected to routine tissue processing, paraffin embedding, and microtome sectioning. Four serial sections were prepared from each tissue block. One section was stained with hematoxylin and eosin (H&E) for histopathological classification, tumour grading, and mitotic figure counting[8]. Tumour grading was performed using the Nottingham modification of the Scarff–Bloom–Richardson system, based on tubule formation, nuclear pleomorphism, and mitotic activity[9]. Mitotic figures were counted in 50 high-power fields, and the mitotic index was calculated accordingly[10]. The remaining serial sections were subjected to AgNOR staining. To enhance AgNOR visibility, co-localization of silver with zinc was performed using Timm's method[11]. Accordingly, three serial sections were stained using Zn-AgNOR-Dithizone, Zn-AgNOR, and AgNOR techniques. These stains were used to quantify cells in different phases of the cell cycle and assess tumour proliferative behaviour[12]. For Zn-AgNOR-Dithizone staining, deparaffinized and rehydrated sections were treated with a solution of $ZnSO_4$, Na_2SO_3, and acetic acid, followed by AgNOR staining using silver nitrate and formic acid–gelatin. Sections were then treated with sodium thiosulphate, exposed to dithizone, cleared in chloroform, and mounted in glycerol. Zn-AgNOR staining followed a similar protocol without dithizone treatment, while AgNOR staining alone involved silver impregnation and mounting in DPX.

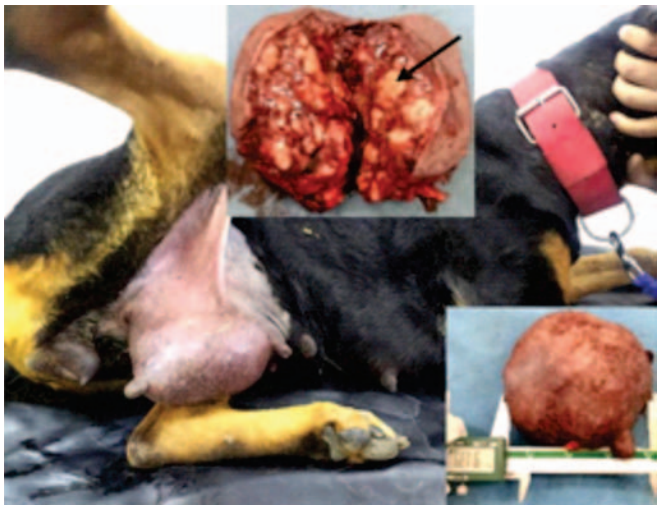

Fig.1. Mammary tumour (91.39 x 85.08 mm) on the right inguinal mammary gland in a Rottweiler (8yr/28.5 kg). Cut section showing hard, bony deposition in tumour mass (black arrow).

RESULTS

Gross examination, in general, revealed fluctuant mass with variable consistency, exhibiting both firm and soft areas. On cut section, the tissue appeared yellowish and contained multiple cavernous spaces filled with greyish fluid.

Histologically, the tumour was characterized by islands of osteoid formation (Fig. 2) and the presence of neoplastic osteoblasts. These cells were short spindle- to triangular-shaped, with plump oval nuclei, arranged in a haphazard manner rather than in organized bundles (Fig. 3). The hallmark feature was the production of osteoid matrix, portions of which were calcified, while other areas remained uncalcified (Fig. 4). In several regions, osteoid was irregularly deposited as fibrillar stroma between pleomorphic cells, with anaplastic cells embedded within the matrix, forming a lace-like pattern. Newly formed osteoid appeared dense, eosinophilia and fibrillar frequently entrapping osteocytes. Occasional multinucleated giant cells and poorly organized cartilaginous islands were also observed. Based on the gross and histopathological findings, the tumours were confirmed as mammary gland osteosarcoma.

The proliferative fraction and growth rate were evaluated by assessing cell-cycle phase distribution using Zn–AgNOR–Dithizone, Zn–AgNOR, and AgNOR staining techniques[13]. Representative histological images showing NOR dots with these three staining methods are presented in Fig. 5, 6 and 7 respectively. The observations are summarized as follows:

Zn-AgNOR-Dithizone Staining

The comparison of mean values of cells in different phases of cell cycle has been presented in Table 1 and Fig. 8. The mean count of cells in S/G2, M as well as S/G2+M phases taken as proliferative fraction of tumour

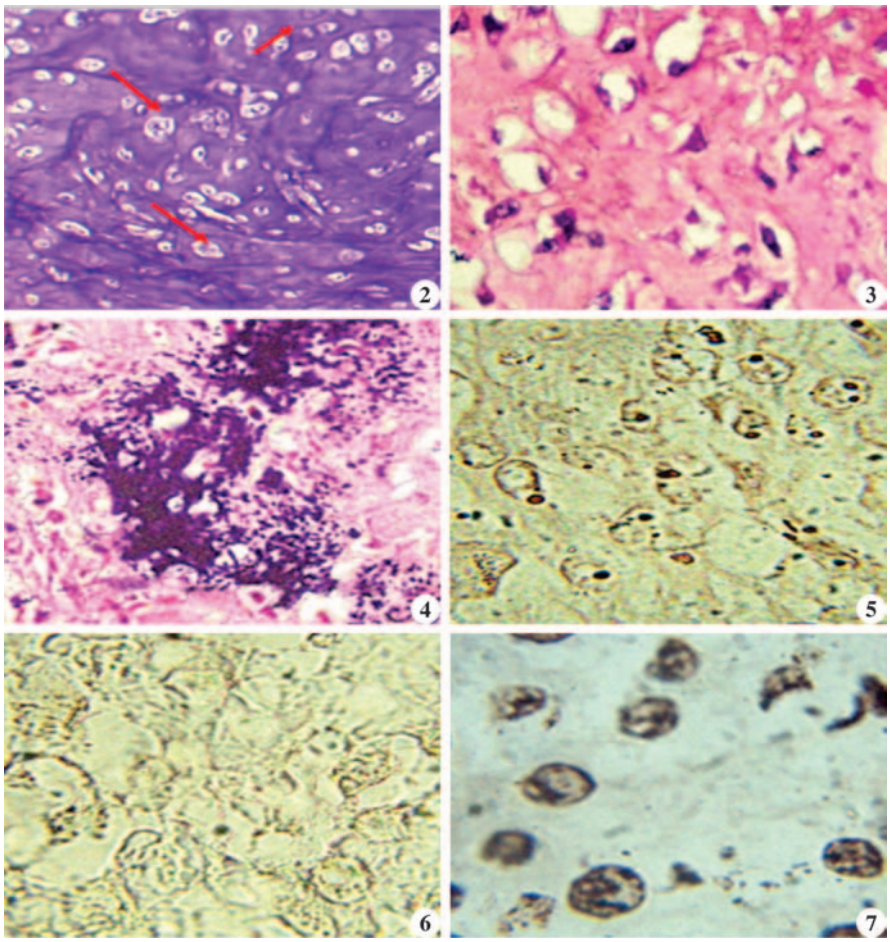

Fig.2. Osteosarcoma of mammary gland characterised by island of basophilic osteoid formation. Mitoses can be seen (H&E x400); **Fig.3.** Osteosarcoma with anastomosing mineralized osteoid (H&E x100); **Fig. 4.** Showing osteoblasts having pleomorphic spindle or triangular shaped nuclei incorporated into bony matrix (H&E x400); **Fig. 5.** Showing cells in different stages of cell cycle in Mammary Osteosarcoma (Zinc-AgNOR-Dithizone x1000); **Fig.6.** Showing cells in different stages of cell cycle in Mammary Osteosarcoma (Zn-AgNOR x1000); **Fig.7.** Showing cells in different stages of cell cycle in Mammary Osteosarcoma (AgNOR x1000).

cells along with mitotic figures were significantly higher in Grade III tumour as compared to Grade II while the count of cells in G_1 phases were significantly lower in Grade III than in Grade II. This clearly indicated more proliferative population of cells in tumours of Grade III than Grade II. At the same time the finding of proliferative population in accordance with the histological behaviour of osteosarcoma support the ability of the system to identify the cells in different phases of the cycle.

Zn-AgNOR Staining

The comparison of mean values is presented in Table 2 and Fig. 9. The observed proliferative fractions, in agreement with the histological behaviour of osteosarcoma, support the capability of this system to identify tumour cells in different phases of the cell cycle. The mean counts of cells in the S/G2 and M phases, as well as the combined S/G2+M proliferative fraction, along with mitotic figures, were significantly higher in Grade III tumours compared to Grade II tumours. Conversely, the mean count of cells in the G1 phase was significantly lower in Grade III than in Grade II tumours.

AgNOR Staining

The comparison of mean values

Table 1. Showing Comparison of counting of percentage of cells in different phases of cell cycle with Zn-AgNOR-Dithizone staining in different Grades of Mammary Osteosarcoma.

	SCORE	G1	S/G2	M	S/G2+M	Abnormal	Mitotic figure
GRADE II	6.21±0.14	67.57±2.75	21.03±1.89	9.59±0.58	29.67±2.38	2.59±0.45	21.71±1.05
GRADE III	9.02±0.00	38.38±1.89	43.49±1.68	13.01±0.51	55.015±2.02	5.41±0.35	28.54±1.18
t- value	-	8.17**	8.17**	3.78**	8.00**	3.93**	4.23**

NS Non Significant, *P<0.05, **P<0.01

Table 2. Showing Comparison of counting of percentage of cells in different phases of cell cycle with Zn-AgNOR stain in different Grades of Mammary Osteosarcoma.

	Score	G1	S/G2	M	S/G2+M	Abnormal	Mitotic figure
Grade II	6.33±0.11	66.35±3.25	20.50±2.28	10.48±0.79	31.00±2.85	2.67±0.55	21.70±1.07
Grade III	9.01±0.00	37.86±3.34	41.51±3.27	13.59±0.54	55.10±3.39	7.08±0.49	28.44±1.19
t- Value	-	6.00**	5.28**	3.29**	5.36**	4.91**	4.25**

NS Non Significant, *P<0.05, **P<0.01

Table 3. Showing Comparison of counting of percentage of cells in different phases of cell cycle with AgNOR stain in different Grades of Mammary Osteosarcoma.

	Score	G1	S/G2	M	S/G2+M	Abnormal	Mitotic figure
Grade II	6.29±0.12	75.81±1.90	10.95±1.37	11.00±0.67	21.00±1.73	3.17±0.40	21.70±1.06
Grade III	8.99±0.00	57.12±1.50	21.76±1.15	14.95±0.96	36.69±1.54	6.21±0.41	28.45±1.14
t- value	-	7.39**	4.80**	4.09**	6.44**	5.50**	4.25**

[NS] Non Significant, *P<0.05, **P<0.01

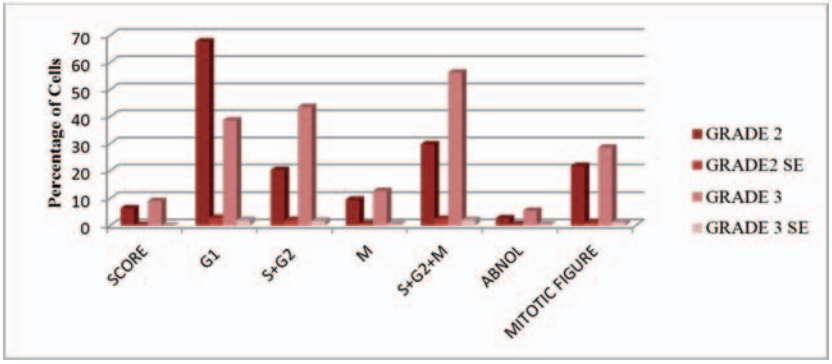

Fig. 8. Showing Comparison of mean values of percentage of cell counts and standard error in different phases of cell cycle with Zn-AgNOR- Dithizone staining in different grades of mammary gland osteosarcoma.

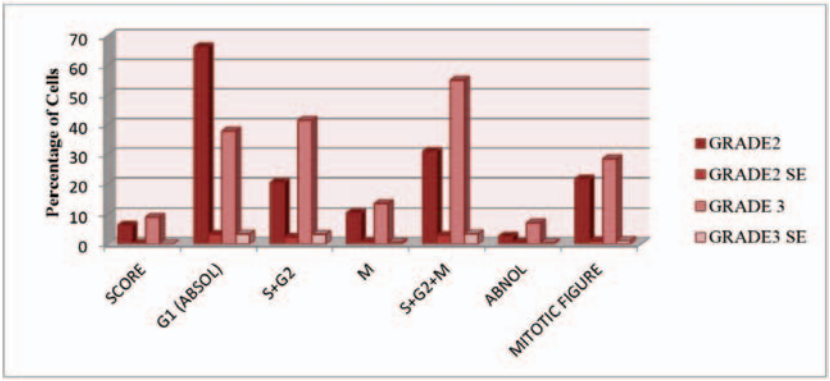

Fig. 9: Showing Comparison of mean values of percentage of cell counts and standard error in different phases of cell cycle with Zn-AgNOR stain in different grades of mammary gland osteosarcoma.

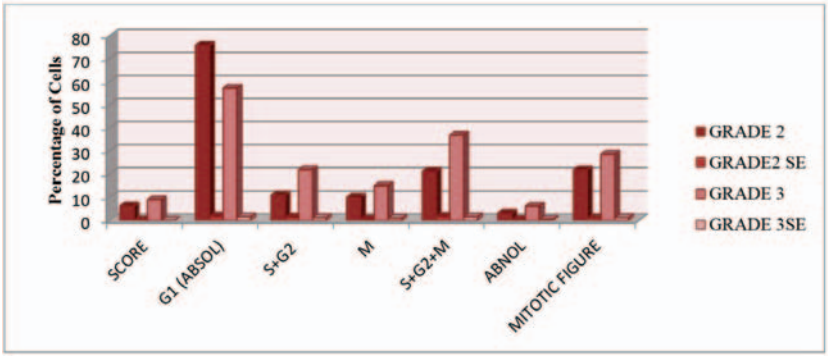

Fig. 10: Showing Comparison of mean values of percentage of cell counts and standard error in different phases of cell cycle with AgNOR staining in different grades of mammary gland osteosarcoma.

is presented in Table 3 and Fig. 10. The observed proliferative rate and growth kinetics, in accordance with the histological behaviour of osteosarcoma, support the effectiveness of this system in identifying tumour cells in different phases of the cell cycle. The mean counts of cells in the S/G2 and M phases, as well as the combined S/G2+M phase considered as the proliferative fraction, along with mitotic figures, were significantly higher in Grade III tumours compared to Grade II tumours. In contrast, the mean count of cells in the G1 phase was significantly lower in Grade III than in Grade II tumours. These findings clearly indicate a higher proliferative cell population in Grade III osteosarcomas.

DISCUSSION

Comparative evaluation of the different staining methods revealed that the percentage of cells in the S/G2 and M phases was consistently highest with Zn–AgNOR–Dithizone staining, followed by Zn–AgNOR, and lowest with AgNOR alone. This finding indicates that Zn–AgNOR–Dithizone staining is more sensitive in identifying S/G2- and M-phase cells, which constitute the most proliferative fraction of the tumour[14]. All three staining techniques demonstrated a significantly higher proportion of cells in the S/G2, M, and S/G2+M (proliferative fraction) phases, along with a lower proportion of cells in the G1 phase, in Grade III tumours compared with Grade II tumours, reflecting increased proliferative activity in higher-grade lesions[15].

Statistical correlation analysis demonstrated a positive and significant association between mitotic figure counts and proliferative phases (S/G2, M, and S/G2+M), and a negative correlation with the G1 phase across all staining

methods, thereby confirming the accuracy of cell-cycle phase identification[16]. Comparative assessment further established that Zn–AgNOR–Dithizone staining consistently detected higher numbers of S/G2- and M-phase cells than Zn–AgNOR or AgNOR alone, underscoring its superior sensitivity and precision in identifying highly proliferative tumour fractions.

Increased cellular proliferation shortens the cell-cycle duration and enhances metabolic activity. Elevated metabolic states are often associated with the presence of multiple extranuclear dots, as reported previously[17]. Mesenchymal cells are intrinsically active in protein synthesis, and tumours of mesenchymal origin exhibit similar behaviour. The intensified protein synthesis accompanying rapid cell cycling is supported by increased transcriptional and translational activity.

It is well established that rRNA ribosomal protein complexes are processed within the nucleolus with the involvement of zinc or silver-binding proteins. Under conditions of accelerated translational activity, these proteins may translocate toward sites of active protein synthesis. Additionally, several translation factors are zinc- or silver-binding proteins, and their increased abundance may contribute to the formation of extranuclear AgNOR granules, reflecting heightened and rapid protein synthesis[18].

Overall, the findings suggest that mammary gland osteosarcoma contains a relatively small but highly proliferative cell population. The tumour is believed to originate from rapidly dividing myoepithelial cells that undergo differentiation and transformation into osteoid tissue under the influence of osteogenic gene expression. During prolonged tumour progression, multiple subclonal populations may emerge, including rapidly proliferating subsets. A notable additional observation in higher-grade osteosarcomas was the presence of intracytoplasmic Zn–AgNOR dots following Zn–AgNOR–Dithizone, Zn–AgNOR, and AgNOR staining, further supporting enhanced proliferative and metabolic activity in advanced lesions.

ACKNOWLEDGEMENT

The authors extend their gratitude to the Dean, BVC and Director Research, BASU for providing the facilities necessary to conduct this study.

Financial support: Funded under Institutional project, BASU, Patna.

Conflicts of Interest: None

REFERENCES

1. Varallo GR, Gelaleti GB, Maschio-Signorini LB, Moschetta MG, Lopes JR, De Nardi AB and De Campos Zuccari DAP. 2019. Prognostic phenotypic classification for canine mammary tumors. *Oncology letters*, **18(6)**, 6545-6553.
2. Bancroft JD, Gamble M. 2019. Theory and Practice of Histological Techniques, 8th ed. Elsevier.
3. Furusawa Y, Takahashi M, Shima-Sawa M, Yamato O and Yabuki A. 2020. Argyrophilic nucleolar organizer regions staining for cytology smears in dogs and cats. J Vet *Med Sci.*:**82(9):**1267-1270.
4. Bertram CA, Donovan TA and Bartel A. 2024. Mitotic activity: A systematic literature review of the assessment methodology and prognostic value in canine tumors. *Vet Pathol*, **61(5),** 752-764.
5. Vijaykumar S, Lakkawar AW, Kumar R, Dhodapkar R and Nair MG. 2018. Histochemical Assessment of AgNORs in Cutaneous Neoplasms of Cattle. *Int. J. Curr. Microbiol. App. Sci*, **7(7),** 523-530.
6. Derenzini M, Treré D. 1991. AgNOR proteins as a parameter of the rapidity of cell proliferation. *J Pathol.*; **165(3):**191–197).
7. Bundgaard-Andersen K, Flagstad A, Jensen AL, Hellmén E and Trerè D. 2008. Correlation between the histopathological diagnosis by AgNOR count and AgNOR area in canine mammary tumors. *J Vet Intern Med*. **22(5):**1174-80.
8. Kumar P, Kumar R, Pawaiya RS and Puttaswamy MB. 2010. Diagnostic significance of mitotic index and AgNOR count in canine mammary tumours. *Braz J Vet Pathol*, **3(1),** 41-45.
9. Elston CW, Ellis IO and Pinder SE. 1998. Prognostic factors in invasive carcinoma of the breast. *Clin Oncol*, **10(1):**14-17.
10. Choviva FU, Sandhika W and Mulawardhana P. 2024. The prognostic role of mitosis index, stage and grade of endometrial cancer in Dr. Soetomo General Academic Hospital Surabaya, Indonesia, in 2018-2020. *J Obst & Gyne Sci*, **136**, 74.
11. Danscher G and Zimmer J. 1978. An Improved Timm Sulphide Silver Method for Light and Electron Microscopic Localization of Heavy Metals in Biological Tissues. *Histochem Springer-Verlag*. **55,** 27-40.
12. Darkwah WK, Aidoo G, Akoto D, Alhassan K, Adormaa BB & Puplampu JB. 2021. Proliferative activity of various grades and types of breast carcinoma using AgNOR (Argyrophilic Nuclear Organizer Region) expression and its prognostic significance. *All Life*, **14(1),** 375-391.
13. Johnson GC, Miller MA and Ramos-Vara JA. 1995. Comparison of argyrophilic nucleolar organizer regions (AgNORs) and mitotic index in distinguishing benign from malignant canine smooth muscle tumors and in separating inflammatory hyperplasia from neoplastic lesions of the urinary bladder mucosa. *J Vet Diag Invest*, **7(1),** 127-136.
14. Nagao T, Ishida Y, Yamazakil K and Kondol Y. 1995. Nucleolar organizer regions in hepatocellular carcinoma related to the cell cycle, cell proliferation and histologic grade. *Pathol-Res Pract*, **191(10),** 967-972.
15. Priyanka DK and KG PK. 2025. The prognostic value of AgNOR parameter in various grades of breast carcinomas. *Int J Acad Med Pharm*, **7(4),** 770-774.
16. Romansik EM, Reilly CM, Kass PH, Moore PF and London CA. 2007. Mitotic index is predictive for survival for canine cutaneous mast cell tumors. *Vet Pathol*, **44(3),** 335-341.
17. Seifi S, Shafigh E and Allaie A. 2011. Quantitative and qualitative analysis of argyrophilic nuclear organizer regions in follicular cyst, keratocystic odontogenic tumor and ameloblastoma. *J Can Res Therap*, **7(3),** 280-285.
18. Salih MM, Abdulgafor DA, Dahlawi HA and Khalifa EH. 2024. The value and significance of nucleolar organizer region proteins as markers of malignancy in breast cancer patients. *Saudi Med J*, **45(10),** 1028.

Indian J. Vet. Pathol., 50(2) : 160-163, 2026: DOI: https://doi.org/10.56093/3e2hb721

SHORT COMMUNICATION

Unraveling the enigma of *Spirocerca lupi* infection in dogs: A hidden menace

Vemula Sravathi, Swathi Bora*, Vagdevi Tangellapally, Haripriya B., Yadala Ravikumar and Sagar Srigadi
Department of Veterinary Pathology, College of Veterinary Science, Rajendranagar,
PVNR Telangana Veterinary University, Hyderabad-500030, Telangana, India
Orcid id: 0000-0003-4141-4026
***Address for correspondence**
Swathi Bora, Department of Veterinary Pathology, College of Veterinary Science, Rajendranagar, PVNR Telangana Veterinary University, Hyderabad-500030; E-mail: drswathibora@gmail.com

Received: 3.2.26; Accepted: 24.2.26

ABSTRACT

Spirocerca lupi is a nematode responsible for causing true malignancies in dogs. Esophageal nodular granulomas are pathological lesions of Spirocercosis. Spirocercosis is a disease occurring predominantly in Canidae, caused by the nematode *Spirocerca lupi*. The present case was noted in 3 years old German shepherd dog with esophageal nodular growth having neoplastic transformation following *S. lupi* infection was histologically elaborated with possible pathologic mechanism. Typical clinical signs are regurgitation, vomition and dyspnoea. Grossly, there was presence of round nodular masses on wall of esophagus occupied almost obliterating the whole lumen of the esophagus. On section, red-colored worms were noticed in the mass and were identified as *Spirocerca lupi* by parasitological examination. The nodular masses were processed routinely and stained by Hematoxylin and Eosin (H & E) and microscopically, esophageal mass revealed numerous parasitic eggs (*Spirocerca lupi*) encircled by proliferating fibrous connective tissue with infiltration of polymorphonuclear cells, predominantly eosinophils and histopathologic lesions of other organs were recorded. Based on parasitic gross, microscopic and immunohistochemical evaluation, the case was diagnosed as Spirocercosis in the dog with acute renal failure.

Key words: Dog, *Spirocerca lupi*, glomerulonephritis, nodule

INTRODUCTION

Spirocercosis is a helminthic disease caused by the nematode *Spirocerca lupi*. The infection is typically characterized by persistent nodular lesions in the oesophagus and aneurysmal changes in the aorta. These lesions may subsequently undergo neoplastic transformation, leading to sarcoma development and can also cause complications such as hemothorax, predominantly reported in dogs and various wild carnivore species[1].

Aside from canids, *S. lupi* infects wild felids, goat, donkey and man by ingesting either the intermediate host (coprophagous beetle) or the paratenic hosts (i.e. reptiles, amphibians, birds and small mammals)[2,3]. After ingestion of infective larvae, it migrates from the stomach *via* the gastric arteries, to the aorta from where they migrate to the caudal thoracic aorta, then, adjacent oesophagus (parasite ectopic migration). In esophagus they mature to adult form and form an inflammatory fibroblastic nodule which may progress to an esophageal sarcoma[4]. The typical clinical signs are related to the presence of esophageal nodules which include regurgitation, vomition, dysphagia and weight loss, together with non-specific signs like pyrexia[5,6].

This study documented histopathology of esophageal tumour induced by *Spirocerca lupi* parasite along with kidney damage (glomerulonephritis).

Clinical history

Thre year old, male, German shepherd dog was presented for postmortem to the necropsy hall, Department of Veterinary Pathology, College of Veterinary Science, Rajendranagar for postmortem with history of weakness, anorexia in the past 7 days, vomiting and sudden onset of hind leg paralysis in the past 10 days.

How to cite this article: Sravathi, V., Bora, S., Tangellapally, V., Haripriya, B., Ravikumar, Y. and Srigadi, S. 2026. Unraveling the enigma of *Spirocerca lupi* infection in dogs: A hidden menace. Indian J. Vet. Pathol., 50(2): 160-163.

MATERIALS AND METHOD

At necropsy, the animal appeared weak, emaciated, pale mucous membrane, dehydration with rough hair coated skin. On flaying the skin, the overall appearance of visceral organs appeared markedly congested. The esophagus showed single large oval shaped firm nodule with mixed fibrous tissue texture, grown outwardly. Esophageal granul oma was located at the distal part of the esophagus about 3 cm from stomach inlet. This lesion was protruded into the lumen causing stenosis of esophagus almost obliterating the lumen. On cut section, single,

well-circumscribed, raised round to oval nodular mass projecting into the lumen and measures approximately 3-5 cm in diameter. It is pink to reddish in colour and mucosal surface over the nodule is ulcerated with firm texture and appears fibrous in consistency. A worm-like structure is visible adjacent to the lesion, suggestive of *Spirocerca lupi* infection. The worms were pulled out from the central cavity a nd were collected in normal saline. For morphological identification, the individual parasites were transferred to hot 70% alcohol and then to glycerol alcohol for clearing. Esophagus, lungs, heart, liver and kidneys were collected in 10% neutral buffered formalin for fixation, subsequently processed, embedded in paraffin wax and sectioned at 4-5 µ thickness. Sectioned tissues were stained with Hematoxylin and Eosin (H&E)[7] to demonstrate eggs in impression smear, immunohistochemical staining (IHC) for demonstrating proliferating nuclear antigen (PCNA) and Heller's method for proteinuria[8].

RESULTS

Grossly, esophages has nodular lesion occupying lumen, severe congestion of lungs, rounding of heart, se vere congestion of liver, lungs and kidneys (Fig.1). On morphology, posterior end of *Spirocerca lupi* showing blunt and rounded, tapering slightly towards the tip and vulval slit was located near the posterior end of the body. Female parasite communicates into esophageal lumen through nodule op ening (Fig.1F).

On impression smear of the esophageal nodule, the cytology shows numerous inflammatory cells, predominantly composed of neutrophils, lymphocytes and eosinophils suggestive of chronic active inflammation with elongated, oval shaped Spirocerca eggs (Fig.2A). Histopathological evaluation of the esophageal tissue revealed a well-developed granulomatous inflammatory response. The granulomas were characterized by concentric layers of proliferating fibrous connective tissue encapsulating parasitic ova, which were surrounded by a dense infiltrate of inflammatory cells. The inflammatory population consisted predominantly of polymorphonuclear leukocytes, chiefly eosinophils, along with lymphocytes and plasma cells, consistent with a chronic active eosinophilic granulomatous esophagitis (Fig. 2B). Within the granulomatous lesions, there was marked fibroblastic proliferation exhibiting cellular atypia. The neoplastic cells were spindle-shaped and arranged in interlacing bundles and whorled patterns. These cells demonstrated anisocytosis, anisokaryosis, hyperchromatic nuclei and frequent mitotic figures, including atypical forms, indicative of anaplasia. Such histomorphological features are consistent with fibrosarcoma (Fig. 2C). Additionally, multifocal nodular areas displayed densely cellular zones composed of closely packed spindle cells arranged in streaming fascicles, with occasional mitotic figures. The overall histomorphological architecture and cytological characteristics support a diagnosis of esophageal fibrosarcoma arising in association with chronic granulomatous inflammation. These pathomorphological changes are coincides with strong immunopositivity of PCNA marker which indicate proliferation of fibroblastic cells (Fig.3 A, B). The granulomas showed different the stage of development with newly developed granulomas showed neovascularization, hyperemia, hemorrhages, tissue necrosis and infiltration of eosinophils and

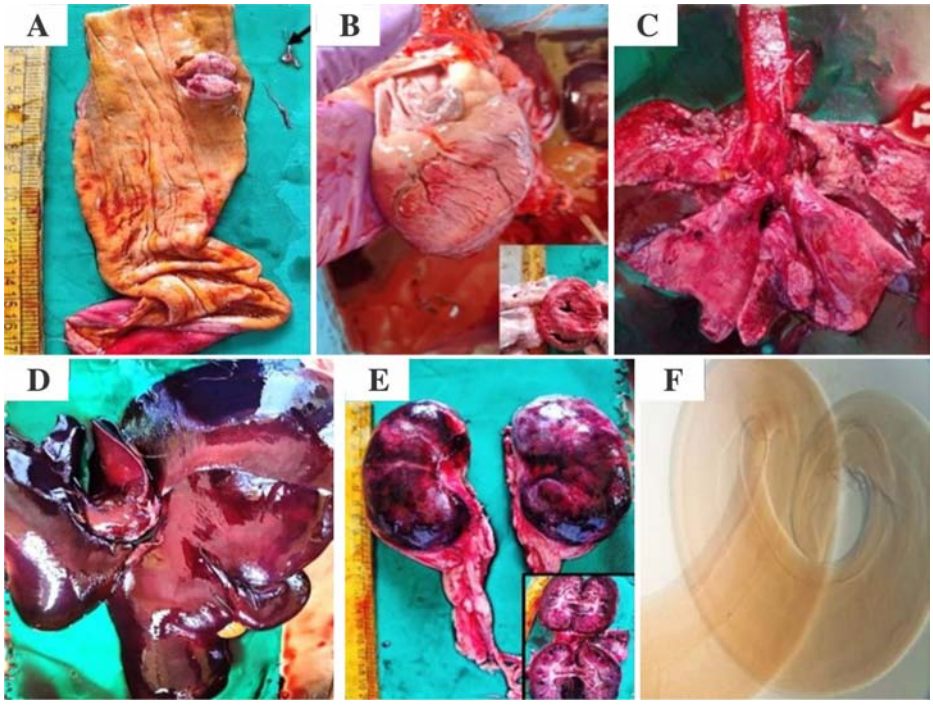

Fig.1A. Gross image of oesophagus showing focal nodular mass occupying oesophageal lumen in a dog. *Spirocerci lupi* worms in an opened nodule. **Arrow-**An individual Worm; **B.** Heart showing rounding due to hypertrophy of left ventricle; **C.** Lung showing odema with severe congestion. **D.** Liver showing severe congetion and rounding of borders; **E.** Kidneys showing haemorrhages and patchy areas of necrosis; **F.** Posterior end of Spirocerca lupi showing vulval slit. Female parasite communicates into esophageal lumen through nodule's opening.

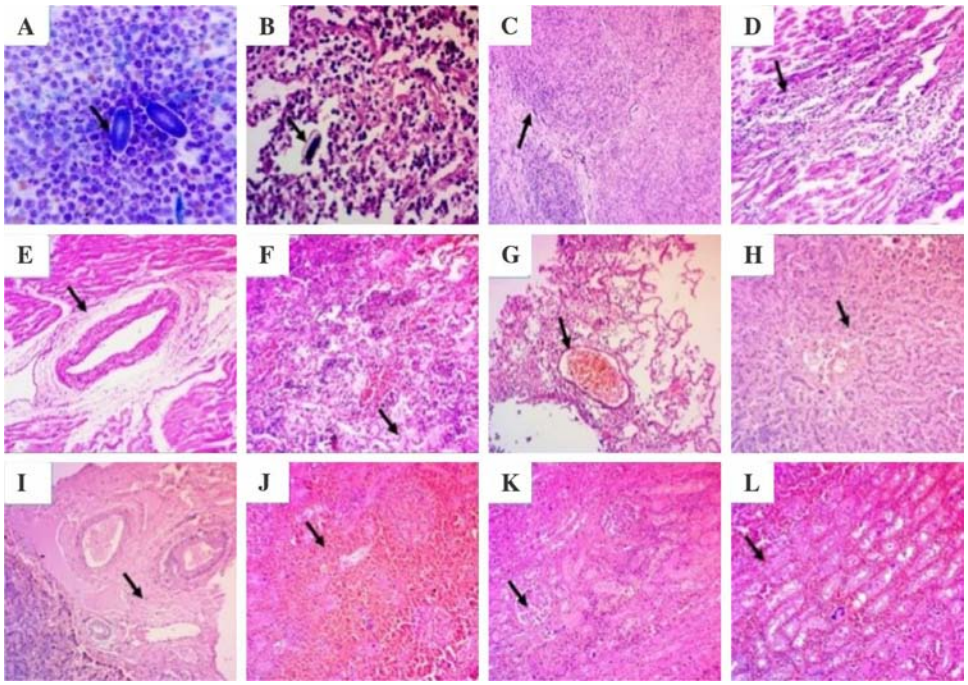

Fig.2. (arrow)A. Impression smear of oesophageal nodule showing *Spirocerca lupi* eggs; **B**. Esophageal nodule showing parasitic eggs surrounded by profused infiltration of eosinophils, MNCs and PMNs (H&E x400); **C.** Esophagus wall showing diffuse infiltration of fibroblast in "whorl" pattern (H&E x100); **D.** Heart showing degeneration of cardiac myocytes with infiltration of PMNs (H&E x100); **E.** Heartsection showing perivascular and intermuscular fibrosis with necrosis and rupture of cardiac myocytes (H&E x100); **F.** Lung section showing haemorrhages, oedema with infiltration of PMNs especially oesinophils (H&E x100); **G.**Lung showing emphysema and distortion of alveoli, congestion of pulmonary blood vessels (H&E x100); **H.** Liver showing severe congestion and haemorrhages, degenerative and atrophic hepatocytes, infiltration of inflammatory cells, distorted hepatic cords with increasing in sinosoidal space (H&E x100); **I.** Liver showing ectesia of portal vein with congestion, oedema and perivascular fibrosis of portal traid (H&E x100); **J&K.** Section of kidneys showing severe necrosis, haemorrhages and presence of hylane cast in degenerating tubules (H&E x100); **L.** Section of kidney showing necrosis of tubular epithelium with degenerated tubules (H&E x100).

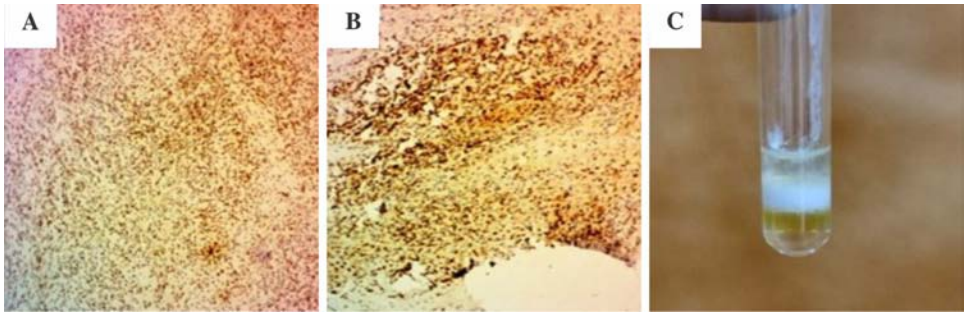

Fig. 3. A-C. Severe nuclear immunopositive reaction with PCNA marker (IHC x100); **C.** Urine sample positive for protein in Heller's method as white ring at the junction.

neutrophils present around the eggs. Further, lymphocytes along myofibroblasts are proliferation occurs along with unorganized fibrous connective tissue.

Heart showed severe infiltration of inflammatory cells with degeneration and necrosis of cardiac myocytes along with perivascular and intermuscular fibrosis (Fig.2E), necrosis and rupture of cardiac myocytes (Fig.2D,E). Where as microscopic picture of lung showing haemorrhages, congestion of pulmonary blood vessels, oedema with infiltration of PMC's especially oesinophils with emphysema and distortion of alveoli (Fig.2F,G). Liver showing extensive congestion and haemorrhages, degenerative and atrophic hepatocytes, mild to moderate infiltration of inflammatory cells, distorted hepatic cords with increasing in sinosoidal space with ectesia of portal vein with congestion, oedema and mild fibrosis of portal traid (Fig.2H,I).

Microscopic picture of kidney showed severe coagulative necrosis of tubular epithelium along with vacular degeneration with infiltration of inflammatory cells, hyline cast in tubules (Fig.2J-L).

To assess kidney function, we went for Heller's method and observed formation of white ring at the junction indicated presence of protein (protenuria) (Fig.3C).

DISCUSSION

We report here a case of esophageal tumor due to Spirocercosis in dog with acute renal failure. The occurrence of acute renal failure (acute kidney injury, AKI) is most likely a secondary complication rather than a direct effect of the parasite. Chronic esophageal tumouration can result in dehydration and hypovolemia due to dysphagia, vomiting, regurgitation, anorexia and reduced water intake, ultimately leading to decreased renal perfusion and ischemic acute tubular necrosis. Spirocercosis in dogs were reportedly found to be associated with pulmonary lesions due to perforation of parasite laden esophageal

growth/ tumor along with acute renal failure due to parasite visceral larval migration. The tumor developed in esophagus showed a tendency to undergo metaplastic changes towards osteoma and myxomatous growth[9].

The molecular pathogenesis of neoplasia associated with *Spirocerca lupi* infection is believed to involve chronic inflammation induced oxidative stress, persistent fibroblast stimulation, and dysregulation of tumor suppressor genes and oncogenes (including altered p53 expression), leading to genomic instability, uncontrolled cellular proliferation and malignant transformation of esophageal mesenchymal cells. The diagnosis of *S. lupi* is not straight f orward compared to other nematodes. Diagnostic technique is hampered by the short and unpredictable period of oviposition, relative ineffective direct fecal preparations and routine flotation and the maturity of the parasite where female inside the nodule produced a passage in the esophageal lumen[10]. Therefore, effective clinical diagnosis is required to diagnosis infection. The condition occurs due to acquiring the infective stage third larvae (L3) by eating either small bird, lizards and dung beetles[3]. After ingestion, L3 enters the body by penetrating the gastric wall and migrates through gastric, gastroepiploic and celiac arteries reaching the caudal thoracic aorta, where they moult into L4[4]. This results in outpouching aneurysm of the thoracic aorta adjacent to the affected esophagus. Later on, the immature adults migrate from aorta to the caudal esophagus and form nodules at the tunica submucosa and adventitia. When the parasite matures, it creates an opening into esophageal lumen where eggs normally pass and forms nodular structure[9].

The present study identified significant sequelae of Spirocercosis, including fibrosarcoma and acute renal failure. Chronic and longstanding infection with *Spirocerca lupi* is well recognized to predispose affected animals to neoplastic transformation, most commonly resulting in sarcoma formation. Among these, fibrosarcoma is the predominant tumour type associated with *S. lupi* infection. Fibrosarcoma is a malignant mesenchymal neoplasm arising from fibroblasts of fibrous connective tissue and is characterized by invasive growth and variable metastatic potential[4].

The probable cause of a death in the present case is as a result of acute renal failure and cardiomyopathy because of degeneration, necrosis of cardiomyocytes in addition to pneumonia leading to generalized toxemic conditions. Other associated pathological changes that contributed in the death of the animal was serious systemic circulatory disturbance which was due to esophageal tumor resulted in vascular constrictions besides acute renal failure. Despite the pathologic effect of spirocercosis, the parasite is often neglected and underestimated by many veterinary practitioners and researchers. Nevertheless, *S. lupi* prevalence worldwide ranges from 10% to 85% where reports are common in tropics and subtropics.

CONCLUSION

The present report should stimulate awareness to all veterinarians in the country about Spirocercosis. It can be regarded as one of the important parasitic infections in canines that usually unnoticed until death and thus act as a silent killer. Spirocercosis should be differentiated from other disease diagnosis while dealing with cases showing clinical signs of vomition or regurgitation, dyspnoea, persistent coughing in dogs greater than 6 months old. During routine deworming, the anthelminthic effective against Spirocercosis should be used.

ACKNOWLEDGEMENT

The authors are thankful to the Department of Veterinary Pathology, C,V.Sc, PVNRTVU, Hyderabad.

Financial support & sponsorship: None.

Conflicts of interest: None.

Use of artificial intelligence (AI)-Assisted Technology for manuscript preparation: The authors confirm that there was no use of AI-assisted technology for assisting in the writing of the manuscript and no images were manipulated using AI.

REFERENCES

1. Portugaliza HP and Torregoza NR. 2015. Post-mortem detection and pathology of canine esophageal worm (*Spirocerca lupi* Rudolphi, 1809) infecting stray dogs in Leyte, Philippines: A case report. *Global Veterinaria* **15**:584-587.
2. Soulsby EJL. 1982. Helminths, arthropods and protozoa of domesticated animals. 7th Edn. London: Bailliere Tindall: 291-294
3. Dvir E, Clift SJ and Williams MC. 2010. Proposed histological progression of the *Spirocerca lupi*-induced oesophageal lesion in dogs. *Vet.Parasitol* **168**: 71–77.
4. Mazaki-Tovi M, Baneth G, Aroch I, Harrus S, Kass PH, Ben-Ari T, Zur G, Aizenberg I, Bark H and Lavy E. 2002. Canine Spirocercosis: clinical, diagnostic, pathologic and epidemiologic characteristics. *Vet Parasitol* **107**:235–250
5. Dvir E, Kirberger RM and Malleczek D. 2001. Radiographic and computed tomography changes and clinical presentation of spirocercosis in the dog. *Vet RadiolUltrasound* **42**:119-129.
6. Luna GLH T. 1968. Manual of histological and special staining techniques. 2nd edition: *The Blakistone Division McGraw-Hill Book Company, Inc. New York, Toronto London* **1**: 9-34.
7. Baka RD, Koutinas CK, Athanasiou LV and Polizopoulou ZS. 2021. Correlation of a quantitative and a semi-quantitative method for proteinuria detection in chronic kidney disease in dogs. *Journal of the Hellenic Veterinary Medical Society* **72**:2897-902.
8. Hamir AN. 1986. Oesophageal perforation and pyothorax associated with Spirocerca lupi infestation in a dog. *The Veterinary record* **119**:276-281.
9. Fox SM, Burns J and Hawkins J. 1988. Spirocercosis in dogs. *Compend Contin Educ Pract Vet* **10**:807-822.

Indian J. Vet. Pathol., 50(2) : 164-167, 2026: DOI: https://doi.org/10.56093/4zgvxs82

SHORT COMMUNICATION

Effects of Di (2-ethylhexyl) phthalate on sperm morphology of Wistar rats

D.C. Monisha*, A. Arulmozhi, P. Srinivasan and P. Sankar
Department of Veterinary Pathology, Veterinary College and Research Institute, Namakkal,
Tamil Nadu Veterinary and Animal Sciences University

***Address for correspondence**
D.C. Monisha, E-mail: dcmonishadpi@gmail.com

Received: 21.11.25; Accepted: 20.12.25

ABSTRACT

Phthalate extensively used as plasticizers in medical devices, cosmetics, children's toys, deodorants and other industries, which is a major environmental toxicant. As they are not covalently bound to polymers and leach easily into the environment and cause a significant health risk. Hence, the present study was carried out to evaluate the effects of Di (2-ethyl hexyl) phthalate on sperm morphology in Wistar rats. Animals were exposed to DEHP at 100, 200 and 400 mg/kg b.wt in corn oil for a period of 28 days. Animals were sacrificed on 29th day and semen was collected from the cauda epididymis and stained with eosin (5%) and nigrosine (10%) staining. Results of this study revealed more sperm abnormalities in all DEHP-exposed groups with more pronounced abnormalities in the high dose group. A highly significant (P<0.01) reduction in the percentage of live sperms and an increase in dead sperms. These results indicated that DEHP has caused many sperm abnormalities and confirm its role as a potent reproductive toxicant.

Keywords: Eosin, nigrosine, phthalate, sperm abnormalities

INTRODUCTION

DEHP is frequently used as a plasticizer in a variety of products like food packaging material, beverage bottles, children's toys, nutraceutical products, cosmetics, deodorants, nail polish, shampoos and skin cleansers. Phthalates, particularly DEHP, leaches readily from products during heating, cleaning and repeated use due to their non-covalent bonding with polymers. DEHP affects endocrine, reproductive, and cardiovascular systems as well as neural development, and causes multiple organs toxicity in humans[1]. DEHP is a potent toxic compound that mainly affects male reproductive system leading to infertility and Testicular Dysgenesis Syndrome (TDS) in humans including insufficient testosterone production during in utero development, undescended testes, malformations of the penis, reduced Anogenital Distance (AGD), decreased sperm motility, poor semen quality and abnormal sperm morphology[2], infertility and testicular cancer[3]. DEHP has negative impacts on fertility by affecting spermatogenesis, sperm functionality, male reproductive hormones and also affects both qualitative and functional characteristics of semen[4].

MATERIALS AND METHODS

An experimental trial was conducted using forty male Wistar rats, which were randomly allocated into four groups as Group I, II, III and IV. Group I acted as control and received corn oil; Group II, III and IV received 100, 200 and 400 mg/kg b.wt. of DEHP respectively. DEHP was administered once daily by oral gavage for a period of 28 days. The animals were sacrificed on 29th day of experimental trial to evaluate the reproductive toxicity induced by DEHP.

The plasticizer Di (2-ethylhexyl) phthalate (50 g) and corn oil were purchased from M/s. Eswarr Scientific & Co, Trichy and stored at room temperature between 20 and 25°C. The corn oil is used as a vehicle (solvent) for the preparation of DEHP suspension.

How to cite this article : Monisha, D.C., Arulmozhi, A., Srinivasan, P., and Sankar, P. 2026. Effects of Di (2-ethylhexyl) phthalate on sperm morphology of Wistar rats. Indian J. Vet. Pathol., 50(2) : 164-167.

Experimental trail was carried out in Laboratory Animal House of the Department of Veterinary Pharmacology and Toxicology, Veterinary College and Research Institute, Namakkal with the approval from Institutional Animal Ethics Committee [No. IAEC/13/VCRI - NKL/2025, Dated: 28.03.2025].

All the rats were sacrificed on 29th day and necropsy was conducted to evaluate the pathological lesions. Semen was collected from the tail of the epididymis of testes from all the groups and smears were prepared on clean glass slides. A drop of eosin (5 %) mixed with four drops of nigrosine (10 %) and a drop of sperm suspension was added. The contents were gently

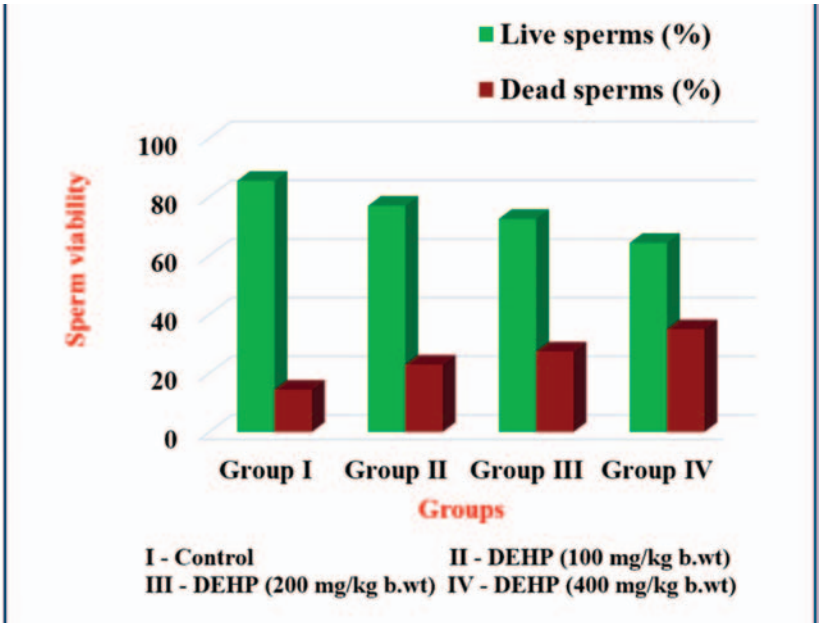

Graph 1. Mean sperm viability of Wistar rats in DEHP induced toxicity

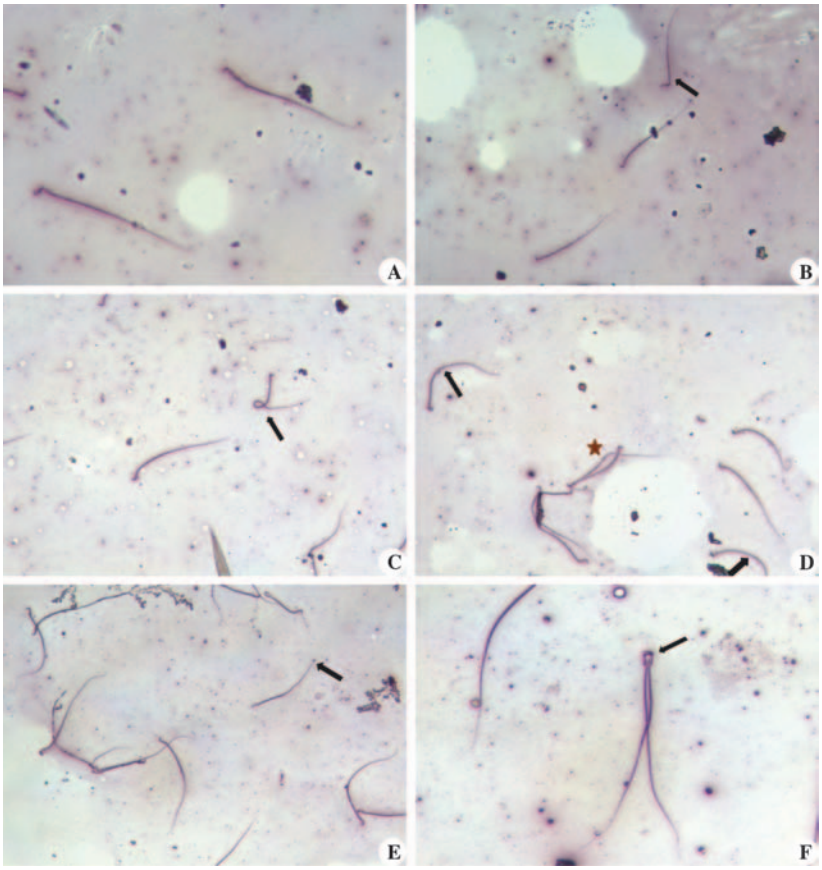

Fig. 1 (A). Control rats showing normal sperm; **(B).** Low dose - DEHP induced rat sperm showing bent neck (arrow); **(C).** Low dose - DEHP induced rat sperm depicting coiled sperm (arrow); **(D).**Medium dose - DEHP induced rat depicting angulated tail (arrows), cytoplasmic vacuolation (star); **(E).** Medium dose - DEHP induced rat sperm revealing microcephaly (arrow); **(F).** Medium dose - DEHP induced rat sperm revealing fusion of head and neck (arrow)

mixed and a small drop of suspension was placed on the slide. A thin smear was prepared using a spreader slide and allowed to air dry. Air-dried stained slides were examined under microscope to study the sperm abnormalities. Under the microscope, live sperm appeared unstained, while dead sperm appeared as pink colour.

At least 100 spermatozoa were counted in different fields of each stained slide to evaluate the proportion of viable and non-viable sperm, and to identify various morphological abnormalities, such as head, midpiece and tail deformities. The observations were recorded in a systematic manner to quantify the percentage of live and dead sperms.

The testes were collected in all the DEHP treated groups and fixed in 10 per cent neutral buffered formalin for histopathological examination. The tissue sections were cut into 4 µm thickness and subjected to routine H & E staining.

RESULTS

In Eosin-Nigrosin staining, live sperm appears as transparent due to their intact membranes, whereas dead sperm exhibit a distinct pink colour. Live and dead sperms in control and DEHP treated groups are presented in Table 1 and Graph 1. In normal healthy rats about 80 % of the sperms are viable, while approximately 20 % are non-viable. The typical sperm morphology in rats is characterized by a hook-shaped head and an elongated tail. Control rats exhibited normal sperm morphology (Fig. 1. A). In contrast, rats treated with a low dose of DEHP showed abnormalities such as bent neck (Fig. 1. B) and coiled sperm (Fig. 1. C) while the medium dose DEHP group showed defects like angulated tail (Fig. 1. D), microcephaly (Fig. 1. E) and fusion of head and neck (Fig. 1. F). Rats exposed to high dose of DEHP revealed various types of sperm abnormalities *viz.*, head fusion (Fig. 1. G), multiple angulations (Fig. 1.H), flat head (Fig. 1. I), head fusion with coiled tail (Fig. 1. J). In addition, multiple anomalies like microcephaly, angulated tail, bent neck, curved tail, coiled tail (Fig.

Table 1. Mean (±SE) of sperm viability in Wistar rats in various toxic dose levels of DEHP induced toxicity

S.No.	Sperm morphology	Group I	Group II	Group III	Group IV
1.	**Live sperms (%)**	85.52±1.08[a]	77.06±0.77[b]	72.60±1.01[c]	64.40±0.80[d]
2.	**Dead sperms (%)**	14.4±22.93[a]	22.93±0.77[b]	27.40±1.01[c]	35.0±0.86[d]

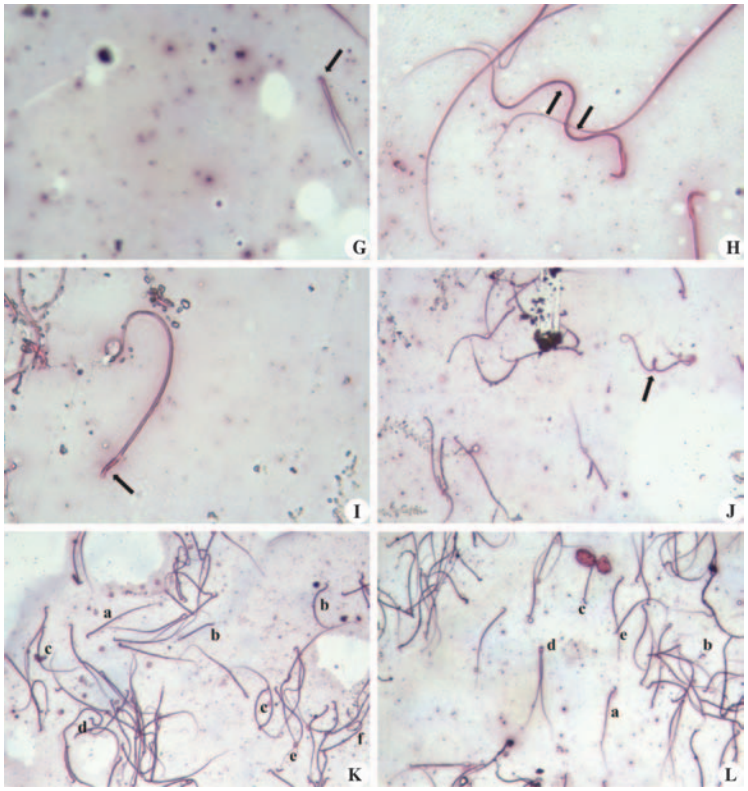

Fig. 1 (G). High dose - DEHP induced rat sperm displaying head fusion (arrow); **(H).** High dose-DEHP induced rat sperm displaying multiple angulations (arrows); **(I).** High dose - DEHP induced rat sperm revealing flat head (arrow); **(J).** High dose - DEHP induced rat sperm revealing head fusion with coiled tails (arrow); **(K).** High dose - DEHP induced rat sperms revealing multiple anomalies (a) Normal sperm (b) Microcephaly (c) Angulated tail (d) Bent neck (e) curved tail (f) Coiled tail; **(L).** High dose DEHP induced rat sperms revealing multiple anomalies (a) Normal sperm (b) Detached head (c) Bent head (d) Pairing of sperm (e) Headless tail

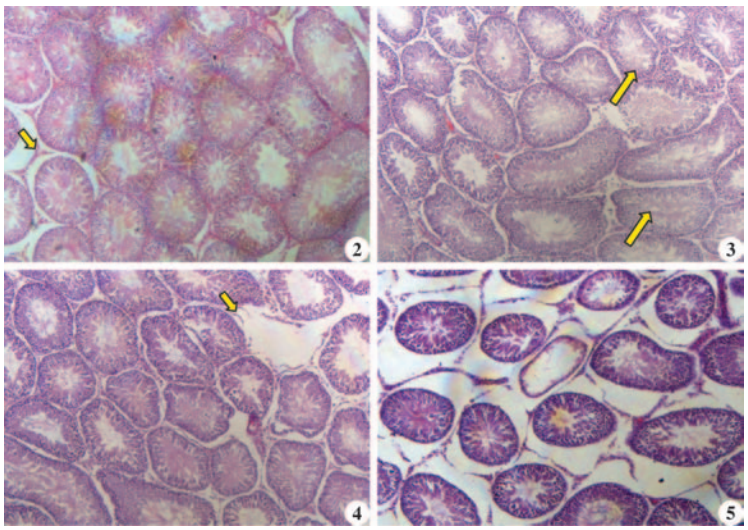

1. K) and combined defects such as detached head, bent head, pairing of sperm and headless tail (Fig. 1. L) were noticed in high dose group.

The control rat exhibited normal testicular architecture with well-organized seminiferous tubules with fully packed spermatozoa and interstitial Leydig cells (Fig. 2). The severity of testicular histopathological lesions in DEHP groups increased in dose-dependent manner. The low dose DEHP treated group revealed mild atrophy of seminiferous tubules with vacuolations (Fig. 3) whereas, medium dose group showed loss of few seminiferous tubules with mild reduction of spermatids in the tubular lumen (Fig. 4). The testes of rats in high dose group exhibited severe atrophy of most of the seminiferous tubules (Fig. 5).

DISCUSSION

Though there were abnormal sperms in all DEHP treated groups, a marked increase in sperm abnormalities was recorded in high dose DEHP treated groups. Similar abnormalities also recorded by[5,6]. The head, midpiece and tail abnormalities might be due to degeneration of seminiferous germinal epithelium and spermicidal action of DEHP. In addition, DEHP also leads to depletion of zinc from spermatids and resulted in sperm abnormalities as zinc plays a crucial role in sperm maturation[7] also caused reproductive toxicity through oxidative stress and lipid peroxidation in testes[8].

This might be due to generation of reactive oxygen species and thereby leading to oxidative stress. Since sperm membranes are rich in polyunsaturated fatty acids and they are highly vulnerable to damage of sperm membrane resulting in reduced sperm viability[9].

Fig. 2. Control - 29th day: Testes showing normal seminiferous tubules with fully packed spermatozoa and clumps of interstitial leydig cells (arrows) (H&E x 40); **Fig. 3**. Low dose DEHP – 29th day: Testes showing mild atrophy and vacuolations in the seminiferous tubules (arrows) (H&E x 40); **Fig. 4.** Medium dose DEHP – 29th day: Testes showing loss of seminiferous tubules (arrow) and mild reduction of spermatids in tubular lumen (H&E x 40); **Fig. 5.** High dose DEHP – 29th day: Testes showing severe atrophy of seminiferous tubules (H&E x 40)

DEHP toxicity damages testes by different mechanism such as production of reactive oxygen species (ROS), oxidative stress, lipid peroxidation, damage to DNA, disruptions in cellular functions, alterations in cellular redox mechanism and mitochondrial dysfunctions in gonocytes of testes[10].

These histopathological lesions of testes might be due to alterations in hypothalamic amino acid neurotransmitters involved in neuroendocrine reproductive regulation[11].

Financial support & sponsorship: None.

Conflicts of interest: None.

Use of artificial intelligence (AI)-Assisted Technology for manuscript preparation: The authors confirm that there was no use of AI-assisted technology for assisting in the writing of the manuscript and no images were manipulated using AI.

REFERENCES

1. Rowdhwal SSS and Chen J. 2018. Toxic effects of di-2-ethylhexyl phthalate: An overview. *Biomed Res. Int* **2018**(1): 1750368.
2. Bloom MS, Whitcomb BW, Chen Z, Ye A, Kannan K and Buck Louis GM. 2015. Associations between urinary phthalate concentrations and semen quality parameters in a general population. *Hum Reprod* **30**(11): 2645-2657.
3. Karabulut G and Barlas N. 2018. Genotoxic, histologic, immunohistochemical, morphometric and hormonal effects of di-(2-ethylhexyl)-phthalate (DEHP) on reproductive systems in pre-pubertal male rats. *Toxicol Res* **7**(5): 859-873.
4. Ogli SA and Odeh SO. 2020. Oral Ascorbic Acid And α-Tocopherol Protect On Di-(2-Ethyl Hexyl) Phthalate (DEHP) Induced Effects on Gonadotoxicity InThe Adult Male Wistar Rats. *Eur J Med Health Sci* **2**(3): 1-8.
5. Agarwal DK, Eustis S, Lamb JC, Reel JR and Kluwe WM. 1986. Effects of di (2-ethylhexyl) phthalate on the gonadal pathophysiology, sperm morphology, and reproductive performance of male rats. *Environ Health Perspect* **65:** 343-350.
6. Erkekoglu P, Zeybek ND, Giray B, Asan E, Arnaud J and Hincal F. 2011. Reproductive toxicity of di (2-ethylhexyl) phthalate in selenium-supplemented and selenium-deficient rats. *Drug Chem Toxicol* **34**(4): 379-389.
7. Foster PM, Foster JR, Cook MW, Thomas LV and Gangolli SD. 1982. Changes in ultrastructure and cytochemical localization of zinc in rat testis following the administration of di-n pentyl phthalate. *Toxicol Appl Pharmacol* **63:** 120-132.
8. Abdel-Kawi SH, Hashem KS and Abd-Allah S. 2016. Mechanism of diethyl hexyl phthalate (DEHP) induced testicular damage and of grape seed extract-induced protection in the rat. *Food Chem Toxicol* **90:** 64-75.
9. Guthrie HD and Welch GR. 2012. Effects of reactive oxygen species on sperm function. *Theriogenology* **78:**1700–1708.
10. Abdollahi M. 2015. Phthalate induced toxicity in various organs with a focus on the reproductive system. *Int J Pharmacol* **100**(2): 95-105.
11. Carbone S, Samaniego YA, Cutrera R, Reynoso R, Cardoso N, Scac chi P and Ponzo OJ. 2012. Different effects by sex on hypotha lamic–pituitary axis of prepubertal offspring rats produced by in utero and lactational exposure to di-(2-ethylhexyl) phthalate (DEHP). *Neurotoxicology* **33**(1): 78-84.

Indian J. Vet. Pathol., 50(2) : 168-170, 2026: DOI: https://doi.org/10.56093/cyjz8y57

CASE REPORT

Concurrent occurrence of intestinal coccidiosis and oral papillomatosis in a buffalo calf

P. Balaram[1], CH. Sudha Rani Chowdary[*], K. Satheesh[2], V. Rama Devi[3] and V. Neeraja[1]
Department of Veterinary Pathology, NTR College of Veterinary Science, Sri Venkateswara Veterinary University, Gannavaram, Andhra Pradesh, India- 521102
[1]M.V.SC Scholars; [2]Professor and Head, Department of Veterinary Pathology, C.V.Sc, Garividi;
[3]Professor and University Head, Department of Veterinary Pathology, NTR CVsc, Gannavaram

***Address for correspondence**
CH. Sudha Rani Chowdary, Assistant Professor, E-mail: drsudha84@gmail.com

Received: 24.12.25; Accepted: 12.1.26

ABSTRACT

This paper describes a unique case of concurrent oral papillomatosis and intestinal coccidiosis in a six-month-old buffalo calf with a history of anorexia, dysentry, and presence of multiple exophytic masses within the oral cavity. Microscopically, the tumors in the oral cavity were characterized by papillary projections with a fibrovascular core and characteristic koilocytes. Simultaneously, the intestines exhibited a thickened, corrugated, and hemorrhagic mucosa grossly, with coccidial oocysts in the intestinal scrapings. On histopathology, proliferative enteritis was recorded. The findings suggest that the physiological stress and immunosuppression induced by intestinal coccidiosis likely predisposed the calf to the mucosal manifestation of papillomatosis.

Keywords: Buffalo calf, coccidiosis, concurrent occurrence, immunosuppression, oral papillomatosis

How to cite this article : Balaram, P., Chowdary, S.R., Satheesh, K., Rama Devi, V. and Neeraja, V. 2026. Concurrent occurrence of intestinal coccidiosis and oral papillomatosis in a buffalo calf. Indian J. Vet. Pathol., 50(2) : 168-170.

INTRODUCTION

The dairy industry is a cornerstone of India's economy, contributing approximately 5% to the national GDP and supporting the livelihoods of over eight crore farmers[1]. However, the sector faces significant challenges due to infectious diseases that impact animal health and productivity. Among these, coccidiosis stands out as a globally prevalent, stress-related intestinal protozoan disease caused by apicomplexan parasites of the genus *Eimeria*. The disease is a major driver of economic loss in the cattle sector, primarily due to high morbidity and mortality in young calves[2,3] . In addition to the parasitic threats, buffalo calves are susceptible to bovine papillomatosis, a contagious viral condition caused by the Bovine Papillomavirus (BPV). This disease is characterized by the development of benign tumors or "warts" on the skin and mucosal epithelium, particularly within the upper alimentary tract[4,5]. Although rarely fatal, papillomatosis can result in stunted growth and reduced milk production[4]. While both conditions are recognized as separate entities in the literature, this case report shows, for the first time, concurrent occurrence of coccidiosis and papillomatosis in a buffalo calf.

A six-month-old female buffalo calf was presented for necropsy to the Department of Veterinary Pathology, NTR College of Veterinary Science, Gannavaram with a history of dysentery and severe dehydration persisting for ten days prior to death. At necropsy, multiple exophytic, hard, sessile masses on the gums and the dorsum of the tongue (Fig.1) were observed. The masses were nodular and measured approximately 2–3 cm in diameter; their cut surfaces appeared grayish-white and fleshy. The abdominal cavity revealed generalized peritonitis, characterized by severe mesenteric and serosal congestion of the intestines, accompanied by localized adhesions between intestinal segments. The intestinal mucosa was severely congested to hemorrhagic, containing mucoid and blood-tinged contents. Notably, the mucosa of the large intestine was markedly thickened and exhibited prominent corrugations (Fig. 2). Direct smear examination of intestinal scrapings confirmed the presence of *Eimeria* spp. oocysts. Representative tissue samples were collected in 10% formalin and subjected to routine tissue processing, paraffin embedding and microtomy. Four to five micron thick paraffin sections were stained by Haemotoxylin and Eosin method. Histologically, the masses in the oral cavity were characterized by exophytic, unbranched to branched papillary projections composed of proliferating stratified squamous epithelium supported by a fibrovascular core. The stratum corneum exhibited hyperkeratosis with a "basket-weave" appearance, while the stratum spinosum showed marked acanthosis and presence of koilocytes, with characteristic perinuclear halos

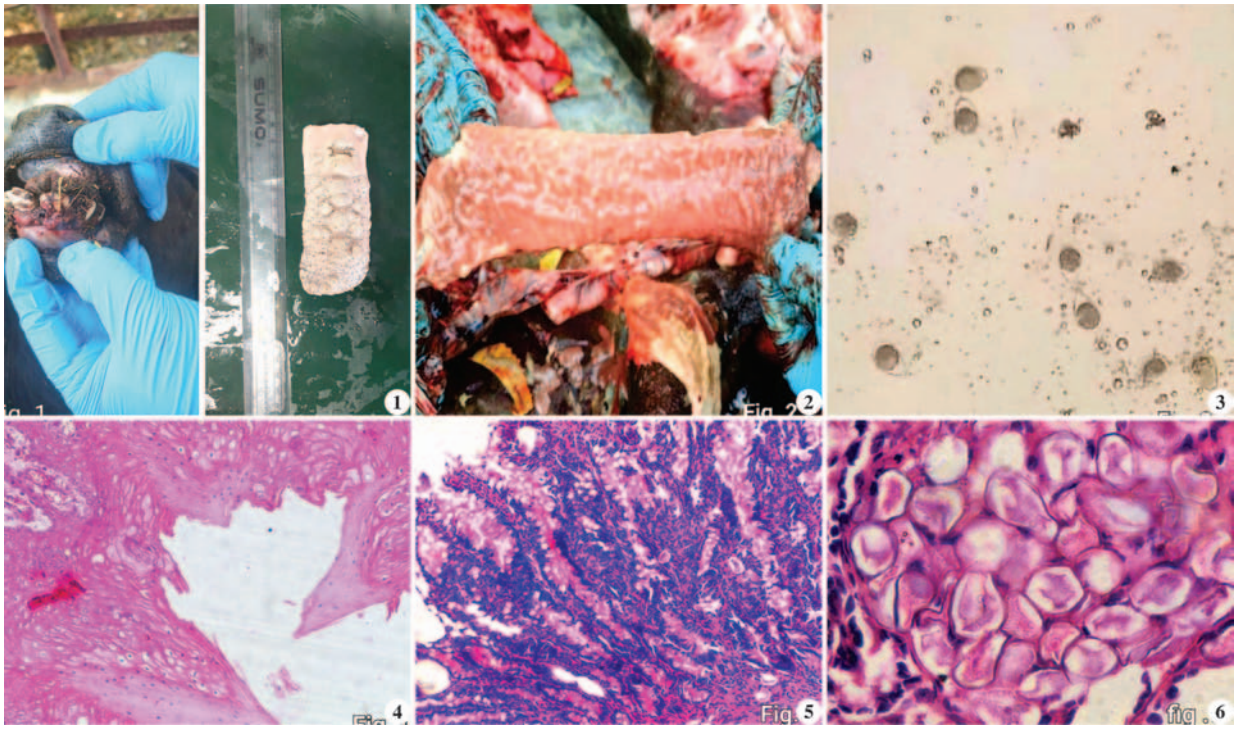

Fig. 1. Papillomas on the gum line and dorsum of the tongue; **Fig. 2.** Intestinal mucosa showing congestion and corrugations; **Fig. 3.** Intestinal scrapings showing a large number of unsporulated oocysts of *Eimeria sp.* x100; **Fig. 4.** Oral papillomatosis showing exophytic, papillary projections with hyperkeratosis, acanthosis and koilocytes, H&E x100; **Fig. 5.** Proliferative enteritis showing severe goblet cell hyperplasia and stages of coccidial organisms. H&E x100; **Fig. 6.** Intestinal mucosa inhabited by stages of coccidial organisms, H&E x400

(Fig. 3). The underlying fibrovascular core was composed of dense collagen, active fibroblasts, and significant neovascularization. Histopathological examination of the intestines revealed proliferative enteritis characterized by mucosa forming polypoid structures, goblet cell hyperplasia and the epithelium inhabited by various developmental stages of *Eimeria* spp. (Fig. 4 & 5). There was a severe infiltration of mononuclear cells within the lamina propria, while the intestinal lumen contained extensive necrotic debris, bacterial colonies, and various stages of *Eimeria* spp.

The present case report documents the concurrent occurrence of oral papillomatosis and intestinal coccidiosis in a buffalo calf. While previous literature has recorded concurrent viral infections in cattle, such as Papillomavirus combined with Parapox or Herpesvirus[6], the specific co-existence of oral papillomatosis and coccidiosis has not been previously documented. Bovine papillomatosis in young cattle is typically associated with several predisposing factors, including immunosuppression, age, poor nutritional status, parasitic infections, and environmental stress[7]. In this instance, it is highly probable that the intestinal coccidiosis induced a state of immunosuppression, thereby predisposing the animal to the papillomavirus infection.

While papillomas typically manifest on the head, neck, and shoulders[8], the growths in this case were localized specifically to the gums and tongue. Such mucosal forms are less frequent and are often categorized as exophytic papillomas, which can be precursors to alimentary or bladder cancers[9]. This unique presentation of concurrent oral papillomatosis and coccidiosis emphasizes the complex interplay between viral and parasitic pathogens in young ruminants and provides a novel reference for future clinico-pathological investigations.

Financial support & sponsorship: None.

Conflicts of interest: None.

Use of artificial intelligence (AI)-Assisted Technology for manuscript preparation: The authors confirm that there was no use of AI-assisted technology for assisting in the writing of the manuscript and no images were manipulated using AI.

REFERENCES

1. Bharia A, Mali MM, Parashar MC, Kumari K and Meena DS 2024. Studies on prevalence and diversity of eimeria species in cattle calves in and around Jaipur, Rajasthan. Ruminant Science **13 (1):** 171-174.
2. Nalbantoglu S, Sari B, Cicek H and Karaer Z. 2008. Prevalence of coccidian species in the water buffalo (*Bubalus bubalis*) in the province of Afyon, Turkey. *Acta Vet Brno* **77 :** 111-116.

3. Bahrami S and Alorzi AR. 2013. Prevalence of subclinical coccidiosis in river buffalo calves of southwest of Iran. *Acta Parasitol* **58(4):** 527-530.
4. Bocaneti F, Altamura G, Corteggio A, Velescu E, Roperto F and Borzacchiello G. "Bovine Papillomavirus: new insights into an old disease," *Transbound Emerg Dis* **63(1):** 14–23.
5. Hamza BS, Naeem LA, Al-Mossawai OF And Khudair ZW. 2024. Histopathological Study Of Papillomatosis Of Cattle Skin In Basrah. *Int J Appl Sci Technol*, **6:** 302-312.
6. Gallina L, Savini F, Canziani S, Frasnelli M, Lavazza A, Scagliarini A and Lelli D. 2020. Bovine papillomatosis hiding a zoonotic infection: Epitheliotropic viruses in bovine skin lesions. *Pathogens* **9(7)**: 583.
7. Ataseven VS, Kanat OY and Ergun O. 2016. Molecular identification of bovine papillomaviruses in dairy and beef cattle: First description of Xi-and Epsilon papilloma virus in Turkey, *Turk J Vet Anim Sci* **40:** 757-763.
8. Etriwati E, Nazaruddin N, Aliza D, Hasan DI and Siagian RA. 2021. Pathomorphology of Papilloma Tumor in Cattle Based on Macroscopic and Microscopic. In 2nd International Conference on Veterinary, Animal, and Environmental Sciences (ICVAES 2020) (pp. 102-106). Atlantis Press.
9. Jana C, Tamang R and Kumar P. 2024. Cutaneous Bovine papillomatosis: Etio-pathology and disease status in India. *Indian J Anim Health* **63(2):** 53-61.

Indian J. Vet. Pathol., 50(2) : 171-172, 2026: DOI: https://doi.org/10.56093/mf01en28

CASE REPORT

Partial intestinal Atresia (Stenosis) in a day-old Beetal goat kid: A case report

Chagi Nagalinga, Abhishek Verma and Geeta Devi Leishangthem*
Department of Veterinary Pathology, College of Veterinary Science,
Guru Angad Dev Veterinary and Animal Sciences University, Ludhiana, Punjab

***Address for correspondence**
Geeta Devi Leishangthem, Department of Veterinary Pathology, College of Veterinary Science, Guru Angad Dev Veterinary and Animal Sciences University, Ludhiana, Punjab; E-mail: drgeetapatho@gmail.com

Received: 20.12.25; Accepted: 26.1.26

ABSTRACT

A one-day-old male goat kid was presented for necropsy with clinical signs of abdominal distension, weakness, and absence of faecal passage since birth. Gross examination revealed a segmental narrowing of the ileum approximately 15–20 cm proximal to the ileocecal junction. The affected part had a markedly reduced lumen diameter, resulting in partial obstruction. The proximal small intestine was severely dilated, haemorrhagic and filled with blood-tinged fluid, while the distal intestine was collapsed and empty with reduced lumen size. Histopathology of distal part showed reduced lumen diameter with intact intestinal wall layers, reduced villi and mild mucosal congestion while the proximal dilated segments showed mucosal flattening, loss of villi, congestion and marked submucosal haemorrhage. The condition was diagnosed as partial intestinal atresia (stenosis), a rare congenital anomaly in goat kids.

Keywords: Congenital anomaly, goat kid, intestinal stenosis, partial atresia, pathology

INTRODUCTION

Intestinal atresia is a congenital anomaly leading to obstruction of the intestinal lumen. It is classified into several types, ranging from complete absence of lumen (Type II, III) to incomplete narrowing (Type I, or stenosis)[1]. While commonly described in calves and lambs, such congenital anomalies are rare in goat kids[2,3]. Furthermore, partial atresia or stenosis is not much reported in goat kids. Partial intestinal atresia allows limited passage of intestinal contents. The condition is often incompatible with life and manifests clinically as failure to pass meconium, abdominal distension, and progressive weakness[4]. This report documents partial intestinal atresia in a neonatal goat kid with gross and histopathological details.

CASE DESCRIPTION

A day-old male goat kid was presented to the department for necropsy with the history of failure to pass faeces since birth, reduced suckling, progressive abdominal distension, weakness and death within 24 hours of birth. A thorough necropsy was performed and representative intestinal tissues were collected in 10% neutral buffered formalin and were routinely proceed and stained with haematoxylin and eosin.

On external examination of carcass, no significant changes were observed except pale conjunctival mucous membrane. On opening of abdominal cavity, dilated loops of proximal small intestine filled with blood-tinged fluid and gas were observed along with congested mesenteric blood vessels (Fig.1). The ileum showed a segment of stenosis approximately 2 cm in diameter, located around 20 cm proximal to the ileocecal junction. The lumen was markedly narrowed but not completely obliterated (Fig. 2). Proximal intestine was dilated and congested, while distal ileum, caecum, and colon were empty and collapsed. Abomasum was filled up with curdled milk. No other congenital anomalies were observed. Lungs, liver and kidneys only revealed mild congestion.

How to cite this article : Nagalinga, C., Verma, A. and Leishangthem, G.D. 2026. Partial intestinal Atresia (Stenosis) in a day-old Beetal goat kid: A case report. Indian J. Vet. Pathol., 50(2) : 171-172.

On histopathological examination, the stenotic segment showed all layers of the intestine but with narrowed lumen, and small and club shaped villi and predominance of goblet cells along with mild congestion and oedema in the mucosa and submucosa (Fig.3). Whereas the proximal dilated segments showed mucosal flattening, loss of villi, congestion and marked submucosal haemorrhages (Fig. 4).

DISCUSSION

Partial intestinal atresia or stenosis corresponds to Type I intestinal atresia in veterinary classification. It differs from complete atresia by presence of a continuous but narrowed lumen. Type I atresia, is characterized by

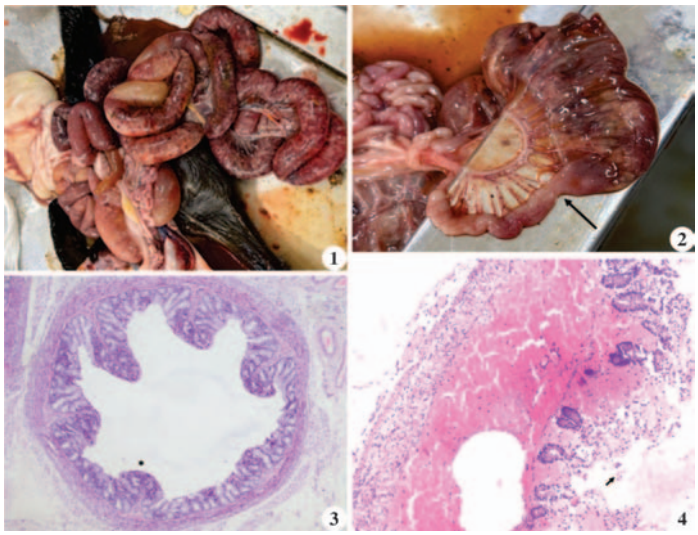

Fig. 1. Gastrointestinal tract of a day-old goat kid showing markedly dilated loops of proximal small intestine due to partial obstruction; **Fig. 2.** Stenotic ileal segment demonstrating reduced lumen (Arrow); **Fig. 3.** Histological section of the stenotic ileum showing narrowing of the lumen (*) with intact mucosa, small and blunted villi, submucosa, and muscularis (H&E 40X); **Fig. 4.** Proximal dilated ileum with submucosal haemorrhages, flattening of villi and denudation of enterocytes (arrow) (H&E 100X).

the presence of a thin intraluminal mucosal or membranous septum that completely or partially occludes the lumen. In this form, the proximal intestinal segment becomes markedly dilated due to accumulation of ingesta and secretions, while the distal segment remains collapsed and devoid of contents. Importantly, the mesentery remains intact and the overall intestinal length is preserved, distinguishing this type from other forms of intestinal atresia[1]. In ruminants, the ileum is most frequently affected. The clinical picture includes abdominal distension, anorexia, and failure to pass faeces. Death usually results from progressive obstruction and toxaemia[5,6]. Vascular accidents during late gestation, such as intrauterine ischemia or thromboembolism of mesenteric vessels, have also been implicated as contributory mechanisms, leading to localized necrosis and resorption of affected intestinal segments[7]. In cattle, a genetic predisposition has been suggested, with several reports indicating familial clustering of atresia coli, particularly in Holstein calves[8].

In small ruminants such as goat kids, surgical correction of congenital intestinal stenosis or atresia is seldom attempted—primarily due to the unfavourable cost-benefit ratio in production animals, limited access to specialist surgical services, and the low economic value of individual animals. Thus, most affected kids are euthanized or die shortly after onset of clinical signs. In contrast, in large animals with higher individual value (e.g., calves and foals), successful surgical correction and survival have been reported. For instance, active surveillance over eight years in dairy herds documented 197 cases of intestinal atresia among 56,454 liveborn calves (incidence ~0.35 %), underscoring that this condition, while rare, is better characterized in bovines[8]. An earlier veterinary series also reported 34 cases of intestinal atresia or stenosis across various species (29 atresia, 5 stenosis), with the majority in calves and a few in lambs or pigs[2]. Palpation of the amniotic vesicle during pregnancy diagnosis between 36 to 42 days of gestation has been considered one of the reasons for atresia at small intestine and colon[9]. In goats, a rare report describes ileal atresia concurrent with absence of the ileo-caecal valve and volvulus in a goat kid, which remains one of the few documented surgical anomaly cases in small ruminants[6]. Thus, this present case contributes to the very limited literature on congenital intestinal stenosis in goats and highlights the importance of documenting such anomalies in small ruminants.

This case report describes partial intestinal atresia (type I) of the ileum in a neonatal goat kid, a rare congenital anomaly causing intestinal obstruction. Pathological examination is essential for accurate diagnosis and differentiation from complete atresia.

Financial support & sponsorship: None.

Conflicts of interest: None.

Use of artificial intelligence (AI)-Assisted Technology for manuscript preparation: The authors confirm that there was no use of AI-assisted technology for assisting in the writing of the manuscript and no images were manipulated using AI.

REFERENCES

1. Oh C. 2023. Jejunoileal Atresia: A contemporary review. *Adv Pediatr Surg*. **29**(2): 89.
2. Van der Gaag I & Tibboel D. 1980. Intestinal atresia and stenosis in animals: a report of 34 cases. *Vet Pathol* **17**(5): 565-574.
3. Brown CC, Baker DC & Barker IK. 2007. Alimentary system. In M.G. Maxie (Ed.), *Jubb, Kennedy & Palmer's pathology of domestic animals*, 5th ed. Vol. 2. **1**:296. Elsevier.
4. Uzal FA, Plattner BL, Hostetter JM. 2016. Alimentary System. In *Jubb, Kennedy & Palmer's Pathology of Domestic Animals*: Volume 2. 2016:1–257.e2. doi: 10.1016/B978-0-70205318-4.00007-3. Epub 2016 Feb 5. PMCID: PMC7811793.
5. Radostits OM, Gay CC, Hinchcliff KW, Constable PD. 2007. In *Veterinary Medicine A text book of disease of cattle, sheep, pigs and horse* 10th ed. Saunders Elsevier, Edinburgh, Pp. 2007:254-60.
6. Kheirandish R & Tajik J. 2017. Ileal atresia concurrent with agenesis of the ileocecal valve and intestinal volvulus in a goat kid. *BJVM*, **20**(1): 73–79.
7. Shweta S and Vaiphei K. 2021. Intestinal atresia: histopathologist view. *Int Surg J* **8**: 226-231.
8. Keane OM, Carthy TR, Hanrahan JP, Matthews D, McEwan JC, Rowe SJ, Kenneally J & Mee JF. 2023. Risk factors for, and genetic association with, intestinal atresia in dairy calves. *Anim Genetics* **54**(2): 104–112.
9. Elsa AT and Onyeyili P. A. 2004. Surgical Management of Small Intestinal Atresia in Sokoto Red Goats. *Pak J Biol Sci*, **7**: 2024-2025.

Indian J. Vet. Pathol., 50(2) : 173-176, 2026: DOI: https://doi.org/10.56093/bhsk5n12

CASE REPORT

Vulvovaginal squamous cell carcinoma: Mimicking chronic prolapse in bitch

Vishal K. Sinha[1], Kaushal Kumar*[1], Deepak Kumar[1], Imran Ali[1], Ramesh Tiwary[2] and Rajesh Kumar[2]
[1]Department of Veterinary Pathology, BVC, BASU, Patna, Bihar, India
[2]Department of Veterinary Surgery & Radiology, BVC, BASU, Patna, Bihar, India

***Address for correspondence**
Kaushal Kumar, Department of Veterinary Pathology, BVC, BASU, Patna, Bihar; E-mail: drkaushal15@rediffmail.com

Received: 1.1.26; Accepted: 28.1.26

ABSTRACT

Squamous cell carcinoma (SCC) is a malignant epithelial neoplasm arising from squamous cells and is infrequently reported in the vulvovaginal region of bitches. Owing to its anatomical location and gross appearance, vulvovaginal SCC may clinically resemble vaginal prolapse leading to diagnostic ambiguity. The present study documents a rare case of vulvovaginal squamous cell carcinoma in a 3-year-6-month-old intact bitch presented to the Teaching Veterinary Clinical Complex, Bihar Veterinary College, Patna with a history of protruding vaginal mass for the past 20 days. Clinically, the mass was reddish-pink, firm, irregular, non-reducible and ulcerated, closely mimicking vaginal prolapse. Based on the chronicity, progressive enlargement and ulcerative surface changes of the mass, a neoplastic condition was clinically suspected and surgical excision was undertaken as a definitive diagnostic and therapeutic approach under general anaesthesia. Haematological evaluation revealed moderate normocytic normochromic anaemia, leucocytosis with neutrophilia and borderline thrombocytopenia, reflecting a non-specific systemic response to neoplasia. Biochemical analysis demonstrated elevated total protein and globulin levels with mild increases in alanine aminotransferase (ALT) suggestive of systemic inflammatory response and hepatic stress. Gross examination of the excised mass revealed an irregular, friable growth with focal pale yellow to grey, soft areas suggestive of necrosis, along with dark red to black, blood-filled regions consistent with haemorrhage. Histopathological examination confirmed the diagnosis of squamous cell carcinoma characterized by invasive cords and nests of neoplastic squamous epithelial cells, marked cellular pleomorphism, hyperchromatic nuclei, prominent nucleoli, frequent mitotic figures and keratin pearl formation within a desmoplastic stroma, consistent with a well to moderately differentiated SCC. Vulvovaginal squamous cell carcinoma though uncommon in young bitches should be considered as an important differential diagnosis in cases of chronic vaginal prolapse-like conditions unresponsive to manual reduction. The present study emphasizes the importance of thorough clinical evaluation, histopathological confirmation and prompt surgical intervention for successful management and prevention of local invasion and recurrence.

Keywords: Histopathology, vaginal prolapse, vulvovaginal squamous cell carcinoma

INTRODUCTION

Squamous cell carcinoma (SCC) is a malignant neoplasm arising from stratified squamous epithelial cells and represents one of the most frequently encountered epithelial tumours in dogs, commonly affecting the skin and mucocutaneous junctions[1,2]. The incidence of SCC in dogs is 6% of all skin tumours[3]. In dogs, the most frequent location occurs on the head, abdomen, limbs, perineum and digits (nailbed). Although cutaneous SCC is well documented, its occurrence in the vulvovaginal region of bitches is comparatively rare and often underreported, largely due to diagnostic challenges and clinical resemblance to non-neoplastic reproductive conditions[4,5]. Vulvovaginal SCC is characterized by locally invasive growth, progressive tissue destruction and a low but potential risk of metastasis, thereby posing significant clinical concern in canine oncology[6]. Malignant tumours like vaginal SCC occur more often in spayed animals[7].

The vulva and vagina are hormonally responsive tissues and endocrine influences particularly prolonged estrogenic stimulation are believed to play a contributory role in the pathogenesis of neoplastic transformation in this region[8,9]. Chronic exposure to endogenous estrogens in intact bitches, pseudopregnancy, repeated estrous cycles, ovarian cysts or estrogen-secreting tumours may induce epithelial hyperplasia and dysplasia, predisposing the mucosal epithelium to malignant transformation[10,11]. Additionally, local irritation, trauma, chronic inflammation and secondary infections also act as promoting factors in the development of vulvovaginal SCC[12].

How to cite this article : Sinha, V.K., Kumar, K., Kumar, D., Ali, I., Tiwary, R. and Kumar, R. 2026. Vulvovaginal squamous cell carcinoma: Mimicking chronic prolapse in bitch. Indian J. Vet. Pathol., 50(2) : 173-176.

Clinically, vulvovaginal SCC often presents as a protruding, ulcerated or proliferative mass that may closely mimic vaginal prolapse, vaginal hyperplasia or transmissible venereal tumour particularly in younger intact bitches[13]. Such resemblance frequently leads to delayed diagnosis and inappropriate management. Affected animals may show vulvar swelling,

bleeding, discharge, dysuria and discomfort significantly impairing quality of life[14].

Haematological and biochemical alterations in dogs with SCC generally reflect chronic inflammation, tumour-associated stress and secondary infection commonly manifesting as anaemia, leucocytosis with neutrophilia and hyperglobulinaemia[6,15]. Histopathological examination remains the definitive diagnostic modality, revealing invasive nests and cords of malignant squamous cells with keratin pearl formation, nuclear pleomorphism and increased mitotic activity[1,5].

Despite its clinical relevance, literature documenting vulvovaginal SCC in bitches particularly from India remains scarce. The present study highlights a rare case of vulvovaginal squamous cell carcinoma in a young bitch mimicking vaginal prolapse, emphasizing the role of hormonal influences and the importance of clinicopathological correlation for accurate diagnosis and effective surgical management.

MATERIALS AND METHODS

The present study was conducted on a clinical case of a vulvovaginal neoplastic growth in a bitch presented to the Department of Veterinary Surgery and Radiology, Teaching Veterinary Clinical Complex, Bihar Veterinary College, Bihar Animal Sciences University (BASU), Patna. The case involved a 3-year-6-month-old intact female dog brought with a history of a protruding vulvovaginal mass for the past 20 days. According to the owner, the mass progressively increased in size and was initially suspected to be vaginal prolapse. The animal also exhibited intermittent serosanguinous discharge, licking of the perineal region and mild discomfort during urination. No prior medical or hormonal treatment was reported.

On clinical examination, the bitch was alert and responsive with normal rectal temperature, normal pulse and respiratory rate. A firm, irregular, reddish-pink, non-reducible mass was observed protruding from the vulva (Fig. 1). Mass was ulcerated at places with focal areas of necrosis. A large, protruding, reddish and lobulated mass from the vulvovaginal region during surgical manipulation appearing firm to friable with marked surface haemorrhage and congestion, necessitating urinary catheterization for procedural management (Fig. 2). Palpation elicited mild pain and regional lymph nodes were not markedly enlarged.

Haematological findings revealed mild to moderate anaemia with marginal leucocytosis while biochemical analysis showed elevated total protein and globulin levels with mild increases in Alanine Aminotransferase (ALT) and Aspartate Aminotransferase (AST) and normal renal parameters (Table 1 & 2).

Table 1. Haematological profile of dog suffering from Vulvovaginal Squamous cell carcinoma.

Parameter	Observed value	Reference range (Canine)
Haemoglobin (Hb) (g/dL)	**9.4**	12–18
Packed Cell Volume (PCV)	**28 %**	37–55 %
Total Erythrocyte Count (TEC) ($\times 10^6/\mu L$)	**4.2**	5.5–8.5
Total Leukocyte Count (TLC) ($\times 10^3/\mu L$)	**17.6**	6–17
Neutrophils	**78 %**	60–77 %
Lymphocytes	**16 %**	12–30 %
Monocytes	**4 %**	3–10 %
Eosinophils	**2 %**	2–10 %
Platelet count ($\times 10^5/\mu L$)	**2.1**	2–5

Table 2. Biochemical profiles of dog suffering from Vulvovaginal Squamous cell carcinoma.

Parameter	Observed value	Reference range (Canine)
Alanine aminotransferase (ALT) (IU/L)	92	10–80
Aspartate aminotransferase (AST) (IU/L)	58	10–50
Alkaline phosphatase (ALP) (IU/L)	138	20–150
Total Protein (g/dL)	8.2	5.5–7.5
Albumin (g/dL)	2.8	2.6–4.0
Globulin (g/dL)	5.4	2.5–4.5
Albumin:Globulin ratio	0.52	>0.8
Blood Urea Nitrogen (BUN) (mg/dL)	18	7–27
Creatinine (mg/dL)	1.0	0.5–1.5

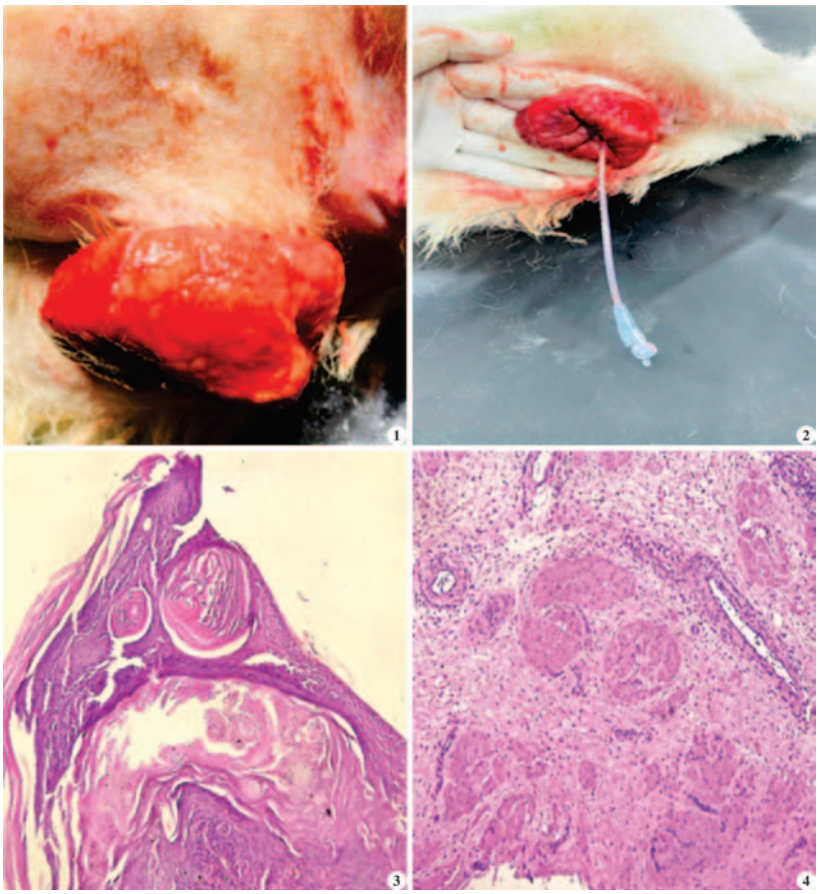

Fig. 1. Image showing a large, exophytic, irregular mass protruding from the vulvovaginal region with a reddish, ulcerated and friable surface; **Fig. 2.** Image showing a large, protruding, reddish and lobulated mass from the vulvovaginal region during surgical manipulation appearing firm to friable with marked surface haemorrhage and congestion, necessitating urinary catheterization for procedural management; **Fig. 3.** Histological section of canine vulvovaginal tumour (H&E 10X) showing infiltrative nests of neoplastic squamous epithelial cells with prominent concentric keratin pearl formation within the tumour mass, consistent with well-differentiated squamous cell carcinoma"; **Fig. 4.** Histological section of vulvovaginal tumour of dog (H&E 10X) showing invasive nests and cords of neoplastic squamous cells embedded in a fibrous stroma, with focal keratinization and associated inflammatory infiltrate.

Surgical excision of the vulvovaginal mass was performed under general anaesthesia with careful blunt and sharp dissection. The animal was pre-medicated with inj. atropine sulphate (0.04 mg/kg body weight, i.m.) and inj. xylazine (1 mg/kg body weight, i.m.) followed by induction with inj. ketamine (5 mg/kg body weight, i.v.). After achieving adequate anaesthesia, the animal was positioned in dorsal recumbency and the perineal region was prepared aseptically. A circumferential incision was made around the base of the mass and the tumour was carefully excised using blunt and sharp dissection. Haemostasis was achieved by ligation of bleeding vessels using absorbable suture material (polyglycolic acid 2/0). The vaginal mucosa was closed in a simple continuous pattern using absorbable sutures, and the skin was closed with nylon 2/0.

The excised tumour mass was immediately fixed in 10% neutral buffered formalin and submitted to the Department of Veterinary Pathology, Bihar Veterinary College, BASU, Patna for histopathological examination. Representative tissue samples were routinely processed by paraffin embedding, sectioned at 4–5 μm thickness and stained with Haematoxylin and Eosin (H&E) for microscopic evaluation.

Postoperatively, the bitch was treated with inj. ceftriaxone (25 mg/kg body weight, i.m.) once daily for five days and inj. meloxicam (0.2 mg/kg body weight, i.m.) for three days. The surgical site was cleaned with povidone-iodine solution twice daily for one week and sutures were removed after 10–12 days. The animal was monitored for postoperative complications and recurrence during follow-up.

RESULTS AND DISCUSSION

Gross examination of the excised vulvovaginal mass revealed an irregular, firm to hard, reddish-pink growth with focal ulceration and areas of necrosis. The cut surface appeared grayish-white with occasional haemorrhagic foci. Such gross features are characteristic of squamous cell carcinoma and have been previously described in vulvovaginal and cutaneous SCC in dogs[1,2,16]. The chronicity of the lesion and its firm, non-reducible nature distinguished it from simple vaginal prolapse or hyperplasia.

The affected bitch showed marked clinical improvement following surgical excision of the vulvovaginal mass. Normal feeding behaviour and activity were resumed within 3–5 days postoperatively. The surgical wound healed uneventfully and sutures were removed on day 10 without any complications. On follow-up examination conducted two months after surgery, no evidence of local recurrence, vaginal obstruction or metastatic spread was observed indicating a favourable postoperative outcome. Similar favourable outcomes following complete excision of vulvar and vaginal tumours in dogs have been reported earlier[8,13].

Histological section of canine vulvovaginal tumour (H&E 10X) showed infiltrative nests of neoplastic squamous epithelial cells with prominent concentric keratin pearl formation within the tumour mass, consistent with well-differentiated squamous cell carcinoma (Fig. 3).

Another Histological section of vulvovaginal tumour of dog showed invasive nests and cords of neoplastic squamous cells embedded in a fibrous stroma, with focal keratinization and associated inflammatory infiltrate (Fig. 4). Based on these findings, the lesion was diagnosed as well to moderately differentiated squamous cell carcinoma, in agreement with earlier reports on canine vulvovaginal SCC[4,5].

Haematological evaluation revealed anaemia characterized by decreased haemoglobin, packed cell volume and total erythrocyte count, consistent with normocytic normochromic anaemia, along with marginal leucocytosis. Biochemical analysis showed elevated total protein and globulin levels with mild increases in ALT and AST suggesting systemic inflammatory response and hepatic stress. Similar hematobiochemical alterations have been documented in dogs with epithelial tumours and chronic neoplastic condition[6,15].

Squamous cell carcinoma accounts for approximately 4–19% of all canine skin tumours; however, its occurrence in the vulvovaginal region is relatively rare[2,10]. Hormonal influence particularly prolonged estrogenic stimulation in intact bitches along with chronic irritation and inflammation has been implicated in the pathogenesis of vulvovaginal SCC[8,14]. The present case highlights the diagnostic challenge posed by such tumours due to their close clinical resemblance to vaginal prolapse.

The absence of recurrence in the present case reinforces that early diagnosis and complete surgical excision remain the treatment of choice for localized vulvovaginal SCC. The findings emphasize the importance of considering neoplasia as a differential diagnosis in cases of chronic or atypical vaginal prolapse to ensure timely and appropriate intervention.

CONCLUSION

Vulvovaginal squamous cell carcinoma in bitches is an uncommon but clinically significant malignant neoplasm that may closely mimic vaginal prolapse particularly in intact animals. Owing to its locally invasive nature and potential for progressive tissue destruction, accurate differentiation from non-neoplastic reproductive conditions is essential for appropriate clinical management. Early diagnosis based on thorough clinical examination supported by haematological, biochemical and definitive histopathological evaluation is crucial for timely intervention. The present study highlights the importance of considering vulvovaginal squamous cell carcinoma as a differential diagnosis in chronic or atypical cases of vaginal prolapse and underscores the need for vigilant postoperative monitoring to ensure long-term therapeutic success.

ACKNOWLEDGEMENTS

The authors express their gratitude to the Vice Chancellor and the Dean of Bihar Veterinary College, Bihar Animal Sciences University, Patna, for providing the necessary facilities to carry out this work.

Financial support & sponsorship: None.

Conflicts of interest: None.

Use of artificial intelligence (AI)-Assisted Technology for manuscript preparation: The authors confirm that there was no use of AI-assisted technology for assisting in the writing of the manuscript and no images were manipulated using AI.

REFERENCES

1. Gross T. L., Ihrke P. J., Walder E. J. and Affolter V. K. (2005) *Skin Diseases of the Dog and Cat: Clinical and Histopathologic Diagnosis*. 2nd ed. Oxford: Blackwell Science.
2. Goldschmidt M. H., Goldschmidt K. H. (2017) Epithelial and melanocytic tumors of the skin. In: Meuten DJ, editor. *Tumors in Domestic Animals*. 5th ed. Ames: Wiley-Blackwell. p. 88–141.
3. Hauck M.L. and Oblak M.L. (2020). Tumors of the skin and subcutaneous tissues. *Withrow and MacEwen's Small Animal Clinical Oncology*. 352-366
4. MacLachlan N. J., Kennedy P. C. (2017) Tumors of the genital systems. In: Meuten DJ, editor. *Tumors in Domestic Animals*. 5th ed. Ames: Wiley-Blackwell. p. 689–721.
5. Meuten D. J. (2017) *Tumors in Domestic Animals*. 5th ed. Ames: Wiley-Blackwell.
6. Withrow S. J., Vail D. M., Page R. L. (2020) *Withrow and MacEwen's Small Animal Clinical Oncology*. 6th ed. St. Louis: Elsevier.
7. Bilbrey S. A., Withrow S. J., Klein M. K., Bennett R. A., Norris A. M., Gofton N., DeHoff W., Sherwood Medical Catheter and Louis S. M. (1989). Vulvovaginectomy and perineal urethrostomy for neoplasms of the vulva and vagina. *Veterinary Sur*, **18(6):**450–453.
8. Klein M. K. (1996) Tumors of the female reproductive tract. *Vet Clin North Am Small Anim Pract*. **26(1):**165–188.
9. Schlafer DH, Miller RB. (2016) Female genital system. In: Maxie MG, editor. *Jubb, Kennedy and Palmer's Pathology of Domestic Animals*. 6th edn. Elsevier.
10. Hayes H. M Jr, Wilson G. P., Fraumeni J. F Jr. (1985) Reproductive factors and risk of canine mammary cancer. *J Natl Cancer Inst*.**75(5):**847–854.
11. Johnston S. D, Root Kustritz M. V, Olson PNS. (2001) *Canine and Feline Theriogenology*. Philadelphia: Saunders.
12. Foster R. A. Female reproductive system. (2016) In: Maxie MG, editor. *Jubb, Kennedy and Palmer's Pathology of Domestic Animals*. 6th edn. St. Louis: Elsevier. p. 358–464.
13. Sontas B. H, Erdogan G, Turna O. (2010) Vulvar and vaginal tumors in dogs: a review. *Vet Med*. **55(7):**329–335.
14. Johnston S. D. (1994) Disorders of the canine vagina and vulva. *Vet Clin North Am Small Anim Pract*. **24(2):**299–316.
15. Ettinger S. J., Feldman E. C. and Côté E. (2017) *Textbook of Veterinary Internal Medicine*. 8th edn. St. Louis: Elsevier.
16. Ramesh S., Nithya P., Senthilkumar K. and Kumar V. (2025). Squamous cell carcinoma in a dog — a case report. *Indian J Vet Pathol.* **49(3):**275–277.

Indian J. Vet. Pathol., 50(2) : 177-179, 2026: DOI: https://doi.org/10.56093/590j4k04

CASE REPORT

Cutaneous junctional melanocytoma in a dog: Clinical, cytological, histopathological and immunohistochemical evaluation

Mani Bharathi M.[1], S. Ramesh[2*], M. Sandhya Bhavani[3], N. Pazhanivel[4], G.V.S. Rao[2], G. Vijayakumar[5], G. Navyasree[6] and R.C. Sundararajan[7]

[1]Ph.D. Scholar, Department of Veterinary Pathology, College of Veterinary and Animal Sciences, Mannuthy, Thrissur, KVASU

[2]Professor (Retd.), Department of Veterinary Pathology, Madras Veterinary College, Chennai, TANUVAS

[3]Assistant professor, Department of Clinics, Madras Veterinary College, Chennai, TANUVAS

[4]Professor, Department of Pathology, Madras Veterinary College, Chennai, TANUVAS

[5]Professor and Head, Department of Clinics, Madras Veterinary College, Chennai, TANUVAS

[6]MVSc Scholar, Department of Veterinary Public Health and Epidemiology, Madras Veterinary College, Chennai, TANUVAS

[7]Phd scholar, Department of Clinical Medicine, Ethics and Jurisprudence, College of Veterinary and Animal Sciences, Mannuthy, Thrissur, KVASU

***Address for correspondence**

S. Ramesh, Professor (Retd.), Department of Veterinary Pathology, Madras Veterinary College, Chennai, TANUVAS; Email: rameshlibya2010@gmail.com

Received: 5.1.26; Accepted: 22.1.26

ABSTRACT

A 4-year-old Rottweiler dog had a black, firm nodule noticed in the dorsal aspect of a paw region in the periungual region at the nail bed/nail fold area of the paw. Cytology revealed brownish-black pigments dispersed throughout the cytoplasm and histopathology revealed melanocytic cells extending from the dermo-epidermal junction into the deep dermis with melanin granules. Immunohistochemistry confirmed strong Melan-A expression.

Keywords: Cytology, dog, histopathology, immunohistochemistry, junctional melanocytoma

INTRODUCTION

Melanocytomas are benign neoplasms originating from melanocytes. In dogs, these tumors commonly noticed on haired skin with a predilection for areas such as the head, limbs and trunk, particularly in middle-aged to older animals. These tumors are well-circumscribed and slow-growing and rarely metastasize. After excision, melanocytomas have a better prognosis, with a low likelihood of local recurrence or systemic spread[1,2]. Cytologically, the cytoplasm often have abundant coarse melanin granules, which appear brownish-black or blue-green on Romanowsky-stained smears. Mild to moderate anisocytosis and anisokaryosis with eccentrically placed nuclei and prominent nucleoli are observed[1,3]. Melanophages—macrophages containing phagocytosed melanin—may also be observed in the background. Diagnostic challenges, particularly in amelanotic variants lacks visible pigment and may mimic other round cell tumors[4].

Grossly, melanocytomas in dogs present as solitary, dome-shaped, raised and well-demarcated nodules. The surface of the tumor is darkly pigmented, appearing black, brown, or grey and lesions are firm and non-ulcerated. These tumors are commonly observed on the head, neck and distal limbs, which are the common anatomic sites for melanocytic neoplasms in dogs[2,5]. Histopathological assessment is necessary for definitive diagnosis. Melanocytomas present as lobulated clusters or nests of neoplastic melanocytes from the dermo-epidermal junction and extending into the superficial and deep dermis. These cells revealed round to oval nuclei, prominent basophilic nucleoli and varying degrees of cytoplasmic melanin[2]. Immunohistochemistry (IHC), melanocytic markers Melan-A, PNL2, TRP-1/TRP-2 and SOX-10 are commonly used. Melan-A and PNL2 have high specificity and sensitivity in canine melanocytic tumors[3,6,7].

How to cite this article : Bharathi, M. M., Ramesh, S., Bhavani, M.S., Pazhanivel, N., Rao, G.V.S., Vijayakumar, G., Navyasree, G. and Sundararajan, R.C. 2026. Cutaneous junctıonal melanocytoma ın a dog: Clınıcal, cytologıcal, hıstopathologıcal and ımmunohıstochemıcal evaluatıon. Indian J. Vet. Pathol., 50(2) : 177-179.

MATERIALS AND METHODS

A 4-year-old male Rottweiler dog was presented with a history of mass in the dorsal aspect of right forelimb in the periungual region adjacent to the nail bed for clinical diagnosis and treatment. Excisional biopsy was performed and the tissue

samples were collected in 10% formalin, processed by routine paraffin embedding method, cut sections were stained by haematoxylin and eosin and subjected to histopathological studies[8]. For immunohistochemical studies, the tissue samples were processed by routine paraffin embedding method and the cut sections were treated with specific marker - Melan-A.

RESULTS

Gross examination revealed a solitary, well-defined, raised, dome-shaped nodule that was distinctly pigmented. The lesion was firm to the touch and clearly demarcated from the surrounding tissues and exicsed mass measured less than 1.8 cm in diameter (Fig.1)

Cytological assessment of the lesion through fine-needle aspiration smears revealed the presence of numerous multinucleated round to oval cells. These cells were abundant, coarse, granular, brownish-black pigments consistent with melanin and dispersed throughout the cytoplasm. The nuclei were eccentrically placed and prominent nucleoli were noticed (Fig.2).

Dermatohistopathological evaluation supported the cytological findings. The sectioned tissue revealed a multilobulated tumor composed of nests and clusters of melanocytic cells extending from the dermo-epidermal junction into the deeper layers of the dermis. The cells showed round to oval nuclei with defined basophilic nucleoli and melanin granules throughout the lesion (Fig.3).

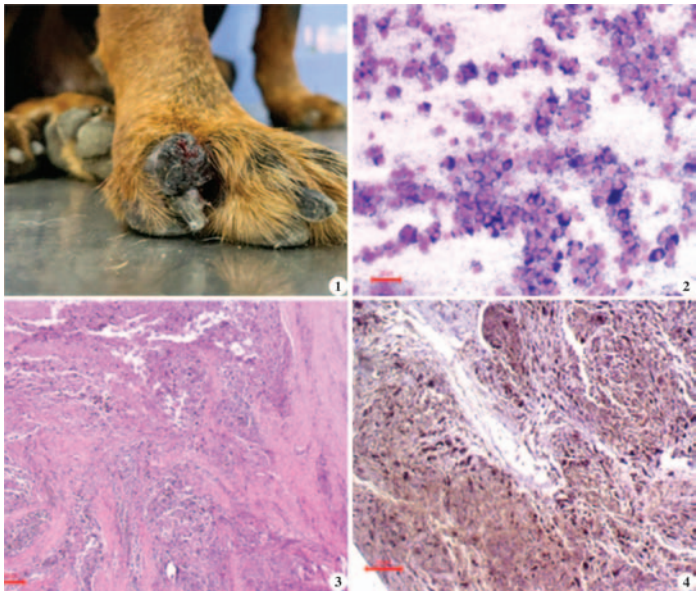

Fig.1. Dog – Melanocytoma – Black, oval, raised nodule in paw; **Fig.2.** Dog – Melanocytoma – Cytology - Granular melanin pigment in the cytoplasm (LG X200); **Fig.3.** Dog – Melanocytoma – HP - Presence of melanin deposition in the deeper part of dermis (H&E X40); **Fig.4.** Dog – Melanocytoma – IHC - Melan A has strongly expressed (H&E X100)

Immunohistochemical examination revealed the neoplastic cells showed strong cytoplasmic expression for Melan A (Fig.4). The strong expression of Melan A in the cytoplasm of the tumor cells confirmed their origin from melanocytes and reinforced the diagnosis of melanocytoma.

DISCUSSION

In the present study, a 4-year-old male Rottweiler with the lesion on the right metacarpal region was noticed, which was known to be the characteristic of melanin tumors. The firm consistency, pigmented appearance and localized nature of the mass are classic features of cutaneous melanocytoma[2,4]. In the current case, fine-needle aspiration revealed such features, with the added presence of coarse melanin granules within the cytoplasm these were in accordance with the presence of melanin pigment was a characteristic diagnostic feature[1,9]. Histologically, melanocytomas consist of lobulated nests of melanocytic cells extending from the dermoepidermal junction into the deeper dermis. In this case, the lesion exhibited a characteristic multilobulated junctional melanocytoma architecture, with prominent melanin deposition and identifiable mitotic figures[10,11] who also observed the importance of histologic depth and mitotic index in prognostic evaluation. Immunohistochemistry (IHC) serves as a useful tool to confirm melanocytic origin, particularly when differentiating from other round cell tumors. Melan A, a melanocyte-specific marker, showed strong cytoplasmic positivity in the neoplastic cells. Melan A has shown to have high grade specificity than markers like S-100 or PNL2[3,12].

CONCLUSION

The characteristic features of heavily pigmented melanocytic cells, multilobulated junctional architecture on histopathology and strong cytoplasmic Melan-A immunoreactivity confirmed the melanocytic origin and nature of the lesion. İt provides the diagnostic value of an integrated approach for accurate identification of canine melanocytic tumors and differentiation from other pigmented cutaneous neoplasms.

Financial Support : No funding

Conflict of Interest : The authors declared that there is no conflict of interest regarding the publication of the manuscript.

Use of Artificial Intelligence : The authors declare that artificial intelligence tools were not used in the design, data collection, analysis or writing of this manuscript.

REFERENCES

1. Contel IJ, Fonseca-Alves CE, Ferrari HF, Laufer-Amorim R and Xavier-Júnior JCC. 2024. Review of the comparative pathological and immunohistochemical features of human and canine cutaneous melanocytic neoplasms. *J. Comp. Pathol.* 211: 26-35.
2. Goldschmidt MH and Goldschmidt KH. 2016. Epithelial and melanocytic tumors of the skin. In: Meuten DJ (editor). *Tumors in Domestic Animals*. 5th ed. Ames, IA, USA: Wiley Blackwell; pp. 88-141.
3. Smith SH, Goldschmidt MH and McManus PM. 2002. A comparative review of melanocytic neoplasms. *Vet. Pathol.* 39 (6): 651-678.
4. Gross TL, Ihrke PJ, Walder EJ and Affolter VK. 2008. *Skin Diseases of the Dog and Cat: Clinical and Histopathologic Diagnosis*. 2nd ed. Ames, IA, USA: Wiley-Blackwell.
5. Smedley RC, Sebastian K and Kiupel M. 2022. Diagnosis and prognosis of canine melanocytic neoplasms. *Vet. Sci.* 9 (4): 175.
6. Fernandes BF, Odashiro AN, Saraiva VS, Logan P, Antecka E and Burnier MN Jr. 2007. Immunohistochemical expression of melan-A and tyrosinase in uveal melanoma. *J. Carcinog.* 6: 6.
7. King E, Cook M, Wittorff H, Dirksen W, Kisseberth WC and Jennings RN. 2024. Evaluation of SOX-10 immunohistochemical expression in canine melanoma and non-melanocytic tumors by tissue microarray. *Vet. Pathol.* 61 (6): 896-903.
8. Suvarna, KS, Layton, C and Bancroft, JD. 2018. Bancroft's theory and practice of histological techniques E-Book. *Elsevier health sciences.*
9. Polton, G, Borrego JF, Clemente-Vicario F, Clifford CA, Jagielski D, Kessler M, Kobayashi T, Lanore D, Queiroga FL, Rowe AT and Vajdovich P. 2024. Melanoma of the dog and cat: consensus and guidelines. *Front. Vet. Sci.* 11: p.1359426.
10. Bergman PJ. 2007. Canine oral melanoma. *Clin. Tech. Small Anim. Pract.* 22 (2): 55-60.
11. Smedley RC, Lamoureux J, Sledge DG and Kiupel M. 2011. Immunohistochemical diagnosis of canine oral amelanotic melanocytic neoplasms. *Vet. Pathol*. 48 (1): 32-40.
12. Giudice C, Ceciliani F, Rondena M, Stefanello D and Grieco V. 2010. Immunohistochemical investigation of PNL2 reactivity of canine melanocytic neoplasms and comparison with Melan A. *J. Vet. Diagnos. Investig.* 22 (3): 389-394.

Indian J. Vet. Pathol., 50(2) : 180-183, 2026: DOI: https://doi.org/10.56093/gexgn295

CASE REPORT

Hepatocellular Carcinoma in dog

Vagdevi Tangellapally, Swathi Bora*, Yadala Ravikumar, Vemula Sravathi and Haripriya B.
Department of Veterinary Pathology, College of Veterinary Science, Rajendranar,
PVNRTVU, Hyderabad-500030, Telengana, India
Orcid id: 0000-0003-4141-4026

***Address for correspondence**
Swathi Bora, Department of Veterinary Pathology, College of Veterinary Science, Rajendranar, PVNRTVU, Hyderabad-500030; Email-rkk.swathi@gmail.com

Received: 9.1.26; Accepted: 3.4.26

ABSTRACT

This report presents clinical, ultrasonographical and pathological findings in a 13-year-old dog with hepatocellular carcinoma (HCC). Ultrasound Sonography (USG) examination of liver revealed anechoic areas with irregular borders. Gross examination of liver and spleen revealed multifocal firm nodules of various sizes. Cut section of liver was greasy. Upon gross examination of lungs, haemorrhagic nodule and pale appearance were noticed. Upon cytological examination, hepatocytes showed multiple nuclei and nuclear atypia along with vacuolated cytoplasm and few naked nuclei. Cytology of spleen revealed multinucleated cells and few hepatocytes which might indicate metastasis. On histopathological analysis, pleomorphic hepatocytes with vacuoles, multinucleated cells and mitotic figures were noticed. These results supported the possibility of hepatocellular carcinoma (HCC). With Masson's Trichrome staining, collagen fibers stained blue colour around the portal triad indicating periportal cirrhosis. Histopathology of spleen revealed islands of fibrous tissue around vasculature which was also confirmed by Masson's Trichrome staining. Immunohistochemical analysis of liver revealed intense immunopositivity for Proliferating Cell Nuclear Antigen (PCNA) and cytokeratin 18 in neoplastic hepatocytes.

Keywords: Cytokeratin, hepatocellular carcinoma, nuclear atypia

INTRODUCTION

Dogs seldom develop primary liver tumours, which account for 0.6% to 1.3% of all canine neoplasms. The most frequent malignant liver tumour is hepatocellular carcinoma (HCC), although others include bile duct carcinoma, carcinoids, sarcomas, lymphomas, and systemic mastocytosis[1]. Hepatocellular carcinomas have been reported in a variety of domestic animal species, including cattle, sheep, pigs, cats, dogs, and horses; however, dogs may be more amenable to HCC than the majority of other animals. HCC is the sixth most prevalent type of cancer in people across the globe which is frequently attributed to chronic liver diseases like cirrhosis, non-alcoholic steroid hepatitis, and hepatitis B and C infection. In domestic animals, factors including persistent infections from parasites, viruses, and bacteria, hereditary factors, or ingestion of chemicals like aflatoxins, pyrrolizidines, and nitrosamines may play a pivotal role in developing HCC[2]. It frequently manifests in dogs with more than 10 years of age and male dogs are more susceptible. Certain dog breeds, including miniature schnauzers, shih tzus, Welsh Corgis, beagles and Scottish terriers with vacuolar hepatopathy have significant risks of acquiring HCC[3].

HCCs can manifest in three different ways: massive form, nodular form and diffuse form. Massive HCC is usually a single neoplasm which often only affects one or two contiguous liver lobes. Nodular HCCs develop scattered nodules, frequently throughout multiple liver lobes. They range in size from tiny, spherical, distinct lesions with a few centimeters in diameter to enormous, diffuse masses with a diameter of more than 10 cm. Minute, hazy masses that are dispersed throughout the liver parenchyma affecting various lobes are the hallmarks of diffuse HCCs. Tumours may vary from well diffuse to highly anaplastic at the microscopic level[2]. Solid, pseudoglandular, cirrhous, clear cell type and trabecular are the histological subtypes of HCC[4]. Others include peritheliomatous, peliod, and cobblestone[5]. The primary objective of this study is to evaluate clinical, ultrasonographical, gross, cytological, histopathological and immunohistological findings of HCC in dog.

How to cite this article : Tangellapally, V., Bora, S., Ravikumar, Y., Sravathi, V. and Haripriya, B. 2026. Hepatocellular Carcinoma in dog. Indian J. Vet. Pathol., 50(2) : 180-183.

Case Description

A 13-year-old female dog was brought to the Veterinary Clinical Complex, College of Veterinary Science in Rajendranagar, Hyderabad, with a history of lethargy and anorexia for the previous 10 days. The animal was in recumbent position. Clinical findings included pit edema, ascites, and melena. On USG examination, anechoic areas with irregular borders and moth eaten appearance of the liver were revealed (Fig. 1A). X-ray of thoracic region revealed opacity in lungs (Fig. 1B).

The animal passed away during treatment and was presented to Department of Veterinary Pathology, Rajendranagar for necropsy examination.

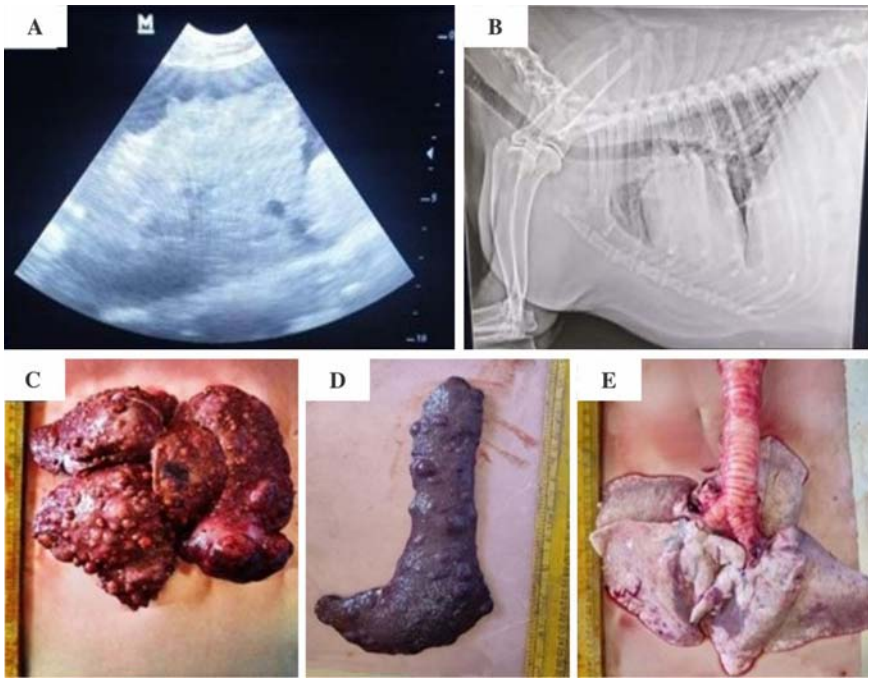

Fig 1. A. USG examination of liver revealed anechoic spaces with irregular borders. **B.** Radiograph of thoracic region revealed opacity in lungs **C.** Multiple random nodules of various sizes which are hard in consistency and haemorrhagic noticed on liver **D.** Multiple random nodules of various sizes which are hard in consistency and haemorrhagic observed on spleen **E.** Gross examination of lung showing haemorrhagic nodule and appears pale.

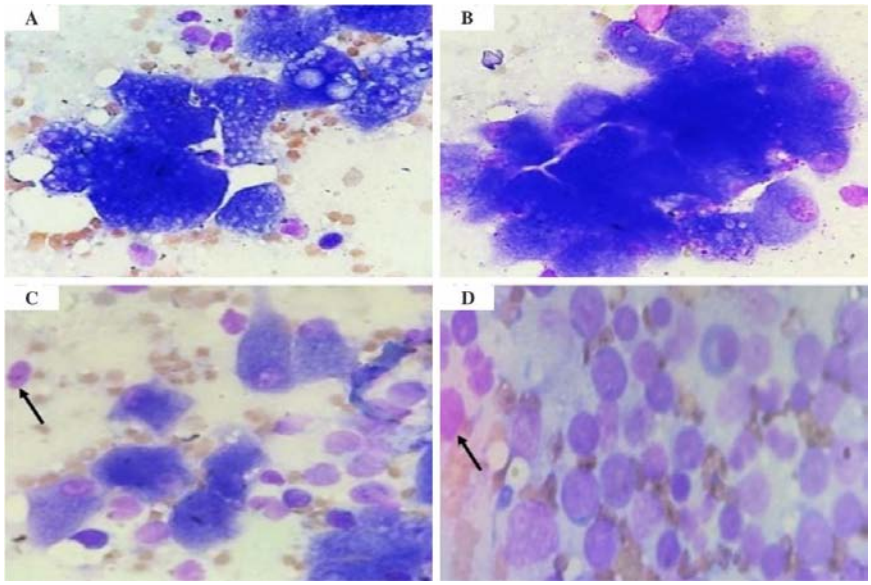

Fig 2. A. Impression smear of liver nodule showing pleomorphic hepatocytes with atypical naked nuclei and vacuolated cytoplasm (Giemsa x1000). **B.** Impression smear of liver nodule showing sheet of neoplastic hepatocytes and few giant cells (Giemsa x1000). **C.** Impression smear of liver nodule showing atypical naked nuclei of hepatocytes. Arrow- naked nuclei (Giemsa x1000). **D.** Impression smear of nodules on spleen showing atypical nuclei of hepatocyte (Arrow) (Giemsa x1000).

On Gross examination of liver, hepatomegaly with greasy appearance along with multifocal haemorrhagic, diffuse firm nodules were noticed (Fig. 1C). On the cut surface, caseous necrosis was noticed at centre of the nodules. Firm nodules of varying sizes were visible upon gross examination of the spleen (Fig. 1D). Gross examination of lungs revealed focal haemorrhagic nodule and appeared pale (Fig. 1E). Fine needle aspirates of liver mass revealed cluster of hepatocytes with few multinucleated hepatocytes, nuclear atypia with anisokaryosis, naked nuclei (Fig. 2C) in some areas and vacuolated cytoplasm (Fig. 2A). Cytology of impression smears of spleen nodules revealed multinucleated cells and few hepatocytes (Fig. 2D) which indicate metastasis. The resected liver and spleen tissues were fixed in 10% neutral buffered formalin, processed routinely and then embedded in paraffin. Paraffin sections of 5 μm thickness were cut and stained with Haematoxylin and Eosin (H&E) and Masson's Trichrome stain (MTS).

Histopathology of liver showed neoplastic hepatocytes with vesicular to vacuolated cytoplasm, hyperchromatic nuclei, pleomorphic and multinucleated cells along with mitotic figures (Fig. 3A). With Masson's Trichrome stain, incremental fibrosis with collagen fibers that stained blue colour were noticed in between the hepatic cords and around the portal triad (Fig. 4A) which indicate periportal cirrhosis. Infiltration of inflammatory cells was also observed. Histopathological examination of spleen revealed islands of fibrous tissue along with fibrous thickenings around the vasculature (Fig. 3C). With Masson's Trichrome staining, collagen fibers which stained blue colour were observed around the splenic vessels (Fig. 4B). Depletion of lymphocytes, prominent trabeculae, haemorrhage, congestion and thickening of splenic vessels were also noticed. Immunohistochemical examination of

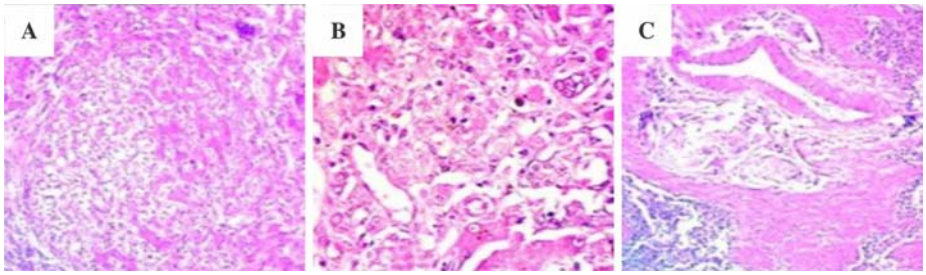

Fig. 3. A. Photomicrograph of liver showing neoplastic hepatocytes with vacuolation and atypical mitotic figures (H&E x100); **B.** acinar pattern forming neoplastic cells and hepatocytes with foamy cytoplasm (H&E x400); **C.** Photomicrograph of spleen showing Islands of fibrous tissue and fibrous thickenings around vasculature with depletion of lymphocytes (H&E x100).

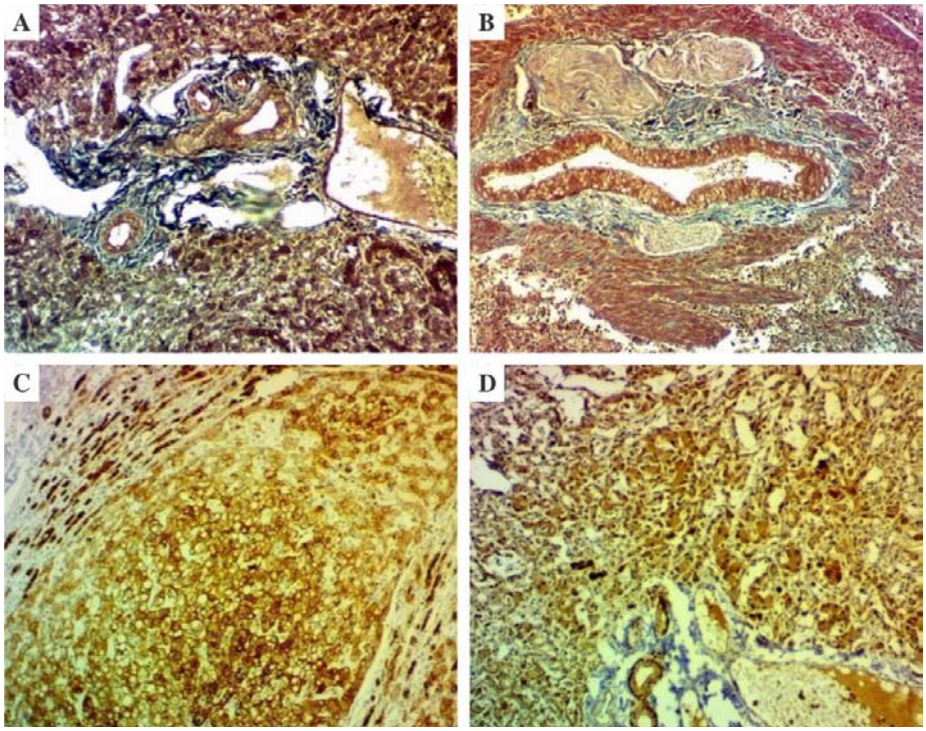

Fig.4. A. Photomicrograph of liver showing fibrous tissue proliferation around portal triad indicating cirrhosis (MTS x100); **B.** Photomicrograph of spleen showing extensive proliferation of fibrous tissue around dilated thickened vasculature (MTS staining x100); **C.** Photomicrograph of liver showing intense immunopositivity for PCNA in the nucleus of neoplastic hepatocytes (IHC-PCNA x100); **D.** Photomicrograph of liver showing intense immunopositivity for cytokeratin 18 in cytoplasm of neoplastic hepatocytes (IHC x100).

liver revealed intense immunopositivity for PCNA in the nucleus of neoplastic hepatocytes (Fig. 4C) and also showed intense immunopositivity for cytokeratin 18 in cytoplasm of neoplastic hepatocytes (Fig. 4D).

DISCUSSION

The most typical primary liver tumour in dogs is hepatocellular carcinoma which accounts for 50% of all hepatic tumours[3]. This study investigates clinical characteristics, USG findings and pathological findings associated with HCC in dog. In the current study, HCC is seen in 13 years old dog indicating age is the risk factor for HCC which was supported by previous studies that reported there will be an increased risk of HCC in dogs greater than 10 years old[6]. USG examination of liver revealed anechoic spaces and irregular borders with moth eaten appearance. X-ray of thoracic region revealed opacity in lungs which represent nodule. Gross examination of liver showed multiple random nodules of various sizes which are hard in consistency and areas of haemorrhages. On cut section, the nodule exhibits a central area of dry, yellowish-white, cheese-like material indicative of caseous necrosis, with a well-demarcated margin separating it from the surrounding tissue. These findings were corroborated by previous studies[2]. The nodular and diffuse forms tend to metastasize more frequently than the massive form[7]. Gross examination of spleen revealed multiple nodules of various sizes which implicated the spleen as metastatic site as reported by previous literature[8]. Upon gross examination, haemorrhagic nodule and pale appearance of lungs were noticed. These findings were supported by previous studies reporting lungs as the frequent metastatic site of HCC[8].

Cytological analysis of liver nodules revealed palisading arrangement of hepatocytes, anisocytosis, anisokaryosis, multinuclearity, vacuolated cytoplasm and naked nuclei which are the most prominent cytological hallmarks of canine HCC[9]. Cytology of nodules on spleen revealed multinucleated cells and few hepatocytes which might indicate metastasis. These findings are similar to studies reported by previous studies[10]. Histopathology of liver showed pleomorphic, multinucleated cells and mitotic figures along with variably sized vacuoles in cytoplasm suggesting Hepatocellular carcinoma. Vacuolated cytoplasm may be

due to fat as gross examination of liver showed greasy appearance. With Masson's Trichrome staining, fibrosis is noticed with collagen fibers in between the hepatic cords and around the portal triad which indicates periportal cirrhosis suggesting cirrhosis as the pathological finding in canine HCC which was reported in previous literature[10]. Histologically, spleen revealed islands of fibrous tissue. With Masson's Trichrome stain, collagen fibers stained blue colour which are observed around the splenic vessels along with depletion of lymphocytes, prominent trabeculae, haemorrhage and thickening of splenic vessels were also noticed. Immunohistochemical analysis of liver showed intense immunopositivity for PCNA and cytokeratin 18 in neoplastic hepatocytes.

CONCLUSION

Based on USG examination, cytological, Histopathological and Immunohistochemical examination, moderately differentiated Hepatocellular carcinoma and metastasis to spleen was confirmed . Periportal cirrhosis was noticed. Histological patterns of Hepatocellular carcinoma should be emphasized more in detail. Diagnosis of tumour is difficult in early stages. To advance our understanding and combat Hepatocellular carcinoma as well as to improve therapeutic outcomes in the future, more thorough and in-depth study on histological patterns of Hepatocellular carcinoma and biomarkers is required .

ACKNOWLEDGEMENT

We extend our gratitude to the Head and staff of the Department of Veterinary Pathology, College of Veterinary Science, Hyderabad for providing the facilities necessary to conduct this study.

Financial support & sponsorship: None

Conflicts of Interest: None

Use of Artificial Intelligence (AI)-Assisted Technology for manuscript preparation: The authors confirm that there was no use of AI-assisted technology for assisting in the writing of the manuscript and no images were manipulated using AI.

REFERENCES

1. Liptak JM, Dernell WS, Monnet E, Powers BE, Bachand AM, Kenney JG and Withrow SJ. 2004. Massive hepatocellular carcinoma in dogs: 48 cases (1992–2002). *J Am Vet Med Assoc* **225:** 1225-1230.
2. Mathewos M. 2021. Pathological and Cytological Studies on Hepatocellular Carcinoma in Cattle Slaughtered at Bishoftu Elfora Abattoir, Central Ethiopia. *Vet Med Int* **2**: 1-6.
3. Oo T, Sasaki N, Ikenaka Y, Ichise T, Nagata N, Yokoyama N, Sasaoka K, Morishita K, Nakamura K and Takiguchi M. 2022. Serum steroid profiling of hepatocellular carcinoma associated with hyperadrenocorticism in dogs: A preliminary study. *Front Vet Sci* **9**: 1014792.
4. Jung JH, Lee M, Yang Y, Seo D, Hwang SH, Kim WH and Kim Y. 2021. A clear cell hepatocellular carcinoma in an obese dog with hyperlipidemia: a case report. *Korean J Vet Res* **61**: e34.
5. Patnaik AK, Hurvitz AI, Lieberman PH and Johnson GF. 1981. Canine hepatocellular carcinoma. *Vet Pathol* **18**: 427-438.
6. Leela-Arporn R, Ohta H, Nagata N, Sasaoka K, Tamura M, Dermlim A, Nisa K, Morishita K, Sasaki N, Nakamura K and Takagi S. 2019. Epidemiology of massive hepatocellular carcinoma in dogs: a 4-year retrospective study. *Vet Sci* **248**: 74-78.
7. Teshima T, Matsumoto H, Shigihara K, Sawada H, Michishita M, Takahashi K and Koyama H. 2013. Hepatocellular carcinoma in a young dog. *Can Vet J* **54**: 845.
8. Liptak JM, Dernell WS and Withrow SJ. 2004. Liver tumors in cats and dogs. *Sarcoma* **36**: 1-6.
9. Masserdotti C, Rossetti E, De Lorenzi D, Della Salda L and Palmieri C. 2014. Characterization of cytoplasmic hyaline bodies in a hepatocellular carcinoma of a dog. *Res Vet Sci* **96**: 143-146.
10. Ciaputa R, Bandoch P, Lewandowska K, Madej JA, Kandefer-Gola M, Janus I and Nowak M. 2016. Immunohistochemical analysis of metastasising hepatocellular carcinomas in dogs. *Vet Med* **61**: 546-552.

Indian J. Vet. Pathol., 50(2) : 184-186, 2026: DOI: https://doi.org/10.56093/engsh030

CASE REPORT

Cavernous splenic hemangiosarcoma in a dog - A pathological study

Marella Bharadwaj[1], P. Balaram[2], CH. Sudha Rani Chowdary[*], Divya Ch[3] and P. Revathi[4]
Department of Veterinary Pathology, NTR College of Veterinary Science, Sri Venkateswara Veterinary University, Gannavaram, Andhra Pradesh, India- 521102
[1]B.V.Sc. & AH student, IV professional year; [2]M.V.Sc. Scholar, [3]B.V.Sc. & AH student, III professional year, [4]Private pet practitioner

***Address for correspondence**
Ch. Sudha Rani Chowdary, Department of Veterinary Pathology, NTR College of Veterinary Science, Sri Venkateswara Veterinary University, Gannavaram, Andhra Pradesh, India- 521102; E-mail: drsudha84@gmail.com

Received: 18.2.26; Accepted: 18.3.26

ABSTRACT

A 12-year-old non-descript male dog was presented with a history of lethargy, vomiting, and loss of appetite. A complete blood count revealed elevated haematocrit, neutrophilia and thrombocytopenia. Abdominal ultrasonography revealed a mass at the splenic tail with a characteristic honeycomb appearance. Cytological examination showed large, pleomorphic, oval to spindle-shaped cells exhibiting nuclear hyperchromasia and a high nuclear-to-cytoplasmic ratio. Splenectomy was performed and the excised mass was subjected to histopathological evaluation. Histological examination revealed large cavernous vascular spaces lined by markedly pleomorphic and plump endothelial cells. Based on the histopathological features, a diagnosis of splenic hemangiosarcoma was made.

Keywords: Dog, hemangiosarcoma, histopathology, spleen, ultrasonography

INTRODUCTION

Hemangiosarcoma (HSA), a malignant mesenchymal tumor originating from the endothelial cells lining blood vessels, poses a serious threat to canine health. Known for its aggressive behaviour, it grows rapidly, spreads easily to other organs, and is associated with a poor prognosis. Current evidence from recent investigations[1] indicates that the cells giving rise to hemangiosarcoma (HSA) originate from pluripotent bone marrow cells at an early, pre-differentiation stage that are capable of migrating to areas of active vascularization, where they may undergo neoplastic transformation[2].The exact causes and biological processes that lead to the development of HSA are still not fully understood. A few studies have proposed a potential association between infections caused by organisms such as *Bartonella* spp. and the development of HSA in dogs, as prolonged exposure to these pathogens can lead to chronic inflammation and angiogenesis both of which are key processes in the initiation and progression of vascular tumors like HSA[3].The most common breeds affected are German Shepherd, Boxer and Maltese Terrier[4].

HSA occurs more frequently in the dog than other species, may originate anywhere in the body with a blood supply and represents 5% of all non-skin primary canine malignant neoplasms[5]. The most common primary sites of visceral HSA include the spleen, right atrium, auricular appendage and liver. The spleen is the primary site for 35–62% of all primary HSAs[6]. Splenic HSA is widely recognized as the leading cause of non-traumatic hemoperitoneum in dogs[7]. In dogs with splenic hemangiosarcoma, the cause of death has been attributed to hypovolemia from tumor rupture, metastatic disease, disseminated intravascular coagulation, and cardiac arrhythmias. Early diagnosis remains a significant challenge, often delaying intervention until the disease is already advanced. The diagnosis of splenic hemangiosarcoma (HSA) requires a combination of imaging and laboratory evaluations, including abdominal ultrasonography, three-view thoracic radiographs, cytology and histopathology. Fine-needle aspiration cytology (FNAC) has limited diagnostic value in diagnosis because the samples are often heavily contaminated with blood, and the procedure carries risks such as tumor cell seeding that may promote metastasis, as well as hemorrhage resulting from rupture of the tumor capsule. A definitive diagnosis of splenic hemangiosarcoma (HSA) is established through histopathological evaluation of the tumor tissue. IHC is not usually needed to diagnose most cases of hemangiosarcoma but can be helpful to identify solid hemangiosarcoma and poorly differentiated neoplasms. Factor VIII-related antigen (von Willebrand factor) typically exhibits diffuse or punctuate cytoplasmic staining appearance in neoplastic endothelial cells.

How to cite this article : Bharadwaj, M, Balaram, P., Chowdary, S.R., Divya Ch and Revathi, P. 2026. Cavernous splenic hemangiosarcoma in a dog - A pathological study. Indian J. Vet. Pathol., 50(2) : 184-186.

The present paper puts on record the clinical and pathological findings of splenic hemangiosarcoma in a dog.

Case Presentation and Clinicopathologic findings

A 12-year-old non-descript, intact male dog was presented to a private veterinary clinic with a history of anorexia, vomiting, dullness and moaning for two weeks. On clinical examination, the animal showed pyrexia, severe dehydration and slightly distended abdomen The animal evinced pain when the abdomen was palpated. Ultrasonography of the abdomen revealed presence of a mass at the tail region of the spleen with a honey comb texture (Fig.1). The mass was subjected to ultrasound guided aspiration and the contents were smeared on to a glass slide. The smear was stained by Leishman's stain and the cytology revealed large number of erythrocytes admixed with a few, moderately pleomorphic, oval to fusiform cells with nuclear hyperchromasia and high nuclear to cytoplasmic ratio. Ultrasoographic and cytologic findings were suggestive of an endothelial tumor. Whole blood was collected from the animal as a pre-operative procedure for complete blood picture. Hematology revealed severe polycythemia, neutrophilia and thrombocytopenia. Subsequently, the dog was subjected to splenectomy by surgical procedure.

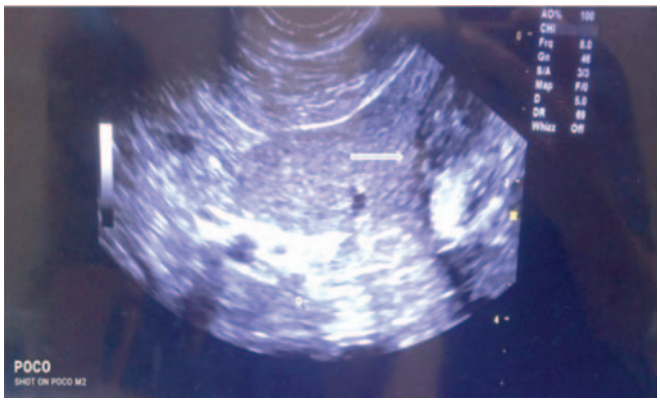

Fig. 1. Abdominal ultrasonography showing a mass at the tail region of spleen (arrow).

Gross and Histopathology

Gross examination of the spleen revealed a soft, reddish brown spherical mass of about 5 cm diameter on the parietal surface at the tail region (Fig. 2). On sectioning the mass, there was severe oozing of blood and the cut sections revealed honey comb like structure. A representative sample of the tumor was collected in 10% formalin and subjected to routine tissue processing by paraffin embedding technique. Four-to-five-micron thick tissue sections were obatained by microtomy and stained by Haematoxylin and Eosin method. Histopathology of the tumor revealed splenic hemangiosarcoma characterized by the presence of cavernous spaces and small to large anastomosing capillaries filled with blood within the lymphoid tissue of the spleen (Figs. 3 & 4). The cavernous spaces were incompletely lined by hyperchromatic, moderately pleomorphic, oval to spindle shaped plump endothelial cells with scanty cytoplasm. In a few foci, endothelial cells were found scattered or are arranged in trabeculae (Fig. 5) in the splenic parenchyma without forming the lumina. There were a few foci of necrosis and presence of hemosiderin in the tumour parenchyma.

DISCUSSION

In the present study, a cavernous splenic hemangiosarcoma was recorded in a non-descript 12 year old, intact male dog. Hemangiosarcoma is the most common splenic neoplasm of the dog, occurring usually between 6 and 17 years of age, and affects many breeds and mixed breeds. In a study on splenic tumors[8], the most common splenic tumor reported was hemangiosarcoma followed by lymphoma and fibrosarcoma. Hemangiosarcoma in dogs occur 80% in spleen[9] as reported. There is no significant sex predilection but a few studies opined that neutering might have an effect on the incidence.

In the present case, the clinical signs at presentation included anorexia, vomiting, pyrexia, distended and

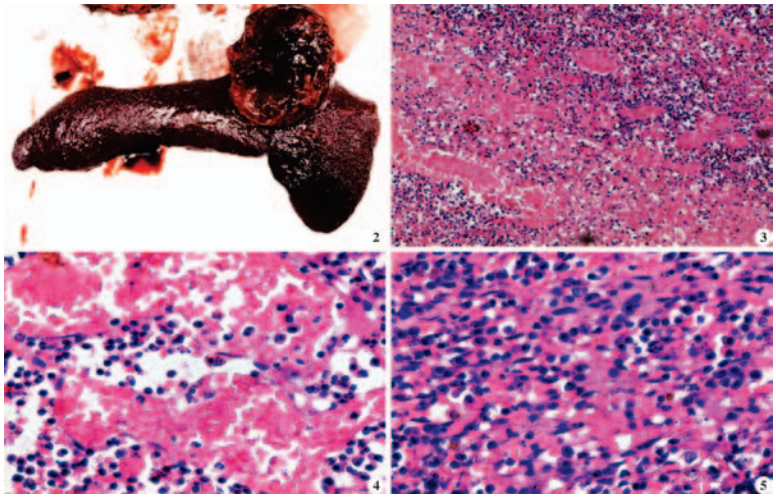

Fig. 2. Spleen showing a reddish brown circumscribed mass on the parietal surface; **Fig. 3.** Photomicrograph showing cavernous spaces and multiple anastomosing capillaries filled with blood within the lymphoid tissue of the spleen (H&E x100); **Fig. 4.** Section of the tumor showing cavernous spaces filled with erythrocytes (H&E x400); **Fig. 5.** Photomicrograph showing loosely arranged plump, moderately pleomorphic and hyperchromatic endothelial cells without formation of definite blood vessels (H&E x400).

sensitive abdomen. Presenting clinical signs in the dog vary and may also include repeated syncope or collapse and subsequent recovery associated with bouts of hypovolemia and autotransfusion following tumor rupture and hemoabdomen. In the present study, the complete blood count abnormalities included polycythemia, neutrophilia and thrombocytopenia. The other abnormalities in dogs with splenic hemangiosarcoma reported were regenerative anemia and reticulocytosis, acanthocytosis, presence of nucleated red blood cells, and schistocytes. The red blood cell abnormalities are helpful aids to the diagnosis, but they are reported in <20% of cases[10].

Polycythemia in the present case could be attributed to severe dehydration caused due to vomiting. In contrast, anaemia could be attributed to hemoperitoneum observed in their study[11] and they also noticed thrombocytopenia in HSA affected dogs like the present study. Dogs with a low platelet count had 21.4 times greater odds of being diagnosed with HSA compared to those with a normal platelet count, while dogs with low haematocrit (HCT) had 3 times greater odds of HSA diagnosis compared to dogs with normal HCT levels[11]. Neutrophilia observed in the present study could be attributed to the inflammatory process occurring in association to the neoplastic process.

In the present study, cytology revealed presence of oval to fusiform, pleomorphic cells with nuclear hyperchromasia like the earlier findings[8]. The gross and histopathological findings of the present study are akin to the findings of Spangler and Kass[12]. HSA can appear as single or multiple nodules of varying sizes[11,13,14] and in some cases, they appear as solid white, tan tumour masses without blood accumulation[14]. In the present study, histopathological examination revealed HSA composed of cavernous spaces and capillaries lined incompletely by oval to spindle shaped plumpy neoplastic endothelial cells in concordance with a previous report[13].

In conclusion, this report throws some light on the occurrence and pathomorphology of splenic hemangiosarcoma in dogs and further prognostic studies could add some insights on the behaviour of HSA in dogs.

Financial support & sponsorship: None.

Conflicts of interest: None.

Use of artificial intelligence (AI)-Assisted Technology for manuscript preparation: The authors confirm that there was no use of AI-assisted technology for assisting in the writing of the manuscript and no images were manipulated using AI.

REFERENCES

1. Kim JH, Graef AJ, Dickerson EB, Modiano JF. (2015). Pathobiology of hemangiosarcoma in dogs: Research advances and future perspectives. *Vet Sci* **2**: 388–405.
2. Griffin MA, Culp WTN, Rebhun RB. (2021). Canine and feline haemangiosarcoma. *Vet Rec* **585**:1-13.
3. Lashnits E, Neupane P, Bradley JM, Richardson T, Thomas R, Linder KE, Breen M, Maggi RG, Breitschwerdt EB. (2020). Molecular prevalence of Bartonella, Babesia, and hemotropic Mycoplasma species in dogs with hemangiosarcoma from across the United States. *PloS One* **15**: 227-234.
4. Christensen N I, Canfield PJ, Martin PA, Krockenberger M B, Spielman DS and Bosward KL. (2009). Cytopathological and histopathological diagnosis of canine splenic disorders. *Aust Vet J* ***87*****(5)**: 175-181.
5. Priester WA and McKay FW. (1980). *The occurrence of tumors in domestic animals*. US Department of Health and Human Services, Public Health Service, National Institutes of Health, National Cancer Institute **54**: 1-210.
6. Kim S E, Liptak JM, Gall TT, Monteith GJ and Woods JP. (2007). Epirubicin in the adjuvant treatment of splenic hemangiosarcoma in dogs: 59 cases (1997–2004). *J Am Vet Med Assoc* **231(10)**: 1550-1557.
7. Aronsohn MG, Dubiel B, Roberts B, Powers BE. (2009). Prognosis for Acute Non-traumatic Hemoperitoneum in the Dog: A retrospective Analysis of 60 Cases (2003–2006). *J Am Anim Hosp Assoc* **45**: 72–77.
8. Varela B, Larranaga C, Yamasaki K and Verdes JM. (2022). Canine splenic tumors: histopathological study of 9 cases in Uruguay, 2019-2020. *Braz J Vet Pathol* **15(3)**:127-132.
9. Leyva FJ, Loughin CA, Dewey CW, Marino D J, Akerman M and Lesser M L. (2018). Histopathologic characteristics of biopsies from dogs undergoing surgery with concurrent gross splenic and hepatic masses: 125 cases (2012–2016). *BMC research notes* **11**: 1-5.
10. Valli VE, Bienzle D and Meuten DJ (2017). Tumors of the hemolayphatic system. In: Meuten DJ, eds. Tumors in domestic animals, NC, USA: John Wiley & Sons, Inc. 203-295.
11. Ziogaite B, Contreras ET and Horgan JE. (2024**)**. Incidence of splenic malignancy and hemangiosarcoma in dogs undergoing splenectomy surgery at a surgical specialty clinic: 182 cases (2017–2021). *PloS one* **19(12):** 314-337.
12. Spangler WL and Kass PH. (1997). Pathologic factors affecting postsplenectomy survival in dogs. *J Vet Intern Med* **11**: 166–171.
13. Suzuki T, Henshaw M J, Yanagi T and Aoshima K. (2024). Current understanding of comparative pathology and prospective research approaches for canine hemangiosarcoma. *Res Vet Sci* **167**: 105-120.
14. Bettini G, Mandrioli L, Brunetti B and Marcato PS. (2001). Canine splenic pathology: a retrospective study of 109 surgical samples, with special emphasis on fibrohistiocytic nodules. *Eur J Vet Pathol* **7(3)**: 101-110.

Title of the Thesis : Antiviral Immune Response and Pathology in Chickens Infected with Fowl and Pigeon Newcastle Disease Virus

Name of the Student : **Faisal Bashir Dar**

Name of Advisor : Dr. Nawab Nashiruddullah,

Degree/Year : M.V.Sc. (Veterinary Pathology)/2024

Name of the University : Sher-e-Kashmir University of Agricultural Sciences & Technology-Jammu (J&K)

Two virulent Newcastle disease virus (vNDV) isolates from pigeons (Genotype II: NDV/P1/22/RSP-2) and chicken (Genotype VII: NDV/F2/22/RSP-2) from spontaneous outbreaks were selected for experimental inoculation in chicks, to study their comparative pathology, cross-transmissibility potential, and exploration of host innate immune response. Forty-five (45) three-week old, healthy, naïve and unvaccinated chicken were segregated as Group I through III, of fifteen birds each. After a week's acclimatization, Group I and II birds were inoculated with 0.1 ml viral inoculums (10^6 EID_{50}/0.1 ml per bird) with pigeon and chicken vNDV isolate respectively, via intranasal/ocular route. Group III was mock infected with sterile PBS. All birds were observed regularly for clinical signs and five birds from each group were randomly selected and for sacrificed at 1, 3 and 7 days post-inoculation (dpi). Clinical signs for both isolates from 3 dpi, showing generalized weakness, depression, conjunctivitis, respiratory distress and nasal exudation. Nervous signs were characterized by tremors, in-coordination, paralysis and coma with both isolates starting from 5-6 dpi, and a 100% fatality was noted by end of 5-6 dpi. Congestive and haemorrhagic gross lesions in the trachea and lungs were near identical, but with early onset of spleen mottling and proventricular/intestinal haemorrhages with the chicken isolate. Microscopic lesions were consistent with splenic lympho-follicular depletion and necrosis, and multifocal necrosis in pancreas. Brain lesions were expressed earlier with the pigeon isolate starting from 1 dpi, characterized by neuronal degeneration, particularly affecting the Purkinjee cells, glial reaction in the neuropil, and perivascular lymphocytic cuffing. Although the pathology of both isolates was analogous in tissue tropism, affections of the pigeon isolate had a distinctive bias towards neuronal tissue, while the chicken isolate had a propensity for the alimentary tract. No clinical signs or lesions were apparent in control, mock infected chicks. Host innate response with both isolates was robust, and conspicuous from transcriptome analysis of select Pattern Recognition Receptors, cytokine/chemokines and anti-apoptotic proteins indicating the rapid systemic dissemination of the viruses and an equally vigorous mRNA expression of innate pathway protein repertoire. Expression of PRRs and cytokines was most dynamic and consistent in the splenic tissue, indicating the early tropism of NDV to lymphoid structures, followed by the respiratory and nervous tissue. The atypical pigeon isolate was notable for its virulence, aggravated pathogenicity, and expression of innate response in chickens may be alarming for speculative natural transmission potential to chickens resulting in perpetuation of ND endemicity in the region.

Title of The Thesis : Seroprevalence and pathomorphological studies of Brucellosis in sheep of Anantapur district

Name of the Student : **Mude Ganesh Teja Naik**

Name of Advisor : Dr. H. Srinivasa Naik

Degree/Year : M.V.Sc./2025

Name of the University : Sri Venkateswara Veterinary University, Tirupati, Andhra Pradesh-517 502

The present study investigated the seroprevalence and pathomorphological effects of brucellosis in sheep from Anantapur district, Andhra Pradesh, India, to assess its prevalence and impact in a region where sheep farming is integral to rural economies. A total of 100 blood samples, comprising 50 male and 50 female sheep, were collected from the selected villages of Anantapur district. Serological screening was performed by RBPT and I-ELISA to confirm the presence of Brucella infection. The RBPT detected a seroprevalence of 16% (16/100), while the I-ELISA revealed a higher seropositivity rate of 30% (30/100). From the seropositive animals that succumbed to the infection, six tissue samples were collected and subjected to polymerase chain reaction (PCR) analysis for molecular confirmation of *Brucella* spp. The PCR, targeting a 223 bp amplicon, confirmed *Brucella* spp. in 33.33% (2/6) of the tissue samples, further validating the serological findings. The study highlighted the widespread prevalence of brucellosis in Anantapur district, with I-ELISA proving to be a more sensitive diagnostic tool compared to RBPT. Hematological analysis of 20 seropositive sheep samples revealed significant alterations ($P < 0.01$) compared to controls. The results indicated decreased hemoglobin, packed cell volume, and total erythrocyte count, while total leukocyte count and neutrophils were markedly increased in Brucella-infected sheep. Biochemical profiles pointed to hepatic dysfunction, with elevated levels of ALT and AST alongside reduced total protein and albumin concentrations, all of which were statistically significant at $P < 0.01$. Histopathological examination of tissues from seropositive adult sheep and fetuses revealed extensive changes despite no gross lesions. In males, testes showed vascular congestion, seminiferous tubule degeneration and spermatogonial loss, while the heart and liver exhibited inflammation and degeneration. In females, the uterus displayed epithelial loss, glandular hyperplasia, vascular congestion and thrombosis and inflammatory infiltration. Placental tissues exhibited hyperemia, hemosiderin deposition, and chronic inflammation. Whereas, the liver, lungs, and spleen showed congestion, emphysema, and white pulp depletion, respectively.

Title of Thesis : Toxicopathological effects of butyl benzyl phthalate on testes and brain of adult zebrafish

Name of the Student : **Kadivar Kaushar Fatemamadbhai**

Name of the Advisor : Dr. Bhavesh Trangadia

Degree/Year : M.V.Sc. /2026

Name of the University : College of Veterinary Science and Animal Husbandry, Kamdhenu University, Junagadh-362001, Gujarat

Butyl benzyl phthalate (BBP) is a common plasticizer and environmental contaminant known for its strong endocrine-disrupting effects. It interferes with hormone functions and impairs reproductive and neurological functions in aquatic organisms. Due to its persistence in aquatic environments, BBP poses a significant ecological and health risks. A total of 174 adult male zebrafish, aged above 3 months were used to evaluate the toxicopathological effects of BBP in testes and brain after daily exposure for 28 days. The study carried out in two phases under standard laboratory conditions. In phase-I, 30 zebrafish were equally divided into 5 groups *viz*., control (RO water), vehicle control (0.01% DMSO), and treatment groups were exposed to BBP at concentrations of TP1 (100 µg/L of water), TP2 (500 µg/L of water), TP3 (1000 µg/L of water). Mortality was not observed throughout the study in fish of any of these groups. However, zebrafish exposed to higher concentration exhibited marked signs of stress, including abnormal swimming behaviour and significantly reduced feed intake as compared to the other groups. Based on these findings, the higher dose levels of BBP were excluded for further testing during phase-II study. In phase-II, 144 fish divided equally in 4 groups *viz*., control (RO water), vehicle control (0.01% DMSO), T1: BBP @ 100 µg/L of water, T2: BBP @ 500 µg/L of water. During Phase-I, behavioural parameters were performed along with histological evaluation of the testes and brain and phase-II focused on the analysis of oxidative stress parameters and corresponding histopathological alterations in these tissues. Anxiety like behaviour and social behaviour evaluated on day 14 and 28 of the experiment using novel tank, light-dark preference, social preference and social recognition tests. Group TP3 exhibited reduced exploratory activity, with significantly fewer entries into the upper zone, increased anxiety-like behavior marked by prolonged time spent in the dark zone, and impaired social recognition, spending less time in the familiar zone as compared to the control group. Superoxide dismutase (SOD) activity and total antioxidant capacity (TAC) levels in the testes of T2 group, were significantly lower, whereas malondialdehyde (MDA) was significantly higher in both T1 and T2 groups as compared to control group. In brain, T2 group exhibited significantly lower SOD activity and TAC level and significantly higher MDA level as compared to the control group. Gross examination of testes and brain did not reveal any significant changes. Histopathology and PCNA immunostaining showed a dose-dependent reduction in spermatozoa along with increase in spermatocytes and spermatogonia in testes of treatment group fish as compared to the control group. While brain did not reveal any appreciable microscopic changes in any of the treatment groups.

Title of the Thesis : Clinical Correlation of Neutrophil Indices and Morphological Changes with Prognosis of Common Disease Conditions of Dogs

Name of the Student : **Krupa D Gundaliyal**

Name of the Advisor : Dr. Dhaval D Fefar

Degree/Year : M.V.Sc./2025

Name of the University : Kamadhenu University, Anand, Gujrat

Neutrophils (Polymorphonuclear cell (PMNs)) are the most abundant leukocytes in dogs, being the main cell population in the inflammatory/infectious response. This study was carried out to aim to correlate the neutrophil indices and morphological changes with different clinical condition in dogs along with their associated prognosis.

In this study, 100 clinically affected dogs and 6 healthy controls underwent comprehensive hematological evaluation, including TLC, DLC, red cell indices, and platelet counts. Neutrophil morphology was assessed and correlated with specific diagnosis and prognosis. Biochemical parameters such as liver enzymes, renal markers, proteins, and bilirubin fractions were measured using standard automated assays. Final diagnoses were established through supportive tests including rapid immunoassays, cytology, imaging, urinalysis, and histopathology.

Among the clinical conditions recorded, viral infections were most prevalent (n=22), followed by gastrointestinal disorders (n=19), pyometra (n=15), ascites (n=12), urinary tract infections (n=8), hepatic dysfunction (n=7), parasitic diseases (n=7), tumors (n=6), and respiratory tract infections (n=4).

A mild to severe left shift was observed in cases of pyometra and hepatic dysfunction, while a mild to moderate left shift occurs in canine distemper virus infection, parvovirus infection, ascites, urinary tract infection, parasitic diseases, tumors, and respiratory tract infections. In contrast, a mild left shift was seen in gastrointestinal disorders. Mild to moderate neutrophilic toxic changes were observed in all conditions except gastrointestinal disorders and tumors, where only mild neutrophilic toxic changes were present. Absolute neutrophilia was observed in cases of pyometra, tumors, and hepatic dysfunction with a leukemoid reaction observed in pyometra.

In this study, 85% of dogs showed a left shift and 82% had neutrophil toxic changes, with an overall case fatality rate of 36%. Although both survivors and non-survivors exhibited these alterations, severe left shift and marked toxicity were absent in survivors but more common in non-survivors. Among dogs with toxic changes, 8% survived less than a week and 28% lived for one week to two months. Overall, mortality increased in association with greater degrees of toxic changes and left shift.

Thus, it can be concluded that the evaluation of alterations in neutrophils number and morphological changes may be helpful in diagnosis and in accessing prognosis of different pathological conditions of dogs.

Title of Thesis : Toxicopathological effects of 4-*tert*-butylphenol on testes and brain of adult zebrafish

Name of the Student : **Nisarga Gowda K S**

Name of the Advisor : Dr. Bhavesh Trangadia

Degree/Year : M.V.Sc. /2026

Name of the University : College of Veterinary Science and Animal Husbandry, Kamdhenu University, Junagadh-362001, Gujarat

4-*tert*-butylphenol (4-*t*-BP), a synthetic phenolic compound widely used in various industrial and consumer products, has emerged as a significant environmental contaminant due to its environmental persistence, resistance to degradation and bioaccumulative nature. Its presence in aquatic ecosystems has raised considerable ecotoxicological concern, as it is known to interfere with endocrine and neural functions in aquatic organisms. Zebrafish (*Danio rerio*), being an established model organism for toxicological studies, is particularly vulnerable to phenolic pollutants that disrupt normal physiological, biochemical and reproductive processes. In the present investigation, a total of 294 adult zebrafish of more than three months of age were utilized to assess the toxicological effects of 4-*t*-BP on the testes and brain following continuous exposure for 28 days. The experiment was carried out in two phases under standard laboratory conditions. In Phase I, 30 zebrafish were randomly divided into five groups *viz.*, control [reverse osmosis (RO) water], vehicle control [0.01% dimethyl sulphoxide (DMSO)] and three treatment groups exposed to 4-*t*-BP at concentrations of 100 µg/L of water (TP1), 500 µg/L of water (TP2) and 1000 µg/L of water (TP3). No signs of toxicity or mortality were reported during this phase. Behavioural analysis using novel tank, light-dark preference, social preference and social recognition tests was conducted on the 14th and 28th days of exposure. Zebrafish in the TP3 group exhibited reduced exploratory activity with significantly fewer entries to the upper zone, increased anxiety-like behaviour characterized by prolonged time spent in the dark zone and reduced social recognition, spending less time in the familiar zone as compared to control group. Based on these observations, concentrations of 500 µg/L (T1) and 1000 µg/L (T2) were selected for Phase II. In this phase, 264 fish were equally divided into four groups: control, vehicle control (0.01% DMSO), T1 (500 µg/L of water) and T2 (1000 µg/L of water) and were assessed for oxidative stress parameters, mRNA expression of *sod*, *cat* and *nrf2* genes and histopathological changes in testes and brain. Proliferative cell nuclear antigen (PCNA) immunostaining in testes was carried out. Biochemical analysis demonstrated significantly reduced superoxide dismutase (SOD) and total antioxidant capacity (TAC) levels, along with elevated malondialdehyde (MDA) concentrations in testes and brain, indicating oxidative stress. mRNA expression of *sod*, *cat* and *nrf2* genes significantly down-regulated in the testes and brain in T2 group. Gross examination of testes and brain did not reveal any significant changes. Histopathology and PCNA immunostaining revealed a dose-dependent decrease in spermatozoa with an increase in spermatogonia in testes of treatment group fish as compared to the control group, while the brain sections did not exhibit any appreciable microscopic alterations. Overall, these findings demonstrate that 4-*t*-BP exposure induce oxidative stress, impair antioxidant gene expression in testes and brain and causes histomorphological alterations in the zebrafish testes, highlighting its potential to disrupt reproductive health in aquatic species.

Title of the Thesis : Pathological Studies and Molecular Characterization of Marek's Disease Virus of Chicken

Name of the Student : **Mutkule Ajay Gopal**

Name of the Advisor : Dr. Kaushal Kumar

Degree/Year : MVSc/2025

Name of the University : Bihar Veterinary College, Bihar Animal Sciences University, Patna, Bihar

Marek's disease is a re-emerging infectious poultry disease, persisting despite extensive vaccination efforts. It is a lymphoproliferative condition in chickens caused by Marek's disease virus (MDV-1), an oncogenic alpha-herpesvirus. MDV exhibits unique virulence-related genes, including vIL-8, pp14, Meq, and pp38, which are associated with its heightened oncogenicity and pathogenicity. The present research was carried out to determine the incidence of MD in various native and cross-bred chicken populations. The study included epidemiological data on mortality due to MD, focusing on factors such as breed, age, and sex of layer chicken from various poultry farms in and around Patna. It involved gross and histopathological examination of various organs, PCR-based detection of Marek's Disease Virus (MDV), and molecular characterization of the field virus through sequencing of the Meq and pp38 gene. The proposed study aims to explore the epidemiology, molecular characteristics, diagnostic advancements in Marek's disease in chicken conventional poultry farming.

In this study, out of 318 birds examined, 34 (10.69%) tested positive for Marek's disease (MD) based on gross pathology, histopathology, and PCR diagnosis. Among the breeds, Vanaraja exhibited the highest incidence rate (26.4%), followed by R.C × R.I.R and BV300, both at 23.5%. Age-wise, the highest incidence was observed in birds aged 40-49 weeks (17.7%), followed by 20-29 weeks, 50-59 weeks, and 60-69 weeks (each at 14.7%). Additionally, female mortality was higher in BV300 and Vanaraja, recorded at 23.5% and 20.6%, respectively. The liver was the most commonly affected organ (76.5%), followed by the spleen (47%), ovaries (38.2%), kidneys (35.3%), and intestines (35.3%). The gross pathological lesions were primarily observed in various visceral organs, including the liver, spleen, proventriculus, kidney, ovaries and intestine etc. Visibly, all affected organs displayed enlargement or thickened mucosa, with multiple greyish-white tumor nodules of varying sizes. Microscopic changes were most consistently observed in tissue sections of liver, spleen, kidney, ovaries and proventriculus representative of all the chicken. The lesions in the hepatic parenchyma were characterized by proliferation of pleomorphic lymphoid cells i.e. lymphoblasts and small to large lymphocytes with Perivascular lymphoid proliferation in some of the tissue sections. There was extensive abnormal infiltration of lymphoid cells which has replaced and distorted the parenchymatous and stromal cell population of spleen, kidney, ovary and proventriculus. Phylogenetic analysis of the nucleotide and amino acid sequences of the *Meq* and *pp38* genes from the field strains in this study revealed that foreign strains, such as those from China and the USA, formed a distinct cluster separate from Indian samples like BASU 5, BASU 4, and BASU 7. The Hyderabad and Chandigarh sequences clustered with the BASU samples, suggesting a geographical similarity among Indian Marek's disease virus (MDV) strains. In conclusion, the study demonstrated that MDV strains from the Indian subcontinent exhibit a high level of sequence similarity, regardless of geographic distribution, compared to foreign MDV isolates.

Title of Thesis : Toxicopathological effects of 4-*tert*-octylphenol on ovary and brain of adult zebrafish

Name of the Student : **Jadhav Sangram Kiran**

Name of the Advisor : Dr. Bhavesh Trangadia

Degree/Year : M.V.Sc. /2026

Name of the University : College of Veterinary Science and Animal Husbandry, Kamdhenu University, Junagadh-362001, Gujarat

4-*tert*-octylphenol (4-*t*-OP) is a phenolic environmental contaminant with significant endocrine-disrupting properties. 4-*t*-OP exhibits toxicity through disrupting reproductive and neurological functions in aquatic organisms and poses serious ecological and health risks. A total of 342 adult female zebrafish, aged above 3 months, were used to evaluate the toxicopathological effects of 4-*t*-OP in the ovary and brain after daily exposure for 28 days. The study was carried out in two phases under standard laboratory conditions. In phase-I, 30 zebrafish were equally divided into 5 groups, *viz*., control (RO water), vehicle control (0.01% DMSO), and the remaining groups were exposed to 4-*t*-OP at concentrations of TP1 100 µg/L of water, TP2 at 400 µg/L of water, and TP3 at 800 µg/L of water. Neither signs of toxicity nor mortality were observed during phase-I of the study. Behavioral assessments on days 14 and 28 (novel tank, light–dark preference, social preference, and social recognition tests), TP3 group exhibited marked anxiety-like behavior and noticeable impairments in social interactions. Microscopic examination of the ovary revealed yolk granule depletion (DYG) in zebrafish of the TP2 group, while DYG and degenerated mature oocyte (DMO) were evident in the ovary of zebrafish from the TP3 group. Histopathological examination of the brain did not reveal any appreciable microscopic changes in any of the treatment groups. Based on phase-I results, exposure concentration of 4-*t*-OP at 400 µg/L and 800 µg/L of water was used for the phase-II study. In phase-II, 312 fish were divided equally into 4 groups, viz., control (RO water), vehicle control (0.01% DMSO), T1: 4-*t*-OP at 400 µg/L of water, and T2: 4-*t*-OP at 800 µg/L of water. Oxidative stress parameters, histopathological changes and mRNA expression profile of *sod, cat* and *nrf2* genes in the ovary and brain were carried out during this phase. Grossly, the ovary and brain of zebrafish from all treatment groups were apparently normal. Histopathological examination of the ovary revealed DYG in mature oocytes in T1 group, while DYG in mature oocytes, along with DMO evident in the ovary of zebrafish from T2 group. Superoxide dismutase (SOD) activity and total antioxidant capacity (TAC) levels in the ovary of T2 group were significantly reduced, whereas malondialdehyde (MDA) was significantly higher in the T1 and T2 groups as compared to the control group. In the brain, SOD activity and TAC level were significantly lower in T2 group; and significantly higher MDA level was reported in T2 as compared to the control group. In the ovary, mRNA expression of *sod, cat* and *nrf2* genes down-regulated in T2 group as compared to the control group. In the brain, *sod* and *nrf2* expression levels were significantly down-regulated in the T2 group, while *cat* gene expression level was significantly down-regulated in both T1 and T2 groups as compared to the control group. Exposure of 4-*t*-OP caused anxiety like behaviour and alteration in social behaviour, also indicating significant oxidative stress and damage in the ovary and brain.

Title of the Thesis : Pathomorphological and Molecular Characterization of *Escherichia coli* in Broiler Chicken

Name of the Student : **Vishal Kumar Sinha**

Name of the Advisor : Dr. Kaushal Kumar

Degree/Year : MVSc/2026

Name of the University : Bihar Veterinary College, Bihar Animal Sciences University, Patna, Bihar

Escherichia coli (E. coli) is one of the most important bacterial pathogens affecting poultry causing colibacillosis that results in significant economic losses (USD 1–2 billion annually) and presents potential zoonotic concerns. The present investigation was conducted to study the pathomorphological alterations and molecular characterization of *E. coli* in broiler chickens in and around Patna, Bihar.

A total of 250 deceased broiler chickens suspected of colibacillosis were examined. Detailed necropsy was performed and representative tissue samples were collected for gross and histopathological evaluation. Additionally, 62 swab samples (34 cloacal and 28 tracheal) and 188 organ samples were processed for isolation, identification and molecular characterization using PCR and whole-genome sequencing (WGS). Gross pathological examination revealed fibrinous perihepatitis (57.5%) and pericarditis (52.5%) as prominent and pathognomonic lesions of colibacillosis. Other consistent findings included airsacculitis, pulmonary congestion, splenomegaly, hepatic necrosis and renal congestion. Age-wise analysis demonstrated the highest mortality in the 0–2 weeks age group (38.1%) followed by birds older than 10 weeks (26.2%) indicating heightened vulnerability during early life. Histopathology revealed severe hepatic degeneration and necrosis, fibrinous exudation, lymphoid depletion in the spleen, interstitial myocarditis and necrotizing enteritis confirming systemic infection.

Of the 250 suspected cases, 101 (40.4%) yielded characteristic *E. coli* colonies on culture. Among these, 59 (58.4%) isolates were biochemically confirmed by IMViC testing. Molecular confirmation targeting the *uidA* gene identified 42 positive isolates resulting in an overall PCR-based prevalence of 16.8%.

Whole-genome sequencing of a representative isolate (BASUEcol01) revealed the presence of 59 antimicrobial resistance genes, 141 virulence-associated genes, 998 transporter genes and 145 metal resistance determinants highlighting marked pathogenic and adaptive capabilities. The genome assembly demonstrated high accuracy with minimal errors. Annotation indicated coexistence of multidrug resistance determinants and multiple virulence factors including iron acquisition and adhesion-associated genes. The isolate belonged to sequence type ST156 and exhibited multidrug resistance potential mediated through efflux systems and regulatory networks.

Phylogenetic analysis based on whole-genome GBDP distances clustered BASUEcol01within a well-supported clade of closely related global *E. coli* strains (bootstrap ~97%) indicating evolutionary relatedness. Overall, this study confirms the presence of genomically diverse, pathogenic and multidrug-resistant *E. coli* strains in poultry from Patna underlining the need for strengthened biosecurity, prudent antimicrobial use and continuous genomic surveillance to mitigate economic losses and public health risks.

Title of Thesis	:	Incidence of respiratory diseases in chicken with special reference to viral etiology
Name of the Student	:	**Sangamoni Pavan Kumar**
Name of the Guide	:	Dr. Swathi Bora
Degree/Year	:	MVSc/2026
Name of the University	:	P. V. Narsimha Rao Telangana Veterinary University, Hyderabad

Respiratory viral diseases represent a major constraint to commercial poultry production due to their high morbidity, mortality, and associated economic losses. The present investigation was undertaken to determine the incidence, seasonal distribution, pathological alterations, and molecular prevalence of major viral respiratory pathogens in chickens from different locations in and around Hyderabad. A total of 439 birds from 32 commercial poultry flocks were examined during the period from June to November 2025. Among these, 262 birds showed gross lesions suggestive of respiratory disease, and 104 cases (23.69%) were confirmed as viral respiratory infections by PCR.

Location-wise analysis revealed considerable variation in incidence with the highest occurrence recorded in Keshampet (34.32%), followed by Rajendranagar (27.65%) and Shadnagar (23.72), while the lowest incidence was observed in Bibinagar (16.70%). Flock level molecular screening demonstrated Newcastle disease virus (NDV) as predominant pathogen, detected in 40.63% of flocks, followed by infectious bronchitis virus (IBV) in 25% and Fowl adenovirus (FAdV) in 12.5% of flocks. Seasonal analysis indicated a significantly higher incidence during the winter months (30.18%) compared to the rainy season (20%), with NDV detected consistently throughout the study period.

Clinically affected birds exhibited respiratory distress, nasal and ocular discharge, diarrhoea, neurological signs, and abnormalities in egg production. Gross pathological findings varied with the viral aetiology and included congested and oedematous lungs, haemorrhagic tracheitis, thickened air sacs, renal alterations, and hepatic lesions.

Disease-wise histopathological examination of respiratory tissues revealed distinct lesions corresponding to individual viral infections. NDV-infected birds showed tracheal epithelial hyperplasia, deciliation, necrosis, submucosal oedema, vascular congestion, and mononuclear cell infiltration, while lungs exhibited congestion, interstitial oedema, heterophilic plugs, and parabronchial epithelial thickening. IBV infection was characterized by severe tracheal epithelial damage with ciliary loss, goblet cell depletion, epithelial sloughing, submucosal oedema, and prominent lymphoid aggregation. Pulmonary lesions in IBV included inter-alveolar septal thickening, congestion, haemorrhages, and mixed inflammatory cell infiltration.

FAdV infected birds showed mild to severe tracheal deciliation and epithelial desquamation with pulmonary congestion and focal haemorrhages. A characteristic feature of FAdV infection was hepatic degeneration and necrosis with prominent intranuclear inclusion bodies. Overall, disease-specific histopathological patterns correlated well with molecular findings, supporting the diagnostic value of histopathology in viral respiratory diseases of poultry.

Molecular detection by RT-PCR and PCR confirmed NDV as the most prevalent virus (62.50%), followed by IBV (22.12%) and FAdV (15.38%). The study highlights the continued predominance of NDV and the significant contribution of IBV and FAdV to respiratory disease complexes in poultry, emphasizing the need for integrated pathological and molecular surveillance to strengthen control and prevention strategies.